# INFORMATION TO USERS

This manuscript has been reproduced from the microfilm master. UMI films the text directly from the original or copy submitted. Thus, some thesis and dissertation copies are in typewriter face, while others may be from any type of computer printer.

**The quality of this reproduction is dependent upon the quality of the copy submitted.** Broken or indistinct print, colored or poor quality illustrations and photographs, print bleedthrough, substandard margins, and improper alignment can adversely affect reproduction.

In the unlikely event that the author did not send UMI a complete manuscript and there are missing pages, these will be noted. Also, if unauthorized copyright material had to be removed, a note will indicate the deletion.

Oversize materials (e.g., maps, drawings, charts) are reproduced by sectioning the original, beginning at the upper left-hand corner and continuing from left to right in equal sections with small overlaps. Each original is also photographed in one exposure and is included in reduced form at the back of the book.

Photographs included in the original manuscript have been reproduced xerographically in this copy. Higher quality 6" x 9" black and white photographic prints are available for any photographs or illustrations appearing in this copy for an additional charge. Contact UMI directly to order.

UMI®

Bell & Howell Information and Learning
300 North Zeeb Road, Ann Arbor, MI 48106-1346 USA
800-521-0600

# An Analytical Investigation of a Panhard Rod Restraint for Beam-Axle Vehicle Suspensions

**Qiang Yin**

**A Thesis**

**in**

**The Department**

**of**

**Mechanical Engineering**

**Presented in Partial Fulfillment of the Requirements for the Degree of Master of Applied Science at Concordia University Montreal, Quebec Canada**

**November 1997**

# Abstract

## An Analytical Investigation of a Panhard Rod Restraint for Beam-Axle Vehicle Suspensions

Qiang Yin

The contributions of the kinematic and dynamic properties of a Panhard rod constraint to the ride and handling performance of road vehicles with beam-axle suspensions are analyzed through study of the roll plane dynamics of a modern high-decker highway bus. A nonlinear kineto-static model of the candidate vehicle is first developed and analyzed to investigate the variations in the coordinates of the suspension roll center and the sprung mass gravity center, the effective roll stiffness as a function of the magnitude of centrifugal force excitation, roll input, vehicle load and the Panhard rod design parameters. Two roll plane dynamic models of the candidate vehicle with nine-DOF and five-DOF are then formulated and analyzed under excitations due to directional maneuvers and road irregularities, as characterized by a harmonic centrifugal acceleration, out-of-phase harmonic displacements, and random unevenness with randomly distributed phase between the right and left tracks. The simulation results show that the Panhard rod inertia and bushings represented in nine-DOF model contribute only to high frequency dynamics of the vehicle. The ride and handling performance of the candidate vehicle under transverse Panhard rod constraint, which relates to the low frequency dynamics of the vehicle is thus evaluated with the simplified five-DOF model by assessing the roll and lateral displacements and accelerations of the sprung mass. The effect of the variations in the suspension and Panhard rod properties, and the vehicle operation conditions are investigated.

# Acknowledgements

The author wishes to thank her supervisors, Dr. S. Rakheja, Dr. I. Stiharu, Dr. S. Sankar and Dr. T. S. Sankar for their guidance and encouragement in the preparation of this thesis.

The author also wishes to thank members of faculty and staff of the CONCAVE (Concordia Computer-Aided Vehicle Engineering) Research Center, Department of Mechanical Engineering, Concordia University for their time and assistance during the progression of this project.

Thanks are also due to the author's husband, Dan Negrin, her parents, Fuyin Tang and Songtao Yin, her brother, Gang Yin for their love, understanding and support during the course of this research.

# Table of Contents

# List of Figures

# List of Tables

# Nomenclature

| Symbol | Description |
|---|---|
| $a_1$ | Half suspension spring track width ( m ) |
| $a_2$ | Half suspension damper track width ( m ) |
| $a_x$ | Centrifugal acceleration imposed on the sprung and unsprung masses, and the Panhard rod, during a cornering/directional maneuver ( $m/sec^2$ ) |
| b | Half tire track width ( m ) |
| c | Half track width of the Panhard rod ( m ) |
| [C] | (5×5) damping matrix |
| $[\overline{C}]$ | (9×9) damping matrix |
| $[C_F]$ | (5×3) equivalent excitation damping matrix |
| $[\overline{C}_F]$ | (9×3) excitation damping and stiffness matrices |
| cg | Center of gravity |
| $[C_P]$ | (5×5) equivalent damping matrix due to Panhard rod |
| $[C_R]$ | (n × m) road excitation damping matrix |
| $[C_s]$ | (n×n) damping matrix |
| $c_s$ | Damping coefficient of the vertical suspension ( N/m ) |
| $c_T$ | Vertical damping coefficient of the tire ( N·s/m ) |
| $c_{tl}$ | Lateral damping coefficient of the tire (N.s/m ) |
| $d_1$, $d_2$ | Initial vertical heights of the Panhard rod bushings with respect to the cg of the sprung and unsprung masses ( m ) |
| $[D_{ax}]$ | (5×1) equivalent excitation mass/inertia matrix |
| e | Half track width of the Panhard rod ( m ) |
| F | Centrifugal force acting on the sprung mass ( N ) |
| $f_A$ | Magnitude of the vertical displacement excitation ( m ) |
| $f_d$ | Damped natural frequency ( Hz ) |
| $f_L$, $f_R$ | Vertical displacements induced at the left- and right- tire-road interface in the roll plane ( m ) |
| $F_L$, $F_R$ | Left and right suspension spring forces ( N ) |

| | |
|---|---|
| $F_{LX}$, $F_{LY}$ | Left suspension spring force components ( N ) |
| $f_n$ | Undamped natural frequency ( Hz ) |
| $F_{RX}$, $F_{RY}$ | Right suspension spring force components ( N ) |
| g | Gravity acceleration ( $m/sec^2$ ) |
| H | Vertical distance between the sprung mass cg and the geometric center of the Panhard rod ( m ) |
| h | Vertical distance between the unsprung mass cg and the geometric center of the Panhard rod ( m ) |
| $\{H_a(i\omega)\}$ | Fourier transform matrix of transfer function under acceleration excitation |
| $\{H_R(i\omega)\}$ | Fourier transform matrix of transfer function under road excitation |
| $h_s$ | Sprung mass cg height ( m ) |
| $h_u$ | Unsprung mass cg height ( m ) |
| $I_L$ | Roll mass moment of inertia of the Panhard rod about its cg ( $kg \cdot m^2$ ) |
| $I_s$ | Roll mass moment of inertia of the sprung mass about its cg ( $kg \cdot m^2$ ) |
| $I_u$ | Roll mass moment of inertia of the unsprung mass about its cg ( $kg \cdot m^2$ ) |
| [K] | $(5 \times 5)$ stiffness matrix |
| $[\overline{K}]$ | $(9 \times 9)$ stiffness matrix |
| $[K_a]$ | $(n \times 1)$ coefficient matrix of centrifugal acceleration excitation |
| $[K_F]$ | $(5 \times 3)$ equivalent excitation stiffness matrix |
| $[\overline{K}_F]$ | $(9 \times 3)$ excitation damping and stiffness matrices |
| $[K_P]$ | $(5 \times 5)$ equivalent stiffness matrix due to Panhard rod |
| $[K_R]$ | $(n \times m)$ road excitation stiffness matrix |
| $[K_s]$ | $(n \times n)$ stiffness matrix |
| $k_s$ | Spring rate of the vertical suspension ( N/m ) |
| $k_T$ | Vertical stiffness of the tire ( N/m ) |
| $k_{tl}$ | Lateral stiffness of the tire ( N/m ) |
| $K_\theta$ | The suspension roll stiffness ( N/m ) |
| L | Panhard rod length ( m ) |

| | |
|---|---|
| $L_L$, $L_R$ | Instantaneous lengths of the left and right suspension springs ( m ) |
| $L_S$ | Free length of the suspension spring ( m ) |
| M | The suspension roll moment ( N·m ) |
| [M] | (5×5) mass/inertia matrix |
| $[\overline{M}]$ | (9×9) mass/inertia matrix |
| $m_L$ | Panhard rod mass ( kg ) |
| $[M_P]$ | (5×5) equivalent mass/inertia matrix due to Panhard rod |
| $[M_s]$ | (n×n) mass/inertia matrix |
| $m_s$ | Sprung mass ( kg ) |
| $m_u$ | Unsprung mass ( kg ) |
| P | Constraint force due to the restraining Panhard rod ( N ) |
| PSD | Power spectral density |
| {q} | Vector of generalized coordinates of the five-DOF analytical model |
| $\{\overline{q}\}$ | Vector of generalized coordinates of the nine-DOF analytical model |
| $\{q_s\}$ | (n×1) vector of generalized coordinates |
| $\{Q_s(i\omega)\}$ | Fourier transform of $\{q_s\}$ |
| r | Radius of the Panhard rod bushing ( m ) |
| R | Height of the sprung mass cg from its base ( m ) |
| $R_0$ | Height of unsprung mass cg from the ground plane ( m ) |
| rc | Roll center of suspension |
| rnd | Random number between 0 and 1 |
| $[S_a(\omega)]$ | (n×n) matrix of the acceleration PSD of $\{q_s\}$ |
| $S_i(\omega)$ | Road displacement excitation spectral density |
| $[S_0(\omega)]$ | (n×n) matrix of the displacement PSD of $\{q_s\}$ |
| [u] | (3×1) vector of excitation coordinates |
| $\{u_R\}$ | (m×1) road excitation vector |
| $\upsilon$ | Vehicle forward speed ( km/h ) |

| | |
|---|---|
| $v_{CG}$ | Velocity of the sprung mass cg ( m/s ) |
| W | Suspension static vertical load ( $W= m_s g$ ) |
| $x_A , y_A$ | Coordinates of the left suspension spring attachment point with the sprung mass ( m ) |
| $x_B , y_B$ | Coordinates of the right suspension spring attachment point with the sprung mass ( m ) |
| $x_{CG}, y_{CG}$ | Coordinates of the sprung mass cg ( m ) |
| $x_L, y_L$ | Coordinates of the Panhard rod cg ( m ) |
| $x_{RC}, y_{RC}$ | Coordinates of the suspension roll center ( m ) |
| $x_s , y_s$ | Coordinates of the Panhard rod joint with the sprung mass ( m ) |
| $x_u, y_u$ | Coordinates of the unsprung mass cg ( m ) |
| $\alpha_0$ | Panhard rod installation angle ( m ) |
| $\alpha, \theta_L$ | Panhard rod roll angle ( m ) |
| $\overline{\alpha}$ | Road roughness coefficient ( $m^{-1}$ ) |
| $\theta_s$ | Sprung mass roll angle ( deg. ) |
| $\Phi(\omega)$ | Displacement PSD of the random road profile ($m^2$/Hz ) |
| $\psi, \theta_u$ | Unsprung mass roll angle ( deg.) |
| $\{\psi_D\}$ | Eigenvector |
| $\lambda_D$ | Eigenvalue |
| $\omega$ | Angular frequency ( rad/s ) |
| $\omega_n$ | Undamped radial natural frequency ( rad/s ) |
| $\omega_d$ | Damped radial natural frequency ( rad/s ) |
| $\zeta$ | Damping ratio |
| $\rho$ | The variance coefficient ( m ) |
| $\tau$ | Phase difference between vertical excitations at left & right tracks ( rad ) |

# Chapter 1

# Introduction and Review of Previous Investigations

## 1.1 General

Vehicle suspensions are primarily designed to support vehicle weight, isolate vehicle body from the road disturbances, and provide directional control. These fundamental requirements can be compiled into three basic criteria: economy, comfort and handling, as illustrated in Figure 1.1 [1]. However, these basic criteria, in principle, are mutually contradictory. Extreme economy is certainly not automatically equated with a high degree of comfort, and excellent handling is generally not attainable with inexpensive designs. Good ride quality inevitably requires soft suspensions. Soft suspensions, however, yield poor control performance with respect to sprung mass attitude and thus deteriorate the handling and roll stability performance of the vehicle. The design of vehicle suspension thus involves a compromise among economy, handling and ride performance characteristics.

Linkage mechanism plays an important role in realizing the vehicle suspension designs that can provide adequate ride and handling performance. Suspension linkages affect the vehicle performance in a significant manner since the handling and directional control characteristics are directly related to the kinematics and dynamics of the suspension linkages, while ride quality of a vehicle is strongly related to the suspension's energy restoring and dissipating properties. A wide variety of suspension linkages have been designed for independent and beam axle vehicle suspensions. Some of the commonly used suspension linkages employed in independent suspensions, such as Double-Wishbone suspension and Macpherson Strut suspension are illustrated in Figure 1.2. The schematic

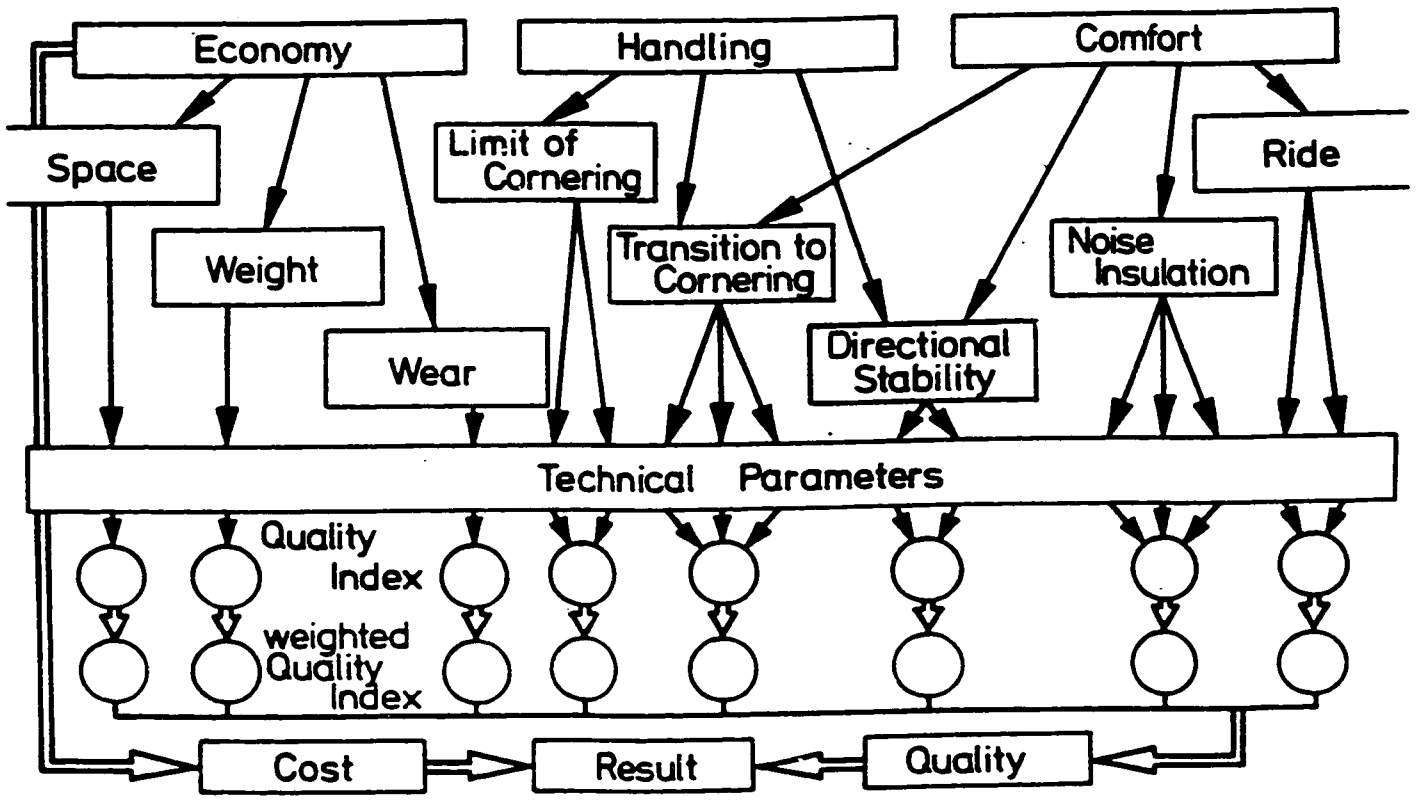


Figure 1.1 Basic criteria for vehicle suspension designs [1]

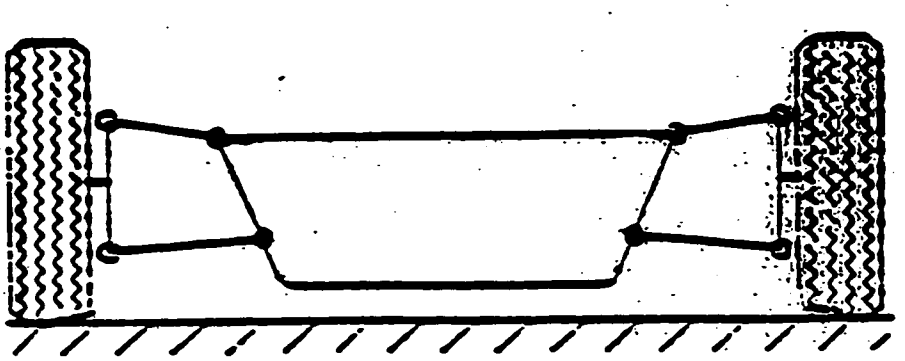

Double-Wishbone suspensions

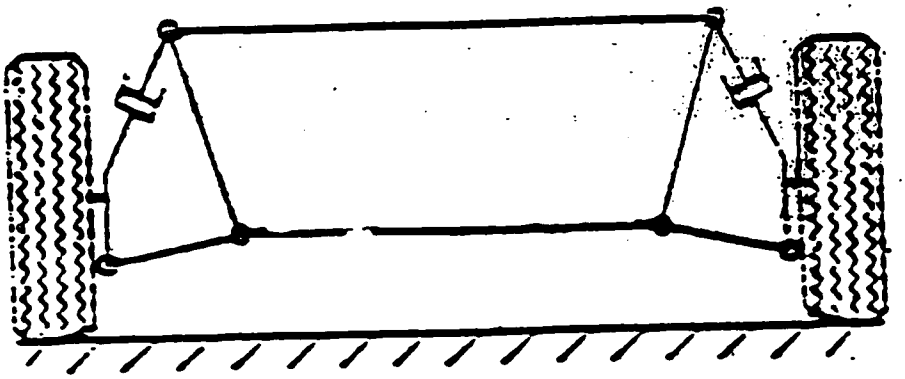

Macpherson Strut suspension

Figure 1.2 Schematics of double Wishbone and MacPherson strut suspensions

diagrams for suspension linkages used in axle suspensions are shown in Figure 1.3. The relative merits of independent and axle suspensions have been addressed in a number of studies [2-4]. Independent suspension linkage designs could lead to improved ride and handling, reduced road damage, and usually are employed when the optimum ride and handling performance compromise for on-road conditions is a priority. Axle suspension linkages, on the other hand, offer significant advantages for highway bus, heavy truck and off-road vehicles. The dependent axle suspensions, in general, are rugged and inexpensive, provide adequate ground clearance and vehicle dynamic performance comparable with those of the independent suspension linkage designs. The kinematics and dynamics of such an axle suspension and the associated linkage is thus investigated in this dissertation.

Among various axle suspensions, beam-axle is one of the most commonly used configurations and therefore is of significant importance. The beam-axle suspensions frequently employed in heavy vehicles are required to transmit excessive power. Such axles thus need to be constrained in the fore-aft plane with certain restraining linkage. In the roll plane, an anti-roll bar is usually employed to restrain the roll motion of the sprung mass encountered due to excitation arising from steering inputs and road irregularities. Suspension linkages installed between the sprung and unsprung masses, such as Panhard rod, Chebyshev linkage, Watt linkage, Roberts linkage and Evans linkage, etc., as shown in Figure 1.4, are frequently utilized in conjunction with softer suspensions to enhance the ride dynamics, the roll and lateral directional stability of highway buses, heavy-duty trucks, racing cars, and off-road vehicles.

The primary objective of the dissertation research is to investigate the ride, handling and roll stability characteristics of road vehicles incorporating beam-axle suspensions with a Panhard rod constraining link, which are strongly related to the

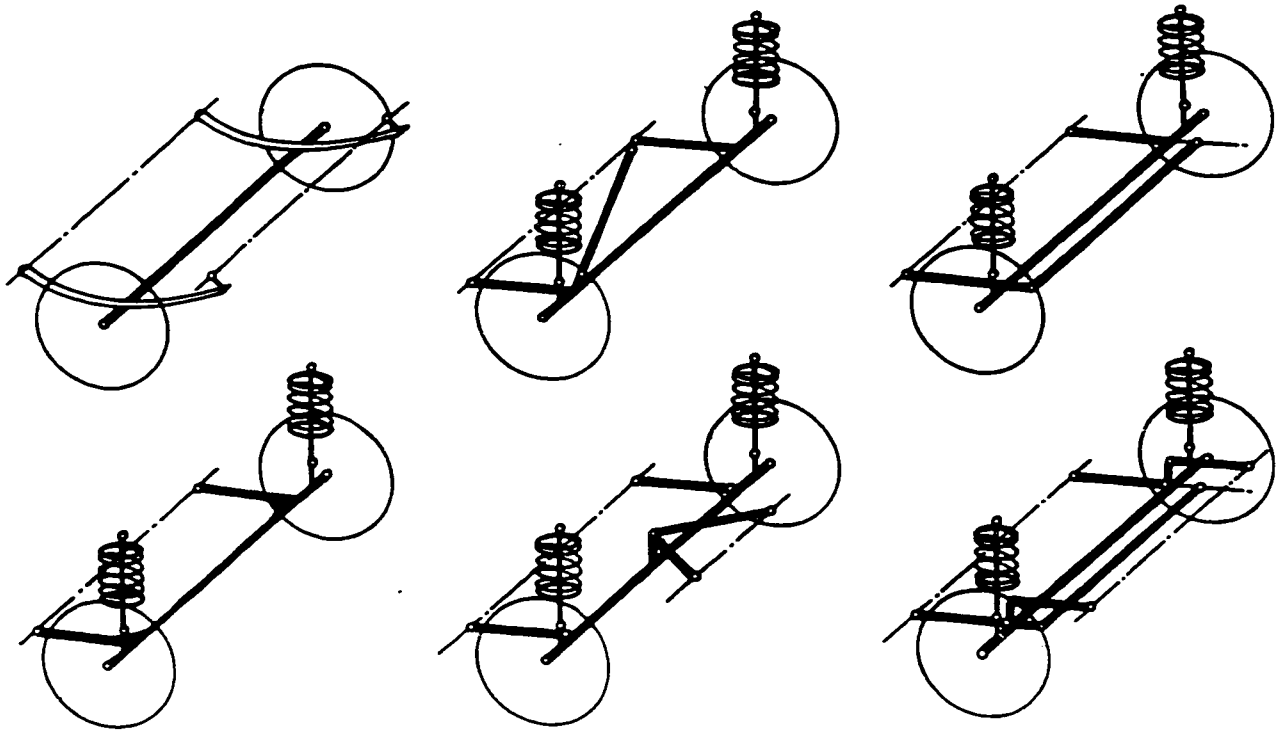

Figure 1.3 Schematics of rigid axles [1]

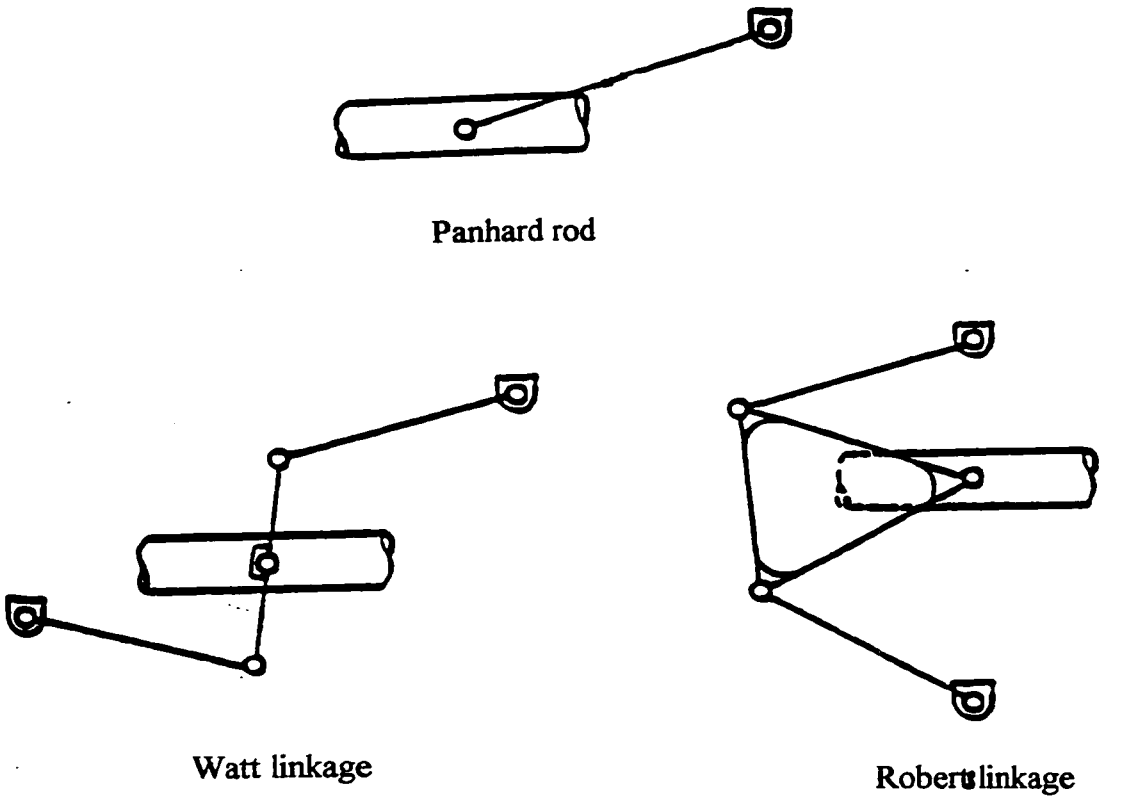


Figure 1.4 Schematics of straight-line constraint linkages

restoring and dissipation properties of the suspension, and the kinematic and dynamic properties of the linkage. A highway bus equipped with beam-axle suspensions is selected as the candidate vehicle. Kinetostatic and dynamic roll plane models of the candidate vehicle are formulated to study the ride, handling and roll characteristics of the candidate vehicle under static, harmonic and random road excitations, and static and harmonic centrifugal acceleration caused by a directional maneuver. The influence of the kinematic and dynamic properties of the Panhard rod, the suspension spring and damping properties, the vehicle speed and the road roughness on the beam-axle suspension performance are discussed.

## 1.2 Literature Review

A review of the relevant reported studies on the suspension design and performance for the road vehicles is briefly presented in the following sections to formulate the scope of this dissertation. The literature review specifically emphasizes the aspects related to ride and handling performance of road vehicles and passive suspension design techniques, which involve vehicle modeling, road surface and tire-road interface descriptions, optimization techniques, suspension linkages, and beam-axle suspensions.

### 1.2.1 Ride and Handling Performance of Road Vehicles

Ride quality of road vehicle relates to many ergonomic design and dynamic considerations. While the driver seating, workstation design, air quality, etc. form the essential components of ergonomic consideration, the dynamic ride quality relates to the whole-body vehicle vibration and noise. The dynamic ride quality is strongly related to the design of vehicle suspension, and is assessed in terms of acceleration due to vibration transmitted to the driver/passenger seats or the sprung mass. The road irregularities,

directional maneuvers, engine and drive-line vibrations and the aerodynamic forces are considered as the major contributing factors to the overall ride vibration environment of the vehicle. Among these, the low frequency vibration arising from the interactions of the vehicle and tires with the irregular road are considered as the most significant contributing factor. The vehicle response to directional maneuvers is also known to yield low frequency vibration (well below 0.5 Hz) at the driver/passenger location. Since the driver/passenger comfort relates to the magnitude of low frequency vibration (below 8 Hz) [ISO-2631], the studies on ride quality of vehicles mostly focus on the road-induced vibration.

The handling performance of a road vehicle refers to its directional characteristics to the drivers' inputs, such as the cornering/directional, braking and acceleration maneuvers. A rapid, precise and steady path following response of the vehicle is considered as the most desirable handling. The handling performance of a vehicle, however, is a complex function of the roll, lateral and yaw motion response of the sprung masses of the vehicles, cornering properties of the tires, and vehicle deflections experienced by the suspension springs. The maximum lateral and roll deflections of the sprung mass when subject to resultant external force caused by directional maneuvers frequently used to assess the handling and roll performance of vehicles.

While soft suspensions yield improved ride performance, the realization of good handling and directional control performance necessitates medium hard to hard suspension springs. Simultaneous demand for better ride and handling characteristics thus poses conflicting design requirements for road vehicle suspensions. A number of designs and concepts in passive suspension have evolved in an attempt to achieve a compromise between ride and handling requirements of road vehicles, which are briefly discussed in the following subsections.

### 1.2.2 Suspensions and Suspension Linkages

The primary functions of a road vehicle suspension are to provide vehicle support, stability, and directional control during handling maneuvers, such as acceleration/braking and cornering, and to provide effective isolation from road disturbances. Furthermore, the suspension should be insensitive to externally applied loads, such as crosswind aerodynamic forces and cargo load variations [5]. Vehicle suspensions can be classified into two categories based on their design: solid axles and independent suspensions.

A solid axle is one in which the wheels are mounted at either end of a rigid beam so that any movement of one wheel is transmitted to the opposite wheel causing them to steer and camber together [6]. Solid axles are often employed in the rear of many cars and most trucks, and within the front axles of many four-wheel-drive trucks. Heavy trucks, where the axles are designed with high load-carrying capacity, the solid beam axles are most frequently employed. Solid axles in the Hotchkiss rear suspension and the four-link rear suspension are shown in Figures 1.5 and 1.6. In Hotchkiss suspension, the leafs perform not only the springing function but also locating the axle laterally and reacting to acceleration and braking torque. The kinematic motion of such suspension, however, is not controlled very precisely. The inherent friction of the leaf springs further yield poor ride and reduced side stability, since long leaf springs are required to achieve lower spring rates. In a four-link suspension, the lower control arms provide longitudinal control of the axle, while the upper arms absorb braking/driving torque and lateral forces. The coil or air springs can be conveniently used to achieve improved noise, vibration and harshness performance by eliminating the coulomb friction characteristics of leaf springs.

In contrast to the solid axles, independent suspensions allow each wheel to move vertically without affecting the opposite wheel. Such suspensions offer superior resistance

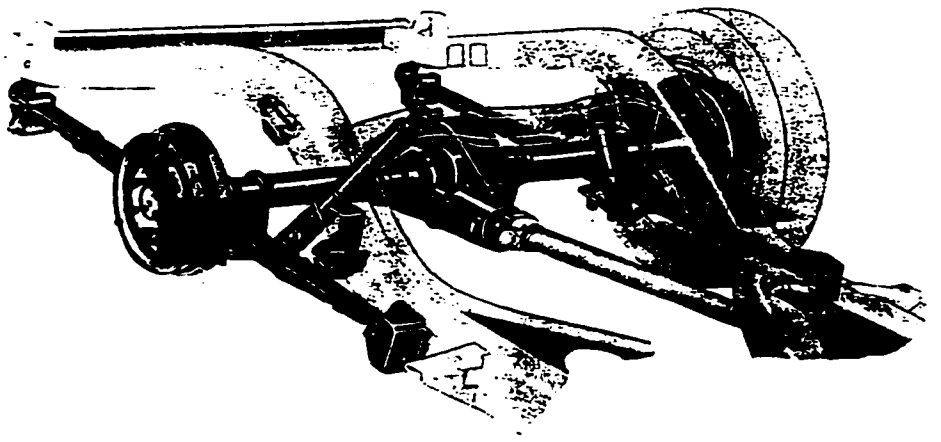

Figure 1.5 The Hotchkiss rear suspension [6]

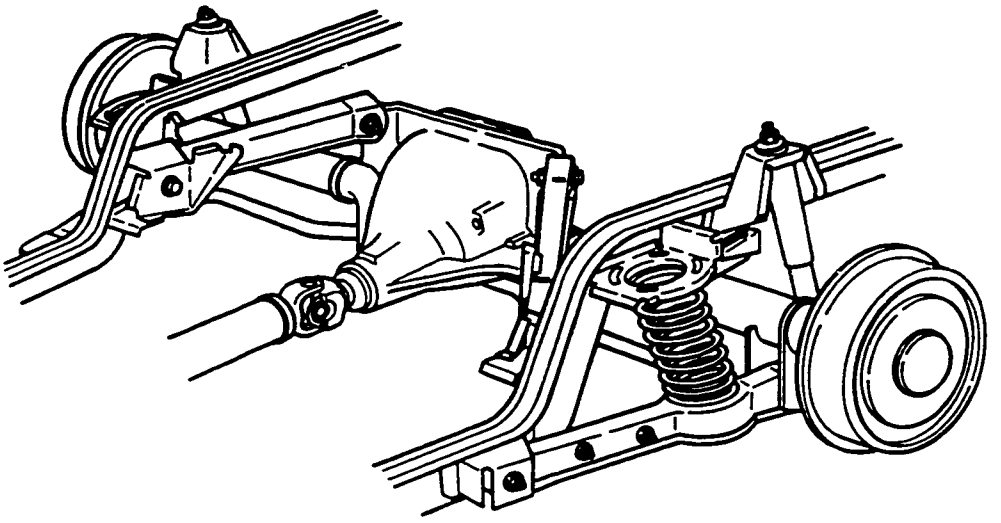

Figure 1.6 The four-link rear suspension [6]

to steering vibration (wobble and shimmy), and provide improved space for locating the engine and drive train. Such suspension is thus most frequently employed in modern automobiles and light trucks. Figures 1.7 and 1.8 illustrate the schematics of independent suspension employed in Ford Taurus and the Corvette. The control arms absorb longitudinal forces and braking moments, control squat and lift. In the Corvette design the U-jointed halfshafts serve as an upper lateral control arm with a simple strut rod serving as the lower lateral arm, in which case, both upper and lower control arms absorb the lateral forces.

### 1.2.3 Passive Suspension Analysis

Ride and handling characteristics of road vehicles with passive suspensions have been extensively investigated in numerous analytical and experimental studies [7-17]. Various linear and nonlinear vehicle models of varying complexities ranging from simple vertical dynamics of two degree-of-freedom (DOF) models to three-dimensional complex models with many DOF, have been developed. Majority of the vehicle models is developed based on the rigid body assumption [18-23], while only few models have incorporated the flexibility of vehicle components that result in considerable computational complexities due to increased dimensionality and higher frequencies of natural vibration involved [24-26]. The vehicle suspension systems are invariably modeled to include progressively hardening force-deflection characteristics of the springs, either linear or variable force-velocity properties of the damping elements. The nonlinearities arising from geometrical configuration are also included in only few studies. A number of analytical techniques have been introduced to perform design optimization of linear and nonlinear suspension under deterministic and random road excitation [27-30].

Figure 1.7 Multi-link rear suspension of Ford Taurus and Stable [6]

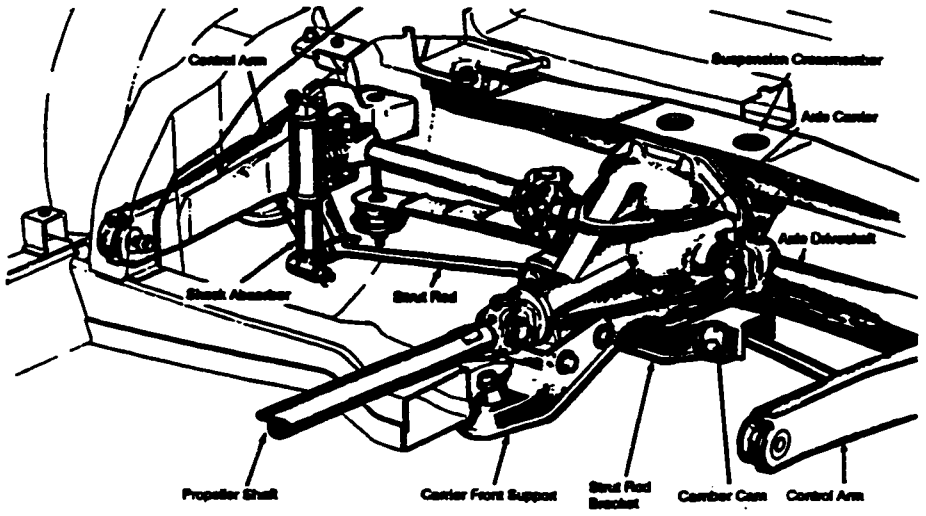


Figure 1.8 The Corvette independent rear suspension [6]

Linear analytical techniques have been extensively used in suspension design and analysis of vehicles to investigate various designs concepts and perform preliminary performance analyses. In cases where nonlinear effects have to be included in the vehicle model, and convenient linear analytical tools are desired to estimate the response characteristics, time and frequency domain equivalent linearization techniques are usually utilized to formulate an equivalent linear suspension models. Many linearization techniques, such as local equivalent and statistical linearization methods have been used to study the response behavior of nonlinear suspensions [31-35]. Majority of analytical investigations in vehicle suspension characteristics, however, is efficiently conducted in a relatively simple manner using linear analytical means for preliminary performance evaluations and parametric sensitivity studies.

Simple two DOF, quarter-vehicle models comprising sprung and unsprung masses constrained to move along the vertical direction, suspension spring and damping properties, and tire characteristics, have been extensively used to gain fundamental understanding of the suspension concepts and parameters on the vehicle ride performance under deterministic or random road disturbances [36-40]. Such models permit the analysis of different vehicle suspension concepts under in-phase vertical excitations in a highly convenient manner. Since the vibration environment of a vehicle comprises various coupled modes of vibration of the sprung and unsprung masses, such models can not be utilized to predict the complex ride and handling performance of vehicles subject to the coupled vertical excitations arising from road irregularities and the excitations due to driver's maneuvers.

A large number of in-phase and three-dimensional analytical models with varying complexities have been developed to investigate the ride and handling properties of vehicles subject to realistic road excitations involving wheel base filtering effects [41-45].

Although a comprehensive three-dimensional model may be considered desirable to study the coupled motions of the vehicles subjected to road irregularities and external forces, analytical models, which are realistic enough to predict the vehicle's behavior of interest with minimum number of DOF, are usually considered desirable. Furthermore, the complexity of the models may depend upon the objectives of the study. The transient handling and stability analyses of road vehicles, for instance, involve nonlinear three-dimension models in conjunction with nonlinear suspension and tire properties to predict the lateral, roll and longitudinally directional response of vehicle. The ride quality analysis of high speed road vehicles are often conducted in the pitch plane to estimate the levels of vertical and pitch vibrations of the vehicles subject to the longitudinally coupled vertical excitation caused by roadway irregularities. Alternatively, roll-plane models are frequently employed to study both the ride and handling properties of vehicles, where the handling assessment is limited to roll and lateral deflections. The analysis of a roll plane model can yield significant insight into the vehicle response to excitations arising from road irregularities at the left and right tire-road interface and driver's steering maneuvers, while neglecting the dynamics associated with the pitch, yaw and longitudinal modes of the vehicles. Roll-plane models are, specifically, well suited for the analysis of dependent suspensions such as beam-axle suspensions with transversal restraining linkages, for instance, the Panhard rod. The measurements on the ride quality of highway buses have revealed that the discomfort experienced by driver/passengers is primarily due to the bounce and lateral vibrations caused by road irregularities and steering maneuvers, while the contributions due to yaw, pitch and fore/aft vibrations are relatively insignificant. Furthermore, the rollover behavior, one of the major concerns for the highway bus handling design, is principally related to the roll plane dynamics. Therefore, the ride and handling qualities related to bounce, lateral and dynamic roll response characteristics of the vehicle subject to road irregularities and cornering/directional maneuvers at high speeds can be effectively investigated using a roll plane model of the vehicle [46-47].

The ride vibration characteristics are directly related to the modes of vehicular vibration and the road roughness. Roads traversed by road vehicles are usually assumed to be perfectly rigid and the profiles under no-load condition represent the vertical displacement excitation to the tire and wheel assembles. Deterministic road surface profiles, such as half round obstacles and sinusoidal course, etc. are frequently employed to assess the transient ride performance of vehicle suspensions. In-phase and out-of-phase harmonic displacement excitations are conveniently used to evaluate the bounce and roll vibration of suspension system under both bounce and roll excitations [46]. Road roughness, however, are random in nature. Various studies have established that road profile is normally distributed and can be mathematically represented by a stationary random process [48-49]. Descriptions of various road surfaces have been proposed in terms of spatial spectral density of the roughness, such as highways, secondary roads for pasture and plowed fields [50-53].

The linear and nonlinear tire models representing the tire-road interactions directly influence the ride and handling performance analysis. While few studies have proposed a fixed or adaptive contact patch tire models, vast majority of studies have been performed assuming bilinear point-contact tire model [54-55]. It has been established that tire-road interactions can be effectively characterized by a point contact, considering high inflation pressure used in modern heavy vehicle tires and non-deformable roads.

Design of a passive suspension for a road vehicle involves designing suspension configuration and selecting suspension parameters to achieve a compromise among conflicting design requirements with satisfactory balance between the ride and handling performance characteristics. The restorative and dissipative properties of suspension force elements, such as spring, damping, bushing and mounts, affect the vehicle dynamic

behavior in a significant manner [56-58]. Enhancement of handling performance, for instance, requires 'hard' suspensions, improvement of ride performance, however, necessitates 'soft' suspensions. Furthermore, a 'harder' suspension will cause higher tire loads and thus result in severer road damage, while a 'softer' suspension will result in larger suspension deflection. Chalasani performed comprehensive evaluations on the effects of suspension spring stiffness and damping coefficients on vehicle response characteristics [56]. Lu et al developed a non-linear programming formulation to achieve optimal design of a four-DOF roll plane passive suspension, where optimal values of suspension spring and damping coefficients, and tire stiffness are generated to achieve desired ride performance by minimizing the mean square value of the vertical acceleration of the sprung mass [41]. ElMadany presented an optimization method to minimize the acceleration and jerk experienced by the driver to improve the vehicle ride quality [59]. A number of other studies have been conducted to determine the fixed optimal suspension parameters through utilizing optimization techniques and various forms of optimization criteria to achieve better vehicle suspension designs [60-64].

### 1.2.4 Panhard Rod Beam-Axle Suspension

The beam-axle suspensions are frequently equipped with a constraint linkage such as Panhard rods, also referred to as the track rods. Such restraining linkages permit nearly vertical motions of the unsprung masses relative to the body, while limiting the relative roll deflections. The restraining linkages further provide enhanced roll stiffness and lateral stability. A Panhard rod provides lateral force reactions between the sprung and unsprung masses. It is desirable that the lateral forces are mostly transmitted along the lateral axis, while only a minimal component is directed along the vertical direction. Beam-axle suspensions with Panhard rods (track bars) are widely used in rear suspensions of road

vehicles, race cars, heavy trucks, and front, drive and rear suspensions of highway buses et al.

Although Panhard rods have been used with beam-axle suspensions, only a limited number of published studies have incorporated the kinematics and dynamics of the Panhard rod to the overall suspension and vehicle response characteristics. George and Sadler investigated the influence of different operating conditions on the performance characteristics of the beam-axle suspension, comprising three commonly used straight-line constraining linkages: Panhard rod, Watt linkage and Robert linkage. The study was directed towards directional control performance analysis of a front-engined high performance-racing vehicle. A kinematic analysis was performed to derive the influence of vertical and lateral loads, and wheel displacements on the linkage orientation, coordinates of the sprung mass center of gravity and roll center, sprung mass roll angle, and suspension roll stiffness [65]. Sadler et al further developed a systematic methodology to study the kinetostatic properties of a beam-axle suspension with a general form of a four-bar restraining linkage [66]. Nalecz and Kaminaga et al analyzed different linkage suspensions for lightweight road vehicles to determine the positions of the roll center and sprung mass gravity center, roll angle and roll stiffness as functions of the center of gravity height, centrifugal force, axle location, vertical loads, etc. These models, however, did not consider wheel displacement [67-68]. Nalecz compared the results of his study with those reported by Ellis. Another important study on the ride and handling performance of Panhard rod beam-axle suspension was conducted by Dulac [46]. In his study, the beam-axle suspension in the roll plane is modeled as a six degree-of-freedom system, while the Panhard rod along with its bushings was simplified and represented by a linear lateral spring.

## 1.3 Scope Of the Dissertation

The overall objective of this thesis is to investigate the ride and handling performance characteristics of road vehicles equipped with beam-axle suspensions and restraining linkages through systematic kinetostatic and dynamic analyses. A modern highway bus is considered as the candidate vehicle, where its front, drive and rear beam-axle suspensions are considered as a single composite suspension constrained by a Panhard rod. Kinetostatic and dynamic characteristics of the candidate suspension with a conventional Panhard rod restraint are analytically studied to gain an insight into the influence on the performance potentials of the candidate highway bus. The specific objectives of the dissertation research are:

1. To develop a roll-plane kinetostatic analysis model of the selected candidate highway bus to investigate the fundamental static characteristics of the suspension, in view of the coordinates of the roll center and sprung mass center of gravity under centrifugal force excitation.
2. To develop a comprehensive roll-plane dynamic analysis model of the candidate vehicle to investigate its fundamental frequency response characteristics related to ride and handling performance.
3. To further develop a simplified roll-plane dynamic analysis model that contains all the important dynamic characteristics of the comprehensive dynamic model.
4. To formulate the excitations to represent the effects of the cornering/directional maneuvers and road irregularities experienced by the right and left tracks of the vehicle.
5. To investigate the influence of kinematic and dynamic properties of Panhard rod on the ride and handling qualities of the candidate vehicle's beam-axle suspension.

6. To investigate the influence of the suspension spring and damping rates on the ride and handling qualities of the candidate vehicle's Panhard rod beam-axle suspension.
7. To investigate the influence of the vehicle speed and road roughness on the ride quality of the candidate vehicle's Panhard rod beam-axle suspension.

In Chapter 2, the widely used vehicle configuration is identified from the reported survey on road vehicles with beam-axle suspensions. A representative non-linear kinetostatic mathematical model of the selected candidate highway bus is developed in the roll plane with an objective to evaluate its lateral and roll deflection characteristics and its parametric sensitivity properties. The mathematical procedure to compute the vehicle's static equilibrium configuration under different centrifugal force and axle roll angle is described. The suspension lateral and roll characteristics are studied, which include the instantaneous location of the suspension roll center, its corresponding suspension roll stiffness, the roll center and the deflection of the sprung mass cg, and their changes relevant to the different magnitudes of centrifugal forces.

In Chapter 3, two analytical models of the composite beam-axle suspension restrained by a Panhard rod are developed for the selected candidate highway bus using Lagrange's energy method to represent the roll-plane dominant ride and handling characteristics. The comprehensive nine-DOF model is formulated to incorporate the flexibility of the Panhard rod bushings and the mass of the Panhard rod, while the simplified five DOF model is developed assuming that the Panhard rod is massless and its bushing flexibility can be ignored. The non-linearity introduced by the Panhard rod constraint is linearized about the suspension static equilibrium. The effect of cornering/directional maneuvers is represented by a harmonic centrifugal acceleration. The effect of road irregularity with roll component is described by an out-of-phase

harmonic displacement at the left- and right-tire interface. The influence of highway random roughness is characterized by a stationary zero-mean Gaussian function. The random phase between the left and right wheels is incorporated in the stochastic analytical model development. Performance criteria comprising the roll and lateral vibrations of the sprung mass are introduced to evaluate the ride and performance of the vehicle suspension subject to Panhard rod constraint. The analytical techniques are presented to solve the differential equations of motions of the candidate vehicle to predict its dynamic behavior under harmonic and random road excitations, and harmonic centrifugal acceleration excitation.

In Chapter 4, eigenvalue analyses of the two mathematical models of candidate vehicle with nine-DOF and five-DOF respectively are carried out to evaluate the resonant frequencies and the corresponding dominant modes. The results are further compared with the available measured data of the candidate vehicle to assess the validity of the analytical models. Dynamic response characteristics of these two models are analyzed and compared in the frequency domain. Simplified five-DOF analytical model is then effectively employed to perform the dynamic ride and handling analyses. The power spectral density characteristics of the candidate vehicle suspension with respect to the random road disturbances are analyzed using the simplified model. A parametric sensitivity study is performed to enhance the understanding on the effects of passive Panhard rod control on the ride and handling performance of candidate vehicle by varying suspension parameters, vehicle speed and road roughness.

The general conclusions together with the recommendations for further work are finally presented in Chapter 5.

# Chapter 2

# Kinetostatic Analysis of Panhard Rod Beam-Axle Suspension

## 2.1 Introduction

High speed road vehicles invariably employ a restraining linkage in the fore-aft plane to achieve enhance roll and lateral directional stability and control. Panhard rod linkages are often employed in conjunction with soft suspension in automobile, racing cars, service vehicles and heavy vehicles, where both good ride and handling properties are considered desirable. While adequately damped soft suspensions yield good ride quality, the handling and directional control characteristics are strongly influenced by the kinematics and dynamics of the restraining linkage and the suspension system. The handling and directional stability of road vehicles are directly influenced by the roll dynamics of the vehicle, which is characterized by the roll stiffness, the roll center coordinates and lateral load transfer properties. These suspension properties can be conveniently derived through kinematic analysis. Although numerous studies on handling and directional dynamics of light- and heavy-road vehicles have been reported in the literature, majority of these studies assume a fixed roll center, while neglecting the kinematics of the suspension linkages.

In this chapter, a roll plane kinetostatic model of a candidate highway bus with Panhard rod beam axle suspension is developed. The influence of various Panhard rod parameters and axle orientation on the suspension roll stiffness, and the variations in the coordinates of the body center of gravity and the suspension roll center is investigated under a lateral force excitation arising from a steady state cornering/directional maneuver. The results of the kinematic analysis are analyzed to enhance an understanding of the

fundamental characteristics of the Panhard rod beam-axle suspension system. Although the analytical model is developed for a modern highway bus, where both the passenger ride comfort and the directional control performance are considered as important design factors, the proposed model is generally applicable for all other road vehicles, which employ the Panhard rod restraining linkage.

## 2.2 Description of a Beam Axle Suspension with Panhard Rod

Road vehicles frequently employ beam axle suspensions with different configurations of restraining linkages. While a generally applicable roll plane model of a beam axle suspension with Panhard rod is developed in Section 2.3, the model is utilized to study the kineto-static roll properties of a modern highway bus. Modern highway buses with baggage compartment beneath the passenger compartment yield poor roll and lateral stability limits due to high location of sprung mass center of gravity (cg). Since the passenger comfort is among the primary criteria for the acceptance of the highway buses, these vehicles are equipped with suspensions that are relatively soft in the vertical mode. The low effective roll stiffness of the soft suspension further contributes to poor roll stability limits of these vehicles. Adequately designed restraining linkages are thus extremely vital to enhance the roll and the lateral stability limits of these vehicles, while maintaining good passenger ride quality. Figure 2.1 illustrates the schematic of a modern high-decker highway bus with a space frame where the engine is located near the drive-axle. The front suspension comprises a Rockwell beam-axle with two rolling sleeve air bellows and two dampers. The axle, located through four parallel trailing links and one transverse Panhard rod, is equipped with a mechanical height control valve to maintain adequate ground clearance. The drive-axle suspension, schematically shown in Figure 2.2, comprises four rolling sleeve air bellows and four dampers supported on a widely spaced H-frame. The axle is located by 3 trailing rods and a Panhard rod with a height control

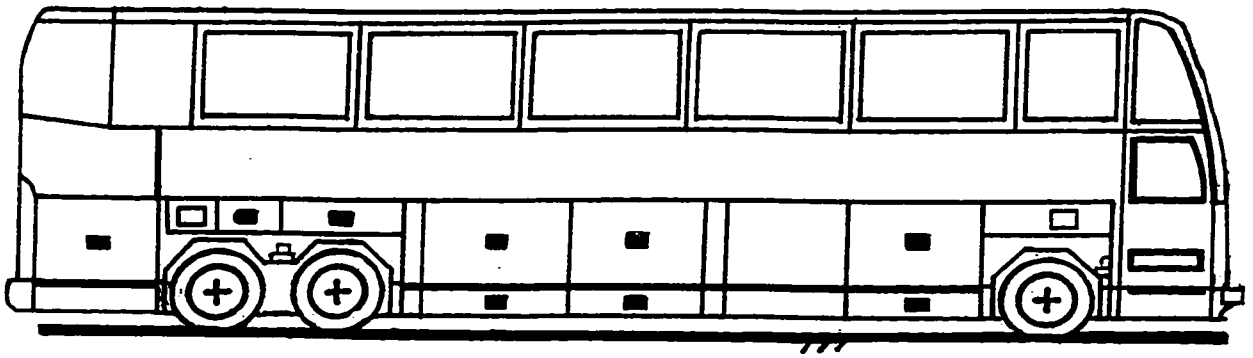

Figure 2.1 Schematic of a modern high-decker highway bus[46]

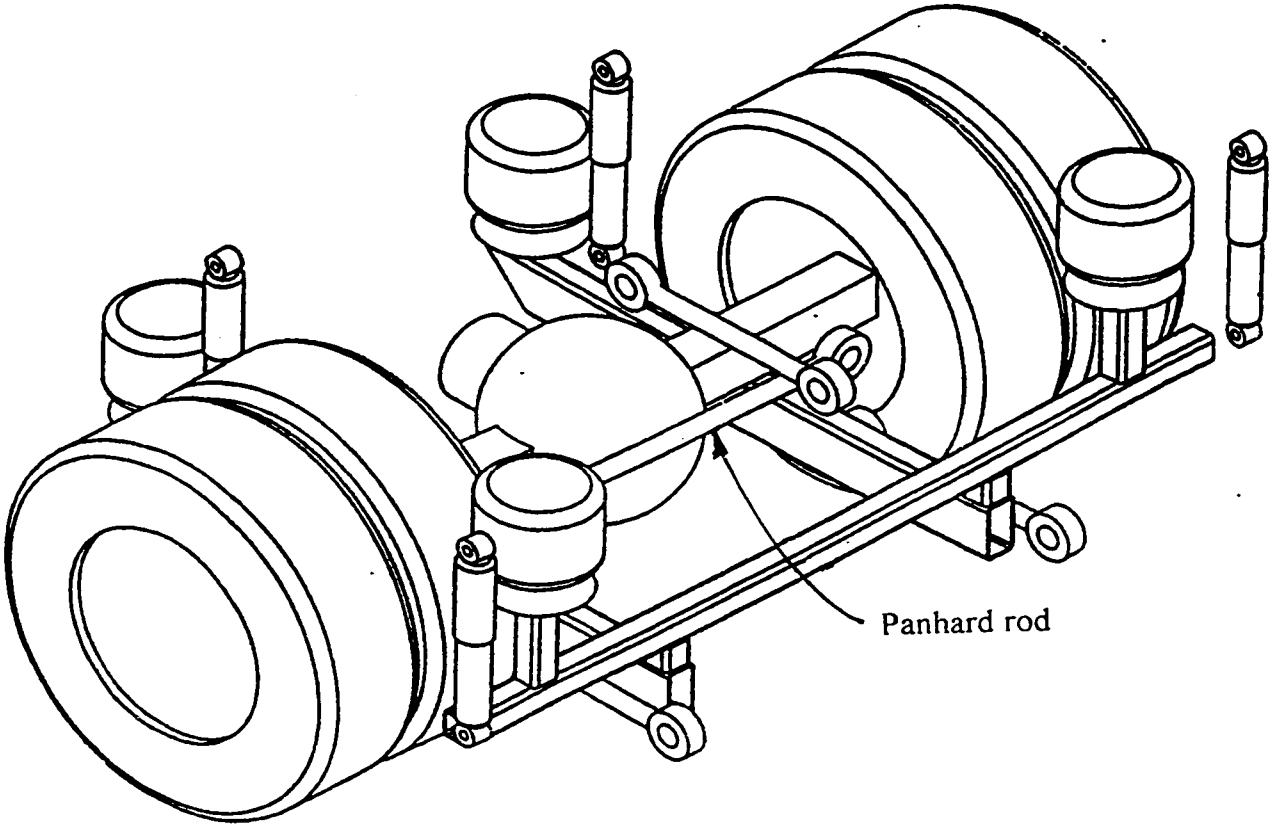


Figure 2.2 Schematic of the drive-axle suspension of the modern high-decker highway bus [46]

valve located on each side of the H-frame. The rear beam-axle suspension also consists of two rolling sleeve air bellows positioned on a relatively narrow base and two dampers installed outside of the bellows. The rear axle is located through one trailing rod, two leading rods and a Panhard rod. The geometric, inertial and suspension properties of the vehicle are summarized in Table 2.1 [46].

## 2.3 Development of a Roll Plane Kinetostatic Model of the Suspension System

The roll and ride behaviors of a vehicle are strongly related to kinematics and dynamics of the suspension and linkages. The variations in the coordinates of the roll center and the sprung mass center of gravity (cg), and the suspension roll stiffness specifically influence the roll dynamics of the vehicle. While majority of the roll plane and three-dimensional vehicle models reported in the literature assume negligible variations in the coordinates of the suspension roll center (rc) and the sprung mass cg, it has been established that various suspension linkage designs yield considerable variations in such coordinates under different directional maneuvers. The variations in the effective roll stiffness, and roll center and sprung mass cg coordinates of the vehicle subject to lateral load transfer and centrifugal forces arising from steady turning maneuvers can be evaluated from the kineto-static analysis of the roll plane vehicle model. A roll plane mathematical model is thus developed by lumping the three Panhard rod beam-axle suspensions into a single composite beam axle suspension in the roll plane. The assumptions involved in formulating the roll-plane model are discussed in the following subsection.

Table 2.1

Technical Data of a Candidate Highway Bus [46]

| Description of Parameters | Value |
|---|---|
| Total mass (fully loaded) | 17727 kg |
| Differential axle unsprung mass | 1882 kg |
| Auxiliary axle unsprung mass | 818 kg |
| Sprung mass cg height | 1.22 m |
| Average unsprung mass cg height | 0.5 m |
| Longitudinal distance between front and differential axles | 7.112 m |
| Longitudinal distance between differential and auxiliary axles | 1.206 m |
| Effective track width of the front axle | 2.175 m |
| Effective track width of the differential axle | 1.958 m |
| Effective track width of the auxiliary axle | 2.082 m |
| Vertical stiffness of the Front suspension springs (each side) | 120 kN/m |
| Vertical stiffness of the drive-axle suspension springs (each side) | 240 kN/m |
| Vertical stiffness of the auxiliary axle suspension springs (each side) | 120 kN/m |
| Roll mass moment of inertia of the sprung mass about its cg | 19300 $kg \cdot m^2$ |
| Roll mass moment of inertia of the front axle about its cg | 923 $kg \cdot m^2$ |
| Roll mass moment of inertia of the dual-tire axle about its cg | 1800 $kg \cdot m^2$ |
| Roll mass moment of inertia of the auxiliary axle about its cg | 893 $kg \cdot m^2$ |
| Damping coefficient due to each suspension damper | 8230 $N \cdot s/m$ |
| Tire diameter | 0.5 m |
| Tire vertical stiffness (Michelin 12R22.5 Radial) | 938.7 kN/m |
| Tire lateral stiffness (Michelin 12R22.5 Radial) | 875.9 kN/m |

### 2.3.1 Assumptions

Figure 2.3 illustrates the roll-plane model of the road vehicle comprising the total sprung mass supported on a composite axle suspension. The properties of the front, drive and rear axle suspensions are lumped and represented by parallel combinations of equivalent vertical spring and damper. The masses due to three axles are lumped together and characterized by a single composite unsprung mass in the roll plane. The tire properties lumped in the roll plane are characterized by vertical and lateral springs, assuming point contact with the road. The energy dissipated by the carcass of the tires is characterized by a viscous damper in parallel with the tire springs. The lumped sprung and unsprung masses are constrained by the transverse Panhard rod as shown in the figure. The sprung and unsprung masses are modeled with three-DOF: vertical, roll and lateral, respectively. The suspension and tire springs, and dampers are assumed to generate forces along their respective axes. The vehicle parameters lumped in the roll plane are summarized in Table 2.2 [46].

The roll plane model is further simplified for the kineto-static analysis, which involves determination of the sprung mass deflection relative to the unsprung mass, and the corresponding variations in the roll center coordinates and roll stiffness under steady lateral and vertical forces acting on the sprung mass. The unsprung mass is thus assumed to be fixed with certain constant roll angle to study the kineto-static behavior under no-roll and roll conditions. Furthermore, the influence of tire flexibility on the roll response of the sprung mass can be considered negligible, and the forces arising from the dissipative elements are considered to be zero. Figures 2.4(a) and 2.4(b) illustrate the kineto-static roll plane model of the vehicle corresponding to zero- and non-zero roll configurations, respectively.

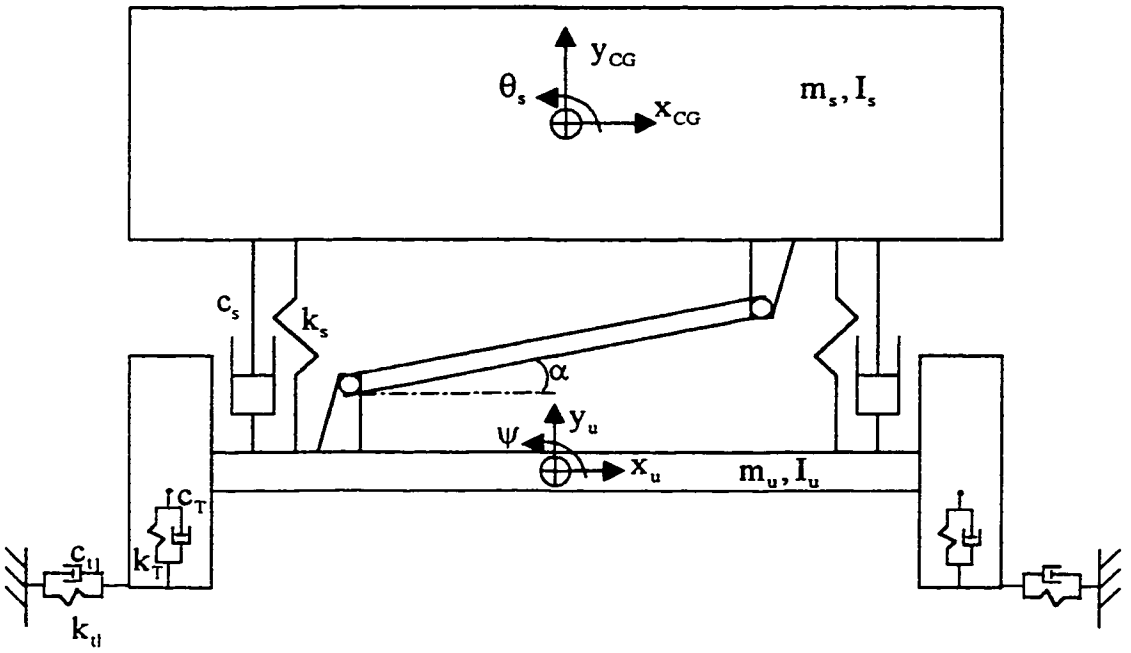


Figure 2.3 Schematic of the lumped roll plane model

Table 2.2

Simulation Parameters for the Composite Roll Plane Model [46]

| Description of Parameters | Value |
|---|---|
| Sprung mass, $m_s$ | 14111 kg |
| Unsprung mass, $m_u$ | 3616 kg |
| Roll mass moment of inertia of the sprung mass about its cg, $I_s$ | 19300 $kg \cdot m^2$ |
| Roll mass moment of inertia of the unsprung mass about its cg, $I_u$ | 3814 $kg \cdot m^2$ |
| Spring rate of the vertical suspension, $k_s$ | 480 kN/m |
| Damping coefficient of the vertical suspension, $c_s$ | 32920 $N \cdot s/m$ |
| Vertical stiffness of the tire, $k_T$ | 3755 kN/m |
| Lateral stiffness of the tire, $k_{tl}$ | 3504 kN/m |
| Vertical damping coefficient of the tire, $c_T$ | 9500 $N \cdot s/m$ |
| Lateral damping coefficient of the tire, $c_{cl}$ | 8000 $N \cdot s/m$ |
| Half suspension spring track width, $a_1$ | 0.7 m |
| Half suspension damper track width, $a_2$ | 0.73 m |
| Half tire track width, b | 1.03 m |
| Unsprung mass cg height, $h_u$ | 0.5 m |
| Vertical distance between sprung mass cg and its base, $h_b$ | 0.2 m |
| Vertical distance between the sprung mass cg and the geometric center of the Panhard rod, H | 0.62 m |
| Vertical distance between unsprung mass cg and the geometric center of the Panhard rod, h | 0.1 m |
| Half track width of the Panhard rod, e,c | 0.4 m |
| Panhard rod installation angle, $\alpha_0$ | $0^0$ |

### 2.3.2 Equations of Kinetostatic Motion

The vertical and lateral forces acting on the sprung mass, and the roll deflections encountered during a steady directional maneuver yield variations in the position and orientation of the sprung mass. The position and orientation coordinates of the sprung mass are thus analyzed in the roll plane under the action of combined vertical and lateral forces, and the roll deflection of the axle. The vehicle is initially assumed to be located on a flat surface with the origin of the fixed X-Y axes system coinciding with the cg of the unsprung mass, as illustrated in Figure 2.4. Although different kineto-static response coordinates may be used to characterize the suspension deflections, the sprung mass roll angle ($\theta_s$) and the Panhard rod orientation angle ($\alpha$) are selected as the generalized coordinates. The suspension springs assume a static equilibrium position under static vertical load ($W=m_s g$) and experience further deflections under the application of lateral force (F) and unsprung mass roll angle ($\psi$), arising from a steady directional maneuver. The vehicle body and the suspension springs then approach a new static equilibrium position under a constant lateral force and axle roll angle. The geometric configuration of the suspension corresponding to the new static equilibrium can be derived from the following nonlinear and coupled algebraic equations:

*Equilibrium of lateral forces:*

$$F + P\cos\alpha - F_{LX} - F_{RX} = 0 \tag{2.1}$$

*Equilibrium of vertical forces:*

$$F_{LY} + F_{RY} + P\sin\alpha - W = 0 \tag{2.2}$$

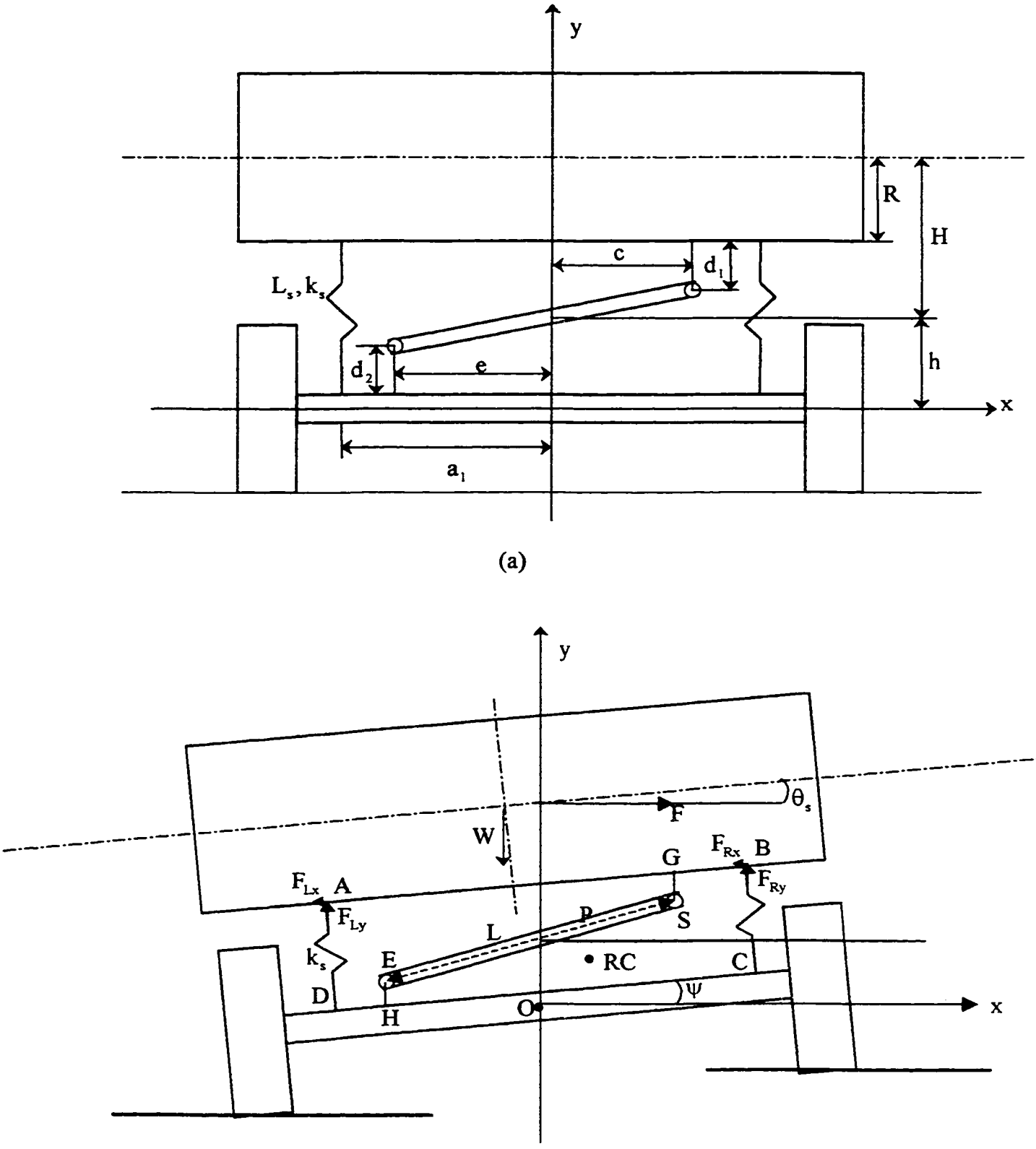


Figure 2.4 Schematic of the kinetostatic roll-plane model. (a) Zero Roll Orientation, (b) Roll angle $\theta$ under F, W, $\psi$.

*Equilibrium of roll moment about the Panhard rod joint S:*

$$F_{LX}(y_A - y_s) + F_{RX}(y_B - y_s) + F_{LY}(x_A - x_s) + F_{RY}(x_B - x_s) - F(y_{CG} - y_s) + W(x_s - x_{CG}) = 0 \quad (2.3)$$

Where P is the constraint force due to the restraining Panhard rod link. $F_{LX}$ and $F_{LY}$ are the components of the left suspension spring force along the X- and Y- coordinates. $F_{RX}$ and $F_{RY}$ are the corresponding force components due to the right suspension spring. $(x_s, y_s)$, $(x_A, y_A)$, $(x_B, y_B)$ and $(x_{CG}, y_{CG})$ are the coordinates of the Panhard rod joint, the left and right suspension spring attachment points and the sprung mass cg, respectively. $m_s$ is the sprung mass and g is the acceleration due to gravity.

Assuming linear properties of the suspension springs, the left and right suspension forces, $F_L$ and $F_R$, can be expressed as:

$$F_L = K_S(L_S - L_L); \text{ and } \quad F_R = K_S(L_S - L_R) \quad (2.4)$$

Where $K_s$ is the linear suspension spring rate, $L_S$ is the free length of the suspension spring, and $L_L$ and $L_R$ are the instantaneous lengths of left and right suspension springs, respectively. The instantaneous length of suspension spring and thus the spring deflections are related to the suspension geometry, and the roll angles of the sprung and unsprung masses in the following manner:

$$L_L = \{[(a-e)\sin\psi + d_2\cos\psi + L\sin\alpha + d_1\cos\theta_s - (a+c)\sin\theta_s]^2 + [(a-e)\cos\psi - d_2\sin\psi + L\cos\alpha - d_1\sin\theta_s - (a+c)\cos\theta_s]^2\}^{1/2}$$

$$L_R = \{[-(a+e)\sin\psi + d_2\cos\psi + L\sin\alpha + d_1\cos\theta_s + (a-c)\sin\theta_s]^2$$

$$+[-(a+e)\cos\psi - d_2\sin\psi + L\cos\alpha - d_1\sin\theta_s + (a-c)\cos\theta_s]^2\}^{1/2} \qquad (2.5)$$

Where a, c, e, $d_1$ and $d_2$ are half suspension track width, half Panhard rod track, and the initial vertical heights of the Panhard rod bushings with respect to the sprung and unsprung masses, as shown in Figure 2.4(a). L is the Panhard rod length, and $\alpha$ is its orientation with respect to the fixed axis system. The components of the suspension forces along the fixed X-Y axis system are derived from the suspension geometry, and equations (2.4) and (2.5):

$$F_{LX} = F_L[-(a-e)\cos\psi + d_2\sin\psi - L\cos\alpha + d_1\sin\theta_s + (a+c)\cos\theta_s]/L_L$$
$$F_{LY} = F_L[(a-e)\sin\psi + d_2\cos\psi + L\sin\alpha + d_1\cos\theta_s - (a+c)\sin\theta_s]/L_L$$

$$F_{RX} = F_R[(a+e)\cos\psi + d_2\sin\psi - L\cos\alpha + d_1\sin\theta_s - (a-c)\cos\theta_s]/L_R$$
$$F_{RY} = F_R[-(a+e)\sin\psi + d_2\cos\psi + L\sin\alpha + d_1\cos\theta_s + (a-c)\sin\theta_s]/L_R \qquad (2.6)$$

From equations (2.5) and (2.6), it is apparent that the suspension forces are related to the roll deflections of the sprung and unsprung masses, Panhard rod orientation, and the spring deflections. The geometric coordinates used in above equations are further related to the suspension geometry and the roll response of the vehicle in the following manner:

$$x_{CG} = -e\cos\psi - d_2\sin\psi + L\cos\alpha - d_1\sin\theta_s - c\cos\theta_s - R\sin\theta_s$$
$$y_{CG} = -e\sin\psi + d_2\cos\psi + L\sin\alpha + d_1\cos\theta_s - c\sin\theta_s + R\cos\theta_s$$
$$x_A = -e\cos\psi - d_2\sin\psi + L\cos\alpha - d_1\sin\theta_s - (a+c)\cos\theta_s$$
$$y_A = -e\sin\psi + d_2\cos\psi + L\sin\alpha + d_1\cos\theta_s - (a+c)\sin\theta_s$$
$$x_B = -e\cos\psi - d_2\sin\psi + L\cos\alpha - d_1\sin\theta_s + (a-c)\cos\theta_s$$
$$y_B = -e\sin\psi + d_2\cos\psi + L\sin\alpha + d_1\cos\theta_s + (a-c)\sin\theta_s$$
$$x_S = -e\cos\psi - d_2\sin\psi + L\cos\alpha$$

$$y_S = -e\sin\psi + d_2\cos\psi + L\sin\alpha \tag{2.7}$$

The above equations are solved to determine the coordinates of the cg, as a function of the roll response of the vehicle. The constraint force P due to the Panhard rod, appearing in equations (2.1) and (2.2), can be eliminated to yield:

$$F_{LY} + F_{RY} + (F_{LX} + F_{RX} - F)\tan\alpha - W = 0 \tag{2.8}$$

Equations (2.3) to (2.8) describe the kinetostatic relationship for the Panhard rod beam-axle suspension under specified vertical load (W), lateral force (F) and unsprung mass roll angle ($\psi$), The solution of equations yields the suspension forces and coordinates of the static equilibrium position, in terms of roll angles of the sprung mass and the Panhard rod, the sprung mass cg, and the suspension roll center (rc) and respective suspension roll stiffness.

### 2.3.3 Numerical Solution of Non-Linear Algebraic Equations

The kinetostatic equations, (2.3) and (2.8), for the roll plane model can in-general be expressed by the following functions of the sprung mass roll angle ($\theta_s$), Panhard rod angle ($\alpha$) and the lateral force (F), for the specified sprung mass vertical load (W) and the unsprung mass roll angle ($\psi$):

$$\begin{aligned} U(\theta_s, \alpha, F) &= 0 \\ V(\theta_s, \alpha, F) &= 0 \end{aligned} \tag{2.9}$$

For a given lateral force F, the non-linear algebraic equations can be solved to yield the sprung mass roll and the Panhard rod orientation angles, corresponding to a new static

equilibrium position. Various numerical techniques can be employed to solve the non-linear algebraic equations. In this study, the sprung mass roll and the Panhard rod orientation angles, corresponding to an equilibrium position, are computed utilizing Newton iteration scheme as follows:

$$\theta_{s_{n+1}} = \theta_{sn} + \frac{1}{J_n}\begin{vmatrix} \frac{\partial U}{\partial \alpha} & U \\ \frac{\partial V}{\partial \alpha} & V \end{vmatrix}_n$$

$$\alpha_{n+1} = \alpha_n + \frac{1}{J_n}\begin{vmatrix} U & \frac{\partial U}{\partial \theta_s} \\ V & \frac{\partial V}{\partial \theta_s} \end{vmatrix}_n \qquad (2.10)$$

Where n and n+1 refer to the iteration number, and $J_n$ is the Jacobian matrix corresponding to iteration $n(\theta_{sn}, \alpha_n)$, given by:

$$J_n = \begin{vmatrix} \frac{\partial U}{\partial \theta_s} & \frac{\partial U}{\partial \alpha} \\ \frac{\partial V}{\partial \theta_s} & \frac{\partial V}{\partial \alpha} \end{vmatrix}_n$$

The iterative algorithm is initiated with the initial static equilibrium position of the suspension with zero sprung mass roll angle ($\theta_{s_0} = 0^0$) and a specified Panhard rod orientation angle ($\alpha_0$). Equations (2.10) are solved to determine the sprung mass roll angle ($\theta_{s_1}$) and the Panhard rod orientation ($\alpha_1$) under the application of a lateral force F. The errors between the computed and previous values are computed, and the iterative procedure is repeated until convergence is attained, such that:

$$|\alpha_{n+1} - \alpha_n| \leq \varepsilon_\alpha \tag{2.11}$$

Where $\varepsilon_\theta$ and $\varepsilon_\alpha$ are the permissible errors in the response variables. The coordinates of the sprung mass cg, suspension attachment points and Panhard rod joint, corresponding to the kinetostatic equilibrium are then derived from equations (2.7). The variations in the coordinates of the sprung mass cg, as influenced by the vehicle roll, lateral force and suspension kinematics, can be determined from:

$$\begin{aligned} x_{CG} &= -e\cos\theta_s - d_2\sin\psi + L\cos\alpha - d_1\sin\theta_s - c\cos\theta_s - R\sin\theta_s \\ y_{CG} &= -e\sin\psi + d_2\cos\psi + L\sin\alpha + d_1\cos\theta_s - c\sin\theta_s + R\cos\theta_s \end{aligned} \tag{2.12}$$

### 2.3.4 Determination of Suspension Roll Center

The suspension roll center is kinematically defined as the instantaneous roll center of the sprung mass with respect to the ground when it experiences a lateral force arising from a directional maneuver. For the kinetostatic analysis, the suspension roll center is defined as a point in the roll plane, where the roll velocity relative to the ground is zero under the application of a steady lateral force and unsprung mass roll deflection. The variations in coordinates of the suspension roll center can be derived from the roll plane analysis and the suspension geometry. Figure 2.5 illustrates the suspension geometry and the dimensional vectors relating the roll center location, indicated by 'rc'. The fixed X-Y coordinate system is attached to the unsprung mass with the origin at its cg. The loop vectors are defined to represent the magnitudes and orientations of the selected geometric vectors with respect to the fixed coordinate system. The vector equation derived from the loop $OESO_1O$ are written as follows:

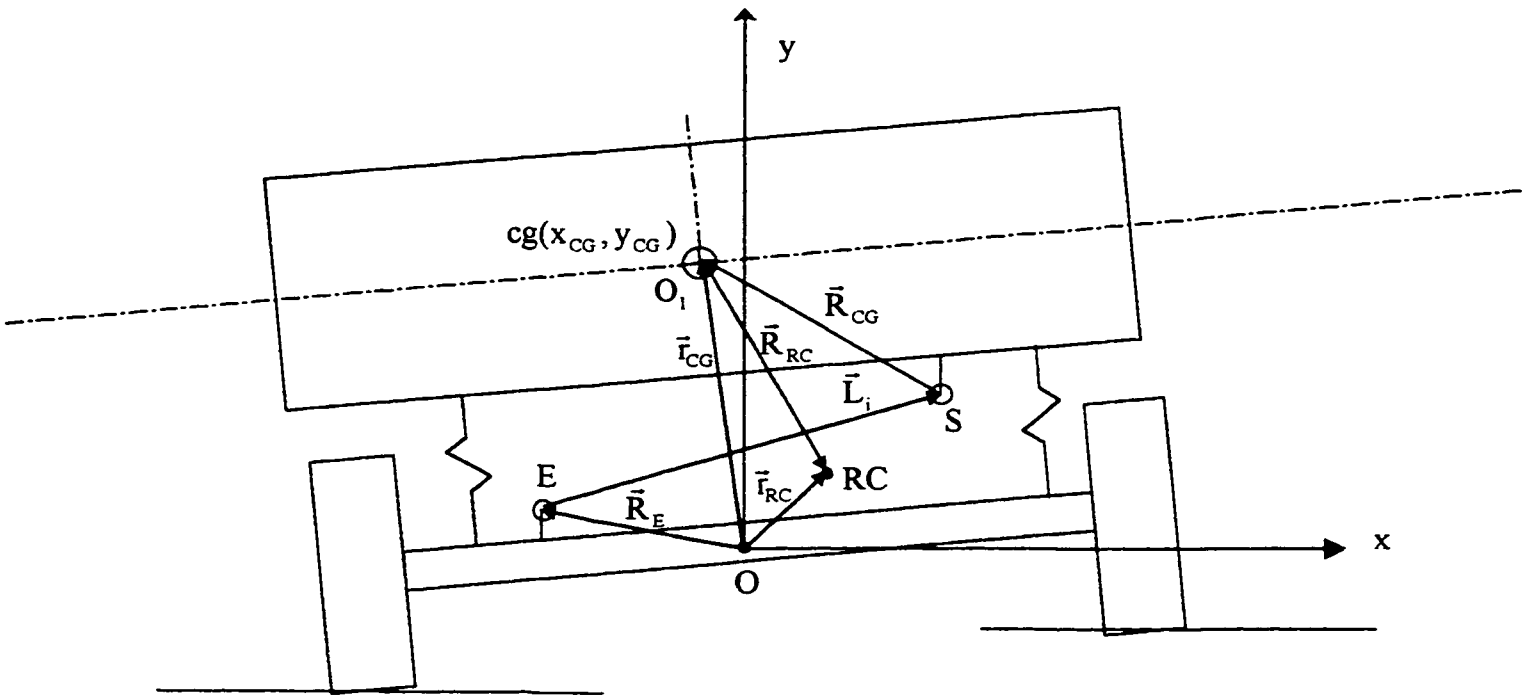


Figure 2.5 Schematic of suspension geometry and dimensional vectors.

$$\vec{r}_{RC} = \vec{r}_{CG} + \vec{R}_{RC}$$
$$\vec{r}_{CG} = \vec{R}_E + \vec{L} + \vec{R}_{CG} \qquad (2.13)$$

Where the vectors $\vec{R}_E$, $\vec{L}$, $\vec{R}_{CG}$, $\vec{R}_{RC}$, $\vec{r}_{RC}$, $\vec{r}_{CG}$ are expressed in the complex algebra form representing the vectors $\overrightarrow{OE}$, $\overrightarrow{ES}$, $\overrightarrow{SO_1}$, $\overrightarrow{O_1RC}$, $\overrightarrow{ORC}$ and $\overrightarrow{OO_1}$, respectively. By definition, the vector $\vec{r}_{RC}$ representing the location of the suspension roll center must satisfy the zero velocity requirement, such that:

$$\dot{\vec{r}}_{RC} = 0 \qquad (2.14)$$

The vectors $\vec{r}_{RC}$ and $\vec{r}_{CG}$ define the locations of the suspension roll center and the sprung mass cg corresponding to the static equilibrium position for given vertical load, lateral force and the unsprung mass roll orientation. These vectors can be derived from the sprung mass roll angle ($\theta_s$) and the Panhard rod orientation angle ($\alpha$) computed in the previous section. The two vectors can be expressed in the following manner:

$$\vec{r}_{RC} = x_{RC} + iy_{RC}$$
$$\vec{r}_{CG} = \vec{R}_E + \vec{L} + \vec{R}_{CG} = x_{CG} + iy_{CG} \qquad (2.15)$$

Where ($x_{RC}$, $y_{RC}$) and ($x_{CG}$, $y_{CG}$) are the components of vectors $\vec{r}_{RC}$ and $\vec{r}_{CG}$ along X and Y, respectively. Similarly, the other geometric vectors corresponding to a static equilibrium position can be expressed in the following form:

$$\vec{R}_E = \vec{R}_{E0} e^{i\psi}$$
$$\vec{L} = L e^{i\alpha}$$
$$\vec{R}_{CG} = \vec{R}_{CG0} e^{i\theta_s}$$
$$\vec{R}_{RC} = \vec{R}_{RC0}(\alpha) e^{i\theta_s} \qquad (2.16)$$

Where $\vec{R}_{E0}$ and $\vec{R}_{CG0}$ describe the position coordinates corresponding to the suspension initial static equilibrium position, which can be derived from the static equilibrium position, as illustrated in Figure 2.4(a):

$$\vec{R}_{E0} = -e + id_2$$
$$\vec{R}_{CG0} = -c + i(d_1 + R) \tag{2.17}$$

$\vec{R}_{RC0}(\alpha)$ describes the position of the rc corresponding to the suspension initial static equilibrium position and the Panhard rod orientation angle. Assuming small variations in the suspension roll center with respect to the changes in Panhard rod orientation:

$$\dot{\vec{R}}_{RC0} = 0 \tag{2.18}$$

Equations (2.3) and (2.15) to (2.17) define the kinetostatic roll motion characteristics of the suspension system under the application of a specified lateral force. The following relation is obtained by differentiating equation (2.13) together with equations (2.14) to (2.18):

$$\vec{R}_{RC} = -\vec{R}_{CG} - \vec{L}\frac{d\alpha}{d\theta_s} \tag{2.19}$$

Substituting equation (2.19) in equation (2.13) yields the instantaneous coordinates of the suspension roll center:

$$\vec{r}_{RC} = \vec{r}_{CG} - \vec{R}_{CG} - \vec{L}\frac{d\alpha}{d\theta_s} \tag{2.20}$$

The coordinates of the rc can also be expressed in the X-Y coordinates in the following manner:

$$x_{RC} = x_{CG} + [c \cdot \cos\theta_s + (d_1 + R)\sin\theta_s - L\cos\alpha \frac{d\alpha}{d\theta_s}]$$
$$y_{RC} = y_{CG} + [c \cdot \sin\theta_s - (d_1 + R)\cos\theta_s - L\sin\alpha \frac{d\alpha}{d\theta_s}] \quad (2.21)$$

Where the differential term $\frac{d\alpha}{d\theta_s}$ represents the change in the Panhard rod orientation angle with respect to variation in the sprung mass roll angle, which may be derived from equation (2.9). The differentials of function U and V yield the following:

$$dU = \frac{\partial U}{\partial \alpha} d\alpha + \frac{\partial U}{\partial \theta_s} d\theta_s + \frac{\partial U}{\partial F} dF = 0$$

$$dV = \frac{\partial V}{\partial \alpha} d\alpha + \frac{\partial V}{\partial \theta_s} d\theta_s + \frac{\partial V}{\partial F} dF = 0 \quad (2.22)$$

Equations (2.22) are solved to yield $\frac{d\alpha}{d\theta_s}$ corresponding to a specified lateral force, given as:

$$\frac{d\alpha}{d\theta_s} = \frac{\frac{\partial U}{\partial F} \cdot \frac{\partial V}{\partial \theta_s} - \frac{\partial V}{\partial F} \cdot \frac{\partial U}{\partial \theta_s}}{\frac{\partial V}{\partial F} \cdot \frac{\partial U}{\partial \alpha} - \frac{\partial U}{\partial F} \cdot \frac{\partial V}{\partial \alpha}} \quad (2.23)$$

Equation (2.21) is solved in conjunction with (2.23) to derive the coordinates of the suspension roll center corresponding to the static equilibrium position under given external input. The corresponding Panhard rod and sprung mass orientation angles, can then be derived using the iterative technique discussed in Section 2.3.3

### 2.3.5 Determination of Suspension Roll Stiffness

The suspension roll stiffness is related to the suspension roll moment M and the applied lateral force F. The suspension roll moment M can be expressed as the function of the roll moments arising from externally applied lateral or centrifugal force and the lateral displacement of the sprung mass:

$$M = F \cdot (y_{RC} - y_{CG}) + W \cdot (x_{RC} - x_{CG}) \tag{2.24}$$

The suspension roll stiffness $K_\theta$ is defined as the change in the suspension roll moment with respect to the change in the sprung mass roll angle, and given by:

$$K_\theta = \frac{dM}{d\theta_s} \tag{2.25}$$

Equations (2.24) and (2.25) yield the following expression for the roll stiffness under varying lateral force acting on the sprung mass:

$$K_\theta = (y_{RC} - y_{CG})\frac{dF}{d\theta_s} - F\left(\frac{\partial y_{CG}}{\partial \theta_s} + \frac{\partial y_{CG}}{\partial \alpha} \cdot \frac{\partial \alpha}{\partial \theta_s}\right) - W \cdot \left(\frac{\partial x_{CG}}{\partial \theta_s} + \frac{\partial x_{CG}}{\partial \alpha} \cdot \frac{\partial \alpha}{\partial \theta_s}\right) \tag{2.26}$$

Where the rate of change in the lateral force with respect to variation in the sprung mass roll angle $\left(\frac{dF}{d\theta_s}\right)$ can be obtained from equation (2.22), which is:

$$\frac{dF}{d\theta_s} = \frac{\frac{\partial U}{\partial \alpha}\cdot\frac{\partial V}{\partial \theta_s} - \frac{\partial V}{\partial \alpha}\cdot\frac{\partial U}{\partial \theta_s}}{\frac{\partial V}{\partial \alpha}\cdot\frac{\partial U}{\partial F} - \frac{\partial U}{\partial \alpha}\cdot\frac{\partial V}{\partial F}} \tag{2.27}$$

Equation (2.26) and (2.27) are solved to determine the variation in effective roll stiffness of the Panhard rod beam-axle suspension with variations in the vertical load, sprung mass roll angle and lateral force.

## 2.4 Kinetostatic Properties of a Panhard Rod Beam-Axle Suspension

The kinematic analysis of the beam-axle suspension with Panhard rod is performed to study the influence of vertical load, lateral forces and unsprung mass roll angle on the variations in suspension roll stiffness and roll center coordinates. The roll plane analytical model, described in Section 2.3, is solved using the parameters of a candidate highway bus described in Tables 2.1 and 2.2. Equation (2.9) is solved to determine the kinetostatic response characteristics of the sprung mass roll angle ($\theta_s$) and the Panhard rod orientation angle ($\alpha$). The coordinates of the suspension roll center ($x_{RC}$, $y_{RC}$) and the suspension roll stiffness ($K_\theta$) corresponding to a static equilibrium position are computed from equations (2.21) and (2.25), respectively. The coordinates of the sprung mass cg ($x_{CG}$, $y_{CG}$) are also computed from equation (2.12). In this study, the kinetostatic response characteristics are evaluated for variations in the lateral force ranging from -44.5 kN to 44.5 kN. The limiting value of the lateral force is based upon the rollover threshold acceleration of the vehicle, which is approximately 0.3g [46]. The kinetostatic analysis is performed for $\alpha$=0 and $\psi$=0, and the results are presented in Figures 2.6 to 2.9.

Figure 2.6 illustrates the variations in the sprung mass roll angle, the Panhard rod orientation angle and the suspension roll stiffness as a function of the lateral force. The

results show that the magnitudes of the sprung mass and Panhard rod angles increase almost linearly with the magnitude of applied lateral force, as illustrated in Figure 2.6(a). The magnitude of roll angle, however, is considerably larger than that of the Panhard rod, irrespective of the magnitude of the lateral force. The magnitudes of the roll angles of the sprung mass and the Panhard rod, when subject to a negative lateral force, are observed to be slightly lower than those encountered under a positive lateral force. The sprung mass roll angles are 3.893 and -4.122 degrees, respectively under -44.5 and 44.5 kN lateral force. The corresponding inclination angles of the Panhard rod are observed to be 2.087 and -1.932 degrees. This behavior can be attributed to the asymmetric motion of the Panhard rod. Figures 2.6(b) and 2.6(c) illustrate the suspension roll stiffness as a function of the applied lateral force and sprung mass roll angle. The beam-axle suspension exhibits larger roll stiffness under application of a negative lateral force when compared to that obtained under the action of a positive lateral force of identical magnitude. The roll stiffness, however, varies nearly linearly with the lateral force and the sprung mass roll angle. The suspension roll stiffness also tends to be larger with positive body roll when compared to that with the negative body roll. When the static lateral force is varied from -44.5 kN to 44.5 kN, the resulting suspension roll stiffness reduces from 493 to 468 kN.m/rad. The variation in the suspension roll stiffness, however, is less than 3%, when compared to the suspension roll stiffness corresponding to the initial static equilibrium position. The similar asymmetric response is also observed with the sprung mass roll angle, as shown in Figure 2.6(c). The asymmetric roll motion of the vehicle is attributed to the asymmetric geometric configuration of the Panhard rod beam-axle suspension. From the results of kinetostatic analysis, it is apparent that the effective roll stiffness of the beam axle suspension and the body roll is dependent upon the direction of the steering maneuver.

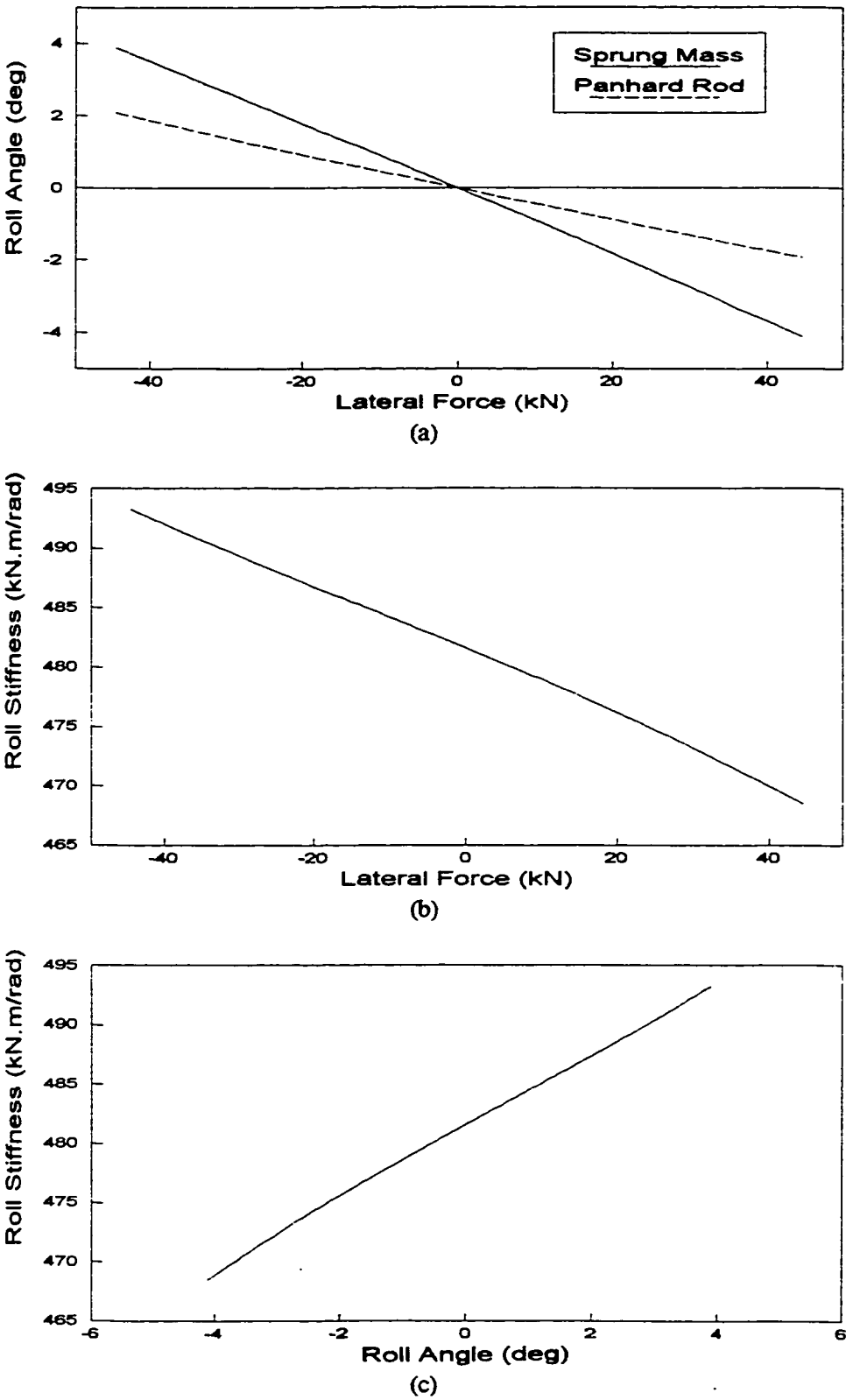


Figure 2.6 Influence of lateral force on sprung mass roll, Panhard Rod roll and suspension roll stiffness

The lateral force encountered during a steady turning maneuver yields displacement of the sprung mass cg as a function of the magnitude of lateral force developed. Equation (2.12) is solved to determine the variations in the cg coordinates as a function of the lateral force. Figures 2.7(a) and 2.7(b) illustrate the variations in the sprung mass cg coordinates, and Figure 2.7(c) illustrates the trajectory of the sprung mass cg when lateral force is varied from -44.5 to 44.5 kN. The results show that the cg coordinates are displaced in an asymmetric manner with variations in the lateral force. While the lateral displacement of the sprung mass cg is more or less linear with variation in the lateral force, the vertical motion of the cg is observed to be highly non-linear function of the lateral force. The magnitude of variations in the lateral coordinates of the cg, however, is observed to be considerably larger than that of in the vertical coordinates. Under the application of lateral force ranging from -44.5 to 44.5 kN, the lateral coordinate of the sprung mass cg varies from -0.042 to 0.045 m, while the vertical position of the sprung mass cg changes from 0.721 to 0.720. The sprung mass cg exhibits vertical motion in the positive direction, irrespective of the direction of centrifugal force acting on the sprung mass cg. The magnitude of the vertical motion under a positive lateral force, however, is slightly lower than that encountered under a negative lateral force

The variations in the lateral and vertical coordinates of the suspension roll center are evaluated for $0^0$ Panhard rod orientation and axle roll angle ($\alpha = \psi = 0^0$). Figures 2.8(a) and 2.8(b) illustrate the roll center coordinates as a function of the lateral force, and Figure 2.8(c) illustrates the trajectory of the suspension roll center. The results show that the application of a negative lateral force yields slightly larger variations in the lateral and vertical coordinates of the suspension roll center when compared to those derived under positive lateral force of identical magnitude. The suspension roll center is displaced vertically by nearly 15% under the application of lateral force ranging from -44.5 to 44.5

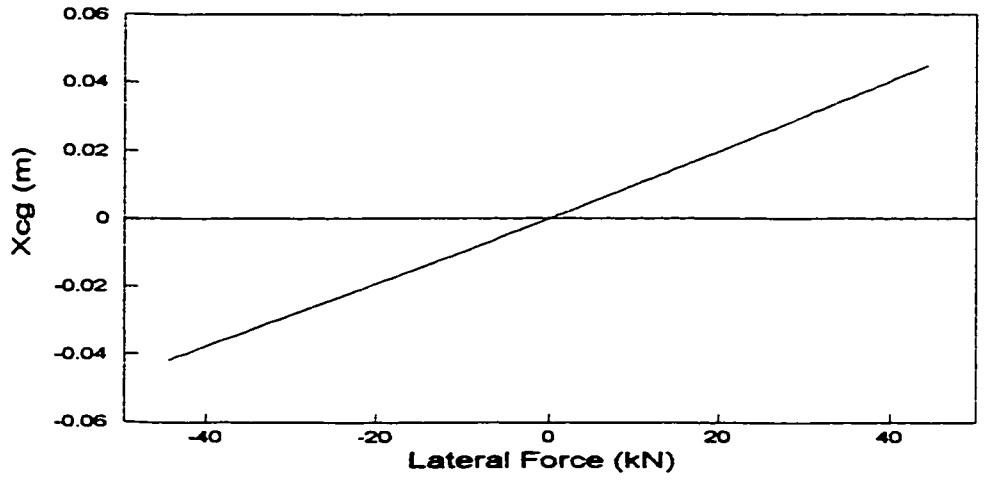


(a)

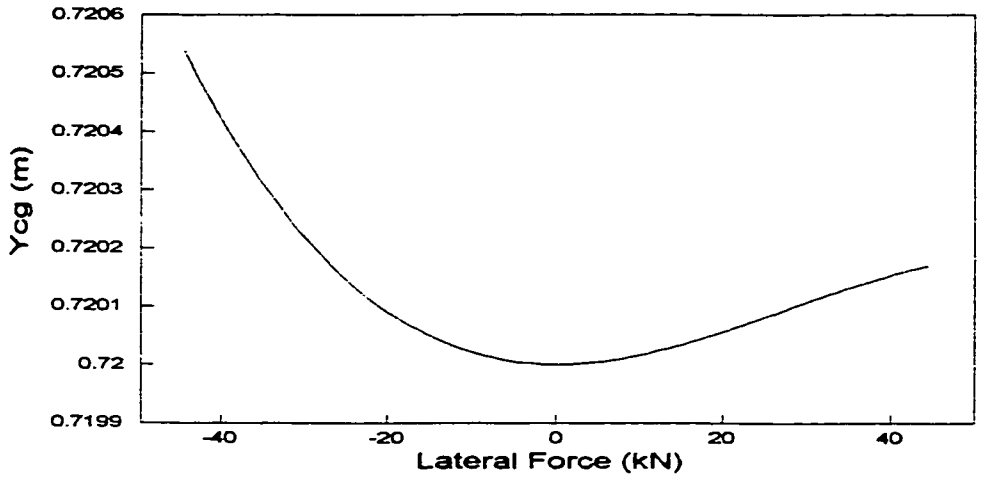


(b)

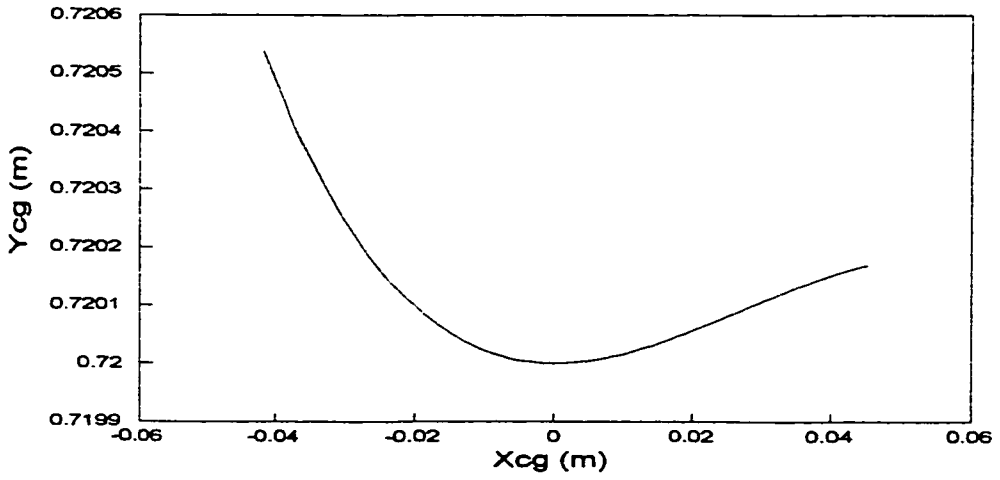


(c)

Figure 2.7 Influence of lateral force on sprung mass cg coordinates

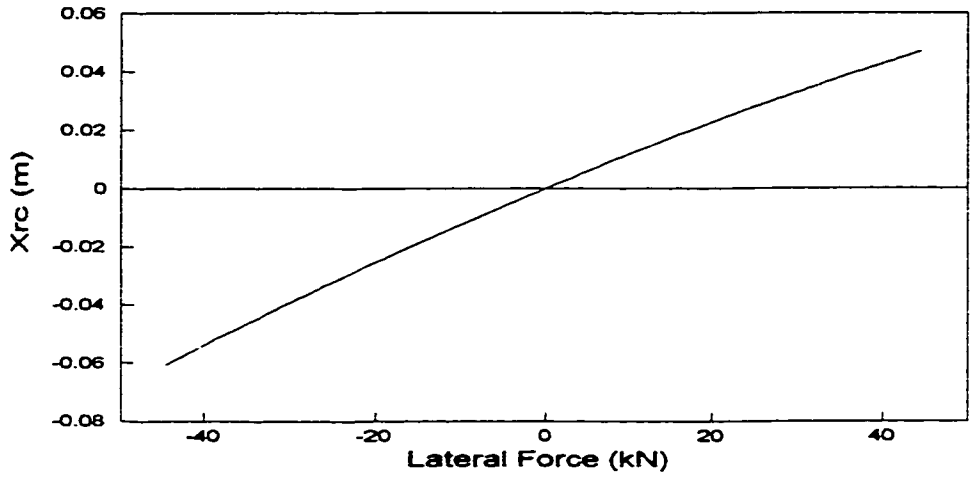


(a)

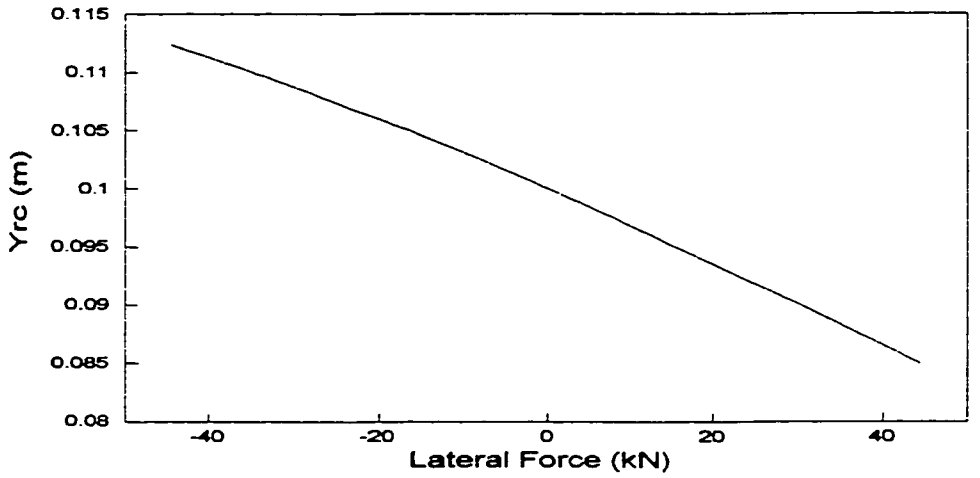


(b)

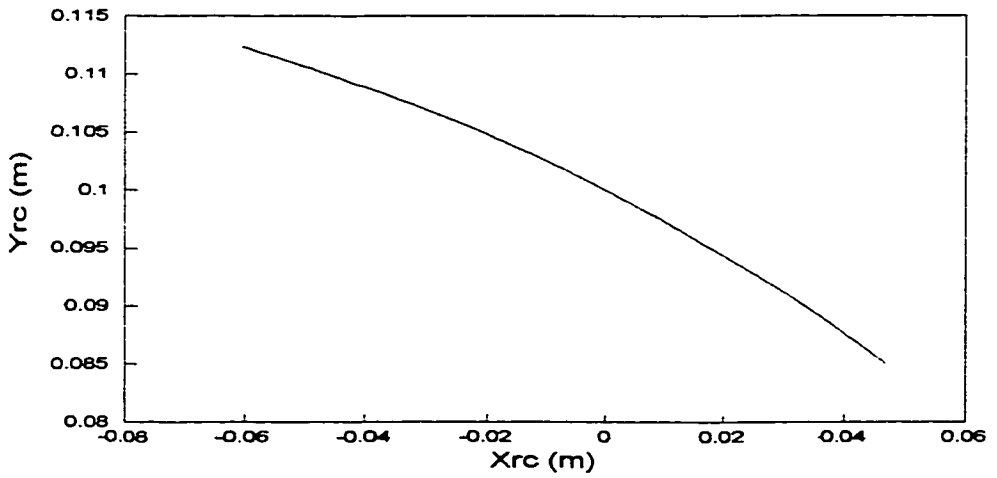


(c)

Figure 2.8 Influence of lateral force on suspension roll center coordinates

kN. The corresponding displacement along the lateral coordinate ranges from -0.061 to 0.047 m.

The variations in the roll center coordinates relative to the sprung mass cg are further evaluated for the range of lateral force, and presented in Figure 2.9. While the variations in the relative lateral displacement of the suspension roll center under application of a positive lateral force are insignificant, a negative lateral force yields considerable deviation in the lateral coordinate. The vertical coordinate of the suspension roll center relative to the sprung mass cg varies in a nearly linear manner with the lateral force, as shown in Figure 2.9(b). The suspension roll center, corresponding to the initial static equilibrium position, lies on the intersection of the vertical axis passing the sprung mass cg and the Panhard rod axis. With application of lateral force, the suspension roll center is observed to move slightly on the left side of the fixed axis system. The variations in the relative coordinates of the suspension roll center with respect to the sprung mass cg are observed to be in the range of -0.019 to 0.002 m for the lateral direction and in the range of -0.608 to -0.635 m for the vertical direction. From the trajectory shown in Figure 2.9(c), it is apparent that the variation in the relative lateral and vertical coordinates are nearly ±1.05% and ±1.9%, respectively.

## 2.5 Influence of Suspension and Vehicle Parameters on the Kinetostatic Response Characteristics

The kinetostatic properties of the beam axle suspension with a transverse Panhard rod, such as effective suspension roll stiffness, suspension roll center coordinates, sprung mass roll angle and sprung mass cg coordinates, are related to various vehicle and suspension parameters. A parametric study is undertaken to establish the influence of selected suspension parameters on the kinetostatic behaviour. The influence of variations

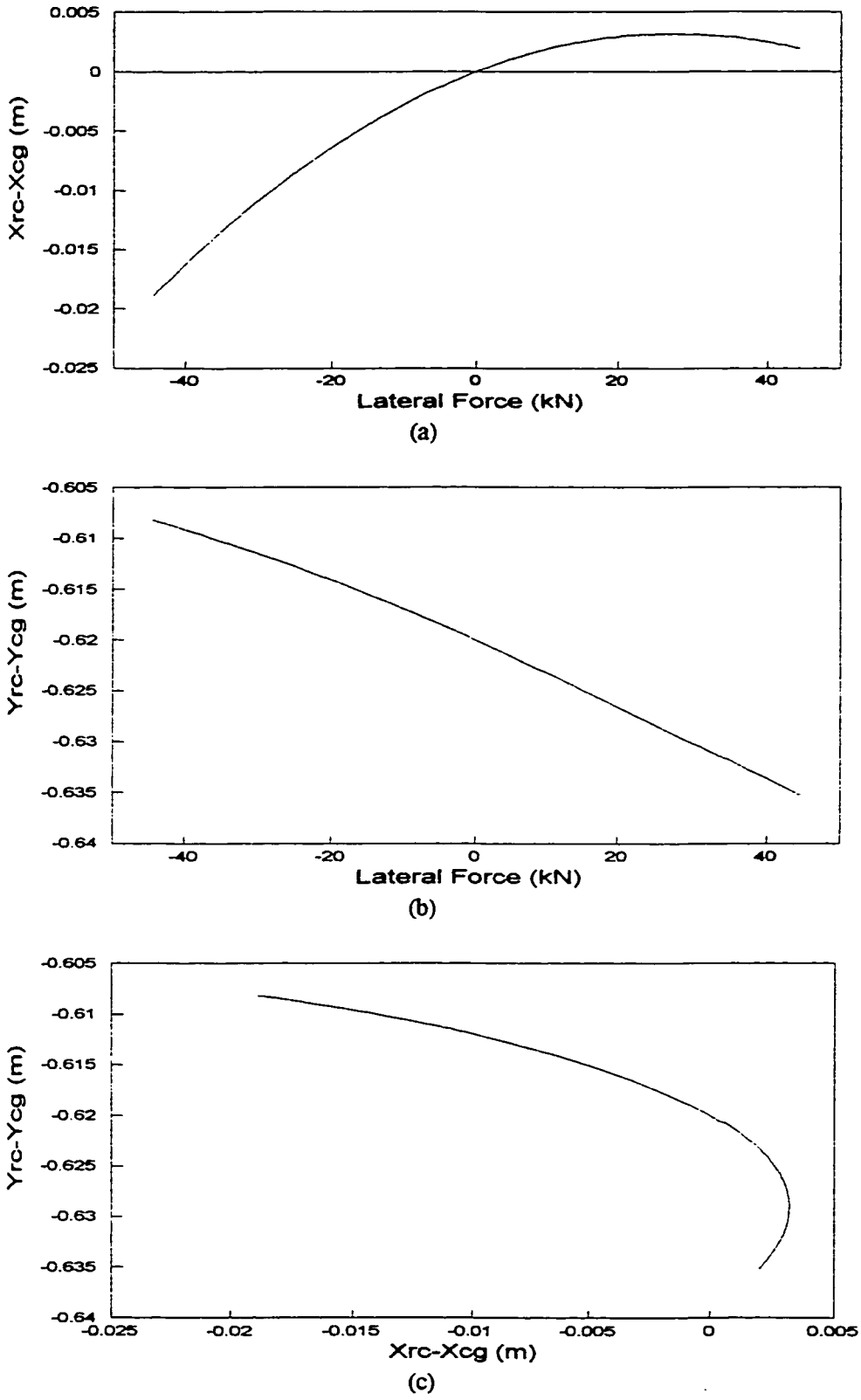


Figure 2.9 Influence of lateral force on suspension roll center vs. sprung mass cg

in the Panhard rod installation angle, unsprung mass roll angle, suspension spring rate, sprung mass, Panhard rod height and Panhard rod track width, is specifically investigated to enhance a thorough understanding of the kinetostatic behaviour of the candidate suspension system.

### 2.5.1 Influence of Panhard Rod Installation Angle

The asymmetric nature of the kinetostatic response behaviour, illustrated in Figures 2.6 to 2.9, is strongly dependent upon the Panhard rod installation angle. Since a large Panhard rod angle poses severe motion constraint, the angle is often limited to below 5 degrees. The kinetostatic properties of the suspension are investigated for different values of the Panhard rod installation angle in the range of -3 to 3 degrees, while the axle roll angle is held zero ($\psi = 0^0$). Equations (2.9), (2.12), (2.21) and (2.26) are solved to determine the sprung mass roll angle, and the coordinates of the sprung mass cg, the suspension roll center and the suspension roll stiffness as the function of the Panhard rod angle ($\alpha$) and the lateral force (F).

Figures 2.10 and 2.11 present the kinetostatic response characteristics for -44.5 kN $\leq$ F $\leq$ 44.5 kN and $-3^0 \leq \alpha \leq 3^0$. While the sprung mass roll angle varies considerably with the magnitude of lateral force, the influence of $\alpha$ on the sprung mass roll angle is apparently insignificant, as shown in Figure 2.10(a). An increase in the magnitude of the Panhard rod angle tends to vary the effective roll stiffness of the suspension considerably, as shown in Figure 2.10(b). A positive inclination ($\alpha = 3^0$) yields considerably larger suspension roll stiffness under negative lateral force, while the application of a positive lateral force results in only slight decrease in the roll stiffness, when compared to that corresponding to $\alpha = 0^0$. The Panhard rod angle, $\alpha = -3^0$, results in slight reduction in roll stiffness for F<0 and considerable increase for F>0. The

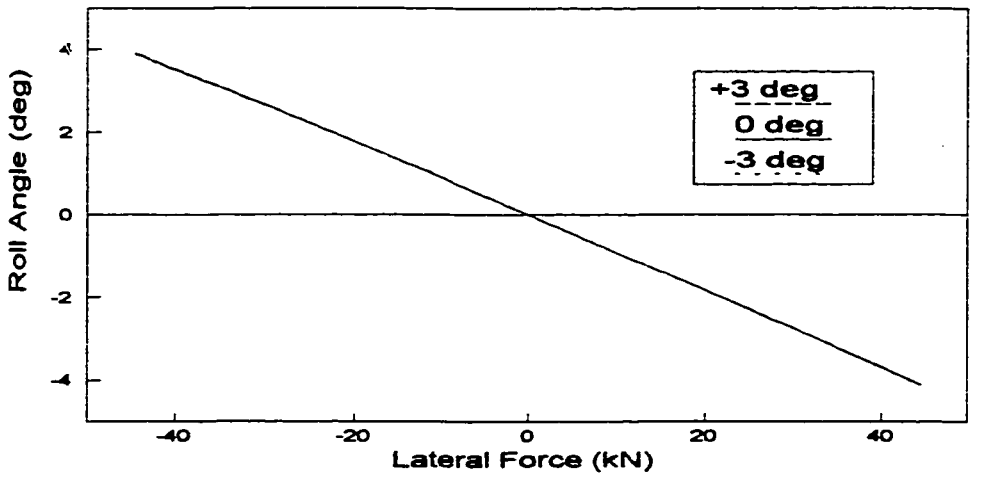


(a)

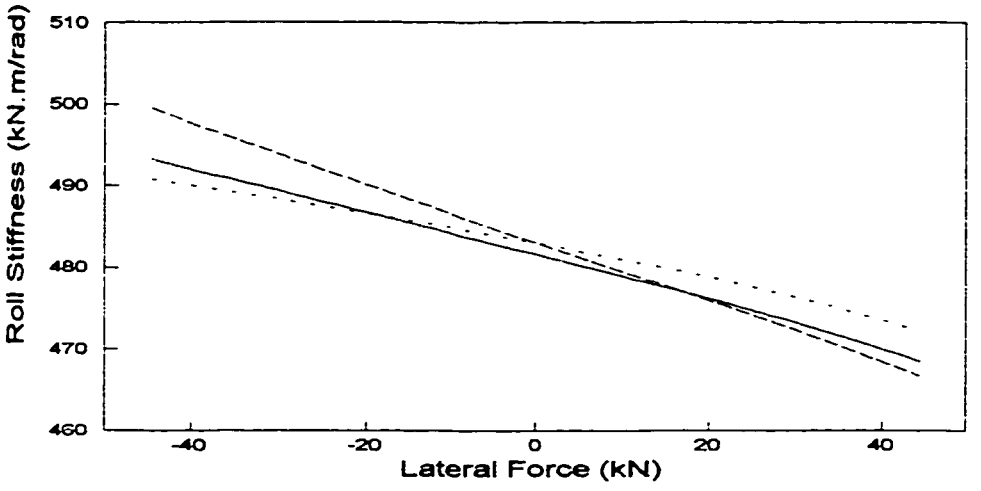


(b)

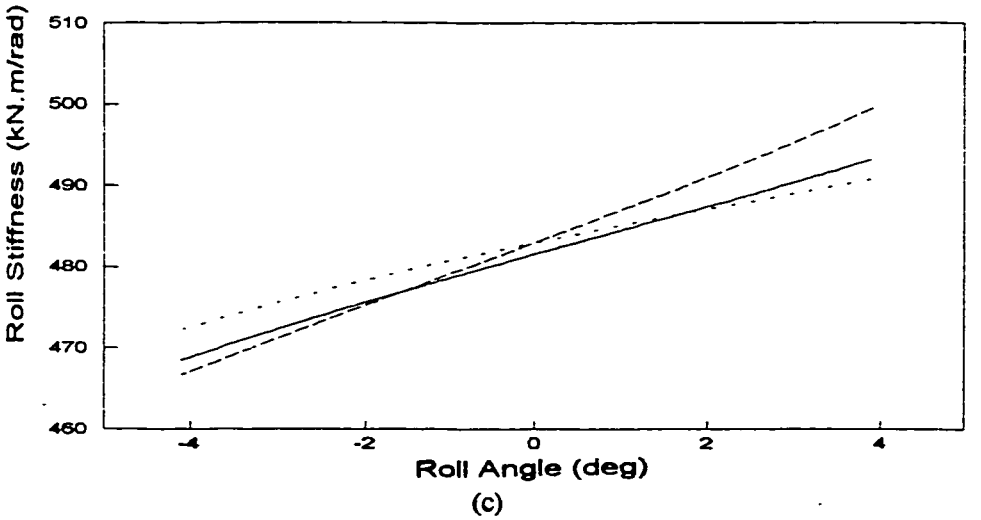


(c)

Figure 2.10 Influence of Panhard rod installation angle on sprung mass roll and suspension roll stiffness

suspension roll stiffness is observed to be an asymmetric function of the lateral force. The suspension roll stiffness properties are most asymmetric for $\alpha = 3^0$ and least asymmetric for $\alpha = -3^0$. For F≥-20 kN, the Panhard rod angle of $\alpha = -3^0$ yields higher suspension roll stiffness, and for F≤20 kN, high roll stiffness is attained with $\alpha = 3^0$. The suspension roll stiffness tends to increase with increase in the roll angle and decrease with decreasing roll angle, irrespective of the lateral force magnitude and Panhard rod angle, as shown in Figure 2.10(c). The roll stiffness varies as a nearly linear function of the roll angle. The Panhard rod with $\alpha = 3^0$ yields considerably larger suspension roll stiffness under positive body roll and slightly lower roll stiffness when the body roll is below -1.7 degrees. The Panhard rod with $\alpha = -3^0$ yields higher suspension roll stiffness under negative body roll and slightly lower roll stiffness when the sprung mass roll angle is above 1.8 degrees. The roll stiffness of the suspension system varies as an asymmetric function of the roll angle in a manner similar to that demonstrated in Figure 2.10(b).

The influence of variations in the Panhard rod angle on the variations in the coordinates of the sprung mass cg and the suspension roll center is illustrated in Figures 2.11(a) and 2.11(b), respectively. The results clearly demonstrate the strong influence of the Panhard rod angle on the trajectories of the sprung mass cg and the suspension roll center. While the limits of lateral displacement of the sprung mass cg ($x_{CG}$) encountered under the application of lateral force (-44.5 kN ≤ F ≤ 44.5 kN) remain almost identical irrespective of the values of $\alpha$, the vertical motion of the cg is strongly affected by the Panhard rod angle. For $\alpha = 3^0$, the vertical location of the sprung mass cg decreases when the lateral force varies from -44.5 kN to 44.5 kN, while for $\alpha = -3^0$, the location of the sprung mass cg increases. For $\alpha = 0^0$, the location of the sprung mass cg decreases slightly when the lateral force changes from -44.5 kN to 0 kN, and then increases slightly when the lateral force changes from 0 kN to 44.5 kN. The coordinates of suspension roll center tend to vary in a similar manner, irrespective of $\alpha$ values, as shown in Figure

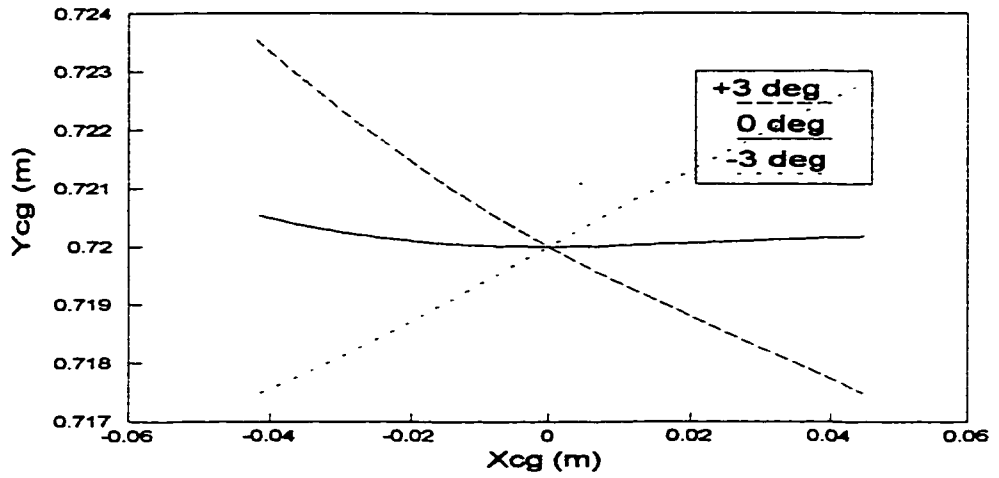


(a)

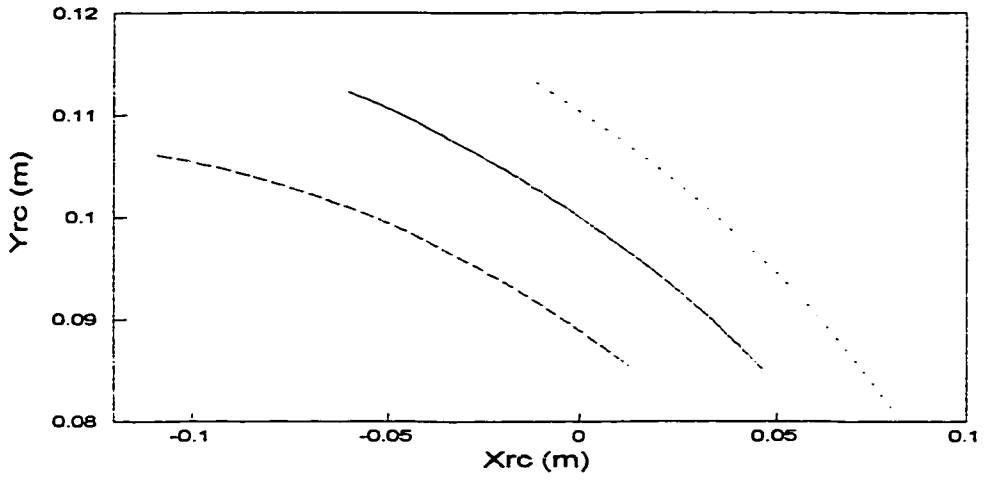


(b)

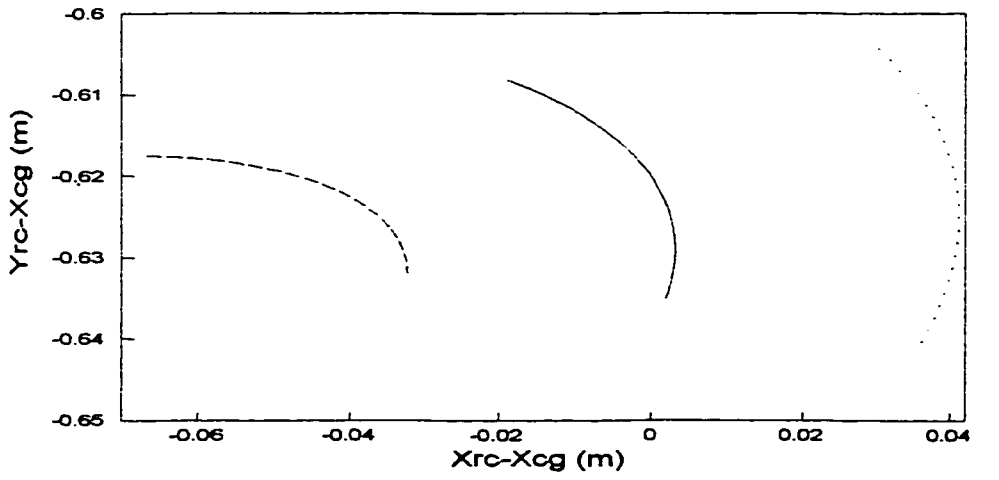


(c)

Figure 2.11 Influence of Panhard rod installation angle on sprung mass cg and suspension roll center

2.11(b). The vertical coordinate tends to decrease, while the lateral displacement increases, when F is varied from 44.5 kN to 44.5 kN. The variations in $\alpha$, however, affect the rate of changes of roll center position. For $\alpha = 3^0$, the suspension roll center experiences larger lateral displacement and smaller vertical displacement than those for $\alpha = 0^0$ and $\alpha = -3^0$, respectively. Furthermore, $\alpha = 3^0$ yields larger negative lateral displacement of the suspension roll center than those for $\alpha = 0^0$ and $\alpha = -3^0$, corresponding to the same lateral force. The influence of $\alpha$ on the variation in the displacement of the suspension roll center relative to the sprung mass cg is clearly shown in Figure 2.11(c). As the lateral force varies from -44.5 kN to 44.5 kN, the vertical distance between the suspension roll center and the sprung mass cg increases irrespective of $\alpha$, while the lateral distance decreases for $\alpha = 3^0$. This variation in the lateral distance, however, reveals different trends for $\alpha = 0^0$ and $-3^0$. The suspension roll center trajectory is further observed to be at the lower left part of the sprung mass cg for $\alpha = 3^0$, at lower right part for $\alpha = -3^0$, and at both lower left and right parts for $\alpha = 0^0$. This asymmetric phenomenon is caused by the asymmetric configurations of the beam axle suspension with different Panhard rod angles, as discussed earlier.

### 2.5.2 Influence of Unsprung Mass Orientation

In Figures 2.6 to 2.9, the kinematic behaviour of the beam-axle suspension with a Panhard rod was described assuming zero unsprung mass roll angle. The road vehicle, in general, exhibits certain roll deflection of the axle due to centrifugal forces and dynamic load transfer encountered during a steering input. Uneven road roughness at the two tracks of the vehicle further yields roll excitations for the unsprung mass. The unsprung mass, however, experiences relatively small motion due to high roll stiffness of the suspension and the anti-roll bars. In this study, the kinetostatic properties of the

suspension are investigated for different values of the unsprung mass roll angle ranging from -3 to +3 degrees, while the Panhard rod installation angle is held zero ($\alpha = 0^0$).

Figures 2.12 and 2.13 present the kinetostatic response characteristics of the sprung mass corresponding to -44.5 kN $\leq$ F $\leq$ 44.5 kN and $-3^0 \leq \psi \leq 3^0$. Figure 2.12(a) clearly shows that the influence of the unsprung mass roll angle on the sprung mass roll angle is apparently significant. It is observed that the variation of the sprung mass roll angle with the magnitude of the lateral force for different unsprung mass roll angle is equivalent to adding a constant angle to the roll response of the sprung mass for $\psi = 0^0$. The positive/negative sign of the added angle is consistent with the sign of $\psi$ and the magnitude of the added angle is proportional to the magnitude of $\psi$. The roll response of the sprung mass corresponding to $\psi = 3^0$ yields nearly $3.6^0$ shift upon that corresponding to $\psi = 0^0$. While the suspension roll stiffness, as shown in Figure 2.12(b), decreases as the lateral force varying from -44.5 kN to 44.5 kN, compared to the suspension roll stiffness corresponding to $\psi = 0^0$, the suspension exhibits higher roll stiffness corresponding to $\psi \geq 0^0$ for all the lateral force studied, and the suspension corresponding to $\psi = -3^0$ yields lower roll stiffness for the lateral force between -44.5 kN to 6 kN and higher roll stiffness for the lateral force between 6 kN to 44.5 kN. The relationship between suspension roll stiffness and resulted roll angle of sprung mass is presented in Figure 2.12(c). When the sprung mass roll angle is between -0.35 to 0.29 degrees, the suspension for $\psi = -3^0$ has higher roll stiffness compared to those corresponding to $\psi = 0^0$ and $\psi = 3^0$. When the sprung mass roll angle is between 0.29 to 4.02 degrees, the suspension for $\psi = 0^0$ yields higher roll stiffness than that with $\psi = 3^0$, while suspension for $\psi = -3^0$ exhibits higher roll stiffness than that with $\psi = 0^0$ when the sprung mass roll angle is between -0.35 to -4.12 degrees. When the magnitude of the sprung mass roll angle is larger than 4.02 and -4.12, the suspension exhibits larger roll stiffness for $\psi = 3^0$ than that for $\psi = -3^0$.

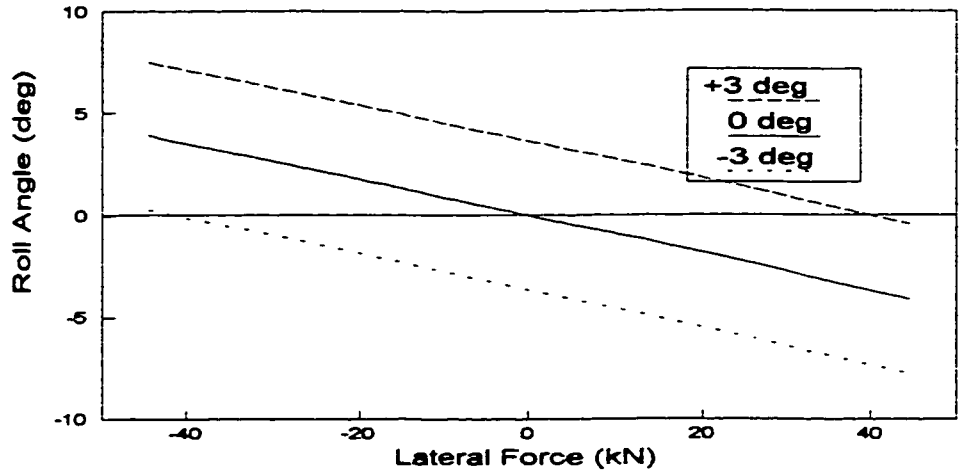


(a)

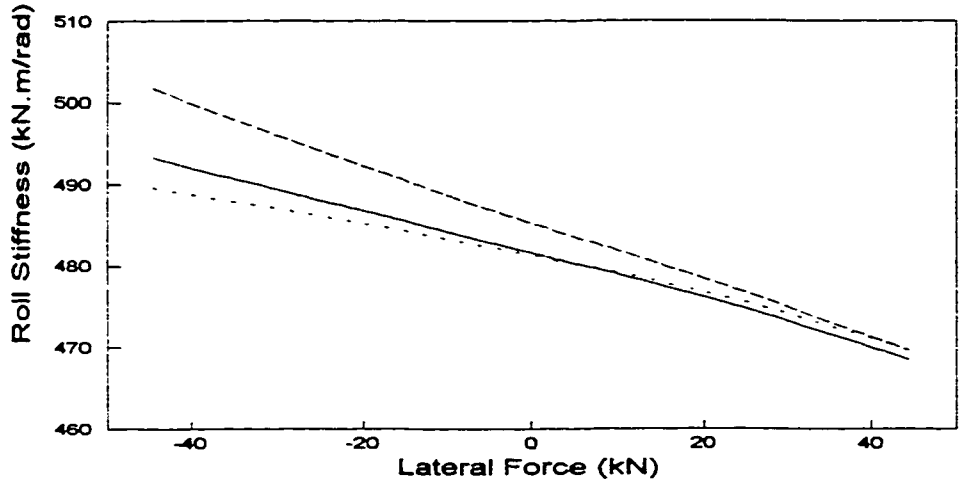


(b)

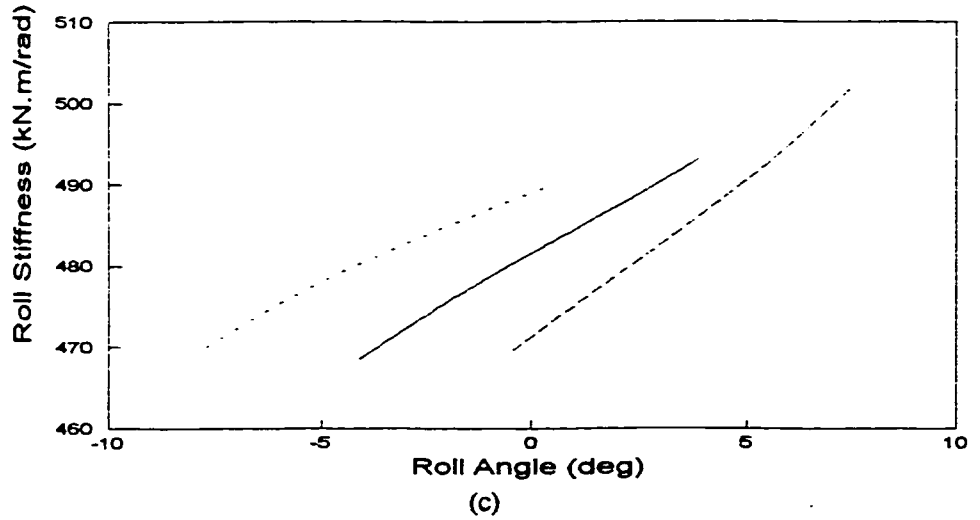


(c)

Figure 2.12 Influence of unsprung mass orientation on sprung mass roll and suspension roll stiffness

The influence of the unsprung mass roll angle on the kinetostatic displacement of sprung mass cg, suspension roll center is presented in Figures 2.13(a) and 2.13(b). It can be observed that the vertical coordinate of the sprung mass cg tends to increase with the decrease in the magnitude of $\psi$ ($>0^0$), and tends to decrease with the increase in the magnitude of $\psi$ ($<0^0$). For $\psi = 3^0$, the sprung mass cg has negative lateral coordinate, while for $\psi = -3^0$, the sprung mass cg has positive lateral coordinate. With respect to the suspension roll center, the influence of $\psi$ on the lateral displacement is apparently illustrated in Figure 2.13(b). With the same vertical coordinate of the suspension roll center, the suspension roll center for $\psi > 0^0$ and $\psi < 0^0$ is at the left and right sides of that for $\psi = 0^0$. And the suspension roll center tends to yield larger lateral deflection when $\psi$ changes from $-3^0$ to $3^0$. The significant effect yielded by $\psi$ on the fluctuation of the suspension roll center with respect to the sprung mass cg is illustrated in the Figure 2.13(c). It is apparent that the suspension roll center yields larger lateral displacement relative to the sprung mass cg corresponding to $\psi$ varying from $-3^0$ to $3^0$ and F changing from -44.5 kN to 44.5 kN. The larger lateral displacement of the suspension roll center appeared in Figure 2.13(b) and 2.13(c) is considered as disadvantageous for the lateral stability.

### 2.5.3 Influence of Panhard Rod Length

The kinetostatic response characteristics of the beam-axle suspension with Panhard rod link is related to its length or track width (L) in a non-linear manner, as evident from equations (2.5) to (2.7), and (2.21). The analytical model is thus evaluated for different lengths of the Panhard rod (L=0.6 m, 0.8 m and 1.0 m), while the angles $\alpha$ and $\psi$ are held at 0 degrees. The influence of variations in the track width of the Panhard rod on the spring mass roll angle and thus the cg coordinates is insignificant for the range of lengths

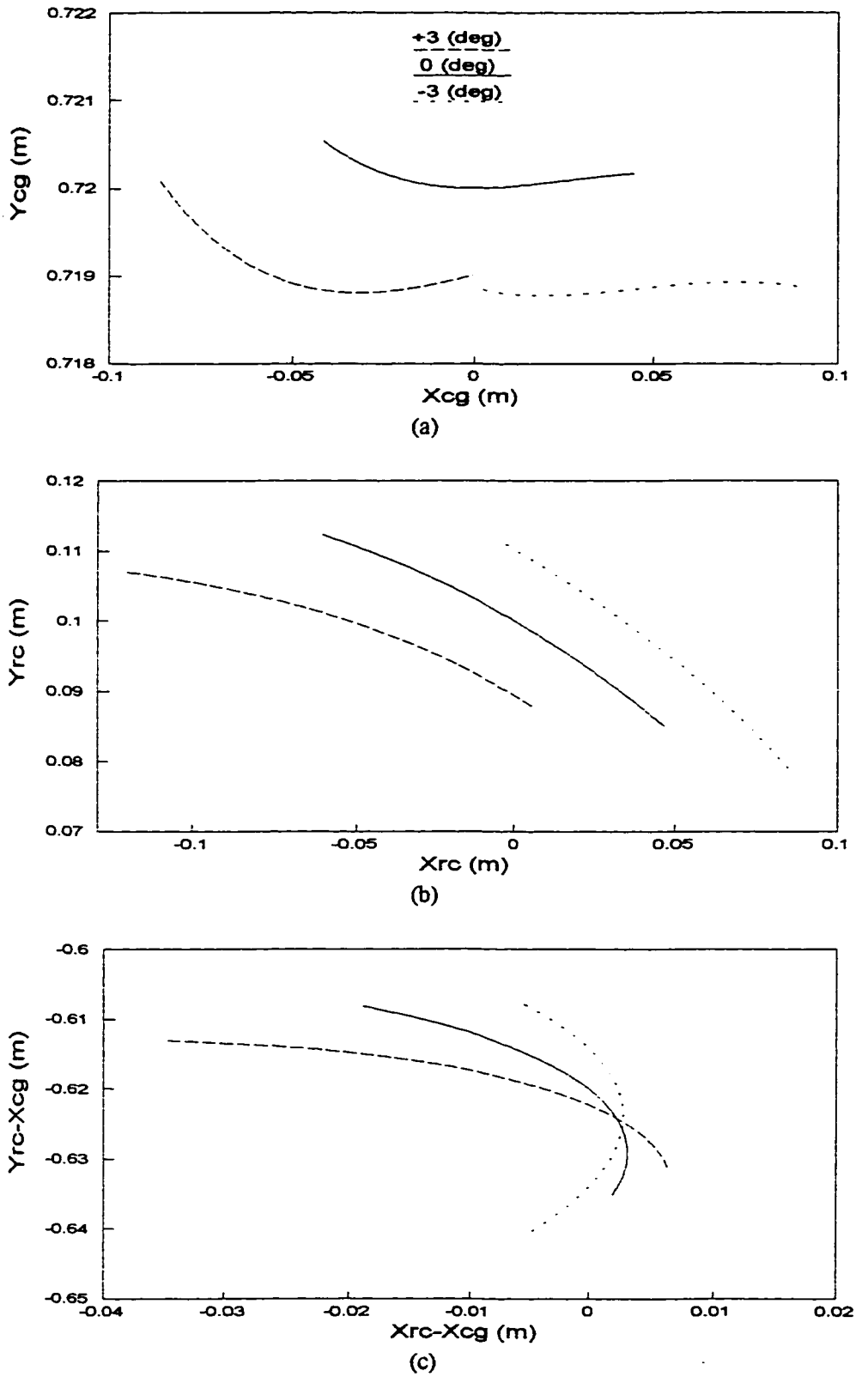


Figure 2.13 Influence of unsprung mass orientation on sprung mass cg and suspension roll center

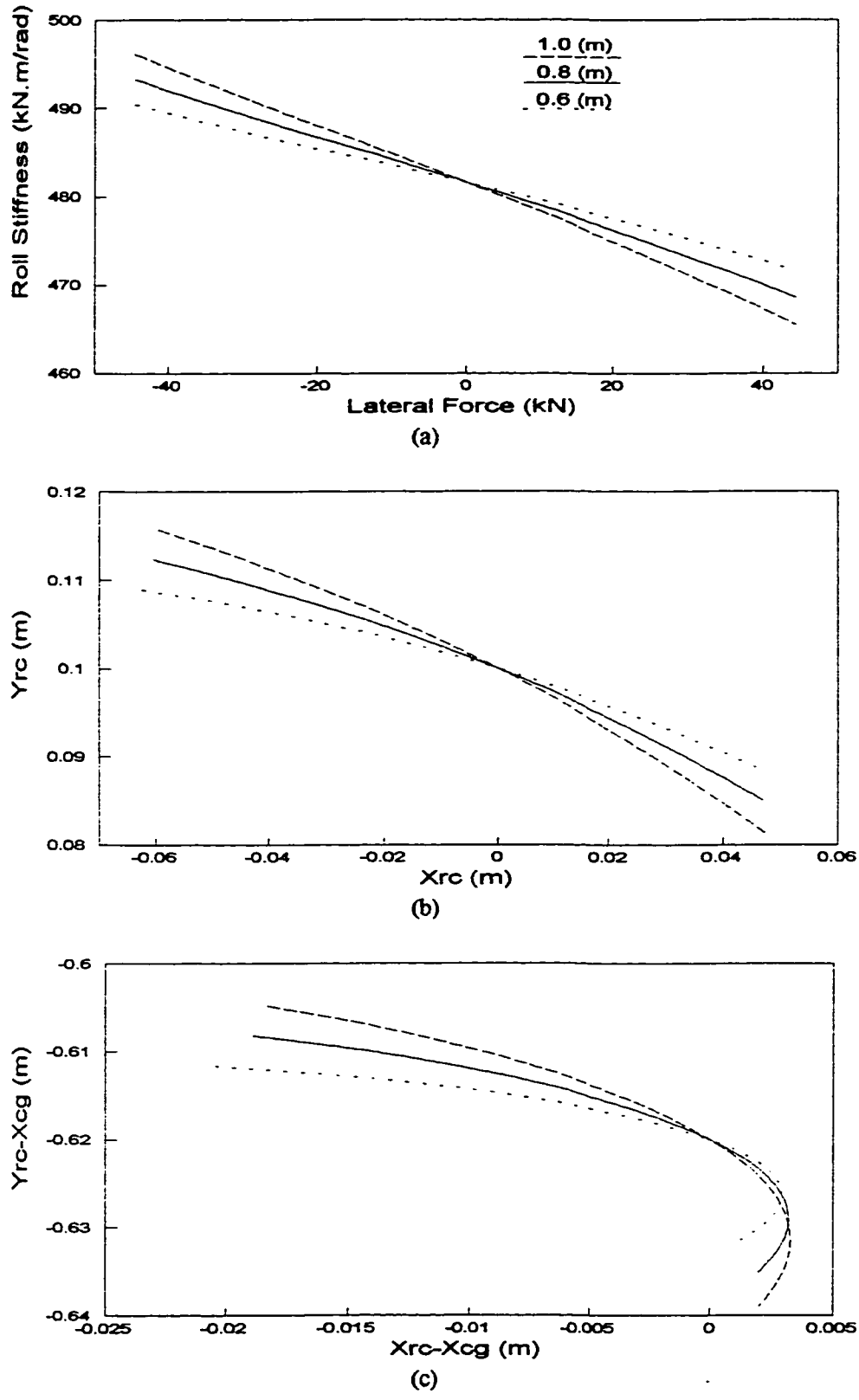


Figure 2.14 Influence of Panhard rod length on sprung mass cg and suspension roll center

and lateral force considered in the study. An increase in the Panhard rod track width, however, yields higher suspension roll stiffness and increase in the vertical coordinate of the roll center for F<0, as shown in Figure 2.14. A shorter Panhard rod track width exhibits higher suspension roll stiffness and increased vertical coordinate of the roll center for F>0.

### 2.5.4 Influence of Suspension Spring Rate

The suspension springs are primarily designed to support the spring weight, reduce the vibrations arising from the road irregularities, and provide adequate directional control performance. An increase in the spring weight yields slightly higher roll stiffness of the suspension over the entire range of the lateral force, which is primarily attributed to the increased static deflection and reduced lateral acceleration. The roll stiffness and the sprung mass angle response characteristics are directly related to the suspension spring rate. An increase in spring rate yields higher effective roll stiffness and lower magnitude of roll deflection, as shown in Figure 2.15. The variations in the lateral force, however, yield only insignificant influence on the roll stiffness, irrespective of the spring rate. The coordinates of the cg and the roll center tend to vary considerably with softer suspension due to reduced roll stiffness, as shown in Figure 2.16.

## 2.6 Summary

A non-linear kinetostatic model of a candidate highway vehicle suspension is developed in the roll plane to study the kinetostatic response characteristics for specified lateral force and vertical load. The kinetostatic model represents a two-degree-of-freedom system compromising generalized coordinates: roll angles of the sprung mass and the Panhard rod. The numerical scheme of Newton iteration is utilized to solve system non-

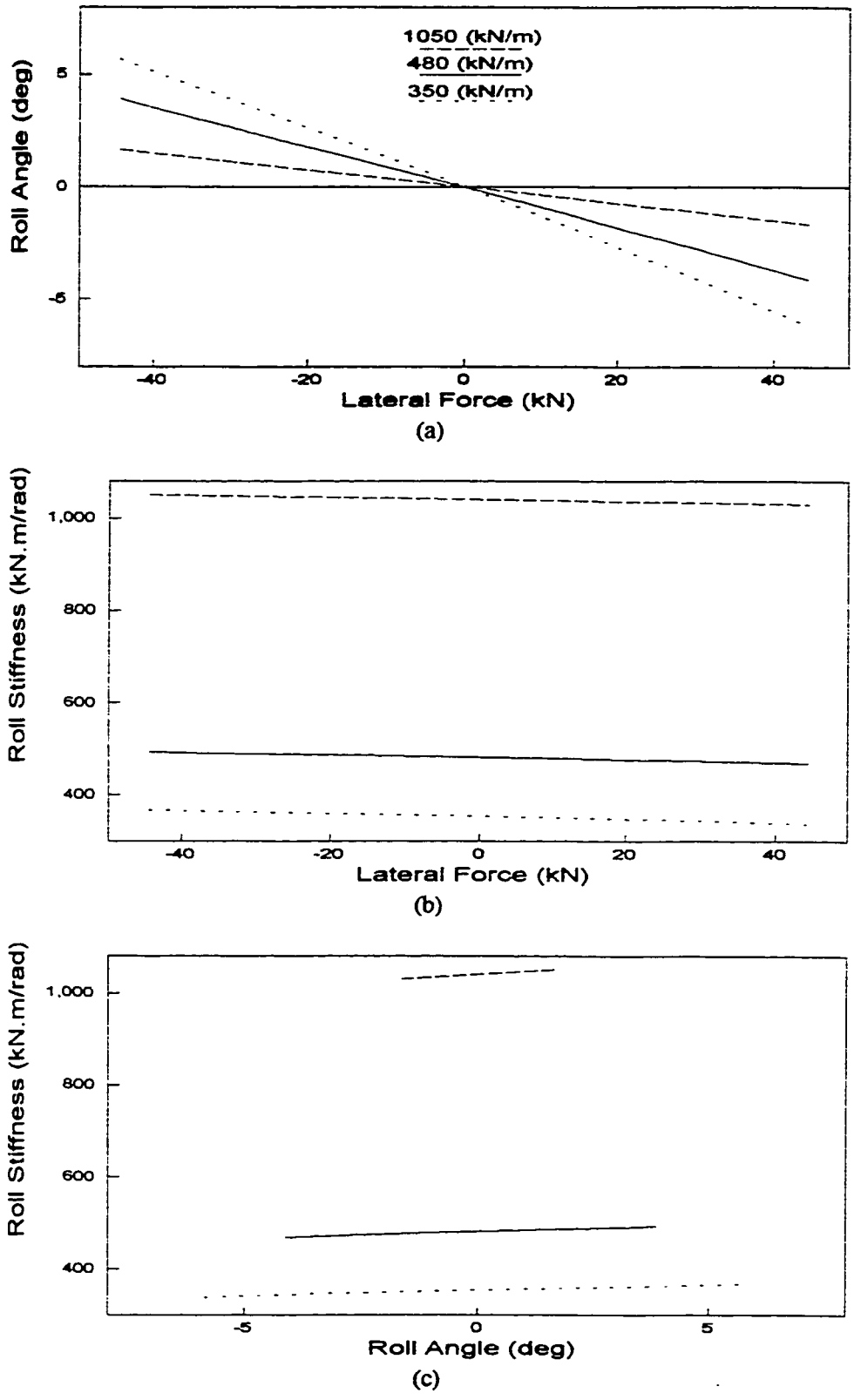


Figure 2.15 Influence of suspension stiffness on sprung mass roll and suspension roll stiffness

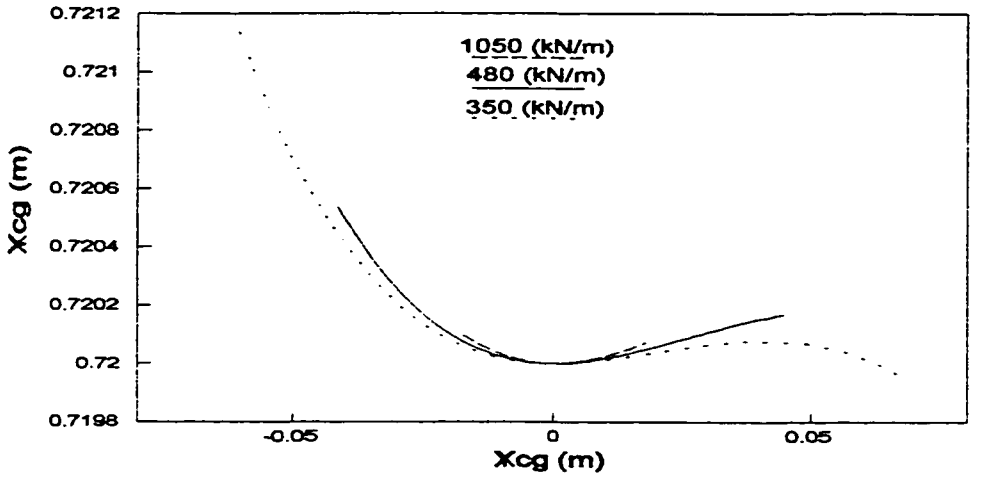


(a)

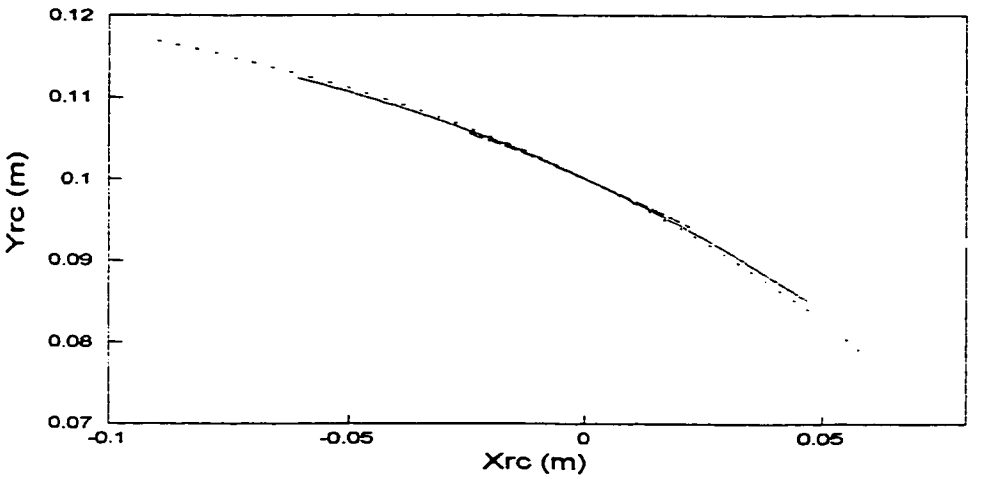


(b)

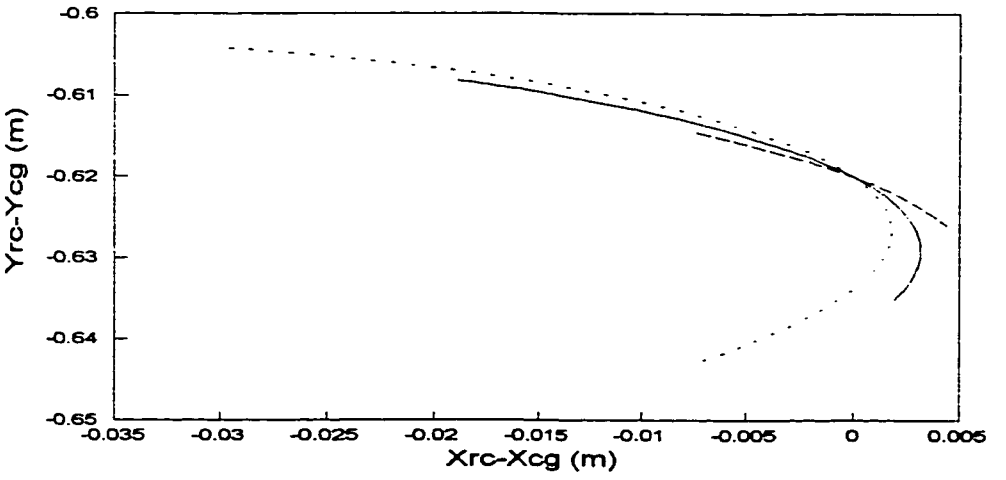


(c)

Figure 2.16 Influence of suspension stiffness on the coordinate of the sprung mass cg and suspension roll center

linear algebraic equations. The variation of the roll angle and the cg coordinates of the sprung mass, the suspension roll stiffness and the suspension roll center coordinates are evaluated as the function of the lateral force changing in the range of -44.5 kN to 44.5 kN, which represents the severe turning condition of the candidate highway bus.

# Chapter 3

# Dynamic Analysis of Panhard Rod Beam-Axle Suspension

## 3.1 Introduction

The ride and handling performance of ground vehicles is related to the kinematics and dynamics of the suspension linkages. The kinematics of the suspension and restraining linkages relates to the suspension roll stiffness, and the variations in coordinates of the suspension roll center and the sprung mass cg under the application of a centrifugal force caused by a cornering/directional maneuver. The dynamic analysis of the suspension and the linkages yields vehicle behavior related to ride and handling performance. The kinetostatic analysis carried out in Chapter 2 revealed that the kinematic variations in the roll center coordinates are relatively small (below 2%), and the suspension roll stiffness varies by less than 3% under the application of a lateral force corresponding to 0.3g centrifugal acceleration. Furthermore, the degree of asymmetry, and the variations in the instantaneous coordinates of the suspension roll center relative to the sprung mass c.g. coordinates under extreme centrifugal forces were observed to be relatively small. The location of the suspension roll center can thus be considered to be constant relative to the sprung mass cg. The study further suggested that the suspension roll center can be determined from the initial static equilibrium position, which is located at the intersection of the vertical axis passing through the sprung mass cg and the Panhard rod axis.

In this chapter, two analytical models of varying complexities of the candidate vehicle incorporating beam axle suspensions and passive Panhard rod constraints are developed to study its roll plane dynamic response characteristics, assuming symmetric characteristics of the suspension for left- and right- directional maneuvers, and fixed roll

center location with respect to sprung mass cg. The analytical models are discussed to evaluate the resonant frequencies and dominant modes, and the influence of passive Panhard rod constraint on the ride and handling performance of the candidate vehicle subject to excitations arising from harmonic and random road irregularities, and the centrifugal force arising from directional maneuvers.

## 3.2 Development of Roll Plane Dynamic Models

The ride and handling characteristics of ground vehicles are related to roll, pitch, yaw, vertical, lateral and longitudinal dynamic motions of the vehicle subject to excitations arising from road roughness and centrifugal forces. Various in-plane and three-dimensional models of road vehicles have been developed to study the ride, handling and directional response characteristics. Two-DOF quarter-vehicle models are often used to study the vertical dynamics of the suspension system and damping mechanisms. Such models yield an effective assessment of uncoupled vertical dynamics of the suspension or damping concepts. Pitch plane models have been used to study the coupled vertical and pitch motions caused by road irregularities, while neglecting the roll dynamics of the vehicle. While the quarter-vehicle and pitch plane models provide the ride dynamics and dynamic tire forces transmitted to the pavements, the roll plane models can yield significant insight into vehicle dynamic response to road irregularities and centrifugal forces arising from the directional maneuvers. Furthermore, the roll plane models can yield the level of vertical, lateral and roll accelerations transmitted to the driver/passenger to assess the ride quality, the roll angle and lateral swing in the view of the handling performance, and the sprung mass lateral acceleration relative to the rollover characteristics of the candidate vehicle.

Two analytical dynamic models of the candidate highway bus with beam axle suspensions and rigid transversal Panhard rod constraints are developed in the roll plane. The primary objective is to study the influence of the Panhard rod constraint on the handling and ride performance of the candidate vehicle subject to harmonic centrifugal acceleration inputs, and harmonic and random roadway disturbances. The initial analytical model is developed to incorporate the dynamics of the Panhard rod and the bushing flexibility of the Panhard rod, while the second analytical model is formulated with the simplifying assumption that the mass of the Panhard rod is relatively small, and that the bushings are relatively stiff.

### 3.2.1 Roll Plane Analytical Model with Panhard Rod Dynamics

The roll plane dynamics of a road vehicle comprising a Panhard rod beam-axle suspension is characterized by a nine-DOF dynamical system, as shown in Figure 3.1. The masses due to body, axle and Panhard rod are lumped in the roll plane, and each lumped mass is considered as a rigid body with three DOF: vertical, lateral and roll. The major assumptions associated with the model development are described below:

1. The composite Panhard rod beam-axle suspension realized upon lumping different axle suspensions in the roll plane, is idealized by a parallel combination of a linear spring and a viscous damper.
2. The suspension spring and damper are constrained to deflect along their axial directions.
3. The tires are represented by parallel combinations of linear springs and dampers in the vertical and lateral directions.
4. The forces arising at the tire-road interface are computed using a point contact tire model assuming undeformable road.

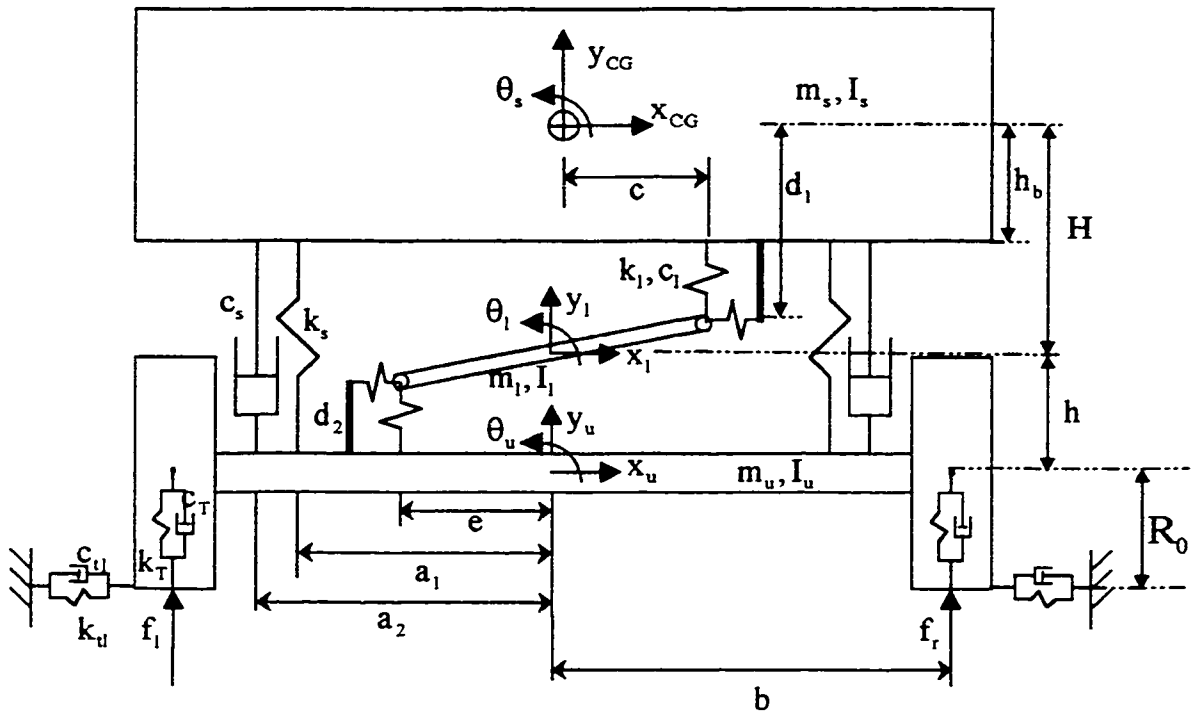


Figure 3.1 Schematic of Nine-DOF Model.

5. The tires are assumed to be in contact with the road at all times.
6. The magnitude of vehicle motions along the generalized coordinates is assumed to be small.
7. The suspension characteristics for left and right directional maneuvers are assumed to be symmetric.
8. The sprung mass roll caused by forces arising from either the tire-road interactions or the directional maneuvers is assumed to occur about a roll center, located at a fixed distance relative to the sprung mass cg. The roll center is located at the intersection of a vertical axis passing through the sprung mass cg and the Panhard rod axis, while assuming negligible displacement of the roll center under external forces.
9. The Panhard rod is connected to the sprung and the unsprung masses by revolute joints, and the radial flexibility of the bushings is represented by equivalent vertical and lateral combinations of a linear spring and a linear damper.
10. The centrifugal force arising from a steering maneuver is assumed to act at the sprung mass cg.

The coupled differential equations governing the roll, lateral and vertical motions of the composite nine-DOF Panhard rod beam-axle suspension under the actions of the centrifugal force and the road induced excitations are formulated using Lagrangian energy equation:

$$\frac{d}{dt}\left(\frac{\partial T}{\partial \dot{\bar{q}}_i}\right)-\left(\frac{\partial T}{\partial \bar{q}_i}\right)+\left(\frac{\partial D}{\partial \dot{\bar{q}}_i}\right)+\left(\frac{\partial V}{\partial \bar{q}_i}\right)=F_i;\quad i=1,2,\ldots,n \tag{3.1}$$

Where T, V and D are the kinetic, potential and dissipation energy functions, respectively. $F_i$ are the generalized forces and $\{\bar{q}\}$ is the vector of generalized coordinates, given by:

$$\{\bar{q}\} = \{y_{RC} \quad y_u \quad y_L \quad \theta_s \quad \theta_u \quad \theta_L \quad x_{RC} \quad x_u \quad x_L\}^T$$

Where "$^T$" designates the transpose. $y_{RC}$, $y_u$, $y_L$ and $x_{RC}$, $x_u$, $x_L$ are the vertical and lateral coordinates of the sprung mass at the suspension roll center, and the unsprung and Panhard rod masses at their cg, respectively, and $\theta_s$, $\theta_u$ and $\theta_L$ corresponding roll deflections.

Assuming the motions to be small relative to the overall dimensions, such that $\sin\theta_i \approx \theta_i$ and $\cos\theta_i \approx 1$, a set of coupled second-order differential equations with constant coefficients is obtained. The roll center is assumed to be located at a fixed distance H, from the sprung mass cg. The resultant velocity of the sprung mass cg, $v_{CG}$, is then described by the following relation:

$$v_{CG}^2 = \dot{y}_{RC}^2 + (\dot{x}_{RC} - \theta_s \dot{H})^2 \tag{3.2}$$

Consequently, the equations of motions describing the roll plane motion of the composite Panhard rod beam-axle suspension are derived as follows:

*Vertical motion of sprung mass:*

$$\begin{aligned} &m_s \ddot{y}_{RC} + 2c_s(\dot{y}_{RC} - \dot{y}_u) - c_L[\dot{y}_L + 0.5\cos\alpha_0 \dot{\theta}_L - \dot{y}_{RC} - (c+r)\dot{\theta}_s] \\ &+ 2k_s(y_{RC} - y_u) - k_L[y_L + 0.5L\cos\alpha_0 \theta_L - y_{RC} - (c+r)\theta_s] = 0 \end{aligned} \tag{3.3}$$

*Vertical motion of the unsprung mass:*

$$m_u\ddot{y}_u - 2c_s(\dot{y}_{RC} - \dot{y}_u) + 2c_t\dot{y}_u - c_t(\dot{f}_L + \dot{f}_R) - c_L[\dot{y}_L - 0.5L\cos\alpha_0\dot{\theta}_L - \dot{y}_u + (e+r)\dot{\theta}_u] - 2k_s(y_{RC} - y_u) + 2k_t y_u - k_t(f_L + f_R) - k_L[y_L - 0.5\cos\alpha_0\theta_L - y_u + (e+r)\theta_u] = 0 \quad (3.4)$$

*Vertical motion of the Panhard rod:*

$$m_L\ddot{y}_L + 2c_L\dot{y}_L - c_L(\dot{y}_{RC} + \dot{y}_u) - c_L[(c+r)\dot{\theta}_s - (e+r)\dot{\theta}_u] + 2k_L y_L - k_L(y_{RC} + y_u) - k_L[(c+r)\theta_s - (e+r)\theta_u) = 0 \quad (3.5)$$

*Roll motion of the sprung mass:*

$$I_s\ddot{\theta}_s + 2a_2{}^2c_s(\dot{\theta}_s - \dot{\theta}_u) - (c+r)c_L[\dot{y}_L + 0.5L\cos\alpha_0\dot{\theta}_L - \dot{y}_{RC} - (c+r)\dot{\theta}_s] - (d_1 - r)c_L[\dot{x}_L - 0.5L\sin\alpha_0\dot{\theta}_L - \dot{x}_{RC} + \dot{\theta}_s H - (d_1 - r)\dot{\theta}_s] + 2k_s a_1{}^2(\theta_s - \theta_u) - (c+r)k_L[y_L + 0.5L\cos\alpha_0\theta_L - y_{RC} - (c+r)\theta_s] - (d_1 - r)k_L[x_L - 0.5L\sin\alpha_0\theta_L - x_{RC} + \theta_s H - (d_1 - r)\theta_s] = 0 \quad (3.6)$$

*Roll motion of the unsprung mass:*

$$I_u\ddot{\theta}_u - 2a_2{}^2c_s(\dot{\theta}_s - \dot{\theta}_u) + 2c_t b^2\dot{\theta}_u + c_t b(\dot{f}_L - \dot{f}_R) + 2c_{tl}(\dot{x}_u + R_0\theta_u)R_0 + c_L[\dot{x}_L + 0.5L\sin\alpha_0\dot{\theta}_L - \dot{x}_u + (d_2 - r)\dot{\theta}_u] \cdot (d_2 - r) + c_L[\dot{y}_L - 0.5L\cos\alpha_0\dot{\theta}_L - \dot{y}_u + (e+r)\dot{\theta}_u](e+r) - 2a_1{}^2k_s(\theta_s - \theta_u) + 2k_t b^2\theta_u + k_t b(f_L - f_R) + 2k_{tl}R_0(x_u + R_0\theta_u) + k_L[x_L + 0.5L\sin\alpha_0\theta_L - x_u + (d_2 - r)\theta_u](d_2 - r) + k_L[y_L - 0.5L\cos\alpha_0\theta_L - y_u + (e+r)\theta_u](e+r) = 0 \quad (3.7)$$

*Roll motion of the Panhard rod:*

$$I_L\ddot{\theta}_L + 2c_L 0.5^2 L^2 \sin^2\alpha_0\dot{\theta}_L + c_L 0.5L\sin\alpha_0(\dot{x}_{RC} - \dot{\theta}_s \cdot H - \dot{x}_u)$$
$$+ c_L 0.5L\sin\alpha_0[(d_1 - r)\dot{\theta}_s + (d_2 - r)\dot{\theta}_u] + 2c_L 0.5^2 L^2\cos^2\alpha_0\dot{\theta}_L$$
$$- c_L 0.5L\cos\alpha_0(\dot{y}_{RC} - \dot{y}_u) - c_L 0.5L\cos\alpha_0[(c+r)\dot{\theta}_s + (e+r)\dot{\theta}_u]$$
$$+ 2k_L 0.5^2 L^2\sin^2\alpha_0\theta_L + k_L 0.5L\sin\alpha_0(x_{RC} - \theta_s H - x_u)$$
$$+ k_L 0.5L\sin\alpha_0[(d_1 - r)\theta_s + (d_2 - r)\theta_u] + 2k_L 0.5^2 L^2$$
$$\cos^2\alpha_0\theta_L - k_L 0.5L\cos\alpha_0(\dot{y}_{RC} - \dot{y}_u) - k_L 0.5L\cos\alpha_0$$
$$\cdot[(c + r)\theta_s + (e + r)\theta_u] = 0 \qquad (3.8)$$

*Lateral motion of the sprung mass:*

$$m_s\ddot{x}_{RC} - m_s\ddot{\theta}_u H - c_L[\dot{x}_L - 0.5L\sin\alpha_0\dot{\theta}_L - \dot{x}_{RC} + \dot{\theta}_s H$$
$$- (d_1 - r)\dot{\theta}_s] - k_L[x_L - 0.5L\sin\alpha_0\theta_L - x_{RC} + \theta_s H$$
$$-(d_1 - r)\theta_s] = -m_s a_x \qquad (3.9)$$

*Lateral motion of the unsprung mass:*

$$m_u\ddot{x}_u + 2c_u(\dot{x}_u + R_0\dot{\theta}_u) - c_L[\dot{x}_L + 0.5L\sin\alpha_0\dot{\theta}_L - \dot{x}_u$$
$$+ (d_2 - r)\dot{\theta}_u] + 2k_u(x_u + R_0\theta_u) - k_L[x_L + 0.5L\sin\alpha_0$$
$$\cdot\theta_L - x_u + (d_2 - r)\theta_u] = -m_u a_x \qquad (3.10)$$

*Lateral motion of the Panhard rod:*

$$m_L\ddot{x}_L + 2c_L\dot{x}_L - c_L(\dot{x}_{RC} - \dot{\theta}_s H + \dot{x}_u) - c_L[(d_1 - r)\dot{\theta}_s$$
$$- (d_2 - r)\dot{\theta}_u] + 2k_L x_L - k_L(x_{RC} - \theta_s H + x_u)$$
$$-k_L[(d_1 - r)\theta_s - (d_2 - r)\theta_u] = -m_L \cdot a_x \qquad (3.11)$$

Where $m_s$ and $m_u$ are the sprung and unsprung masses, respectively, lumped in the roll plane, and $m_L$ is the lumped mass of the Panhard rod. $k_s$ and $c_s$ are the stiffness and damping coefficients of the suspension spring and damper. $k_L$ and $c_L$ are the linear stiffness and damping coefficients representing the radial flexibility of the Panhard rod revolute joint bushings. $k_t$ and $c_t$ represent the linear vertical spring and damping coefficients due to the tire, respectively, and $k_u$ and $c_u$ are the respective lateral stiffness and damping coefficients. L is the length of rigid Panhard rod and $\alpha_0$ is its installation angle. r is the radius of the Panhard rod bushing and c is the half-track length of Panhard rod relative to the sprung mass (the lateral distance between the bushing connecting the Panhard rod and the sprung mass, and the vertical axis passing through the sprung mass cg). e is the half track length of Panhard rod relative to the unsprung mass (the lateral distance from the center of bushing connecting the Panhard rod to the unsprung mass and the unsprung mass cg) $f_L$ and $f_R$ are the vertical displacements induced at the left- and right- tire-road interface in the roll plane. $I_s$, $I_u$ and $I_L$ are the roll mass moments of inertia of the sprung mass, unsprung mass and Panhard rod with respect to their cg, respectively. $a_1$ is half the suspension spring track width, while $a_2$ is half the suspension damper track width. $d_1$ is the vertical distance between the sprung mass cg and the bushing which connects the Panhard rod and the sprung mass, while $d_2$ is the vertical distance between the unsprung mass cg and the bushing which connects the Panhard rod and the unsprung mass. $R_0$ is the height of unsprung mass cg from the ground plane and $a_x$ is the centrifugal acceleration imposed on the sprung mass, unsprung mass and the Panhard rod, during a cornering/directional maneuver.

The coupled differential equations of motion, (3.5) to (3.11), describe the roll plane dynamics of the vehicle with the beam-axle suspension and the rigid Panhard rod constraint, subject to a centrifugal force arising from a directional maneuver and vertical

road excitations. The above equations of motion may be expressed in the following matrix form:

$$[\overline{M}]\{\ddot{\overline{q}}\}+[\overline{C}]\{\dot{\overline{q}}\}+[\overline{K}]\{\overline{q}\}=[\overline{C}_F]\{\dot{u}\}+[\overline{K}_F]\{u\} \tag{3.12}$$

Where $[\overline{M}]$, $[\overline{C}]$ and $[\overline{K}]$ are $(9\times9)$ mass/inertia, damping and stiffness matrices, respectively. $[\overline{C}_F]$ and $[\overline{K}_F]$ are $(9\times3)$ excitation damping and stiffness matrices, respectively. $[\overline{q}]$ is a vector of generalized coordinates and [u] is a vector of excitation coordinates, given by:

$$\{u\}=\{f_L \quad f_R \quad a_x\}^T$$

### 3.2.2 Roll Plane Analytical Model with Massless Panhard Rod and Rigid Panhard Rod Bushings

The nine-DOF analytical model, described by equation (3.12), characterizes the roll dynamics of the candidate vehicle incorporating the dynamics due to the restraining Panhard rod. The mass due to the Panhard rod, however, is extremely small when compared to those of the unsprung and the sprung masses (<0.06% of the sprung mass). Furthermore, the stiffness due to the Panhard rod bushings is extremely high. The Panhard rod can thus be considered as a rigid two-force link, which connects the sprung and unsprung masses laterally. The analytical model can then be simplified by assuming negligible inertia effects of the Panhard rod and high bushing stiffness. Figure 3.2 illustrates the schematic of the roll plane model assuming rigid Panhard rod link. The simplified model comprises the unsprung mass with three-DOF characterized by its vertical, lateral and roll coordinates ($y_u$, $x_u$ and $\theta_u$) and the sprung mass with two-DOF characterized by the vertical and roll coordinates at the suspension roll center ($y_{RC}$, $\theta_s$). The lateral motion of the sprung mass is coupled to that of the unsprung mass through the

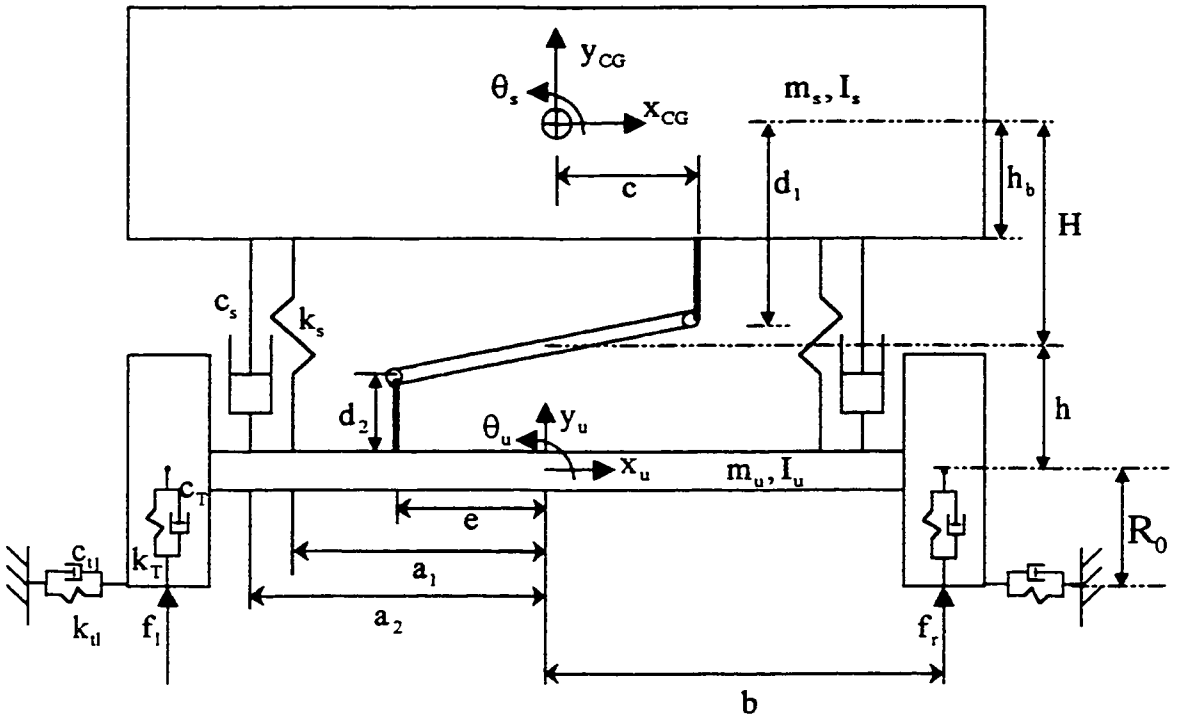


Figure 3.2 Schematic of Five-DOF Model.

transversal Panhard rod constraint. The equations of motion of the simplified five-DOF analytical model, derived using the Lagrange's energy method subject to assumptions described in Section 3.2.1, are summarized as follows.

*Vertical motion of the sprung mass:*

$$m_s\ddot{y}_{RC} + 2c_s(\dot{y}_{RC} - \dot{y}_u) + 2k_s(y_{RC} - y_u) = F\sin\alpha \tag{3.13}$$

*Vertical motion of the unsprung mass:*

$$\begin{aligned} &m_u\ddot{y}_u - 2c_s(\dot{y}_{RC} - \dot{y}_u) + 2c_t\dot{y}_u - c_t(\dot{f}_L + \dot{f}_R) - 2k_s(y_{RC} - y_u) \\ &+2k_t y_u - k_t(f_L + f_R) = -F\sin\alpha \end{aligned} \tag{3.14}$$

*Roll motion of the sprung mass:*

$$I_s\ddot{\theta}_s + 2a_2{}^2c_s(\dot{\theta}_s - \dot{\theta}_u) + 2a_1{}^2k_s(\theta_s - \theta_u) = F(c\sin\alpha + d_1\cos\alpha) \tag{3.15}$$

*Roll motion of the unsprung mass:*

$$\begin{aligned} &I_u\ddot{\theta}_u - 2a_2{}^2c_s(\dot{\theta}_s - \dot{\theta}_u) + 2c_t b^2\dot{\theta}_u + c_t b(\dot{f}_L - \dot{f}_R) \\ &+ 2c_u(\dot{x}_u + R_0\dot{\theta}_u)R_0 - 2a_1{}^2k_s(\theta_s - \theta_u) + 2b^2k_t\theta_u \\ &+ 2k_u(x_u + R_0\theta_u)R_0 + bk_t(f_L - f_R) = F(e\sin\alpha + d_2\cos\alpha) \end{aligned} \tag{3.16}$$

*Lateral motion of the sprung mass:*

$$m_s\ddot{x}_{RC} - m_sH\ddot{\theta}_s = F\cos\alpha - m_sa_x \tag{3.17}$$

*Lateral motion of the unsprung mass:*

$$m_u\ddot{x}_u + 2c_u(\dot{x}_u + R_0\dot{\theta}_u) + 2k_u(x_u + R_0\theta_u) = -F\cos\alpha - m_ua_x \tag{3.18}$$

*Geometric non-linear constraint due to Panhard rod:*

$$[(y_{RC}-y_u)+(h_s-h_u)+(c\theta_s+e\theta_u-d_1-d_2)]^2$$
$$+[(x_{RC}-x_u)+(c+e+d_1\theta_s+d_2\theta_u)]^2=L^2 \qquad (3.19)$$

where F is the constraint force due to Panhard rod link and $\alpha$ is the instantaneous orientation angle. $h_s$ and $h_u$ are the heights of the sprung and unsprung mass cg, respectively, with respect to the ground plane, corresponding to the static equilibrium position. The non-linear geometric constraint arising from the rigid massless Panhard rod can be linearized about the static equilibrium position using Taylor series expansion. Assuming small motions and negligible asymmetry due to the restraining Panhard rod, as discussed in Chapter 2, the linearized constraint equation about the suspension static equilibrium position can be expressed as follows.

$$\sin\alpha_0\cdot(y_{RC}-y_u+c\cdot\theta_s+e\cdot\theta_u)+\cos\alpha_0\cdot(x_{RC}-x_u+d_1\cdot\theta_s+d_2\cdot\theta_u)=0 \qquad (3.20)$$

The lateral displacement of the unsprung mass c.g., derived from the constraint equation (3.20), can then be expressed by:

$$x_u=\tan\alpha_0(y_{RC}-y_u+c\theta_s+e\theta_u)+(x_{RC}+d_1\theta_s+d_2\theta_u) \qquad (3.21)$$

Equation (3.18) and (3.21) are solved to yield the constraint force as a function of the dynamic motion of the vehicle and the suspension geometry:

$$\begin{aligned}F=&-\tan\alpha_0/\cos\alpha_0(m_s\ddot{y}_{RC}+2c_u\dot{y}_{RC}+2k_uy_{RC}-m_s\ddot{y}_u-2c_u\dot{y}_u-2k_uy_u)\\&-(c\cdot\tan\alpha_0-H+d_1)/\cos\alpha_0(m_u\ddot{\theta}_s+2c_u\dot{\theta}_s+2k_u\theta_s)\\&-(e\tan\alpha_0+d_2)/\cos\alpha_0(m_u\ddot{\theta}_u+2c_u\dot{\theta}_u+2k_u\theta_u)\\&-2c_uR_0/\cos\alpha_0\dot{\theta}_u-2k_uR_0/\cos\alpha_0\theta_u-(m_u\ddot{x}_{RC}\\&+2c_u\dot{x}_{RC}+2k_ux_{RC})/\cos\alpha_0-m_u/\cos\alpha_0a_x\end{aligned} \qquad (3.22)$$

Upon substituting for the constraint force from equation (3.22), the coupled second order differential equations of motion for the five-DOF roll plane model can be expressed in the following matrix form:

$$[M - M_P]\{\ddot{q}\} + [C - C_P]\{\dot{q}\} + [K - K_P]\{q\} = [D_{ax}]\{a_x\} + [C_F]\{\dot{u}\} + [K_F]\{u\} \qquad (3.23)$$

Where [M], [C] and [K] are (5×5) mass, damping and stiffness matrices, respectively. $[M_P]$ , $[C_P]$, and $[K_P]$ are (5×5) matrices of mass, damping and stiffness coefficients due to linearized Panhard rod geometric constraint. $[D_{ax}]$ is the effective force coefficient matrix due to linearized Panhard rod geometric constraint. $[C_F]$ and $[K_F]$ are (5×3) excitation damping and stiffness matrices, respectively. $\{q\}$ and $\{u\}$ are vectors of generalized response and excitation coordinates, given by:

$$\{q\} = \{y_{RC} \quad y_u \quad \theta_s \quad \theta_u \quad x_{RC}\}^T$$
$$\{u\} = \{f_L \quad f_R \quad a_x\}^T$$

## 3.3 Description of Excitations

The study of ride and handling performance characteristics of a road vehicle primarily involves response analyses under external excitations. The road vehicles, in general, are subject to excitations arising from tire-road interactions, centrifugal forces attributed to directional maneuvers, longitudinal forces caused by braking and acceleration, and the aerodynamic forces and moments. The ride dynamic properties of road vehicles are, in general, evaluated for deterministic and stationary random excitation at the tire-road interface, assuming constant forward speed. The constant speed handling properties of a vehicle relate to its roll, yaw and lateral dynamic response, when subject to a centrifugal force caused by a steering maneuver. The analytical models, described in the

previous section, can be effectively utilized to evaluate the vertical and lateral ride properties, and handling performance related to roll and lateral dynamics of the vehicle. The analysis, however, necessitates identification of representative excitations encountered by the vehicle.

### 3.3.1 Description of Cornering Maneuver Excitation

The vehicle body and axles experience a centrifugal force during a directional maneuver. The resulting lateral acceleration of the vehicle accounts for the primary overturning moment imposed on the vehicle. The handling performance of a vehicle relates to its ability to counteract the overturning/roll moment arising from the lateral or centrifugal acceleration excitation. Figure 3.3 illustrates the lateral acceleration of the sprung mass of a highway bus measured during a typical lane change maneuver at a speed of 110 km/h [46]. The measured data reveals that the lateral acceleration excitation can be represented by a harmonic excitation, at a frequency of approximately 0.3 Hz. The lateral acceleration excitation corresponding to a typical lane change maneuver at a highway speed can thus be characterized as:

$$a_x = 0.3g \cdot \sin 2\pi ft$$

Where $a_X$ is the lateral acceleration in g unit and $f$ is the predominant steering frequency. The magnitude of the harmonic lateral acceleration excitation may decrease when the directional maneuver is carried out at a lower speed.

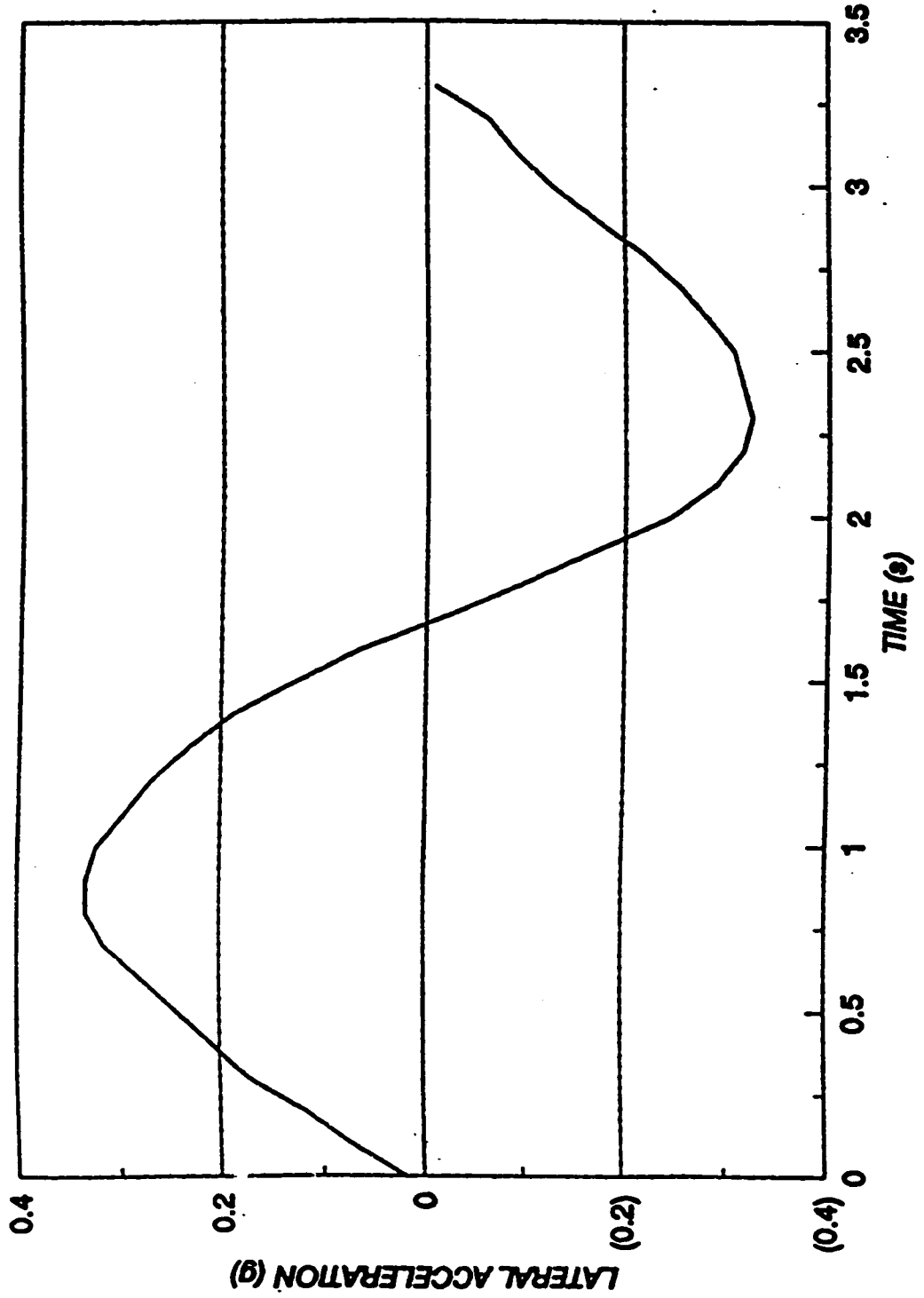


Figure 3.3 Measured transient lateral acceleration of the candidate highway bus [46]

### 3.3.2 Description of Road Excitation

While the ride performance analyses require description of excitations arising from a randomly rough road, the fundamental response behavior of a suspension system can be conveniently derived from deterministic excitations. The roll plane analytical models are thus analyzed for both deterministic and random road excitations described as follows.

#### Deterministic Road Excitations

The roughness and cross-slope of the road profiles, primarily, induce vertical and roll excitations to the vehicle. The fundamental vertical and roll response of the vehicle suspension can thus be investigated assuming in-phase and out-of-phase harmonic excitations at the tire-road interface. While the in-phase harmonic excitations yield the influence of restraining linkage under pure vertical excitation, the out-of-phase excitations provide significant insight into the role of restraint under pure roll excitations. The excitation arising at the tire-road interface are thus expressed as:

$$\begin{aligned} &\underline{\text{In-phase:}} && f_L = f_R = f_A \sin\omega t \\ &\underline{\text{Out-of-phase:}} && f_L = -f_R = f_A \sin\omega t \end{aligned} \qquad (3.24)$$

Where $f_A$ is the magnitude of the displacement excitation.

#### Random Road Excitations

The ride dynamic analysis of the beam-axle suspension and Panhard rod thus necessitates characterization of a representative random road profile. Various studies on characterization of the road profiles have established that the road profile can be described by a stationary Gaussian process with zero mean. The road roughness has been described

by a single sided displacement power spectral density (PSD) function with zero-mean stationary Gaussian random distributions:

$$\Phi(\omega) = \frac{2\bar{\alpha}\upsilon\rho^2}{\pi(\bar{\alpha}^2\upsilon^2 + \omega^2)} \tag{3.25}$$

Where $\Phi(\omega)$ is the displacement PSD of the random road profile, $\omega$ is the temporal angular frequency, $\bar{\alpha}$ is the road roughness coefficient, $\rho$ is the variance and $\upsilon$ is the forward speed of the vehicle. The displacement PSD corresponding to smooth, medium rough and rough road are evaluated using the coefficients presented in Figure 3.1. The displacement PSD of different road profiles at a speed of 110 km/h is further illustrated in Figure 3.4.

**Table 3.1 The Roughness Coefficients and Variance of Different Road Profiles** [53]

| Road Roughness | Roughness Coefficients | | |
|---|---|---|---|
| | $\bar{\alpha}$ ($m^{-1}$) | $\rho$ (m) | $\upsilon$ (km/h) |
| Smooth | 0.15 | 0.0033 | 110 |
| Medium Rough | 0.2 | 0.0056 | 110 |
| Rough | 0.4 | 0.012 | 110 |

Equation (3.25) describes the mean road profile to evaluate the vehicle response under pure vertical excitations. The analysis of the roll response necessitates the description of two terrain profiles at the right- and left-tire tracks. Alternatively, roll excitations may be generated by introducing a constant or speed dependent phase to represent the cross-slope present in the road in the following manner:

$$f_L(t) = f_R(t)e^{j\tau}$$

and

$$\tau = 2\pi \cdot (0.5 - \text{rnd})] \tag{3.26}$$

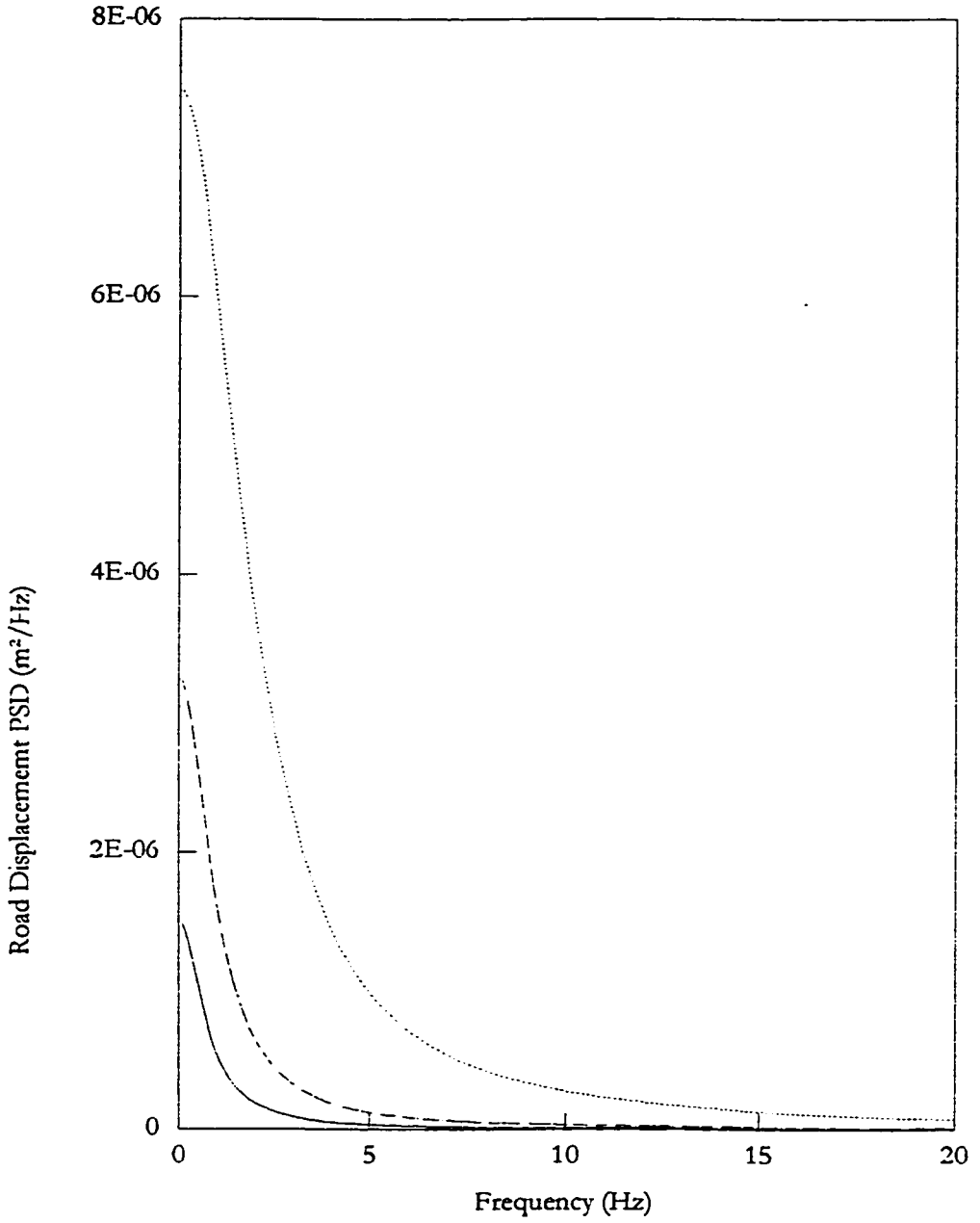


Figure 3.4 Road displacement PSDs for different random road roughness
( ——— Smooth; - - - - - - Medium Rough, ····· Rough )

Where $\tau$ represents the phase difference between the vertical excitations at left and right tracks ranging from $-\pi$ to $\pi$, and rnd is a random number generated between 0 and 1.

## 3.4 Performance Indices

A performance index, in general, is selected to assess specific designs and the objectives. The performance objectives of the candidate beam axle suspension with a transversal Panhard rod include vehicle ride and handling qualities. The roll plane models formulated in this study can be conveniently used to derive the handling performance of the candidate vehicle in terms of the roll deflection ($\theta_s$) of the sprung mass about the suspension roll center, and the lateral deflection of the sprung mass at its cg ($x_{CG}$). The lateral swing acceleration of the sprung mass at its cg ($\ddot{x}_{CG}$) can be further analyzed to assess the rollover stability characteristics of the vehicle.

The vehicle ride quality is a complex function of workstation design, placement of controls, seat design, noise and vibration environment, etc. Subjective rankings are often used to assess the ride quality related to the seat and the work station design, and objective methods are used to assess the impact of noise and vibration on the driver ride comfort. Although the ride quality associated with whole-body vehicular vibration is assessed using the acceleration response at the driver/passenger-seat interface and weighting filters representing the human response to vibration, a relative measure of vehicle ride quality can be conveniently derived from the acceleration response of the sprung mass. The ride quality of the candidate vehicle can thus be assessed by evaluating the vertical, lateral and roll acceleration response of the sprung mass.

## 3.5 Dynamic Analysis Of Panhard Rod Beam Axle Suspension Models

The dynamic characteristics of road vehicles under various excitations associated with the terrain irregularities and steering maneuvers are strongly related to the various vibration modes of the vehicle. A free vibration analysis is performed to identify the natural frequencies associated with different vibration modes. The computed natural frequencies are compared to the frequencies of dominant vibration measured on a highway bus.

### 3.5.1 Free Vibration Analysis

The differential equations of motion for the vehicle models under free vibration are expressed in the following matrix form:

$$[M_s]\{\ddot{q}_s\}+[C_s]\{\dot{q}_s\}+[K_s]\{q_s\}=\{0\} \tag{3.27}$$

Where $[M_s]$, $[C_s]$ and $[K_s]$ are $(n\times n)$ mass, damping and stiffness matrices, respectively. n is the number of degrees-of-freedom and $\{q_s\}$ is the corresponding vector of generalized coordinates. The natural frequencies of the damped vehicle models are determined from the following eigenvalue problem:

$$[A_D-\lambda_D I]\cdot\{\psi_D\}=\{0\} \tag{3.28}$$

Where $[A_D]=[M^*]^{-1}\cdot[K^*]$, and $[M^*]$ and $[K^*]$ are the $(2n\times 2n)$ matrices, given by:

$$[M^*]=\begin{bmatrix}[M_s] & [0]\\ [0] & [M_s]\end{bmatrix} \qquad [K^*]=\begin{bmatrix}[0] & [M_s]\\ -[K_s] & -[C_s]\end{bmatrix}.$$

The solution of the eigenvalue problem yields the eigenvector $\{\psi_D\}$ and eigenvalue $\lambda_D$, which are related to the damped and undamped natural frequencies ($\omega_{d_j}$ and $\omega_{n_j}$) and the daming ratios ($\zeta_j$):

$$\lambda_{D_j} = (-\zeta_j \omega_{n_j} \pm i\omega_{d_j})^2; \quad j = 1,2,...n$$

### 3.5.2 Dynamic Response To Excitations Arising From Steering Maneuver

The dynamic response characteristics of the candidate composite beam axle suspension with Panhard rod constraint subject to such harmonic centrifugal acceleration excitation discussed in section 3.3.2, can thus be evaluated in the convenient frequency domain. The equations of motion of the vehicle model subject to a centrifugal acceleration excitation, $a_x$, alone can be expressed in the following matrix form:

$$[M_s]\{\ddot{q}_s\} + [C_s]\{\dot{q}_s\} + [K_s]\{q_s\} = [K_a]\{a_x\} \tag{3.29}$$

where $[K_a]$ is $(n \times 1)$ coefficient matrix of centrifugal acceleration excitation. The Fourier transform of equation (3.29) yields the following expression for the complex frequency response function:

$$[H_a(i\omega)] = [[K_s] - \omega^2[M_s] + i\omega[C_s]]^{-1} \cdot [K_a] \tag{3.30}$$

The displacement response vector is thus derived for a harmonic centrifugal acceleration excitation of 0.3g amplitude, which corresponds to the acceptable level of rollover threshold of heavy vehicle [46]:

$$\{Q_s(i\omega)\} = 0.3g[H_a(i\omega)] \tag{3.31}$$

The corresponding acceleration response vector is given by:

$$\{\ddot{Q}_s(i\omega)\} = \omega^2 \cdot \{Q_s(i\omega)\} \qquad (3.32)$$

### 3.5.3 Dynamic Response to Road Excitation

Dynamic response characteristics of the linear and linearized vehicle models can be conveniently derived in the frequency domain, for both deterministic and random road excitations. The linearized equations of motion for the vehicle models are expressed in the following matrix form.

$$[M_s]\{\ddot{q}_s\} + [C_s]\{\dot{q}_s\} + [K_s]\{q_s\} = [C_R]\{\dot{u}_R\} + [K_R]\{u_R\} \qquad (3.33)$$

Where $[C_R]$ and $[K_R]$ are the $(n \times m)$ road excitation damping and stiffness matrices, respectively, and $\{u_R\}$ is the $(m \times 1)$ road excitation vector, given by:

$$\{u_R\} = \{f_L \quad f_R\}^T$$

Fourier transform of equation (3.33) yields:

$$\{Q_s(i\omega)\} = [H_R(i\omega)] \cdot \{U_R(i\omega)\} \qquad (3.34)$$

Where $\{Q_s(i\omega)\}$ and $\{U_R(i\omega)\}$ are the Fourier transforms of the $(n \times 1)$ and $(m \times 1)$ vectors of generalized response and excitation coordinates, respectively, and $[H_R(i\omega)]$ is the $(n \times m)$ complex frequency response function matrix. Solution of equation (3.34) yields the dynamic response characteristics of the vehicle models subject to out-of-phase vertical harmonic road excitations of constant displacement amplitude.

The dynamic response to random road excitations can be evaluated from the frequency response function matrix, $[H_R(i\omega)]$ and the road displacement excitation spectral density, $S_i(\omega)$:

$$[S_i(\omega)] = \Phi(\omega) \cdot \begin{bmatrix} 1 & e^{j\tau} \\ e^{-j\tau} & 1 \end{bmatrix} \tag{3.35}$$

And,

$$[S_0(\omega)] = [H_R(i\omega)] \cdot [S_i(\omega)] \cdot [H_R(i\omega)]^*$$
$$[S_a(\omega)] = [S_0(\omega)] \cdot \omega^4 \tag{3.36}$$

Where $[S_0(\omega)]$ and $[S_a(\omega)]$ are the $(n \times n)$ matrices of the displacement and acceleration PSDs of generalized coordinates, respectively. '*' designates the complex conjugate transpose.

## 3.6 Summary

In this chapter, the roll plane dynamics of the passive beam-axle suspension with rigid Panhard rod constraint is represented using two mathematical models. A nine-DOF analytical model is formulated to incorporate the flexibility of the Panhard rod bushings and the mass of the Panhard rod, while a simplified five DOF model is developed assuming the Panhard rod bushings are rigid and the mass of the Panhard rod can be neglected. The geometric non-linearity caused by the Panhard rod constraint is expressed by a linear relationship in order to derive system of linear differential equations characterizing the roll plane dynamics. The excitation arising from directional maneuver is represented by a harmonic centrifugal acceleration excitation, while those due to road roughness are described by both deterministic harmonic and random stationary zero-mean Gaussian

functions. The analytical techniques are briefly discussed to predict the fundamental frequency response characteristics and the random response characteristics of the candidate vehicle suspension under steering and roadway induced excitations.

# Chapter 4

# Dynamic Response Characteristics of Panhard Rod Beam-Axle Suspension Models

## 4.1 Introduction

The ride, handling and directional performance characteristics of road vehicles impose conflicting design requirements for the suspension and the linkage mechanisms. The suspension design for highway buses necessitates a careful compromise between the ride and handling. Since both factors are considered equally important in view of passenger comfort and directional control performance. The dynamic response characteristics related to the performance indices, discussed in Chapter 3, are strongly affected by the deflection modes of the vehicle and the corresponding resonant frequencies. The magnitudes of dynamic deflections and response accelerations are further related to dynamic behavior of the suspension and restraining linkage.

Free vibration analyses of the two analytical models, developed in Chapter 3, are performed to identify the natural frequencies and associated deflection modes of the candidate highway bus. The results of the study are compared to the available measured data to achieve a limited validation of the models. Dynamic response characteristics of the analytical models are evaluated for harmonic lateral acceleration excitation encountered during cornering/directional maneuvers, and harmonic and random roadway excitations. A comprehensive parametric study is performed to establish an understanding of the interactions of the transverse Panhard rod with the roll plane dynamics of the candidate vehicle.

## 4.2 Free Vibration Analysis

The eigenvalue problem, formulated in Chapter 3, is solved to identify the natural frequencies, damping ratios and the associated deflection modes of the two analytical models of the candidate vehicle. The results, summarized in Table 4.1, reveal that the free vibration response characteristics of the simplified five-DOF model are quite close to those of the nine-DOF model, when five lower deflection modes are considered. These include the models associated with roll, vertical and lateral deflection modes of the sprung mass and the vertical and roll deflection modes of unsprung mass. The sprung mass resonances occur at relatively low frequencies: 0.6581~ 0.6583 Hz for the roll mode, 1.2328 ~ 1.2524 Hz for the bounce mode, and 3.0711 ~ 3.0753 Hz for the lateral vibration mode. The composite unsprung mass exhibits resonances at relatively higher frequencies: 7.3584 ~ 7.3506 Hz for the vertical mode and 8.4469 ~ 8.4684 Hz for the roll mode. The peak error between the damped natural frequencies of the two models is 1.32% for all these five modes. This high degree of correlation between the free-vibration response characteristics of the two models is attributed to the high stiffness of the Panhard rod bushings and relatively small mass of the Panhard rod.

The results also reveal relatively high damping ratio corresponding to the vertical deflection modes of the sprung ($\zeta \approx 0.23$) and unsprung ($\zeta \approx 0.26$) masses. The damping ratio corresponding to the lateral deflection modes are observed to be low (below 0.06) for both the models. Table 4.1 further reveals that the nine-DOF analytical model exhibits very high resonant frequencies and extremely light damping associated with the lateral, vertical and roll deflection modes of the Panhard rod, which is attributed to its small mass and high stiffness bushings. Since such high frequency resonant modes of the nine-DOF analytical model do not contribute to the ride and handling properties of the candidate vehicle, the simplified five-DOF analytical model, is considered for further analysis of ride

Table 4.1 Comparison of Resonant Frequencies and Damping Ratios between Nine-DOF and Five-DOF Analytical Models

| 9-DOF model | | | 5-DOF model | | | | |
|---|---|---|---|---|---|---|---|
| Damped Resonant Frequency $f_d$ (Hz) | Undamped Resonant Frequency $f_n$ (Hz) | Damping Ratio $\zeta$ | Damped Resonant Frequency $f_d$ (Hz) | Undamped Resonant Frequency $f_n$ (Hz) | Damping Ratio $\zeta$ | Dominant Resonant Coordinate | % Difference in damped Resonant Frequency |
| 0.6581 | 0.6649 | 0.1426 | 0.6583 | 0.6650 | 0.1418 | $\vartheta_s$ | 0.03 |
| 1.2328 | 1.2682 | 0.2347 | 1.2165 | 1.2524 | 0.2378 | $y_{CG}$ | 1.32 |
| 3.0711 | 3.0765 | 0.0595 | 3.0753 | 3.081 | 0.0606 | $x_{CG}$ | 0.14 |
| 7.3584 | 7.6098 | 0.2743 | 7.3506 | 7.6024 | 0.2553 | $y_u$ | 0.11 |
| 8.4469 | 8.5327 | 0.1415 | 8.4684 | 8.5544 | 0.1414 | $\vartheta_u$ | 0.25 |
| 52.3797 | 52.3803 | 0.0217 | / | / | / | $x_u$ | / |
| 1916.09 | 1916.09 | 0.0001 | / | / | / | $x_L$ | / |
| 1916.19 | 1916.19 | 0.0001 | / | / | / | $y_L$ | / |
| 3317.99 | 3317.99 | 0.0002 | / | / | / | $\vartheta_L$ | / |

and handling performance. The nine-DOF model, however, may be considered desirable for the study of dynamic behavior of the transverse constraint.

The natural frequencies of the candidate vehicle models are compared with the dominant ride vibration frequencies identified from the road test data. A limited number of road tests were performed on a highway bus to measure the ride vibration response of the sprung and unsprung masses [46]. The dominant ride frequency of the vertical motion of the sprung mass, and the vertical, roll and lateral motions of the unsprung mass, identified from the limited measured data, compared with the resonant frequencies of proposed model in Table 4.2, show that the natural frequencies derived for the analytical models are results comparable with the dominant ride frequencies. The natural frequencies associated with vertical modes of the sprung and unsprung masses are close to the measured frequencies with errors of 8.12% and 18.35%, respectively. The analytical roll mode frequency of the unsprung mass is somewhat lower than the corresponding measured frequency with approximated 15.3% difference. This difference between the measured and computed frequencies are mostly attributed to the assumptions associated with the roll plane models comprising a single composite axle. A considerable difference between the computed and measured values of lateral mode frequency of the unsprung mass is also observed, which can also be attributed to the single composite axle used in roll plane vehicle model.

## 4.3 Frequency Response Characteristics of the Vehicle Models

An assessment of the ride and handling performance characteristics of the beam-axle suspension with a transverse Panhard rod requires the selection of appropriate performance index. The passenger ride quality has been directly related to vertical, lateral and roll acceleration perceived by the passengers. Since the vibrations at passengers'

Table 4.2 Comparison of Damped Resonant Frequencies of the Roll Plane Models with the Measured Dominant Frequencies

| Dominant Vibration Mode | Measured Dominant Natural Frequency (Hz) | 9-DOF Model Natural Frequency (Hz) | % Error | 5-DOF Model Natural Frequency (Hz) | % Error |
|---|---|---|---|---|---|
| $\vartheta_s$ | † | 0.6581 | / | 0.6583 | / |
| $y_{CG}$ | 1.49 | 1.2328 | 17.26 | 1.2165 | 18.35 |
| $x_{CG}$ | † | 3.0711 | / | 3.0753 | / |
| $y_u$ | 8.00 | 7.3584 | 8.02 | 7.3506 | 8.12 |
| $\vartheta_u$ | 10.00 | 8.4469 | 15.53 | 8.4684 | 15.32 |
| $x_u$ | 15.00 | 52.3797 | 249.20 | / | / |

† not reported

locations are directly related to the sprung mass vibration, the measure of passengers' comfort can be expressed in terms of acceleration response of the sprung mass. Furthermore, the drive and passenger exposure of whole-body ride vibration is frequently carried out in the frequency domain in order to apply the necessary weighting filters in a convenient manner. Although the ride analyses, in-general, are performed under the resonance behaviour, the effectiveness of vibration attenuation mechanisms and the role of Panhard rod constraint can be effectively investigated under harmonic excitation. In this study, the ride performance of the candidate vehicle is evaluated in terms of vertical, lateral and roll accelerations of the sprung mass under harmonic and random roadway inputs and harmonic steering maneuver excitation.

The handling performance of a ground vehicle, under constant forward speed, can be fully described by the lateral, roll and yaw motions of the vehicle. While the yaw and lateral motions are determined from the yaw plane dynamics of the vehicle, the roll plane model yields the handling response in terms of lateral acceleration, lateral and roll motions of the sprung and unsprung masses. Since the lateral accelertion excitations encountered during a typical lane change or cornering maneuver can be approximated by a sinusoidal function, the response characteristics can be conveniently derived from the harmonic response of the vehicle models. Other external excitations causing suspension roll and swing, such as roadway disturbances with roll component, also affect the handling performance. In this thesis, the handling performance of the candidate vehicle is evaluated in terms of frequency response characteristics of the roll and lateral displacements of the sprung mass.

### 4.3.1 Response to Cornering Maneuver Induced Harmonic Lateral Acceleration Excitation

The frequency response characteristics of the candidate vehicle models are evaluated for a harmonic lateral acceleration excitation with magnitude of 0.3g, which represents the centrifugal acceleration encountered during a directional maneuver. The results are presented in terms of roll and lateral motions of the sprung mass in order to gain an insight into the handling and ride characteristics of the vehicle with respect to a steering input. Although typical steering maneuvers of the candidate highway bus occur at frequencies well below 0.5 Hz, the response characteristics are illustrated between 0 to 3 Hz to gain better understanding on the overall dynamic behavior of the vehicle in the vicinity of the sprung mass resonances. Equations (3.29) to (3.32) are solved to yield the frequency response characteristics of the sprung and unsprung masses using the parameters listed in Table 2.2, assuming zero inclination angle of the Panhard rod. Figures 4.1 and 4.2 illustrate the corresponding frequency response characteristics of the roll and lateral displacements and accelerations of the sprung and unsprung masses. It should be noted that the roll response of the sprung mass is evaluated about its roll center, and the resulting vertical motions of the sprung and unsprung masses are considerably small and negligible. The response characteristics derived from the simplified (model I) and comprehensive (model II) models are also compared to investigate the influence of inertial and compliant properties of the Panhard rod. The results show that the two analytical models exhibit almost identical frequency response characteristics under specified lateral acceleration excitation. The similarity of the two models is attributed to insignificant contribution of very small inertia of the rod, and high stiffness of the bushings. It can thus be concluded that the lateral dynamics of the vehicle can be effectively analyzed assuming rigid Panhard rod constraint.

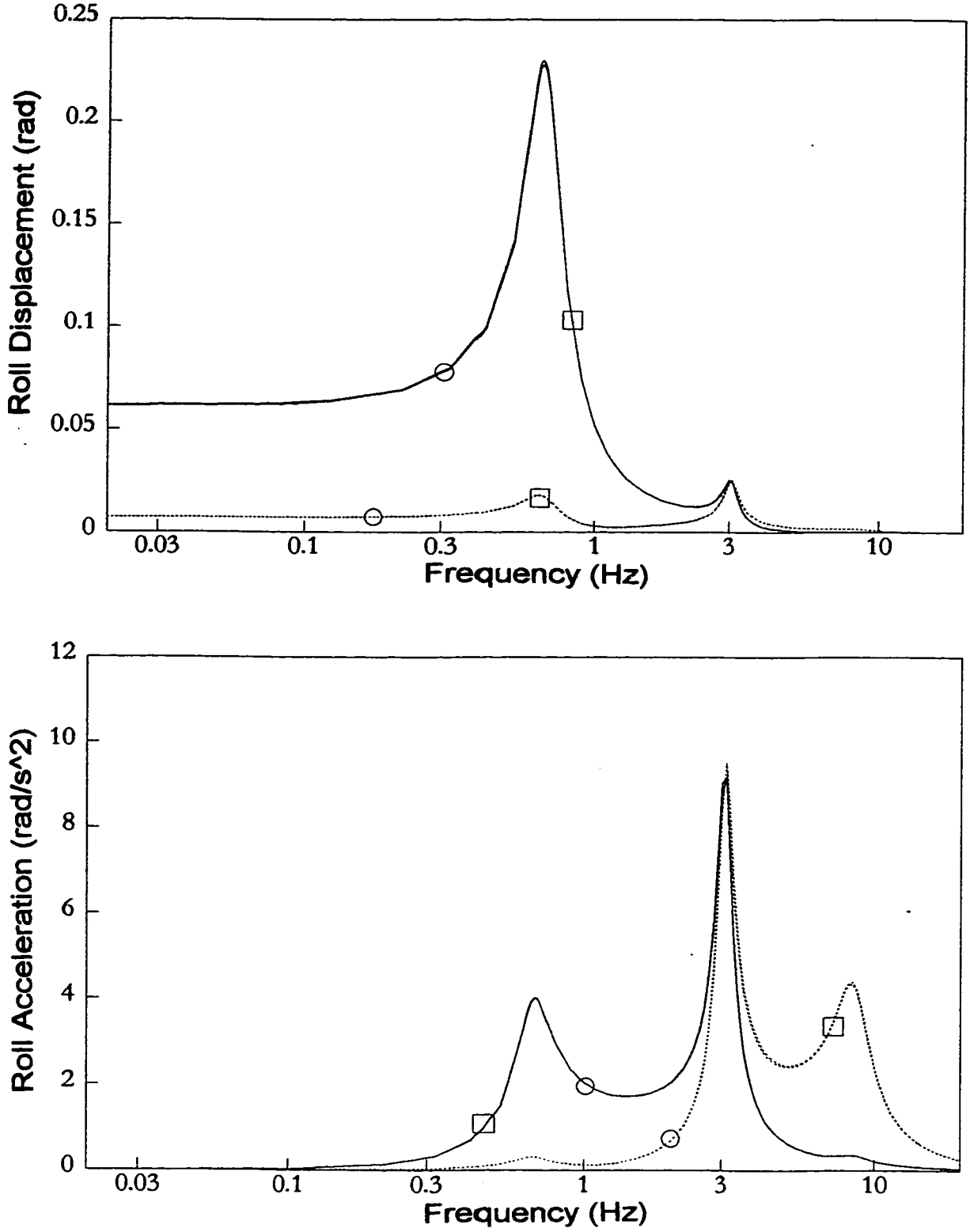


Figure 4.1 Roll response characteristics of the sprung and unsprung masses (——— sprung mass ····· unsprung mass; □ model I, O model II; Excitation: 0.3g lateral acceleration harmonic)

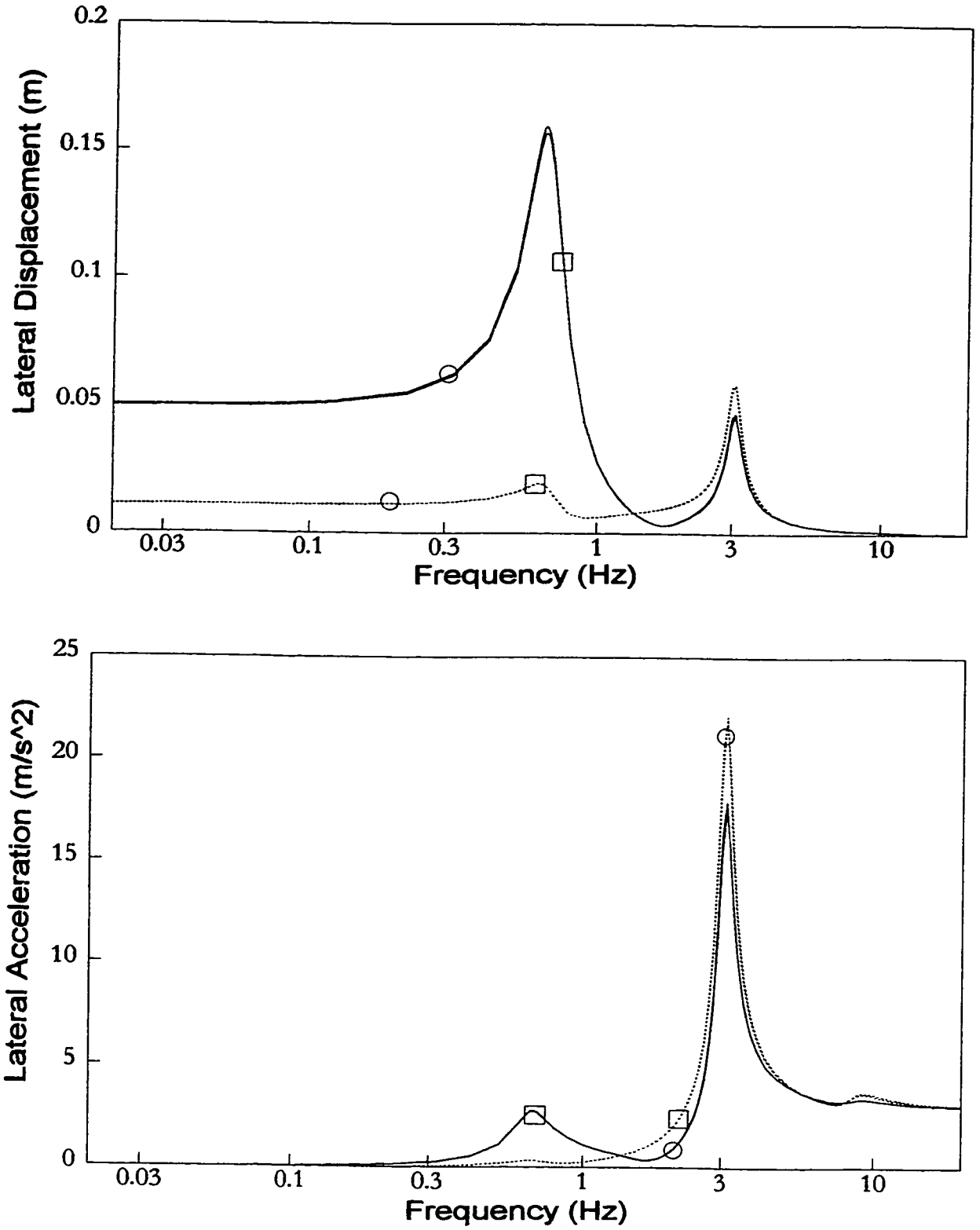


Figure 4.2 Lateral response characteristics of the sprung and unsprung masses (——— sprung mass ····· unsprung mass; □ model I, O model II; Excitation: 0.3g lateral acceleration harmonic)

The roll displacement and acceleration frequency response characteristics, illustrated in Figure 4.1, exhibit peak roll displacement of approximately 12.6 degrees of the sprung mass in the vicinity of its roll resonant frequency, 0.67 Hz. The static roll angle of the sprung mass under harmonic lateral acceleration excitation is observed to be near 3.4 degrees. The unsprung mass roll displacement response exhibits peaks near sprung mass roll and lateral mode natural frequencies. The peak unsprung mass roll displacement of approximately 1.4 degrees occurs near the lateral mode resonant frequency of the sprung mass, 3.1 Hz. Although the results show considerably high roll acceleration peaks of the sprung and unsprung masses (approximately 9 rad/$s^2$ ) in the vicinity of 3.1 Hz, this frequency is well above the steering frequencies encountered during typical maneuvers. Since most steering frequencies occur well below 0.5 Hz, the roll angle response in the 0 - 0.5 Hz needs to be specifically examined to study the handling related dynamic behavior of the vehicle. The peak roll angle response of the sprung and unsprung masses in this frequency range are approximately 7.2 and 0.4 degrees, respectively. The corresponding roll response accelerations of the sprung and unsprung masses are observed to be well below 2 m/$s^2$ and 1 m/$s^2$ , respectively.

The lateral displacement and acceleration response characteristics of the sprung mass, as shown in Figure 4.2, exhibit distinct peaks corresponding to the roll and lateral resonant frequencies of the sprung mass, respectively. The lateral displacement and acceleration response of the unsprung mass also reveals significant peaks in the vicinity of the sprung mass lateral resonant frequency. The frequency response characteristics also reveal that the static displacement of the sprung and unsprung masses under 0.3g lateral acceleration are approximately 0.05 m and 0.01 m, respectively. The sprung mass experiences a peak displacement of approximately 0.14 m and peal acceleration of 3.0 m/$s^2$ near its roll resonant frequency 0.67 Hz. The peak acceleration response of the sprung and unsprung masses approach nearly 18 m/$s^2$ and 22 m/$s^2$ in the vicinity of the

sprung mass lateral resonant frequency (3.1 Hz). This high acceleration response may be considered less important for handling analysis, since the dominant steering frequencies occur at frequencies well below 3.1 Hz.

### 4.3.2 Response to Harmonic Roll Excitation due to Road Unevenness

The frequency response characteristics of the two vehicle models, developed in Chapter 3, are evaluated for out-of-phase harmonic road excitations of constant displacement amplitude of 0.01 m. Equation (3.34) is solved using the parameters listed in Table 2.2 and zero Panhard rod installation angle. The roll response of the sprung mass are presented about the suspension roll center, while the roll responses of the unsprung mass are presented about its cg. The corresponding amplitudes of roll and lateral displacement and acceleration response characteristics of the sprung and unsprung mass masses are illustrated in Figures 4.3 and 4.4, respectively. The results show that the two analytical models yield identical frequency response characteristics, at frequencies below 3.5 Hz, while only small differences are observed at higher excitation frequencies, which is attributed to the compliant bushings of the Panhard rod. It can thus be concluded that the contributions due to the Panhard rod inertia and the compliance of the bushings are insignificant under excitations arising from the tire-road interaction.

The roll displacement and acceleration response characteristics of the sprung and unsprung masses of the vehicle subject to out-of-phase harmonic road excitations, shown in Figure 4.3, exhibit peaks near the roll (0.67 Hz) and lateral (3.1 Hz) resonant frequencies of the sprung mass and the roll resonant frequency (8.5 Hz) of the unsprung mass. The coupling between the roll and lateral modes, caused by the Panhard rod constraint, is clearly evident from the frequency response characteristics derived for both analytical models. While the sprung mass experiences large roll deflection at low

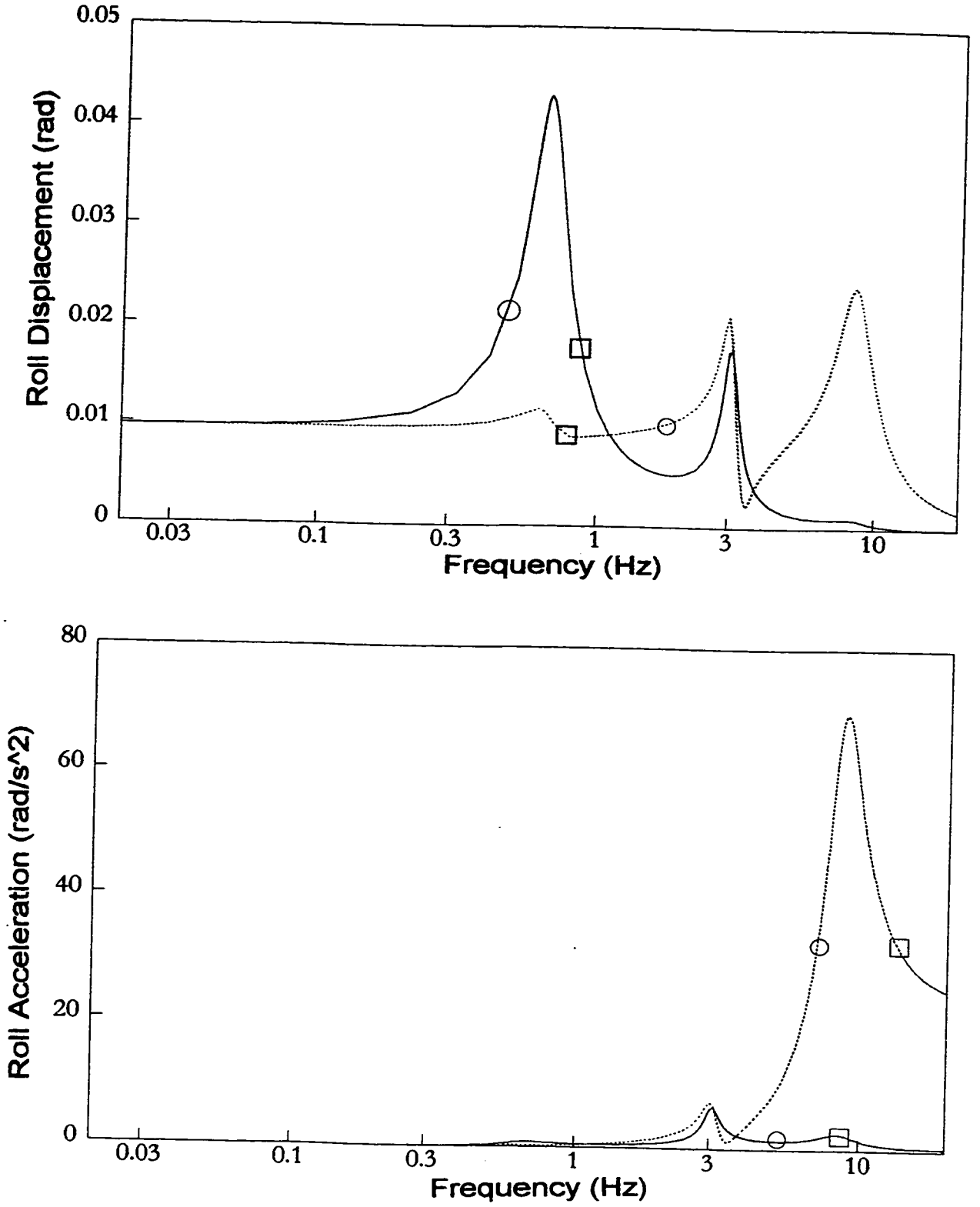


Figure 4.3 Roll response characteristics of the sprung and unsprung masses (——— sprung mass ····· unsprung mass; □ model I, O model II; Excitation: 0.01 m harmonic out-of-phase displacement)

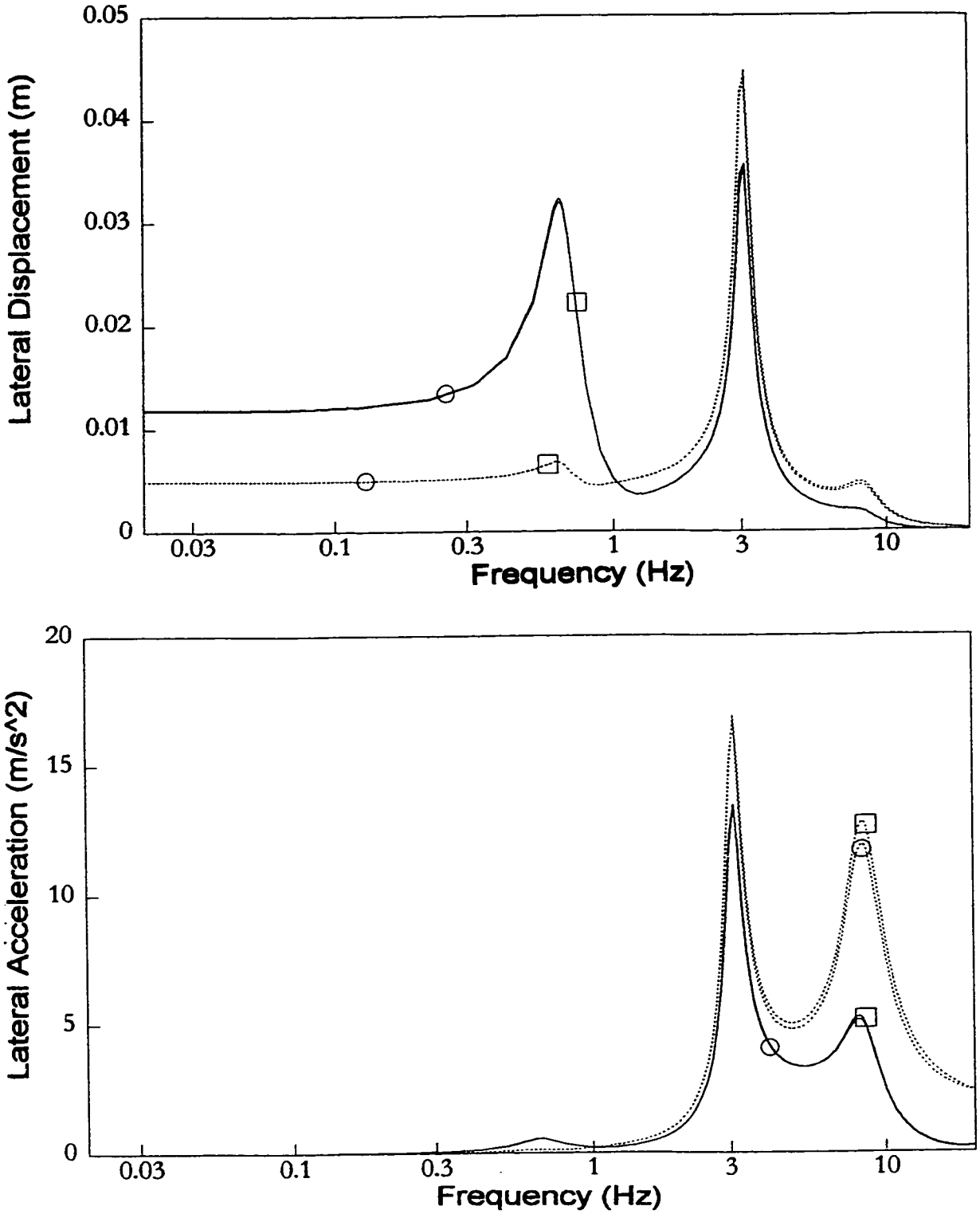


Figure 4.4 Lateral response characteristics of the sprung and unsprung masses (——— sprung mass ····· unsprung mass; □ model I, ○ model II; Excitation: 0.01 m harmonic out-of-phase displacement)

frequencies near its roll resonance, high roll deflections of the unsprung mass occur in the vicinity of lateral mode resonance of the sprung mass and the roll resonant frequency of the unsprung mass. The acceleration response of the unsprung mass thus approaches very high magnitude at higher frequencies. The high roll deflections of both sprung and unsprung masses near the lateral mode resonance of the sprung mass are mostly attributed to the kinematic constraint imposed by the transverse Panhard rod.

The lateral displacement and acceleration response characteristics of the sprung and unsprung masses of both analytical models exhibit peaks in the vicinity of roll and lateral resonant frequencies of the sprung mass, and roll resonant frequency of the unsprung mass, as shown in Figure 4.4. The sprung and unsprung masses both exhibit high magnitude lateral displacement and acceleration peaks near the lateral resonant frequency of the sprung mass (3.1 Hz).

## 4.4 Response to Random Road Excitation

The results presented in section 4.3 clearly revealed that the contributions due to compliance of the bushings and the Panhard rod are relatively insignificant. The ride and handling analysis of a beam-axle suspension with Panhard rod constraint can thus be performed using the simplified five-DOF model based upon rigid Panhard rod. The ride response characteristics of the candidate bus to realistic random excitations arising from the road roughness are thus evaluated using the simplified model. Equations (3.35) to (3.36) are solved to determine the power spectral densities (PSD) of the displacement and acceleration coordinates under Gaussian distributed random road profile with random phase between the left- and right-tire-road interface. The response characteristics are evaluated under excitations arising from a rough road, as described in Chapter 3. The

random phase between the left- and right-tire tracks is introduced to represent the cross-slope of the road, as discussed earlier in section3.

Figures 4.5 to 4.10 illustrate the PSD of vertical, roll and lateral displacement and acceleration response of the sprung and unsprung masses in the frequency range of 0.1 to 20 Hz. It should be noted that the vertical and lateral response presented in the figures represents the motion of the cg of the sprung and unsprung masses, while the roll response of the sprung mass is presented about the roll center. The PSD characteristics of the vertical displacement response of the sprung mass exhibit a peak near the vertical resonant frequency (1.2 Hz) of the sprung mass, while the PSD characteristics of its acceleration response show peaks near both vertical resonant frequencies of the sprung mass (1.2 Hz) and unsprung mass (7.4 Hz), as illustrated in Figure 4.5. The unsprung mass yields high amplitude vertical displacement response PSD peaks near the vertical resonant frequencies of the sprung mass (1.2 Hz) and the unsprung mass (7.4 Hz), while its acceleration response PSD peak is shown near its vertical resonant frequency (7.4 Hz), as presented in Figure 4.6. The PSD characteristics of the roll and lateral displacement response of the sprung mass exhibit peaks near the dominant roll (0.66 Hz) and the lateral (3.07 Hz) resonant frequencies of the sprung mass, while their acceleration response PSD characteristics show peaks near the dominant lateral resonant frequency of the sprung mass (3.07 Hz) and the roll resonant frequency of the unsprung mass (8.5 Hz), as illustrated in Figures 4.7 and 4.9. The roll displacement response PSD characteristics of the unsprung mass presents the peaks near the roll (0.66 Hz), lateral (3.07 Hz) resonant frequencies of the sprung mass, and the roll resonant frequency of the unsprung mass (8.5 Hz), while its acceleration response PSD characteristics show a significant peak near the roll resonant frequency of the unsprung mass (8.5 Hz), as illustrated in Figure 4.8. The lateral displacement and acceleration response of the unsprung mass show similar resonant

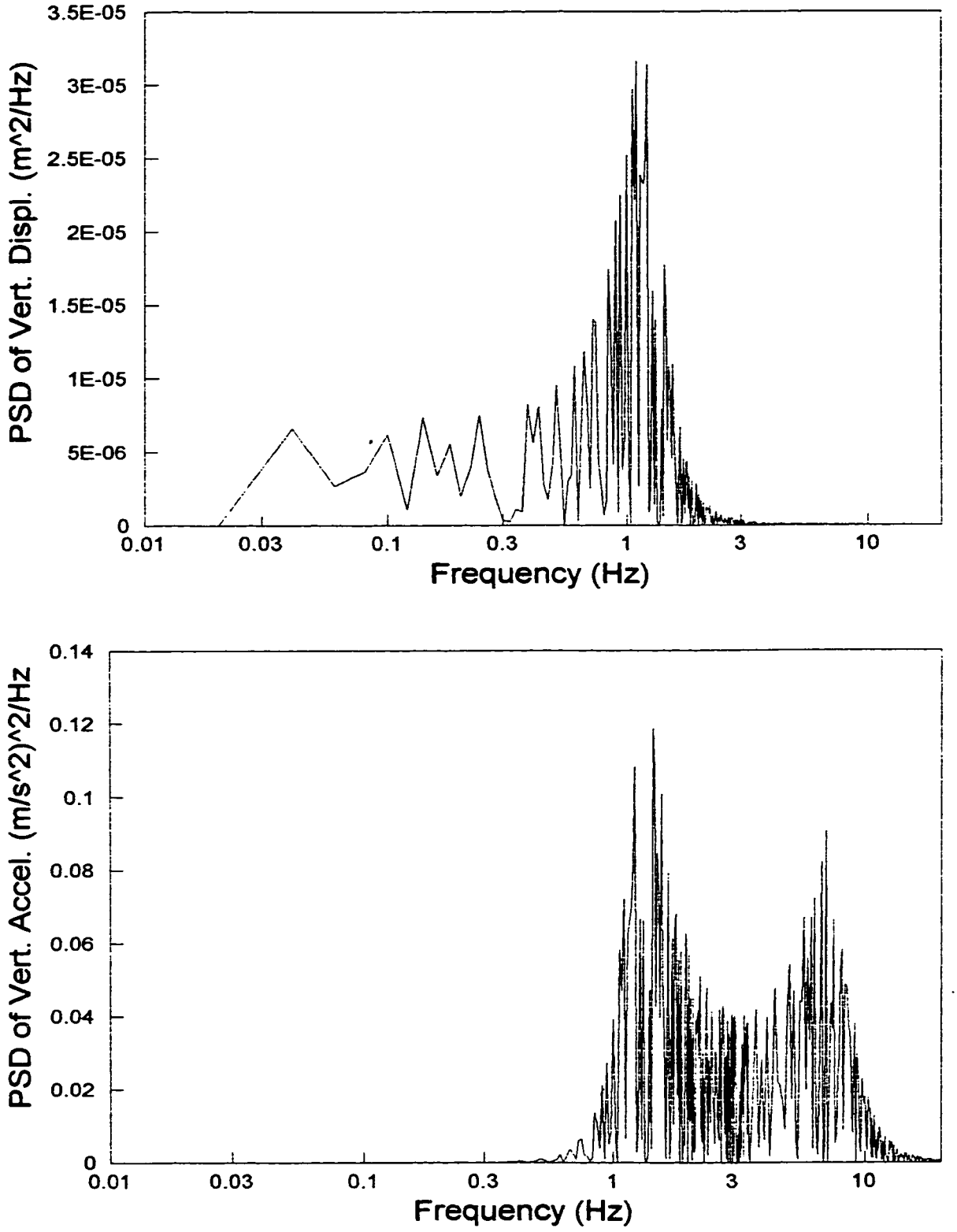


Figure 4.5 PSD of vertical displacement and acceleration of the sprung mass for rough random road with random cross-slope between left and right wheels.

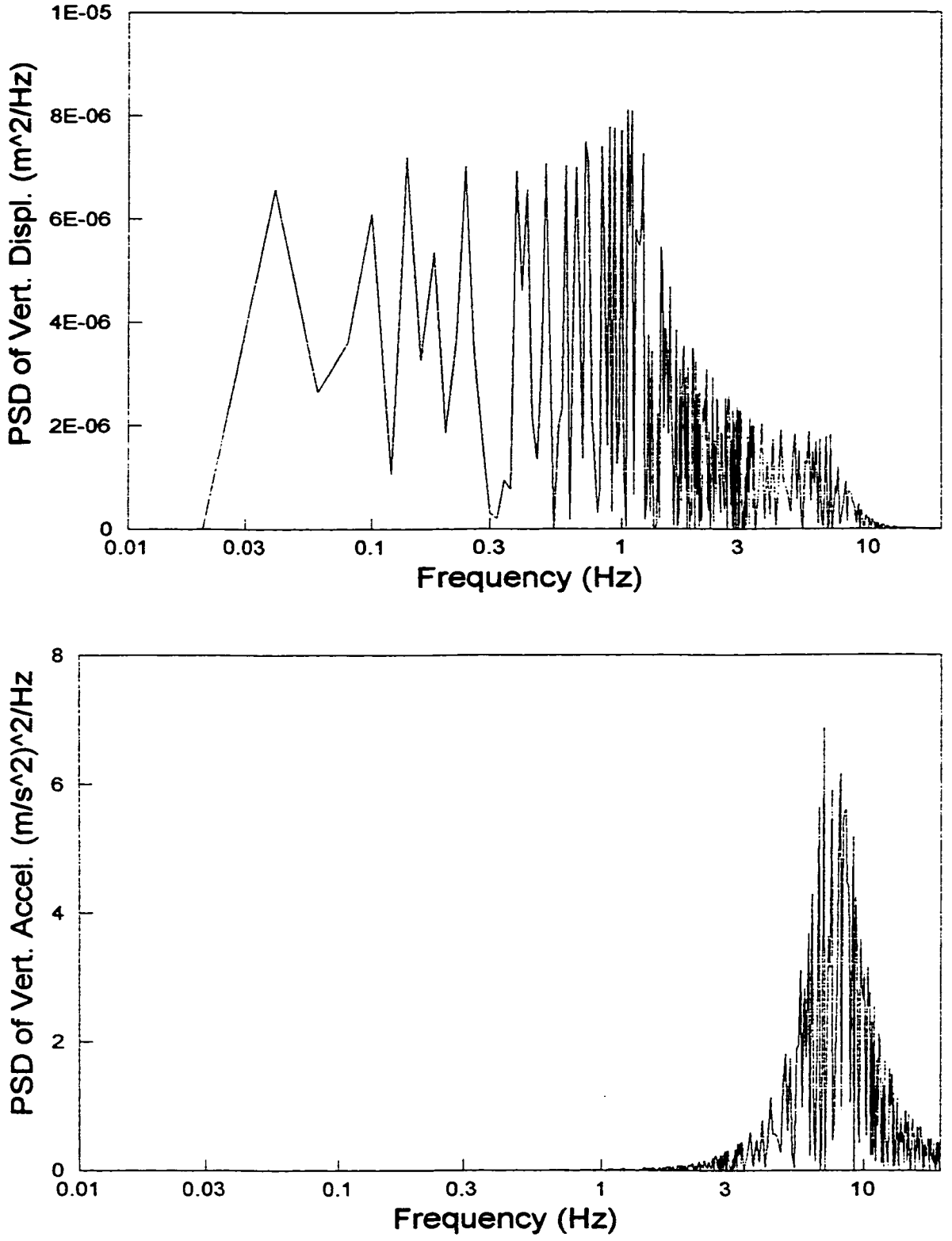


Figure 4.6 PSD of vertical displacement and acceleration of the unsprung mass for rough random road with random cross-slope between left and right wheels.

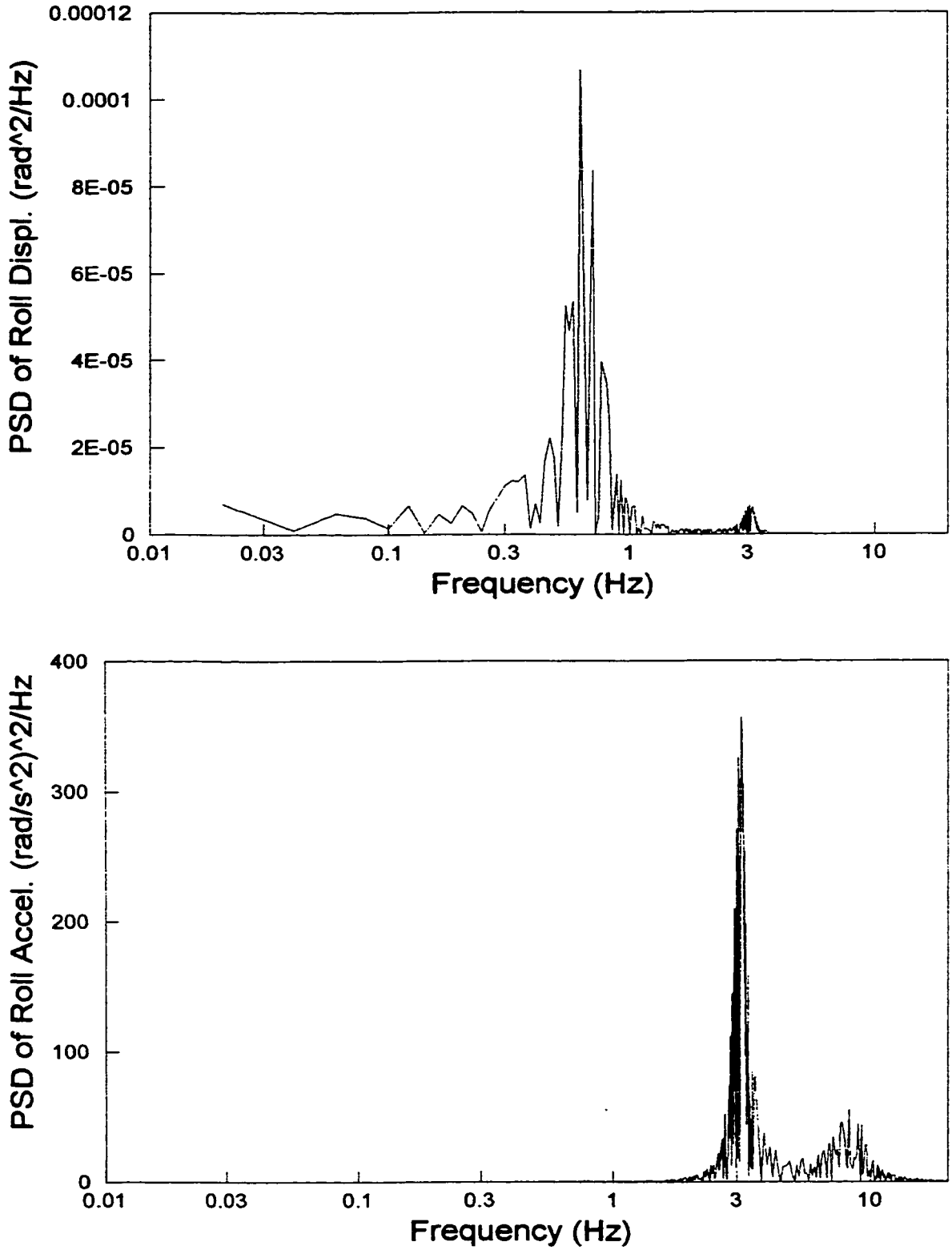


Figure 4.7 PSD of roll displacement and acceleration of the sprung mass for rough random road with random cross-slope between left and right wheels.

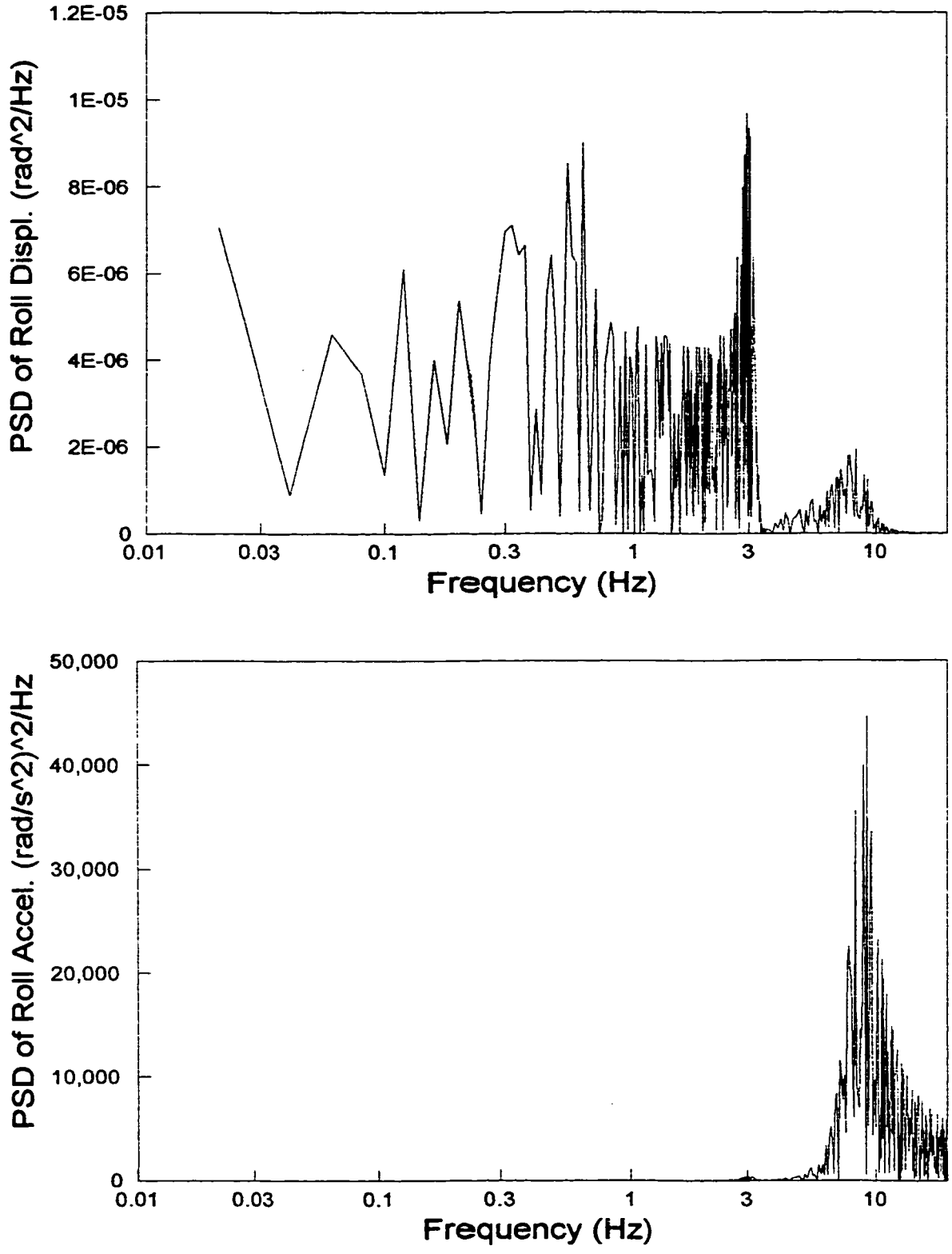


Figure 4.8 PSD of roll displacement and acceleration of the unsprung mass for rough random road with random cross-slope between left and right wheels.

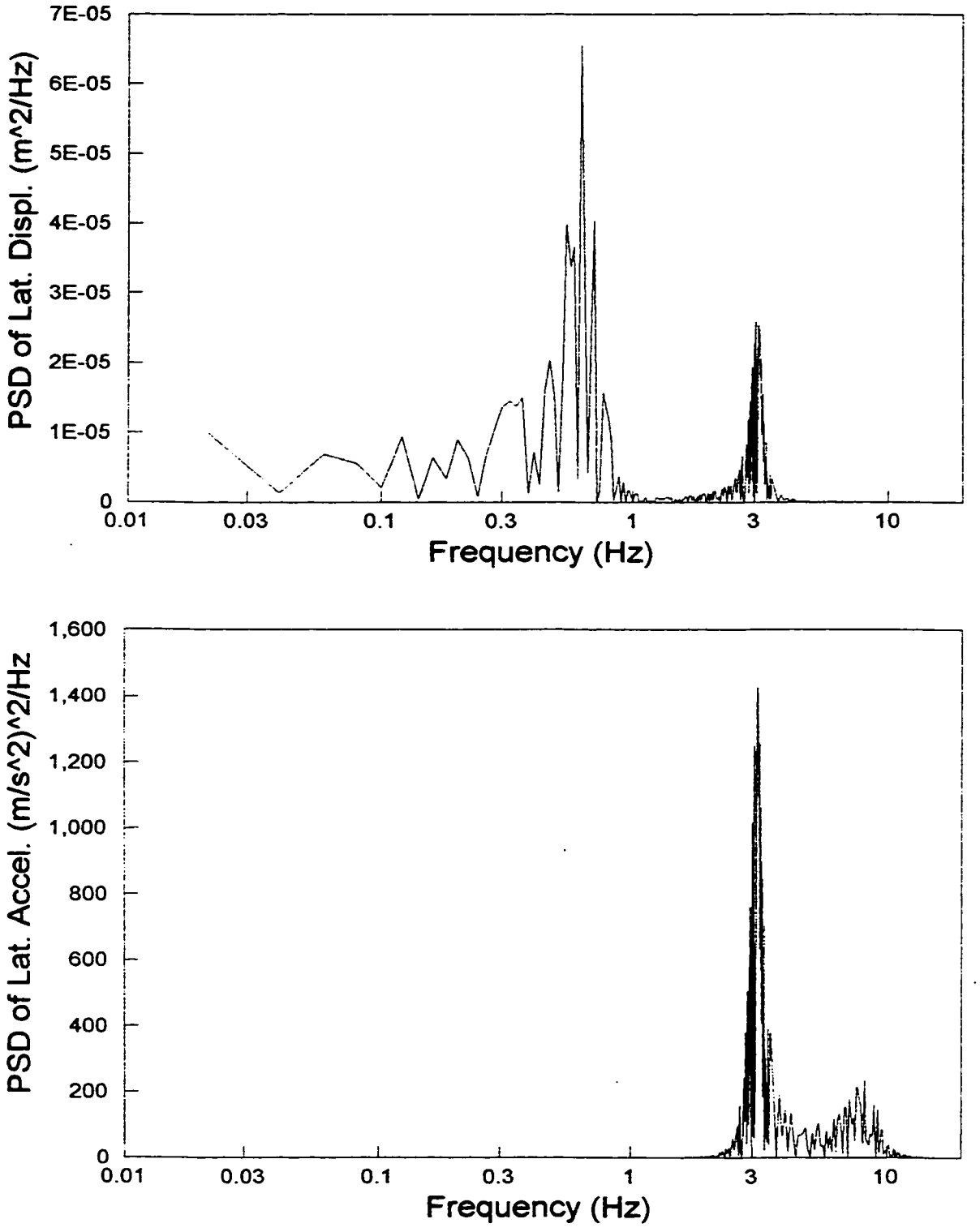


Figure 4.9 PSD of lateral displacement and acceleration of the sprung mass for rough random road with random cross-slope between left and right wheels.

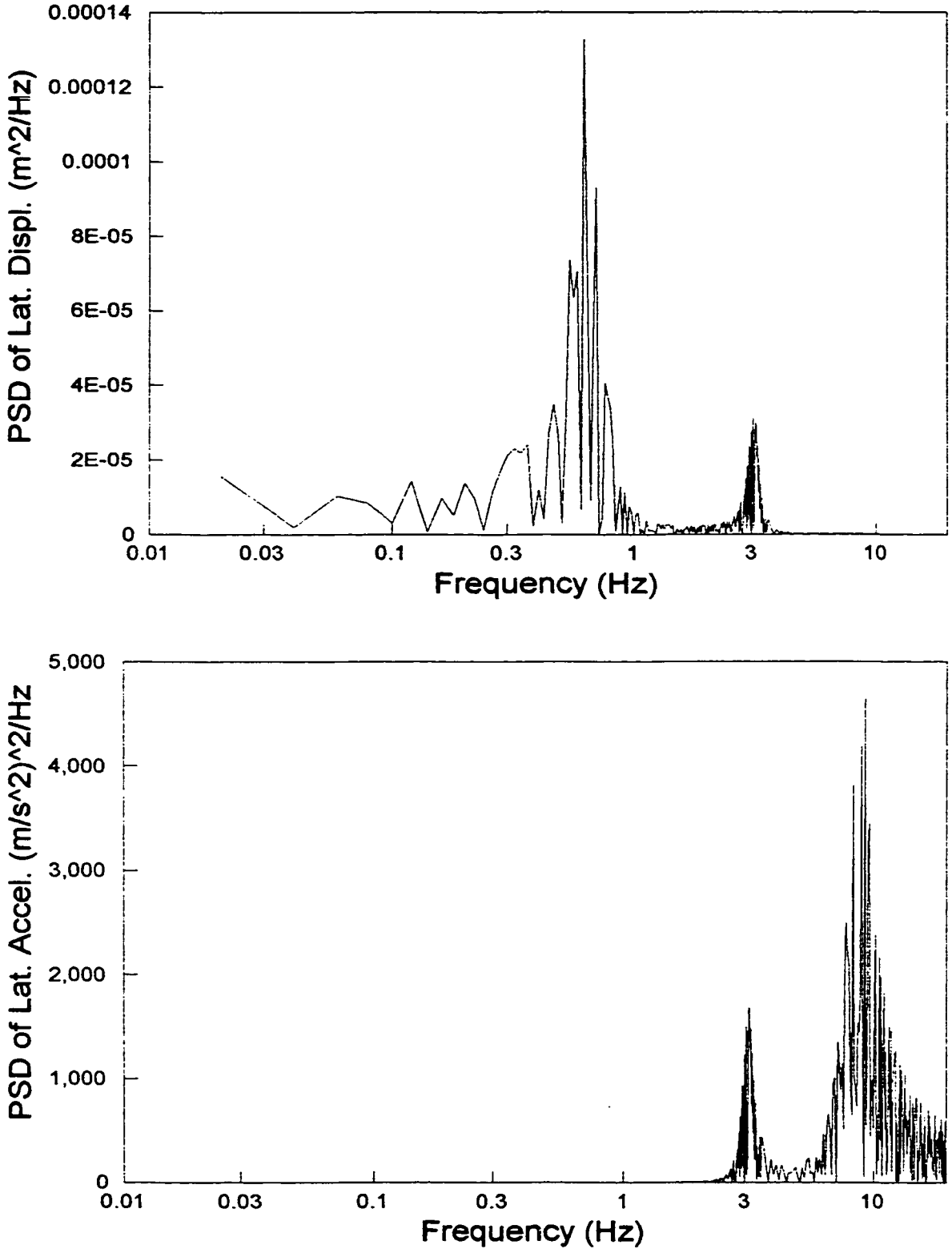


Figure 4.10 PSD of lateral displacement and acceleration of the unsprung mass for rough random road with random cross-slope between left and right wheels.

characteristics as that of the sprung mass, except for the acceleration response is dominated by the roll resonant frequency of the unsprung mass, as shown in Figure 4.10.

## 4.5 Influence of Suspension Parameters on Dynamic Response Characteristics

The handling and ride performance characteristics of a road vehicle are directly influenced by the suspension and tire properties, geometry, load, and Panhard rod property etc. Sensitivity of system parameters on the suspension performance is studied based on the simplified five-DOF analytical model with variations in a single parameter at a time. The results of this study are utilized to gain understanding of the effect of Panhard rod with respect to varying system parameters on the ride and handling performance of the candidate vehicle. The variations in the design parameters considered in the study include:

1. Suspension spring rate,
2. Suspension damping rate,
3. Tire vertical stiffness rate,
4. Sprung weight,
5. Vehicle speed,
6. Road roughness.

The variations in ride and handling performance characteristics with variations in the above design parameters are evaluated under lateral harmonic acceleration excitation arising from directional maneuver, harmonic out-of-phase roadway excitation and Gaussian random road excitation with random crosslope between the left and the right tire-road interface. Since ride and handling performance of a road vehicle is mostly related to the dynamic behavior of the sprung mass, the investigation carried out in the following

sections is concentrated on the sprung mass dynamics alone. Equations (3.29) to (3.32) are solved to yield the frequency response amplitudes of the sprung mass under 0.3g lateral acceleration excitation. Equations (3.34) to (3.36) are solved to yield the frequency response amplitudes and the random response of the sprung mass under 0.01 harmonic out-of-phase and random road excitations, respectively. For random vibration analysis, the vehicle is assumed to operate at 110 km/h and a relatively rough profile is selected. The nominal design parameters are taken as those presented in Table 2.2. Since the vertical response amplitudes of the sprung mass under given excitations are insignificant, the results are presented in terms of lateral and roll response of the sprung mass. The roll response of the sprung mass are derived with respect to the suspension roll center, while the vertical and lateral response represent the motion at the cg.

### 4.5.1 Influence of Suspension Spring Rate

The influence of the suspension spring rate on the ride and handling performance characteristics of the suspension are investigated by varying the spring rate from 350 kN/m to 1050 kN/m, while the nominal value is 480 kN/m. The response characteristics of the sprung mass under 0.3g harmonic lateral acceleration excitation, harmonic out-of-phase and random road excitations are illustrated in Figure 4.11 to 4.18. Since the effective roll stiffness is directly related to the suspension spring rate, the variations in the spring rate affect the roll and lateral dynamics of the vehicle in a significant manner. The suspension spring affects the roll and lateral response behaviour of the sprung mass most significantly under lateral acceleration excitations at frequencies below 2.0 Hz, as shown in Figures 4.11 and 4.12. The results show that the roll and lateral displacements and accelerations of the sprung mass exhibit peaks at frequencies attributed to the sprung mass roll and lateral resonant frequencies, which tend to increase with increase in spring rate. The increase in roll stiffness due to increase in spring rate, 480 kN/m to 1050 kN/m, yields

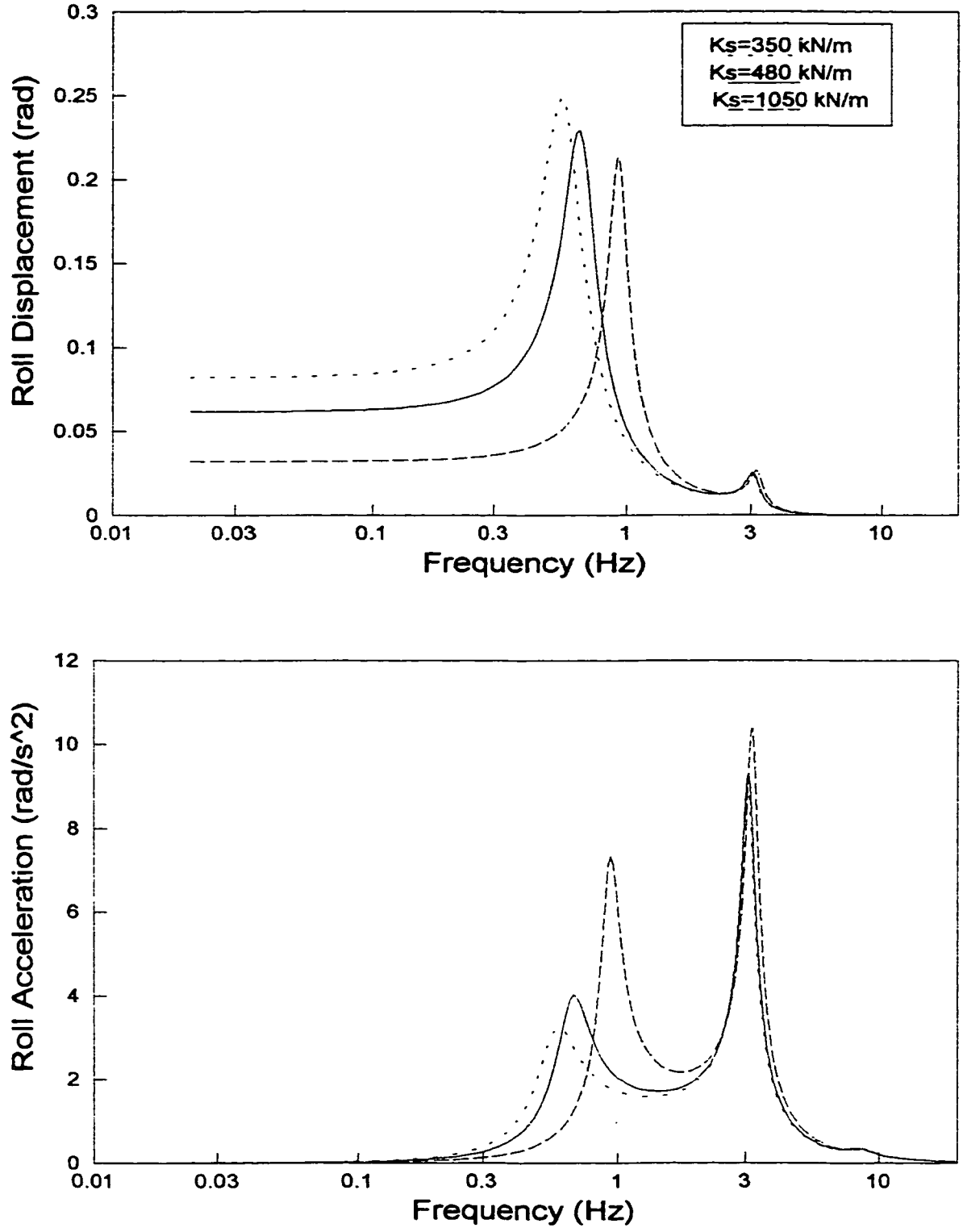


Figure 4.11 Influence of suspension stiffness on the roll response characteristics of the sprung mass (Excitation: 0.3g harmonic lateral acceleration)

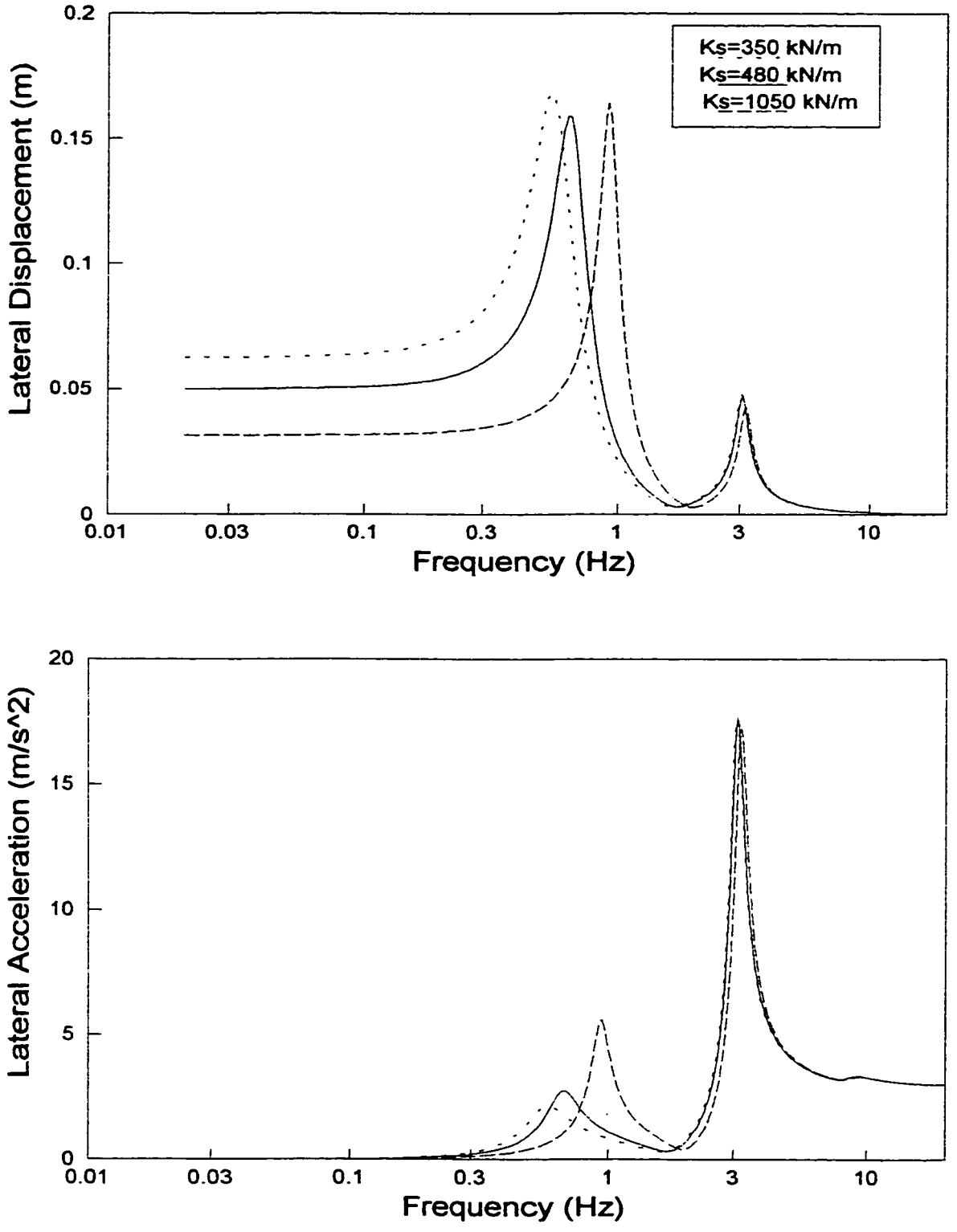


Figure 4.12 Influence of suspension stiffness on the lateral response characteristics of the sprung mass (Excitation: 0.3g harmonic lateral acceleration)

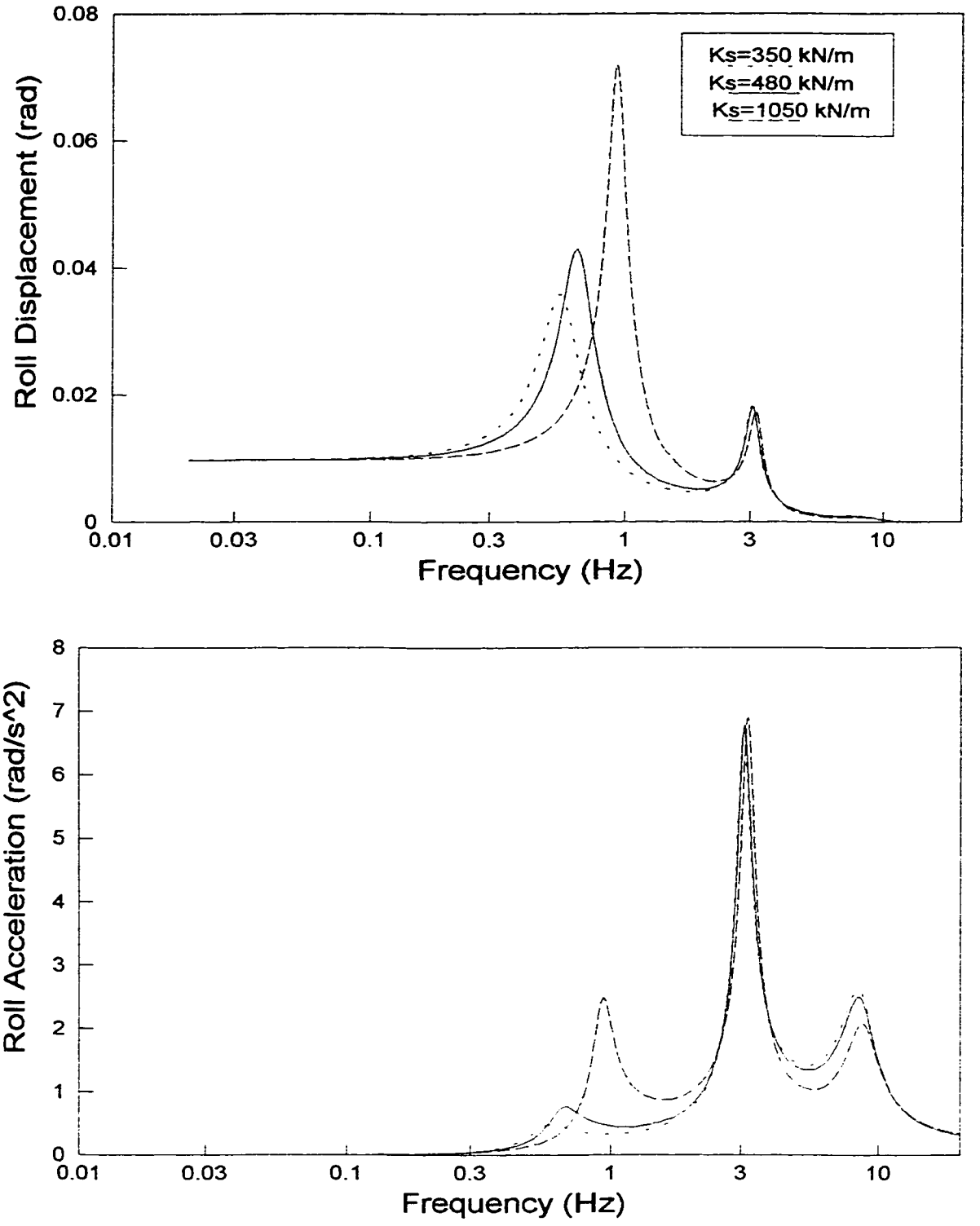


Figure 4.13 Influence of suspension stiffness on the roll response characteristics of the sprung mass (Excitation: 0.01 m harmonic out-of-phase displacement)

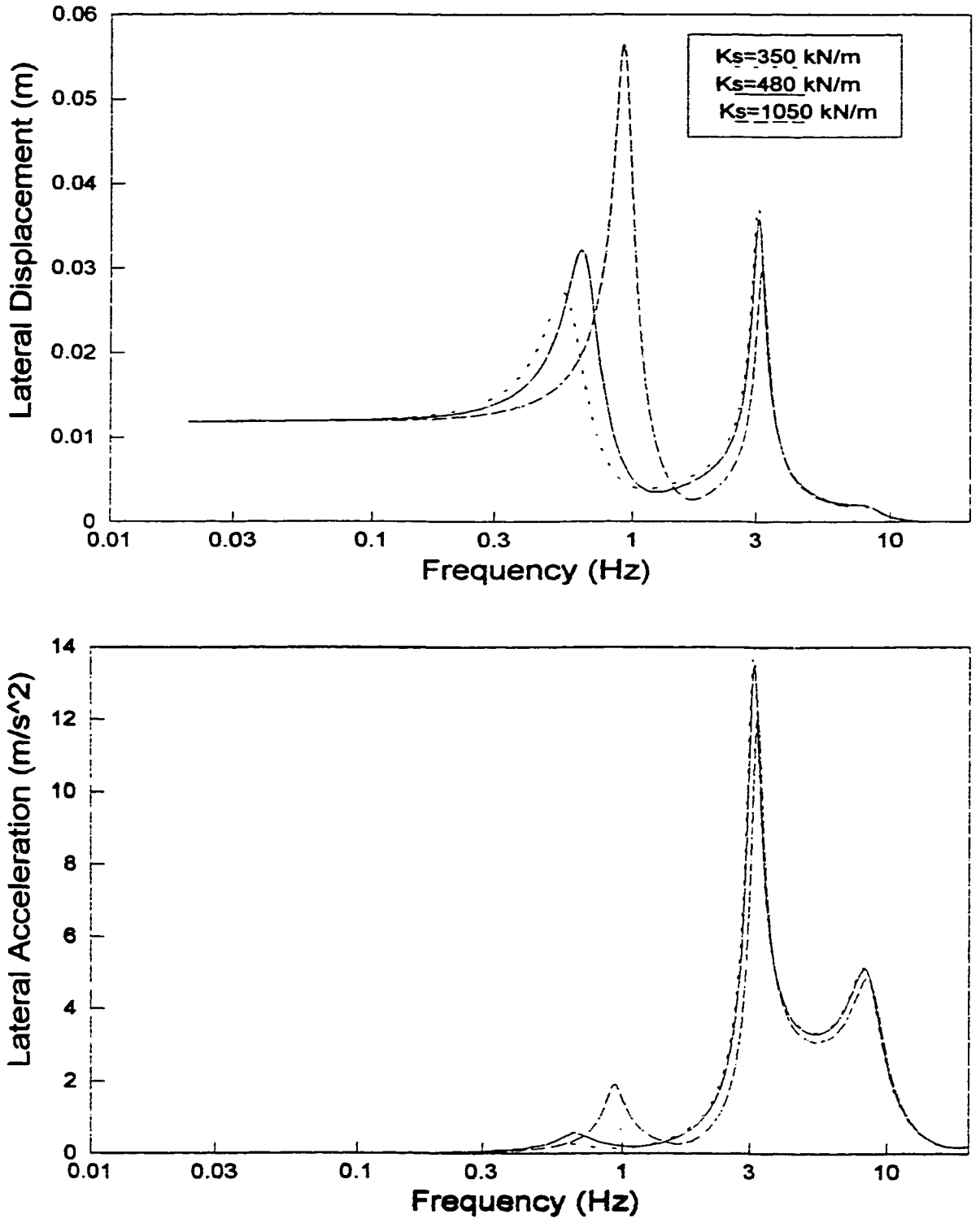


Figure 4.14 Influence of suspension stiffness on the lateral response characteristics of the sprung mass (Excitation: 0.01 m harmonic out-of-phase displacement)

an considerable increase in the sprung mass roll natural frequency from 0.56 Hz to 0.92 Hz. The influence of the suspension spring rate on the lateral mode natural frequency, however, is nsignificant. Frequency response characteristics further reveal that a stiffer suspension spring yields lower roll displacement due to increased roll stiffness. The static roll and lateral deflections of the sprung mass also decrease when the suspension stiffness is increased. Since the directional maneuvers are invariably performed at lower frequencies (well below 0.5 Hz), the stiffer suspension spring rate can yield improved handling performance. The corresponding magnitudes of roll and lateral acceleration peaks of the sprung mass, however, tend to increase due to increase in the roll and lateral natural frequencies. The enhancement of driver/passenger ride quality may thus necessitate the use of soft suspension springs.

The influence of the suspension spring rate on the ride and handling performance of the vehicle subject to constant displacement out-of-phase harmonic roadway excitation is displayed in Figures 4.13 and 4.14. The peak magnitudes of roll and lateral displacements in the vicinity of the roll resonant frequencies tend to increase with increase in suspension roll stiffness, as observed earlier in Figures 4.11 and 4.12. The road excitations also tend to excite the unsprung mass roll mode, which is apparent in the acceleration response near 8.5 Hz. It should be noted that the variations in the spring rate affect the sprung mass response mostly in the vicinity of its roll resonant frequency, while the effects at higher frequencies are minimal.

The influence of variations in suspension spring rate, from 380 kN/m to 1050 kN/m, on the suspension ride performance is further investigated under Gaussian random road excitation with random phase between the left- and right-tire-road interface. The PSD characteristics of the roll and lateral displacement and acceleration response of the sprung mass are presented in Figures 4.15 and 4.18. The dominant peak amplitudes of the

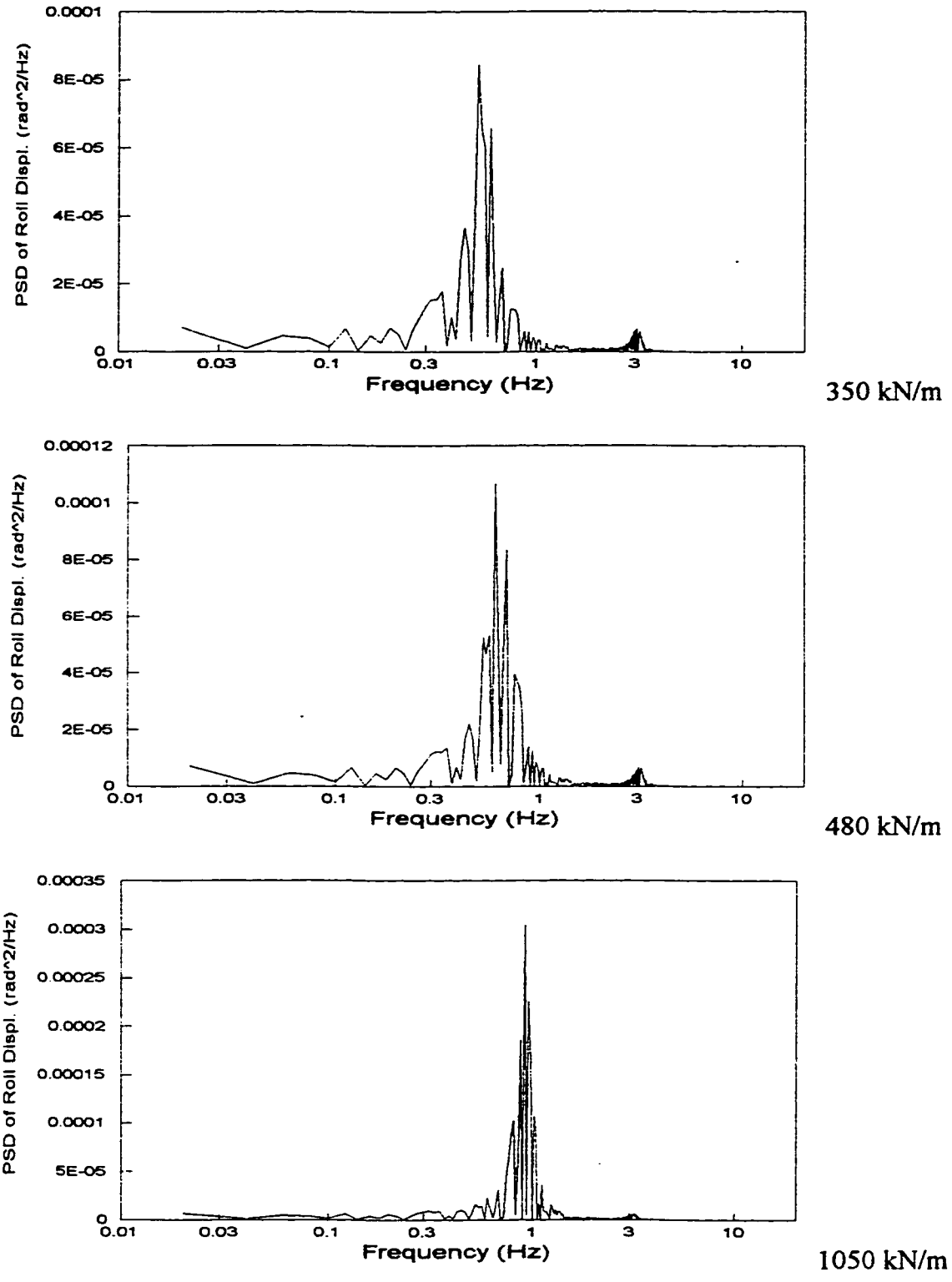


Figure 4.15 Influence of suspension stiffness on PSD of roll displacement of the sprung mass for rough random road with random cross-slope between left and right wheels.

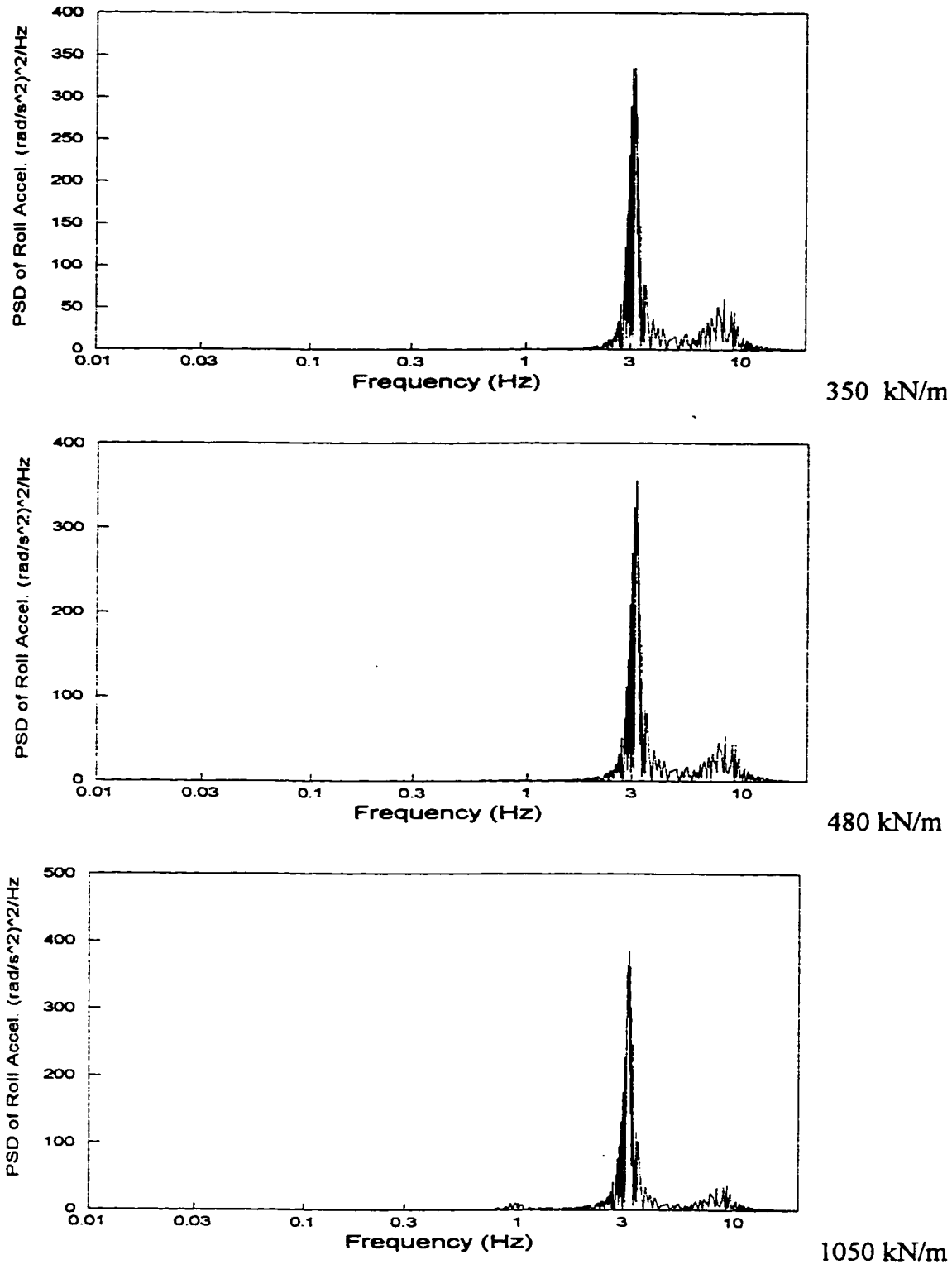


Figure 4.16 Influence of suspension stiffness on PSD of roll acceleration of the sprung mass for rough random road with random cross-slope between left and right wheels.

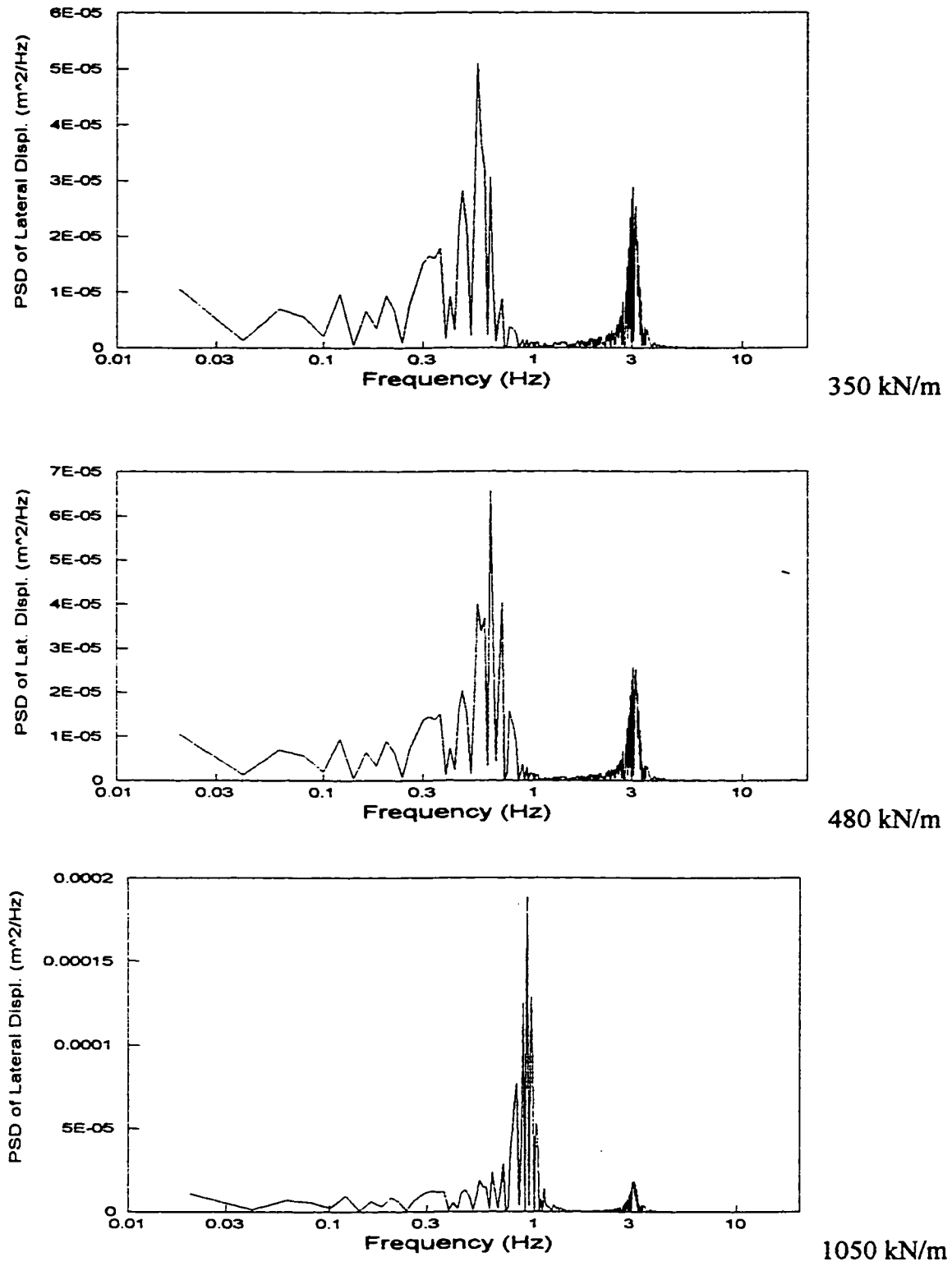


Figure 4.17 Influence of suspension stiffness on PSD of lateral displacement of the sprung mass for rough random road with random cross-slope between left and right wheels.

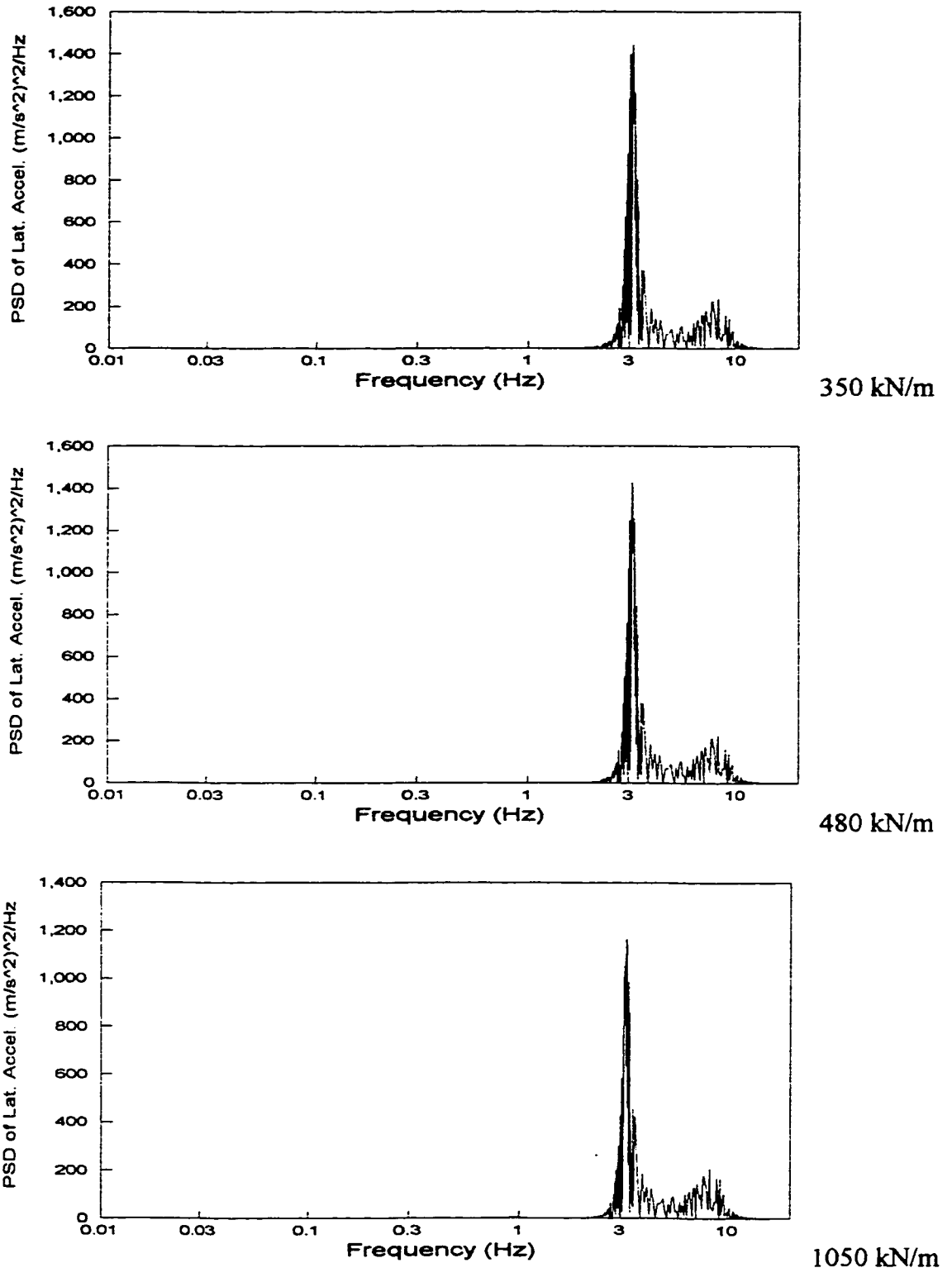


Figure 4.18 Influence of suspension stiffness on PSD of lateral acceleration of the sprung mass for rough random road with random cross-slope between left and right wheels.

roll displacement and acceleration response PSD of the sprung mass near the roll (for displacement) and lateral (for acceleration) resonant frequencies of the sprung mass tend to increase with increase in the spring rate, while the peak amplitudes near the lateral resonant frequency of the sprung mass (for displacement) and the roll resonant frequency of the unsprung mass (for acceleration) tend to decrease with increase in the spring rate, as shown in Figures 4.15 and 4.16. The dominant peak magnitude of the lateral displacement response PSD of the sprung mass near its roll natural frequency increases with increase in the suspension spring rate, while the peak value in the vicinity of its lateral resonant frequency decreases accordingly, as displayed in Figure 4.17. The dominant peak value of the lateral acceleration response of the sprung mass corresponding to its lateral resonant frequency tends to decrease with increase in the spring rate, while the peak magnitude near the unsprung mass roll resonant frequency is not apparently affected by the spring rate, as illustrated in Figure 4.18.

### 4.5.2 Influence of Suspension Damping

The ride and handling performance of a road vehicle is strongly dependent upon the effective suspension damping. Adequately damped suspensions effectively suppress the resonant peaks, while lightly damped suspensions yield better vibration isolation in the ride frequency range. Figures 4.19 to 4.26 illustrate the influence of suspension damping on the ride and handling performance of the vehicle subject to excitation arising from the steering maneuvers and tire-road interactions. Figures 4.19 and 4.20 illustrate the roll and lateral dynamic response of the sprung mass under a 0.3g centrifugal acceleration excitation for different damping coefficients varying from 28.12 kN.s/m to 48.69 kN.s/m. The results clearly show that the magnitudes of peak roll and lateral displacements occurring in the vicinity of respective resonant frequencies tend to decrease considerably with increase in suspension damping coefficient. The variations in suspension damping

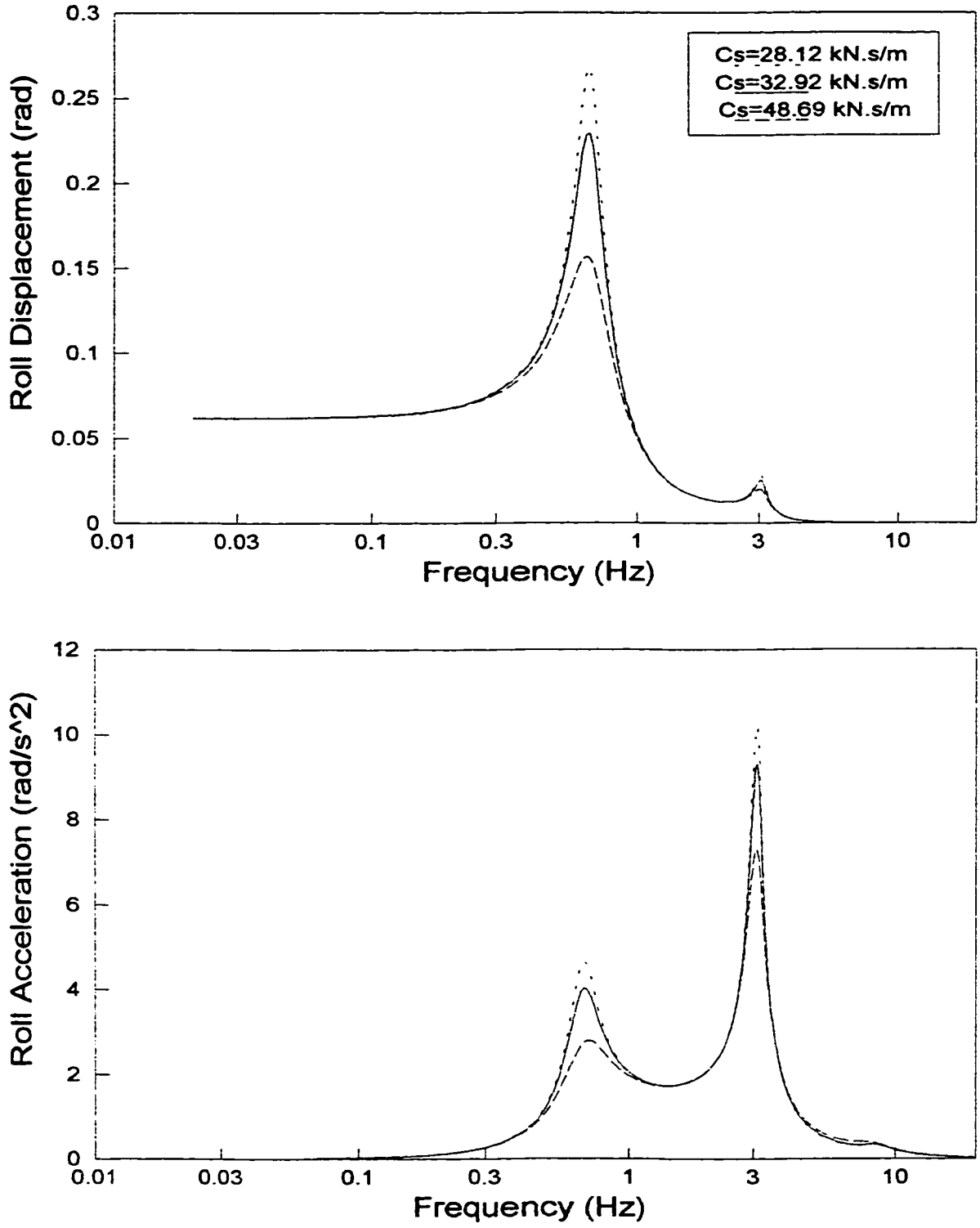


Figure 4.19 Influence of suspension damping on the roll response characteristics of the sprung mass (Excitation: 0.3g harmonic lateral acceleration)

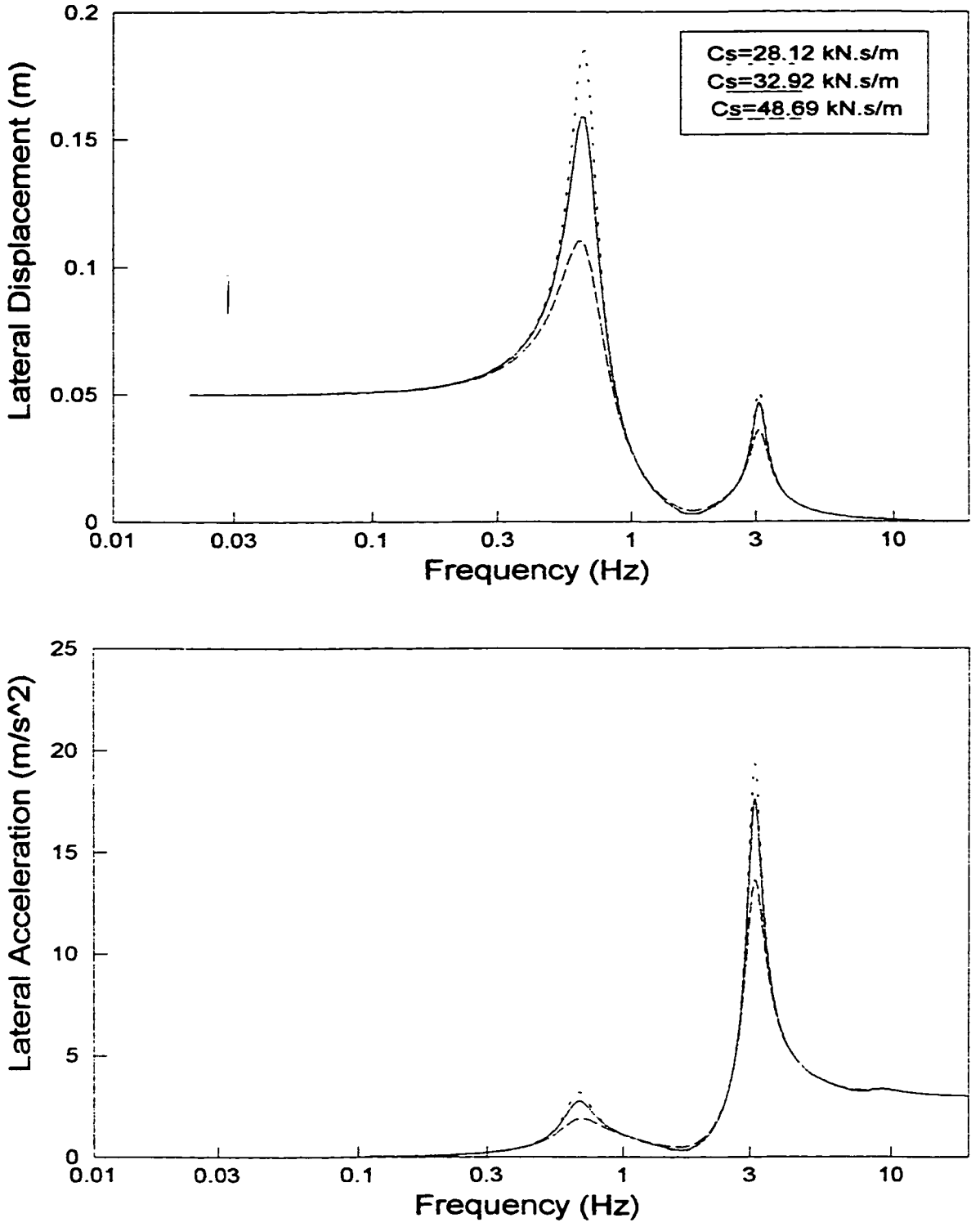


Figure 4.20 Influence of suspension damping on the lateral response characteristics of the sprung mass (Excitation: 0.3g harmonic lateral acceleration)

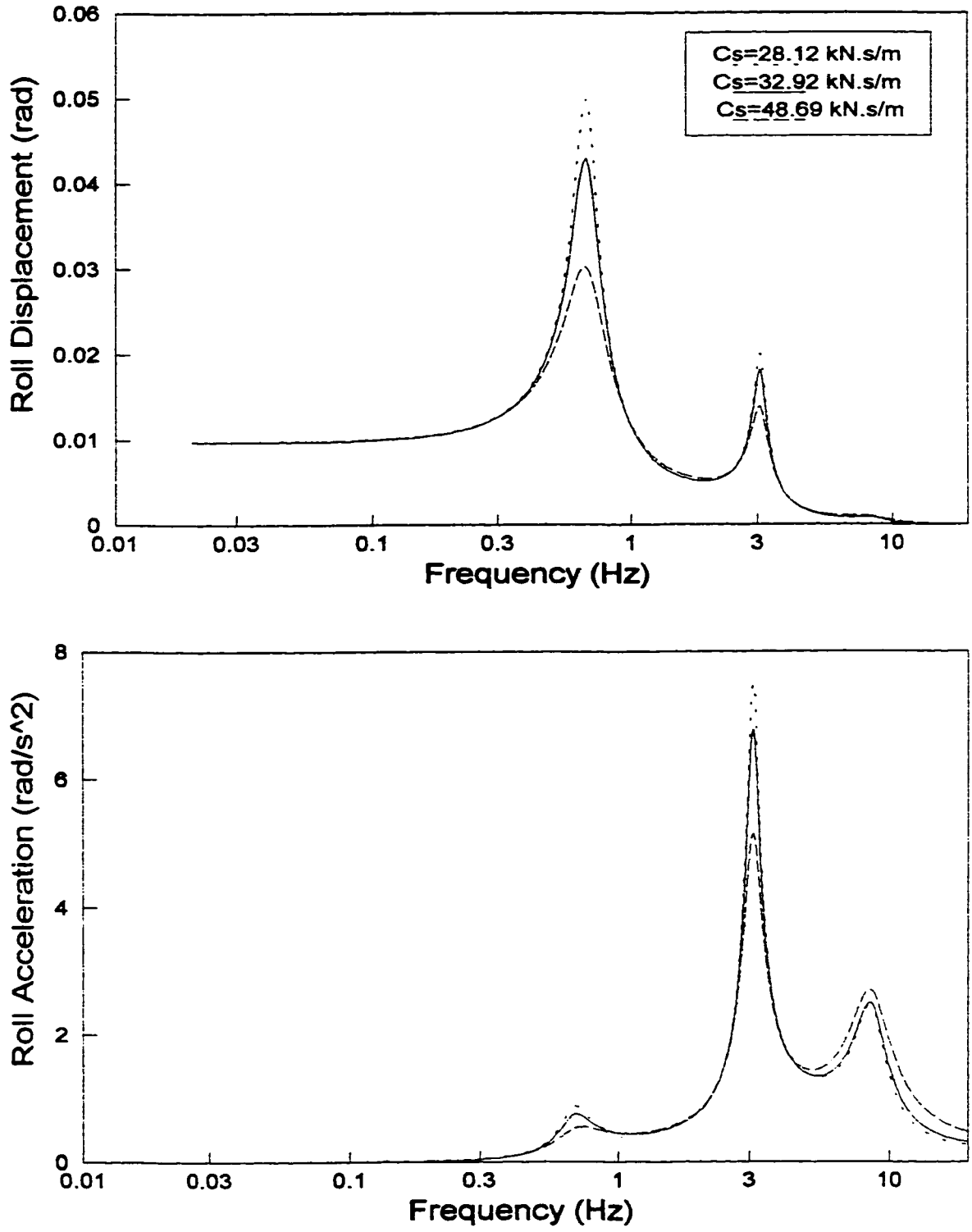


Figure 4.21 Influence of suspension damping on the roll response characteristics of the sprung mass (Excitation: 0.01 m harmonic out-of-phase displacement)

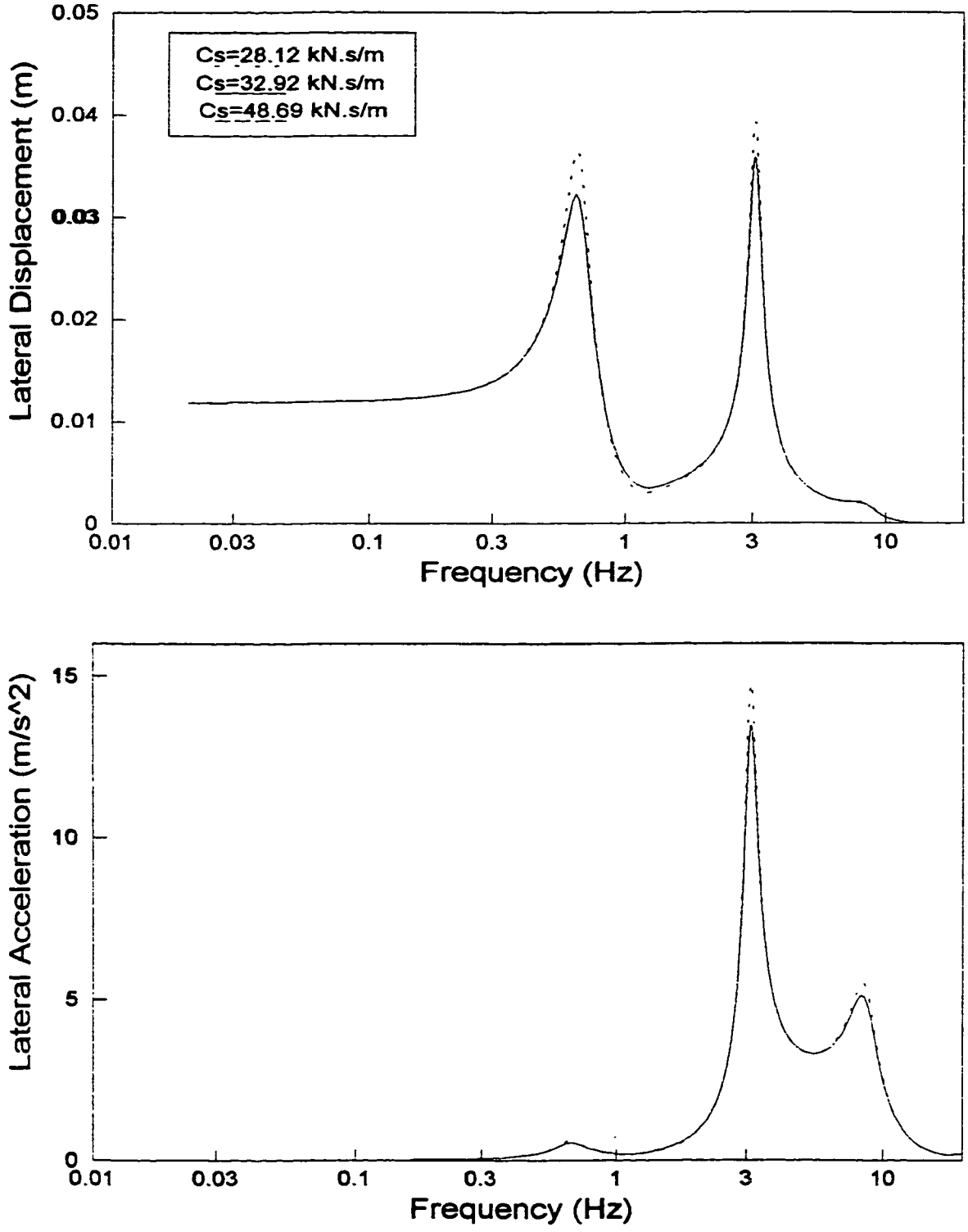


Figure 4.22 Influence of suspension damping on the lateral response characteristics of the sprung mass (Excitation: 0.01 m harmonic out-of-phase displacement)

cause only insignificant influence on the damped natural frequencies. The peak acceleration response of the sprung mass also decrease with increase in damping due to corresponding increase in the roll damping properties of the suspension. The variations in suspension damping, however, do not affect the static roll and lateral deflections of the sprung mass. From the results, it can be concluded that suspensions with higher damping can provide improved handling performance by reducing the magnitudes of roll and lateral deflections, and improved ride performance related to roll and lateral accelerations of the sprung mass.

The influence of the suspension damping on the ride and handling performance of the vehicle subject to harmonic out-of-phase road excitation is presented in Figures 4.21 and 4.22. The peak magnitudes of roll and lateral displacements and accelerations in the vicinity of roll and lateral mode resonances tend to decrease considerably, when high suspension damping is employed. Highly damped suspension, however, apparently increases the roll acceleration responses near the unsprung mass roll resonant frequency and at higher frequencies, as shown in Figure 4.21. The corresponding peak magnitude of the lateral acceleration of the sprung mass near the unsprung mass roll resonant frequency is apparently reduced by using highly damped suspension, as shown in Figure 4.22.

The significant influence of the suspension damping on the vehicle response to the Gaussian random road excitations is illustrated in Figures 4.23 and 4.26. The results clearly show that the dominant peak amplitudes of the displacement and acceleration response PSD characteristics of the sprung mass can be effectively reduced by using highly damped suspension: the roll and lateral response PSDs are dominated by the sprung mass roll resonant frequency, while the corresponding roll and lateral acceleration response PSDs are dominated by the sprung mass lateral resonant frequency. The suspension damping doesn't show apparent influence on the peak magnitudes of the roll and lateral

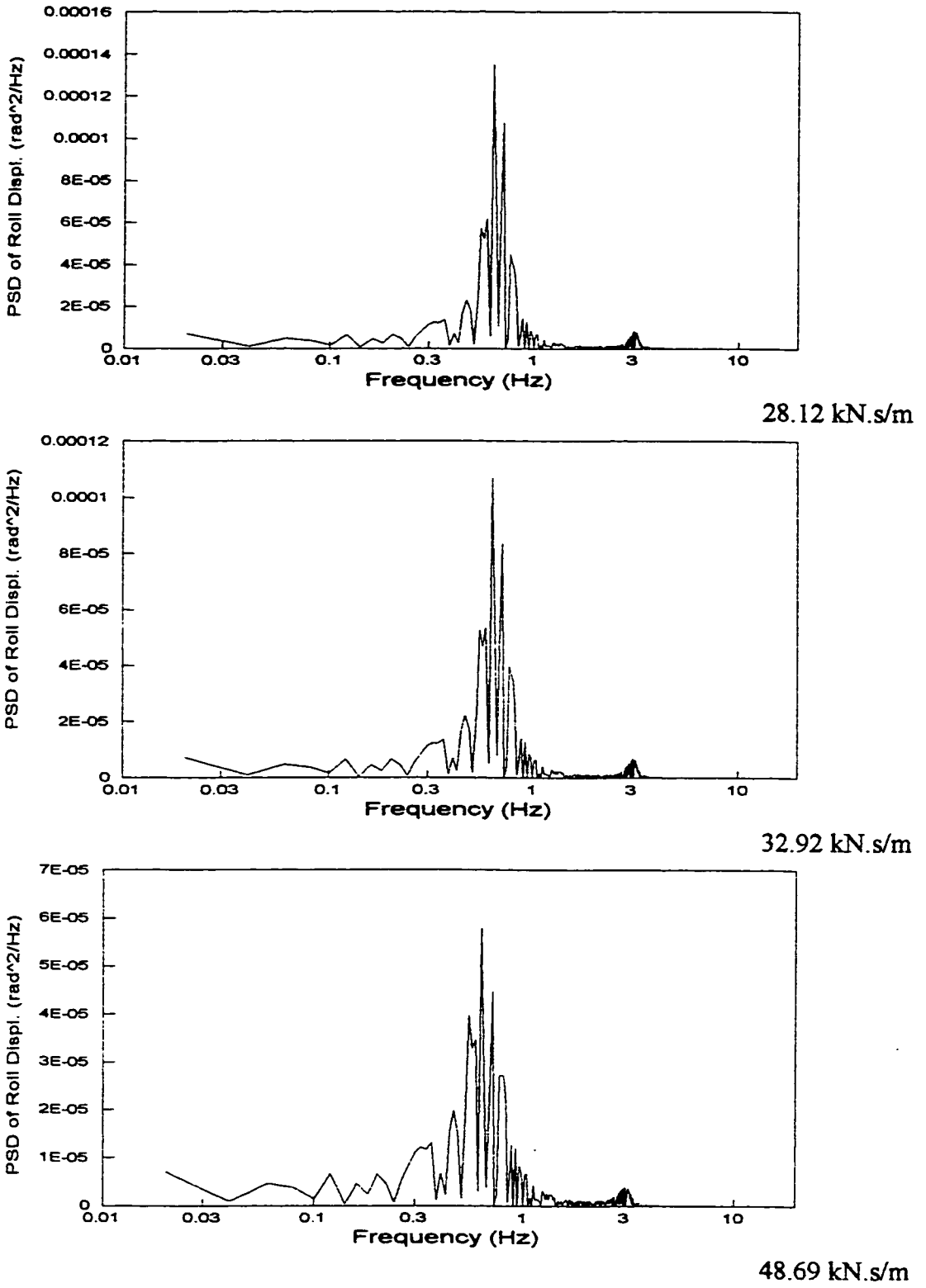


Figure 4.23 Influence of suspension damping on PSD of roll displacement of the sprung mass for rough random road with random cross-slope between left and right wheels.

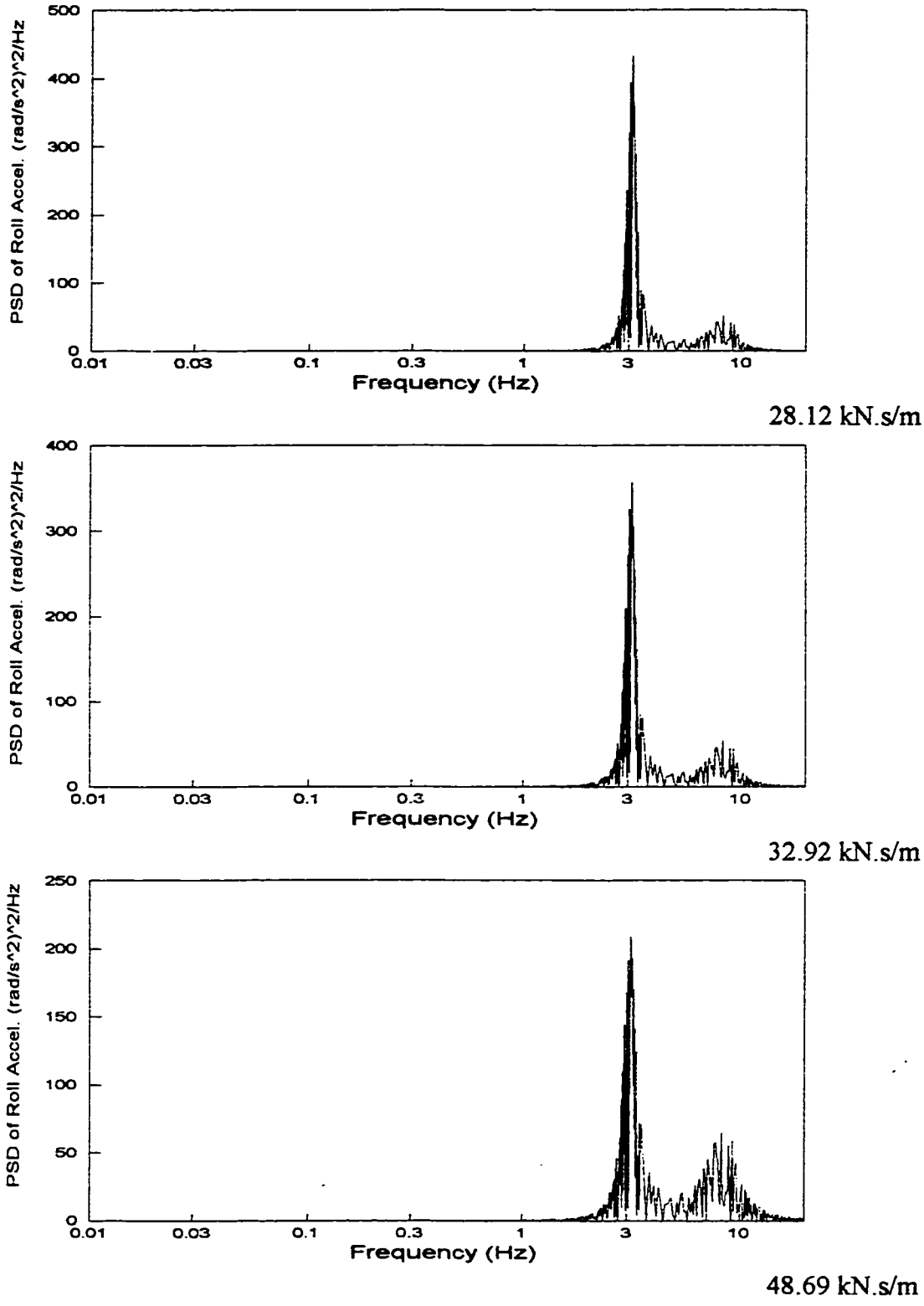


Figure 4.24 Influence of suspension damping on PSD of roll acceleration of the sprung mass for rough random road with random cross-slope between left and right wheels.

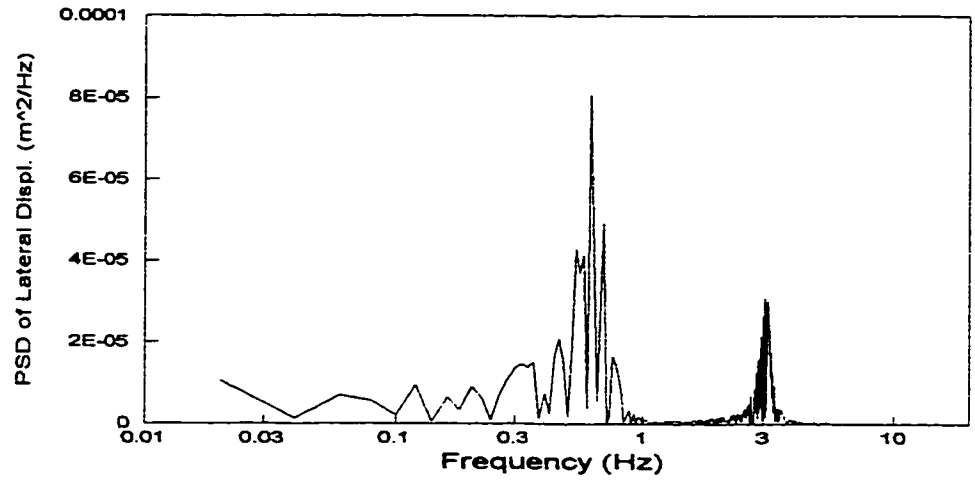


28.12 kN.s/m

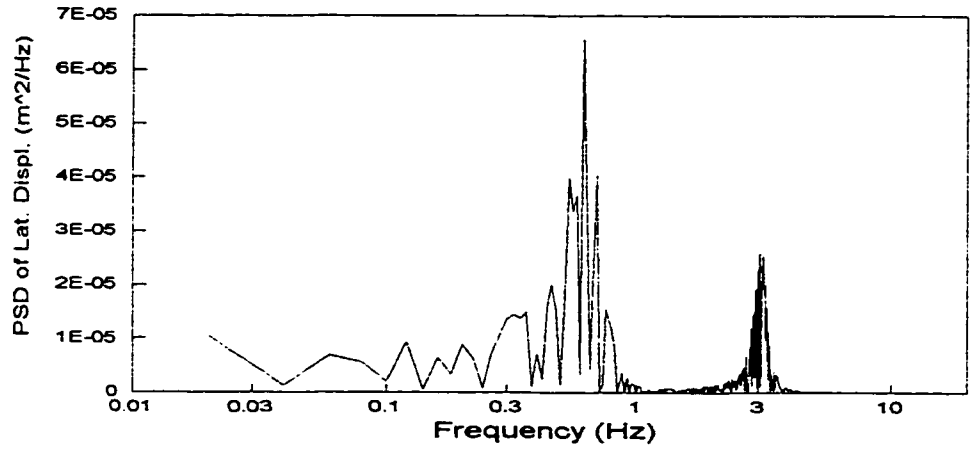


32.92 kN.s/m

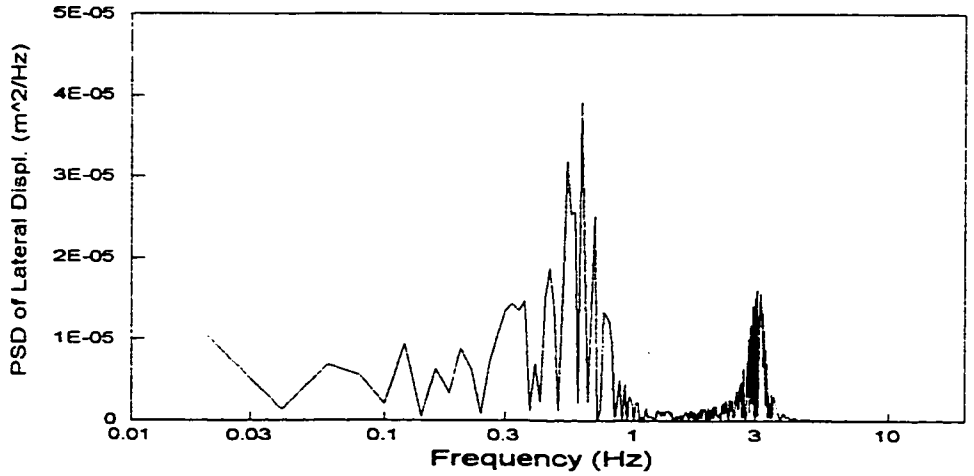


48.69 kN.s/m

Figure 4.25 Influence of suspension damping on PSD of lateral displacement of the sprung mass for rough random road with random cross-slope between left and right wheels.

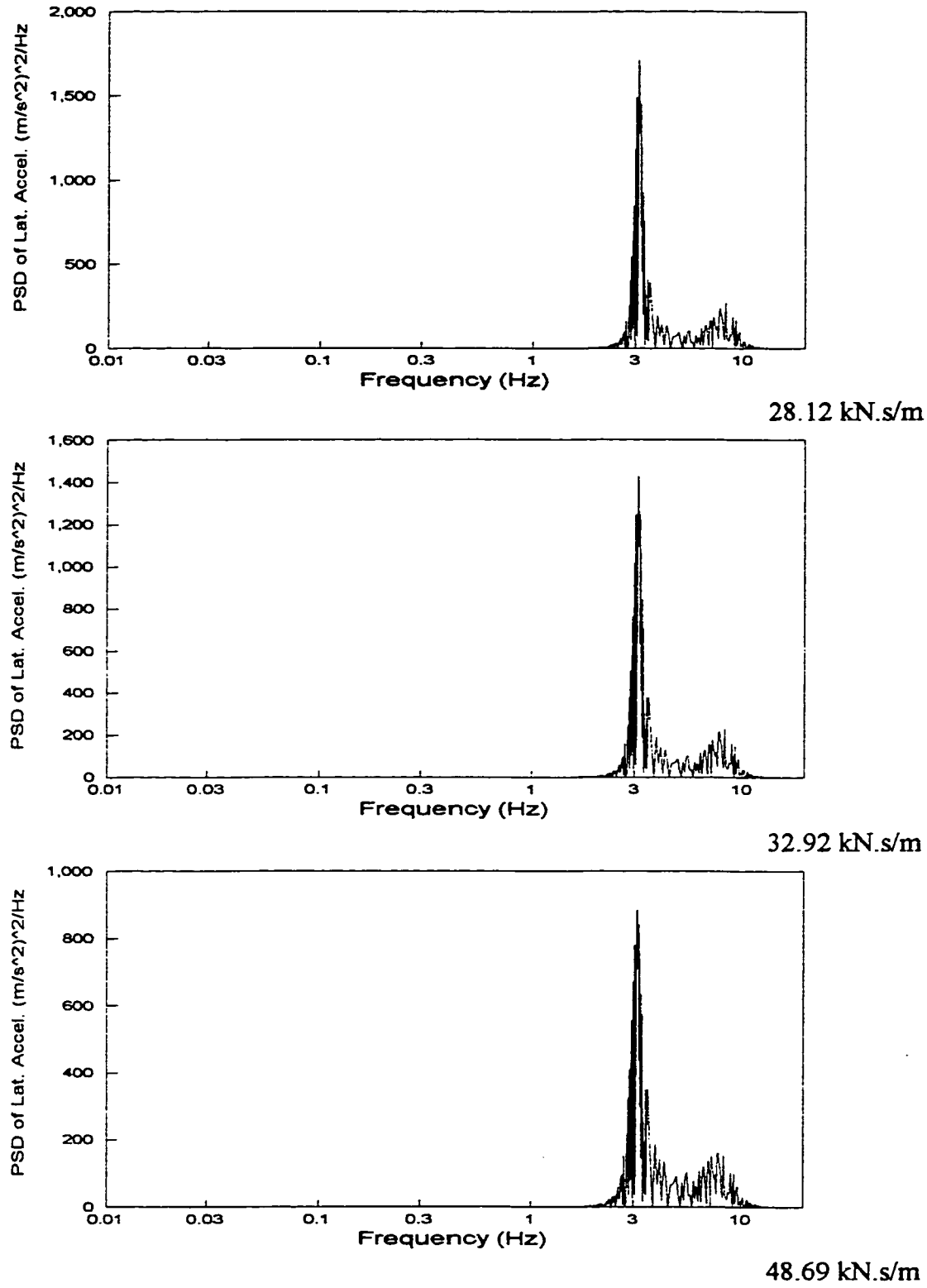


Figure 4.26 Influence of suspension damping on PSD of lateral acceleration of the sprung mass for rough random road with random cross-slope between left and right wheels.

displacement response PSDs near the sprung mass lateral resonant frequency, however, the peak values of the roll and lateral acceleration response PSDs near the unsprung mass roll resonant frequency tend to increase with increase in the suspension damping.

### 4.5.3 Influence of Tire Vertical Stiffness

The effect of variations in the vertical stiffness of tires on the ride and handling performance of the vehicle is studied for lateral acceleration and roadway excitations, by varying the tire vertical stiffness from 2755 kN/m to 4755 kN/m. The corresponding roll and lateral displacement and acceleration response characteristics of the sprung mass are illustrated in Figures 4.27 to 4.34. An increase in the effective roll stiffness of the tires due to increase in the vertical stiffness yields reduction in static and dynamic roll and lateral deflection response in the veicinity of the roll mode resonance of the sprung mas subject to lateral acceleration excitation, as shown in Figures 4.27 and 4.28. The increase in tire vertical stiffness, however, yields slight increase in the roll and lateral mode resonant frequencies of the sprung mass. Furthermore, the magnitudes of roll and lateral displacements and accelerations tend to increase near the lateral mode (3.07 Hz)with stiffer tires. This increase may be attributed to high roll stiffness and reduced damping ratio. The effect of tire vertical stiffness on the roll and lateral dynamics of the vehicle subject to harmonic and out-of-phase roadway excitations (Figures 4.29 and 4.30) is also similar to that observed under centrifugal acceleration excitations. While the variations in tire stiffness cause only slight variations in the magnitude of response at low frequencies, the response behaviour corresponding to higher frequencies modes is strongly influenced by the tire stiffness. The unsprung mass roll mode is strongly influenced by the tire stiffness. The unsprung mass roll mode frequency increases considerably with increase in tire stiffness due to corresponding increase in the roll stiffness, as shown in Figures 4.29 and 4.30. Under excitations arising from a randomly rough roadway with randomly

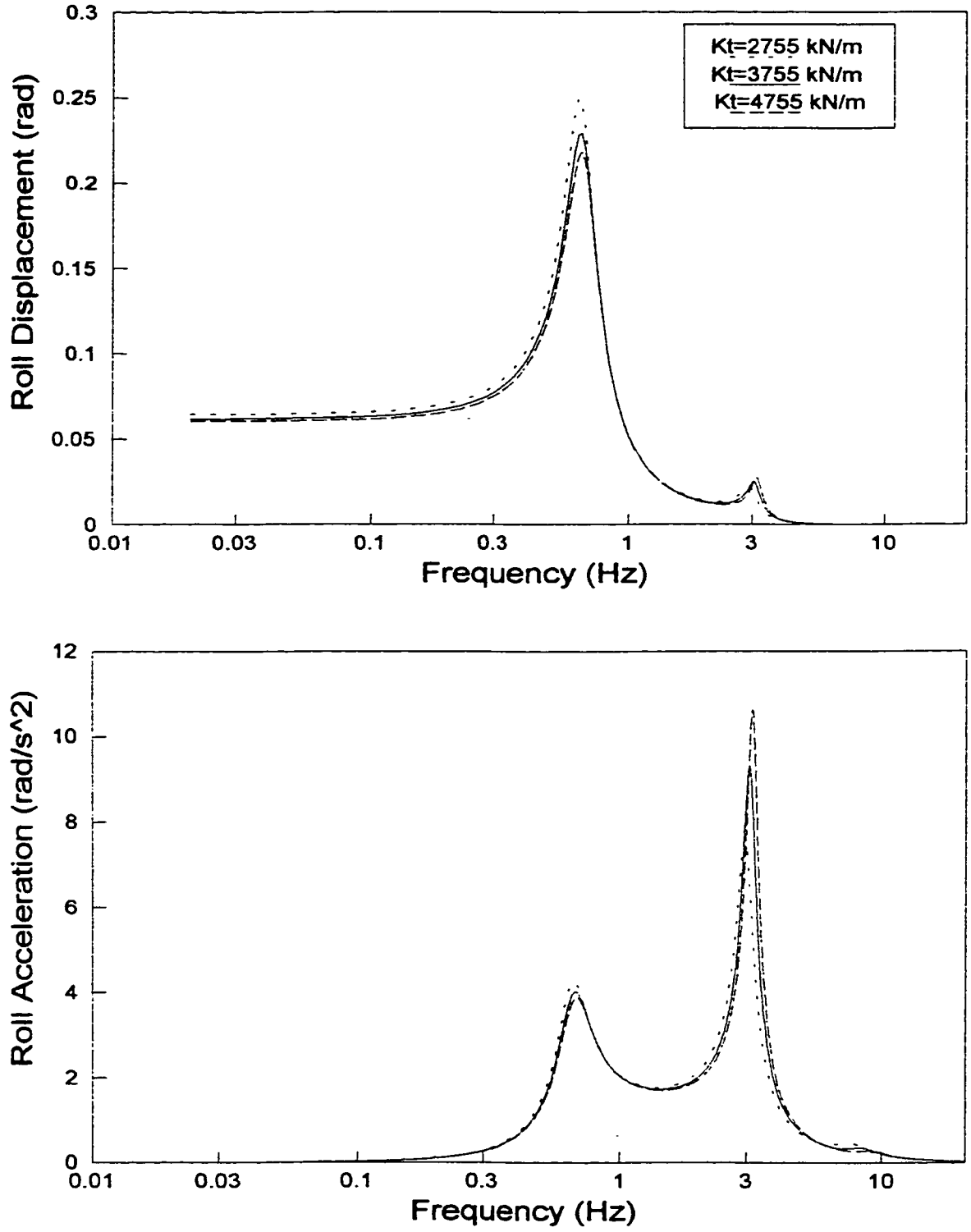


Figure 4.27 Influence of tire vertical stiffness on the roll response characteristics of the sprung mass (Excitation: 0.3g harmonic lateral acceleration)

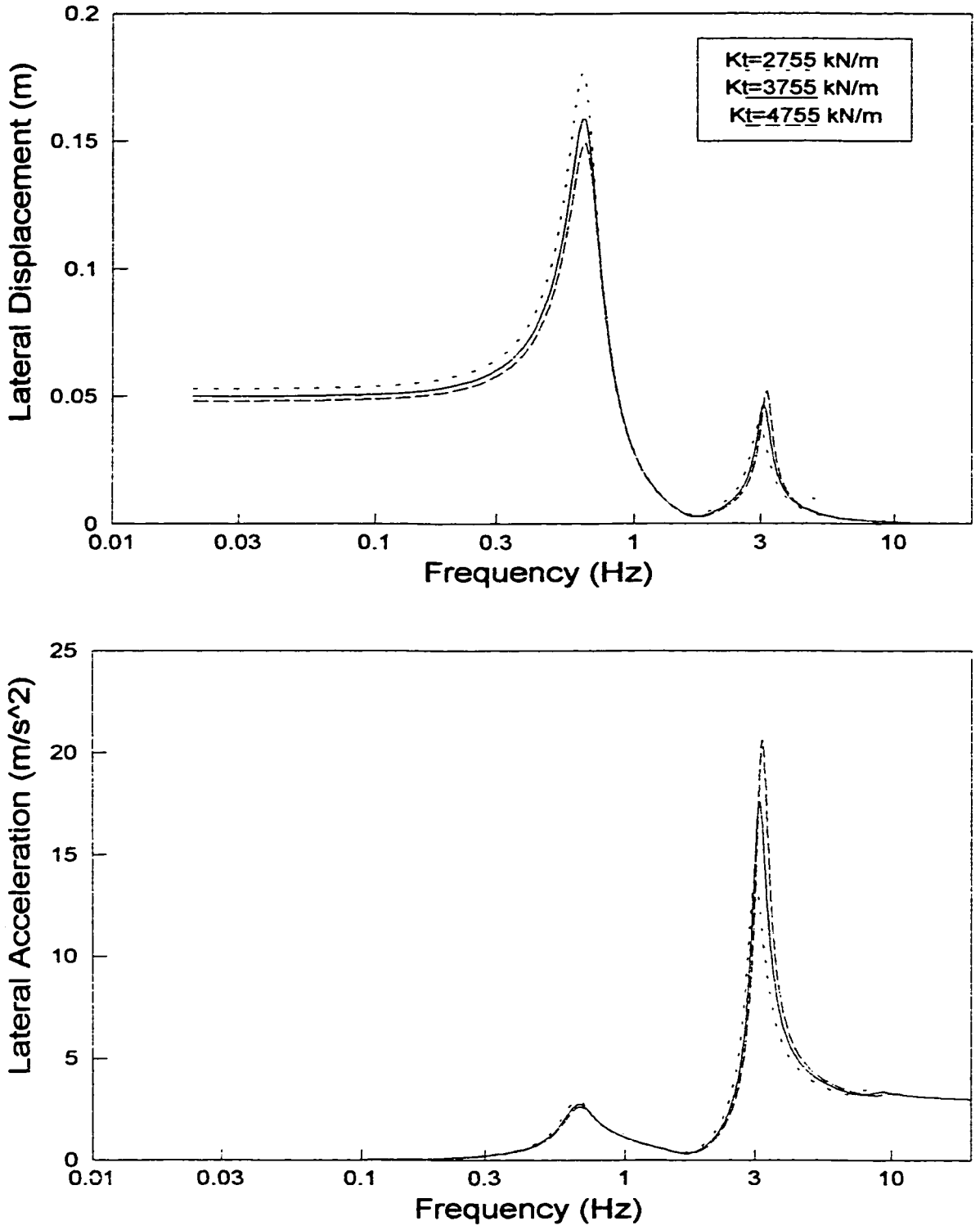


Figure 4.28 Influence of tire vertical stiffness on the lateral response characteristics of the sprung mass (Excitation: 0.3g harmonic lateral acceleration)

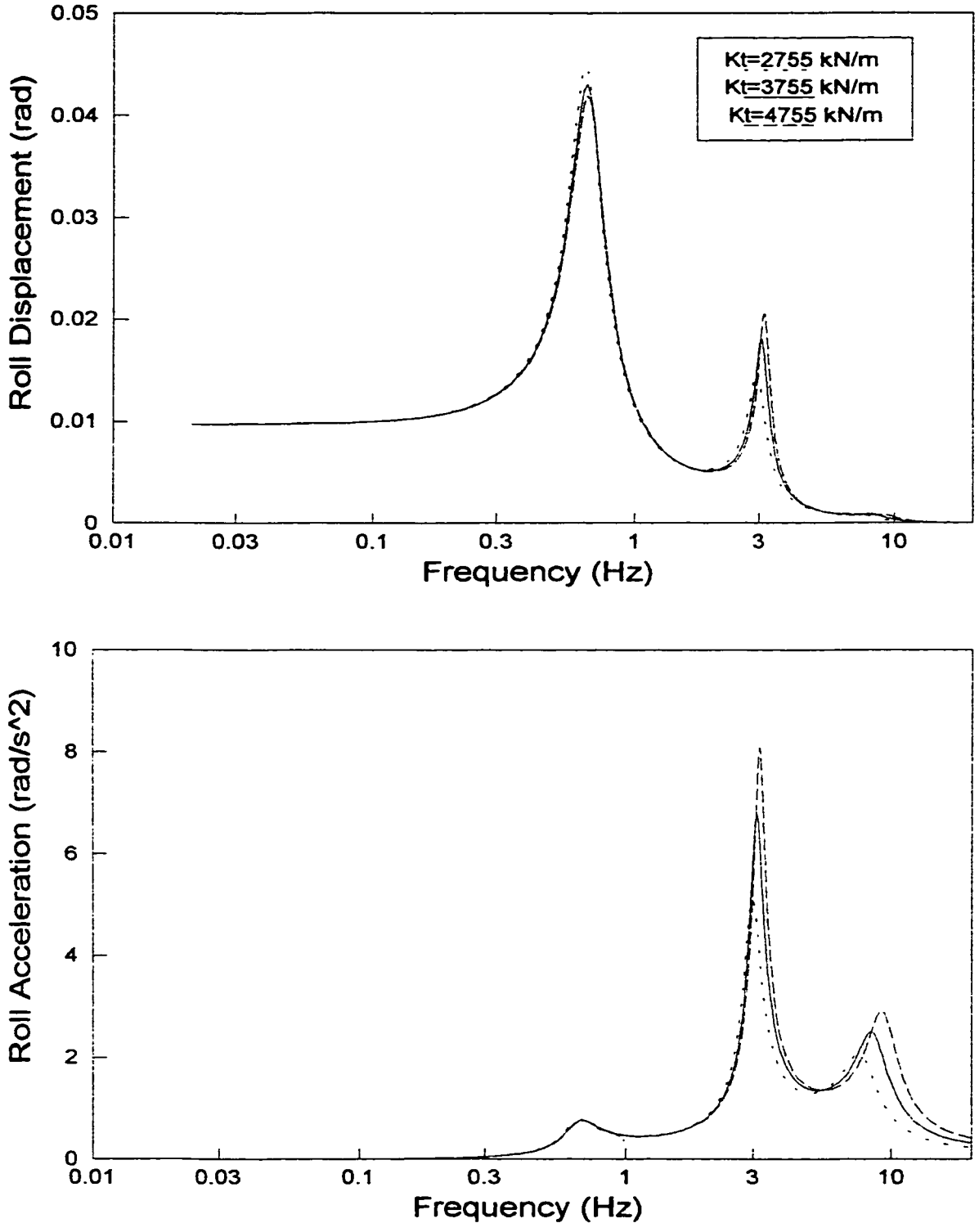


Figure 4.29 Influence of tire vertical stiffness on the roll response characteristics of the sprung mass (Excitation: 0.01 m harmonic out-of-phase displacement)

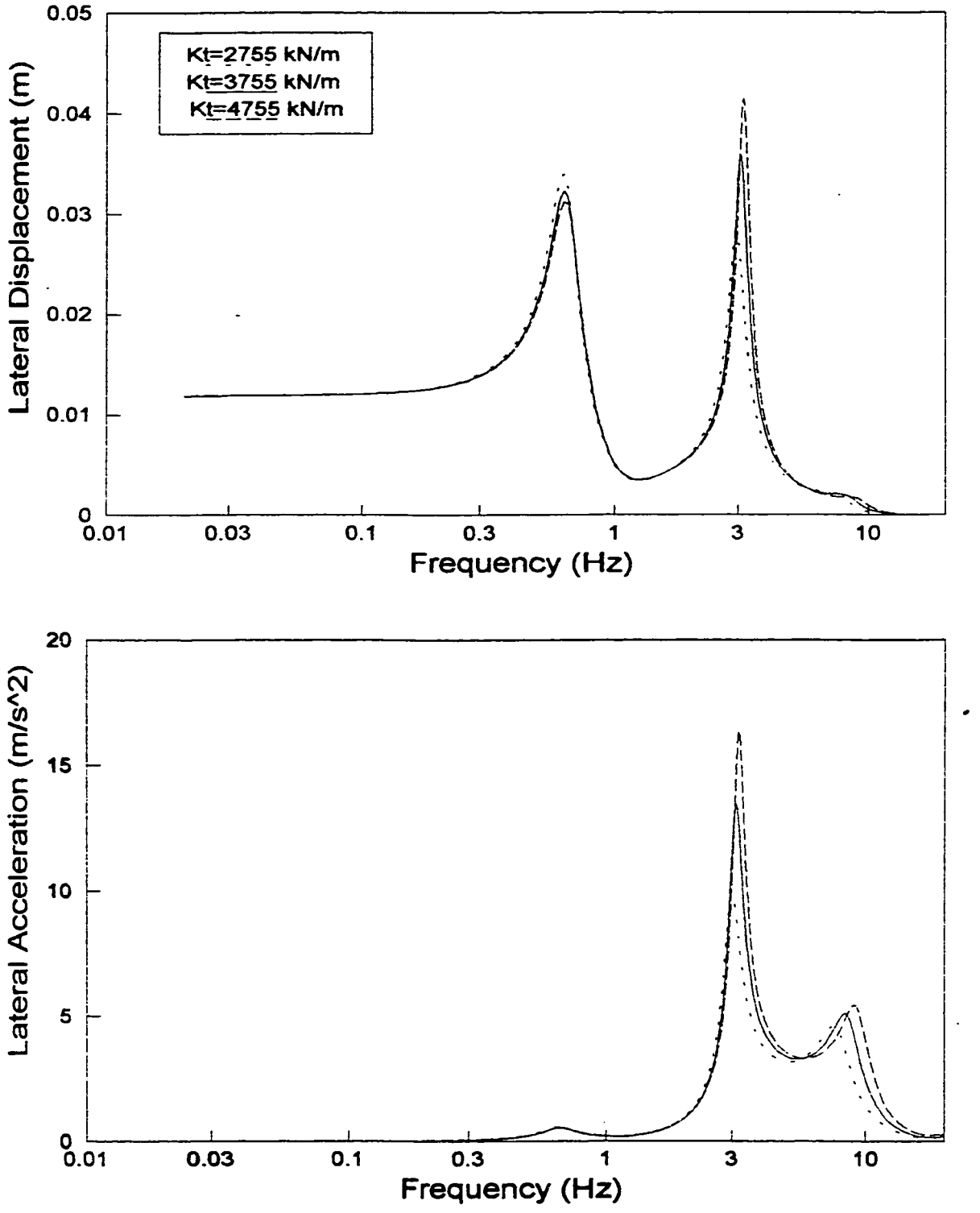


Figure 4.30 Influence of tire vertical stiffness on the lateral response characteristics of the sprung mass (Excitation: 0.01 m harmonic out-of-phase displacement)

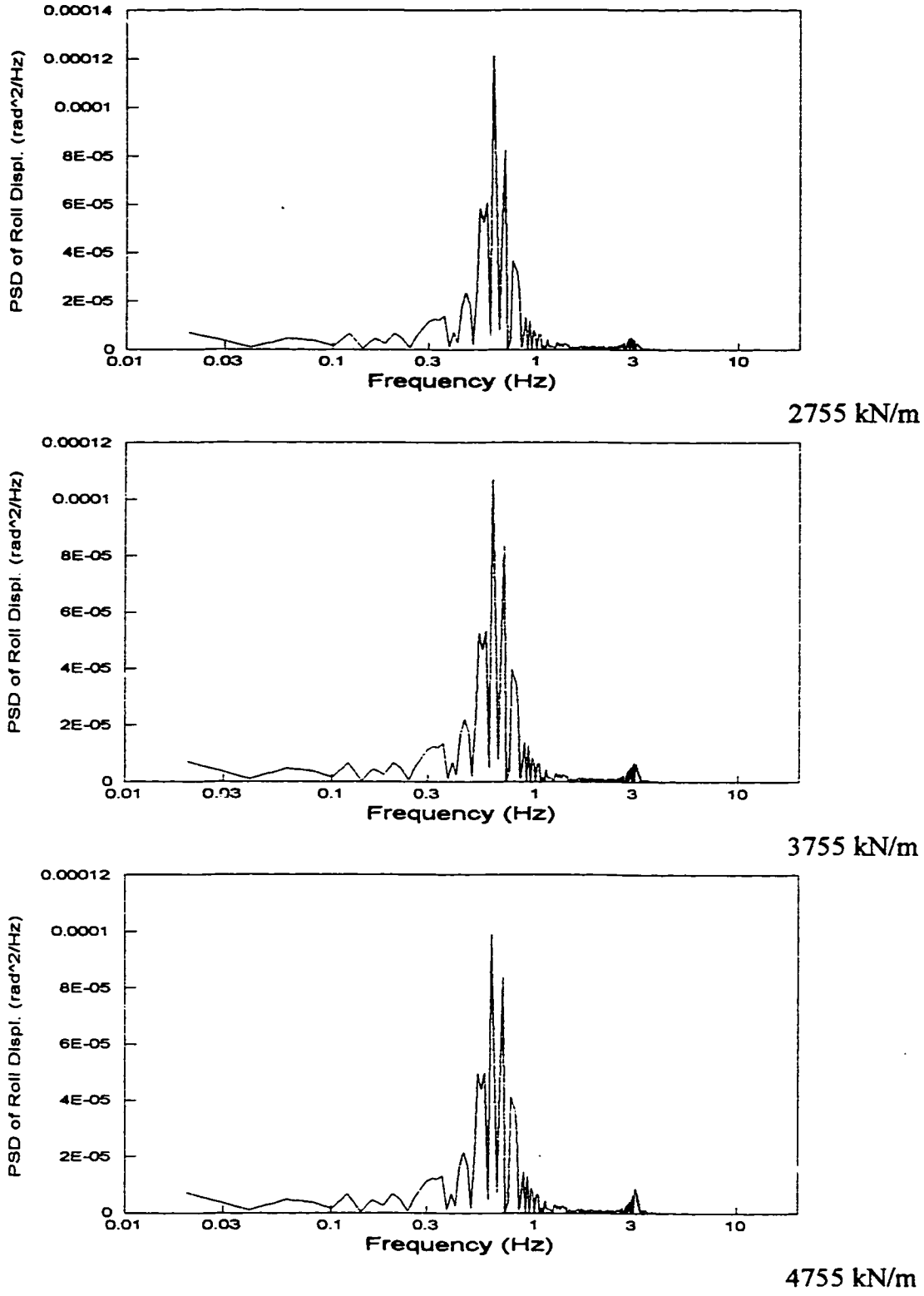


Figure 4.31 Influence of tire vertical stiffness on PSD of roll displacement of the sprung mass for rough random road with random cross-slope between left and right wheels.

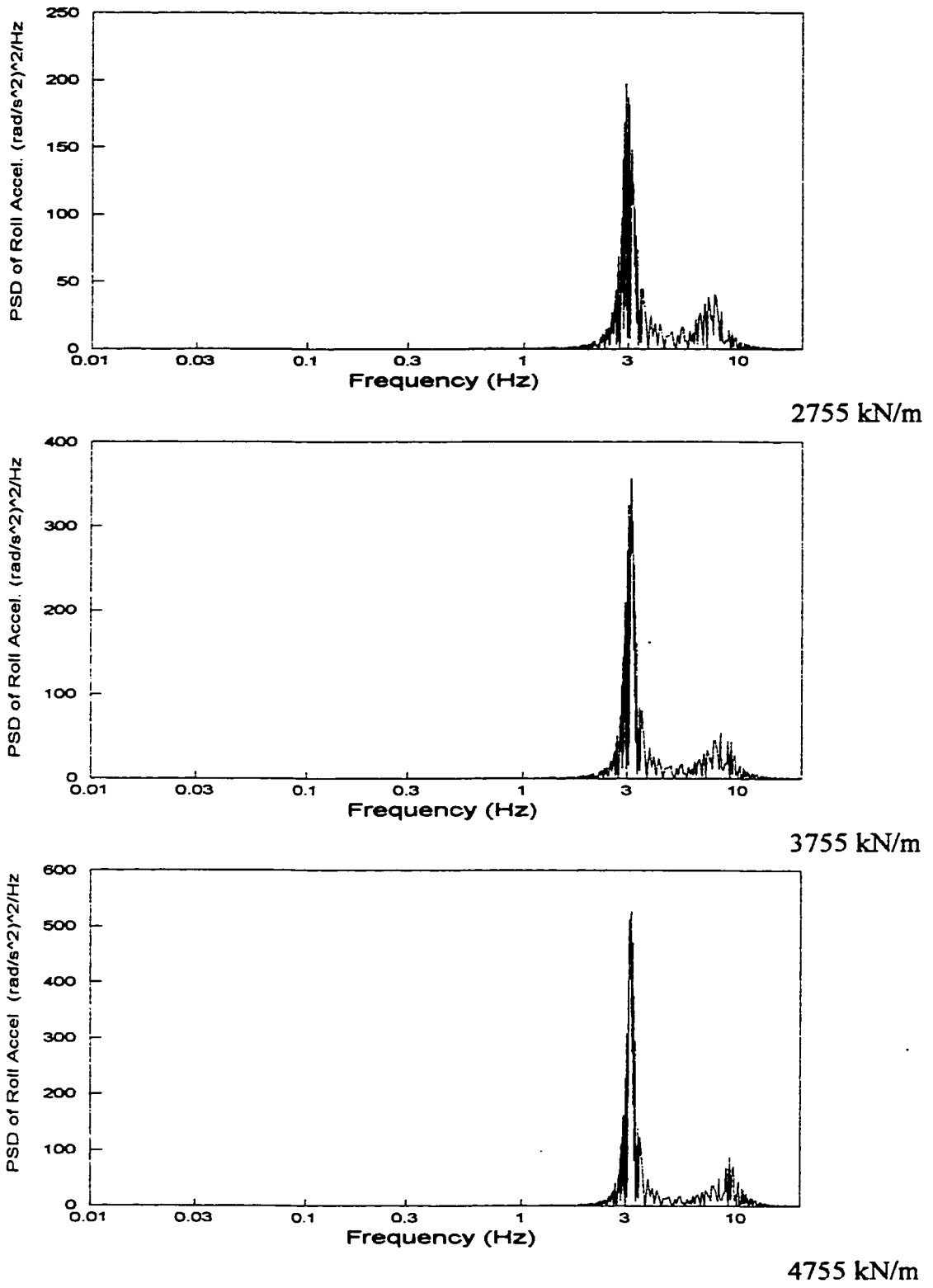


Figure 4.32 Influence of tire vertical stiffness on PSD of roll acceleration of the sprung mass for rough random road with random cross-slope between left and right wheels.

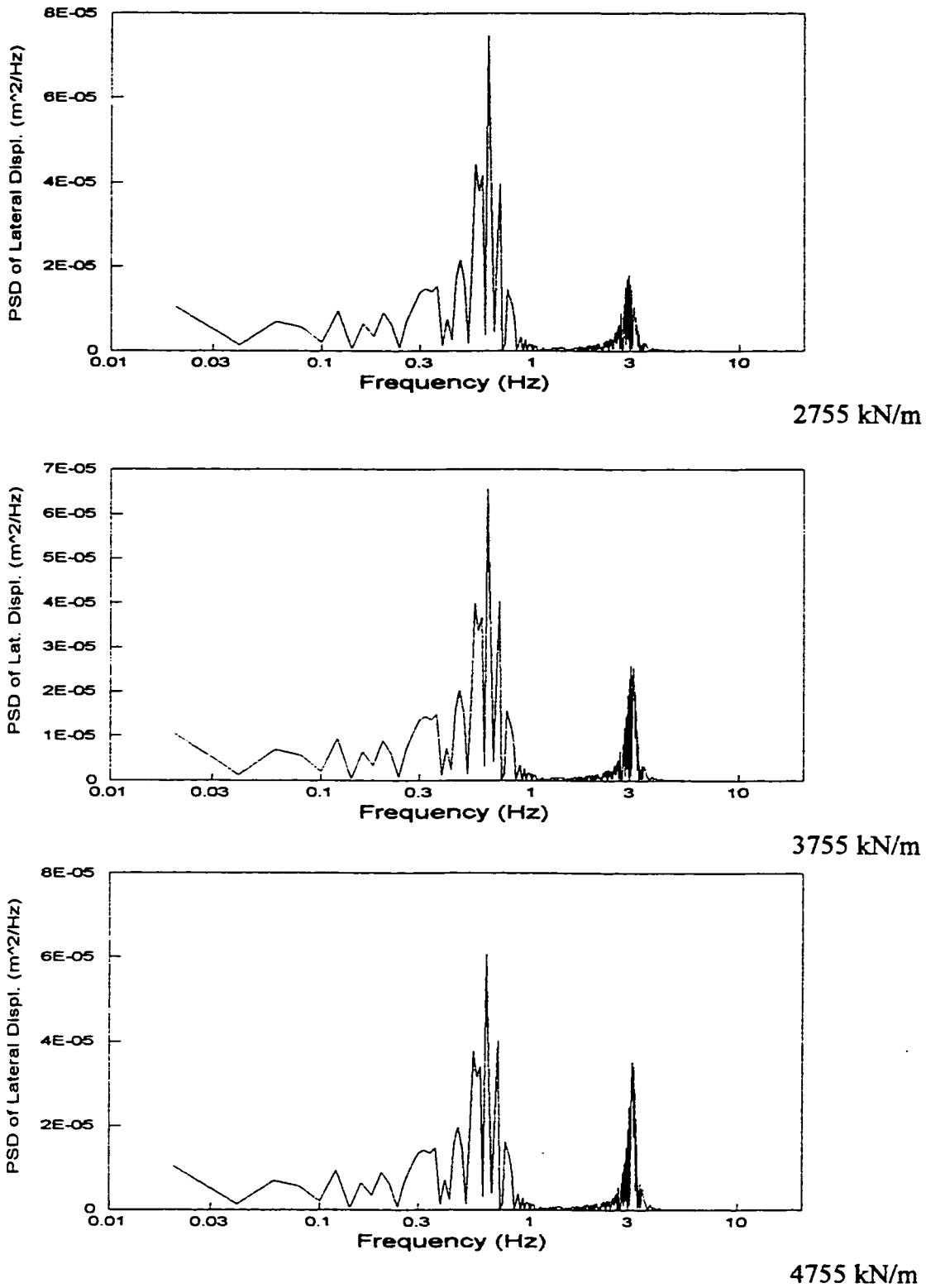


Figure 4.33 Influence of tire vertical stiffness on PSD of lateral displacement of the sprung mass for rough random road with random cross-slope between left and right wheels.

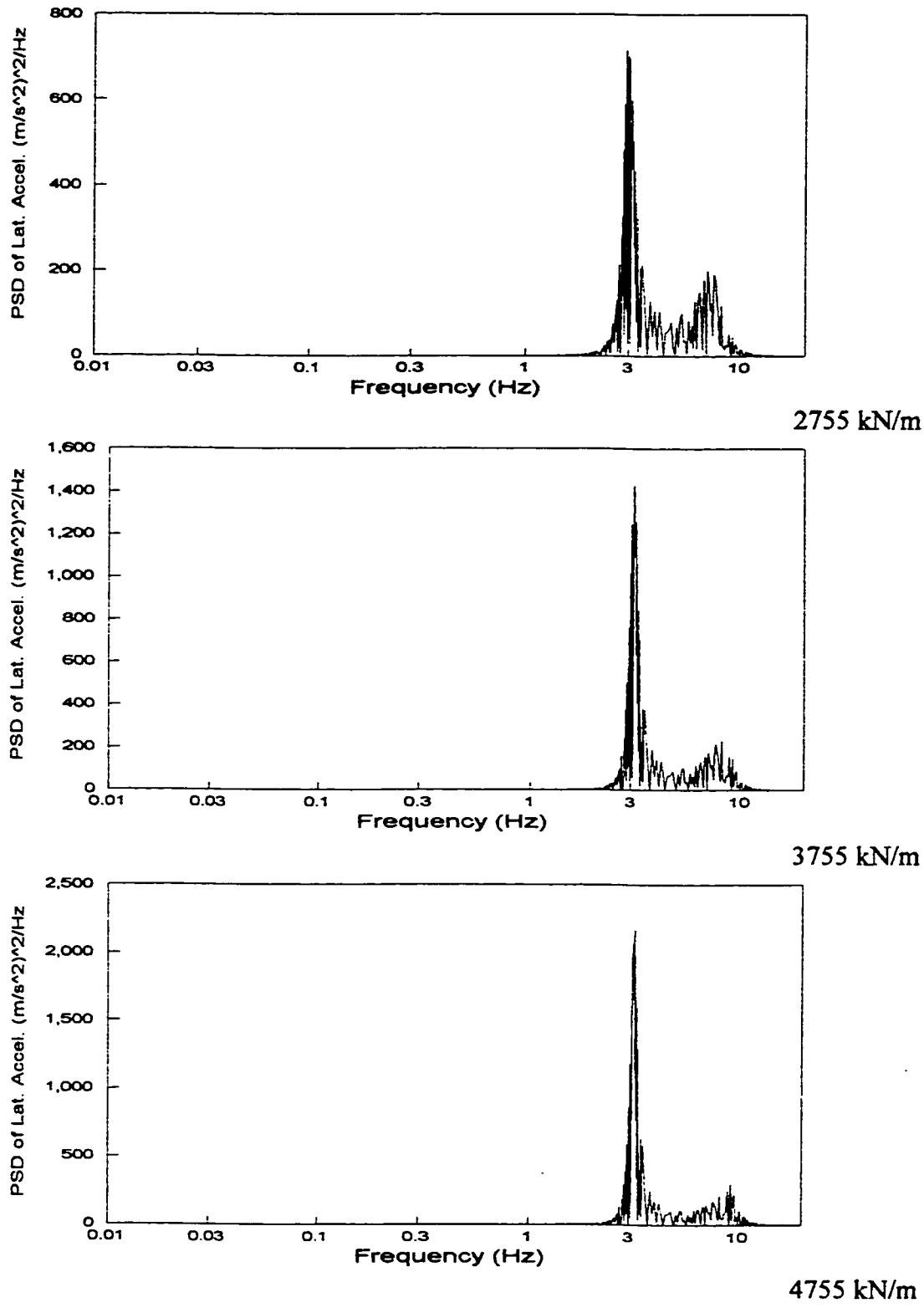


Figure 4.34 Influence of tire vertical stiffness on PSD of lateral acceleration of the sprung mass for rough random road with random cross-slope between left and right wheels.

distributed phase, an increase in tire stiffness yields reduced body roll at the roll mode frequencies at the roll mode frequencies but considerably larger roll acceleration near the lateral mode resonance, as shown in Figures 4.31 and 4.34. The random response PSD characteristics of the sprung mass show dominant roll and lateral displacement resonances at the sprung mass roll resonant frequency, and dominant roll and lateral acceleration resonances at the sprung mass lateral natural frequency. The results show that these dominant roll and lateral displacement peak amplitudes can be reduced with increase in the tire vertical stiffness rate, however, the corresponding roll and lateral acceleration peak magnitudes will increase accordingly. By contrast, the roll and lateral displacement resonant peaks attributed to the sprung mass lateral frequency mode tend to increase with increase in the tire vertical stiffness rate, while the roll and lateral acceleration resonant peaks due to the unsprung mass roll frequency mode tend to decrease as the result of it.

### 4.5.4 Influence of Sprung Weight

The effect of the suspension sprung weight on the handling and riding performance of the candidate vehicle is investigated for varying suspension sprung mass from 13111 kg to 15111 kg and given lateral acceleration and roadway excitations. The frequency responses and random response PSD of the sprung mass are presented in Figures 4.35 to 4.42.

The effect of sprung weight on the dynamic behavior of the sprung mass for the given lateral acceleration input is illustrated in Figures 4.35 to 4.36. The frequency response characteristics show that heavier loaded suspension will yield lower sprung mass roll and lateral natural frequencies and higher resonant peaks except for the lateral response peaks about the sprung mass lateral resonant frequency. Lighter suspension sprung weight yields smaller roll and lateral responses of the sprung mass in the vicinities

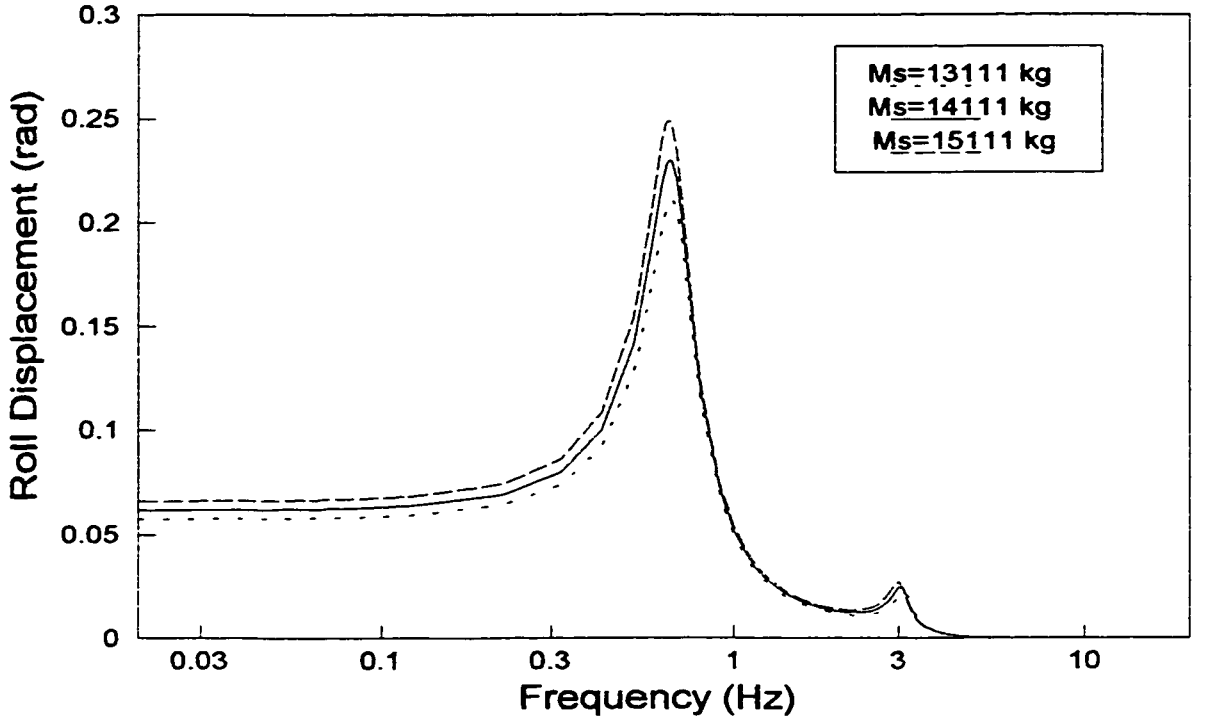


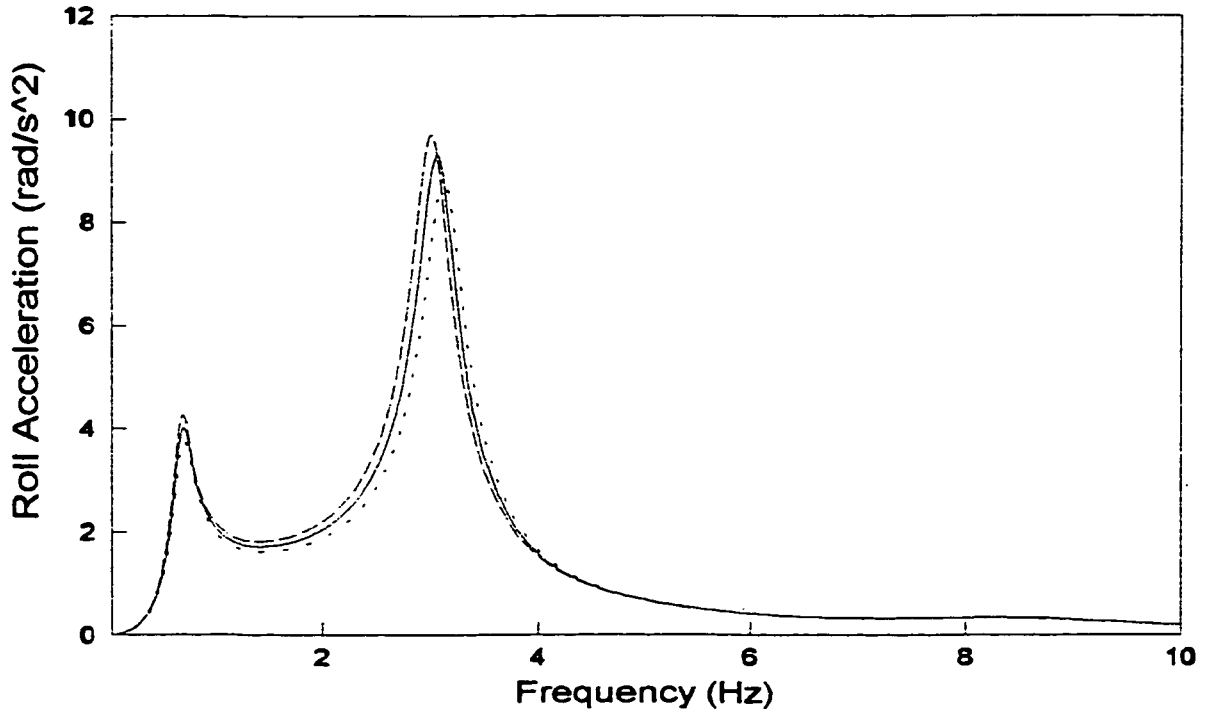


Figure 4.35 Influence of sprung mass weight on the roll response characteristics of the sprung mass (Excitation: 0.3g harmonic lateral acceleration)

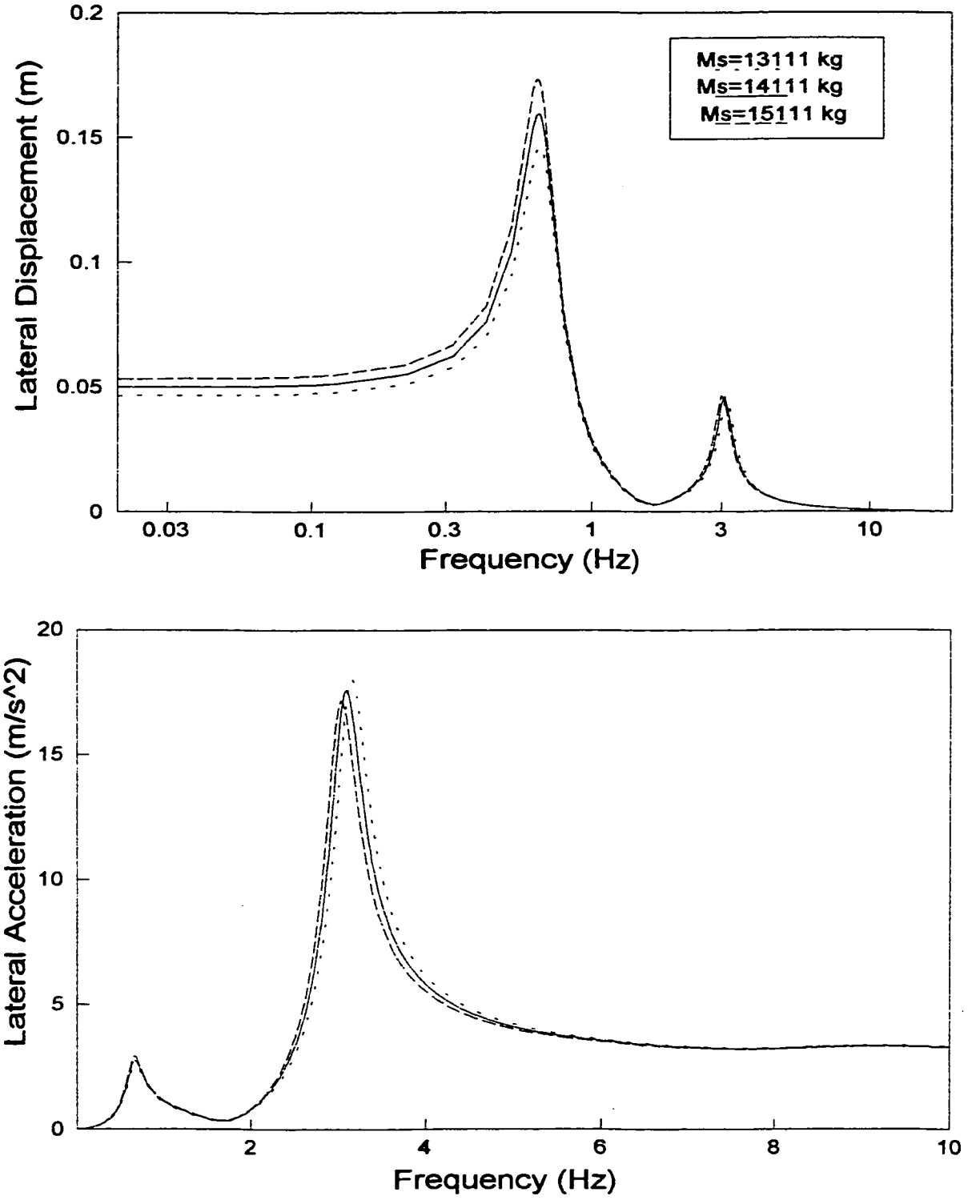


Figure 4.36 Influence of sprung mass weight on the lateral response characteristics of the sprung mass (Excitation: 0.3g harmonic lateral acceleration)

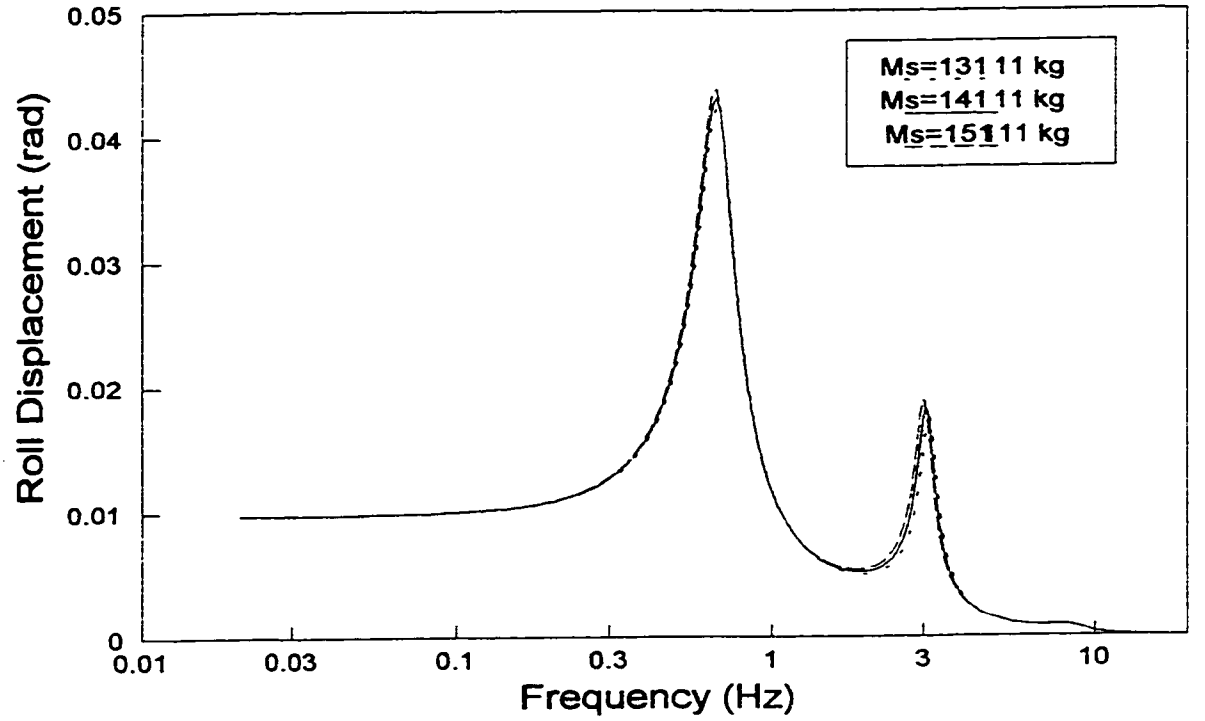


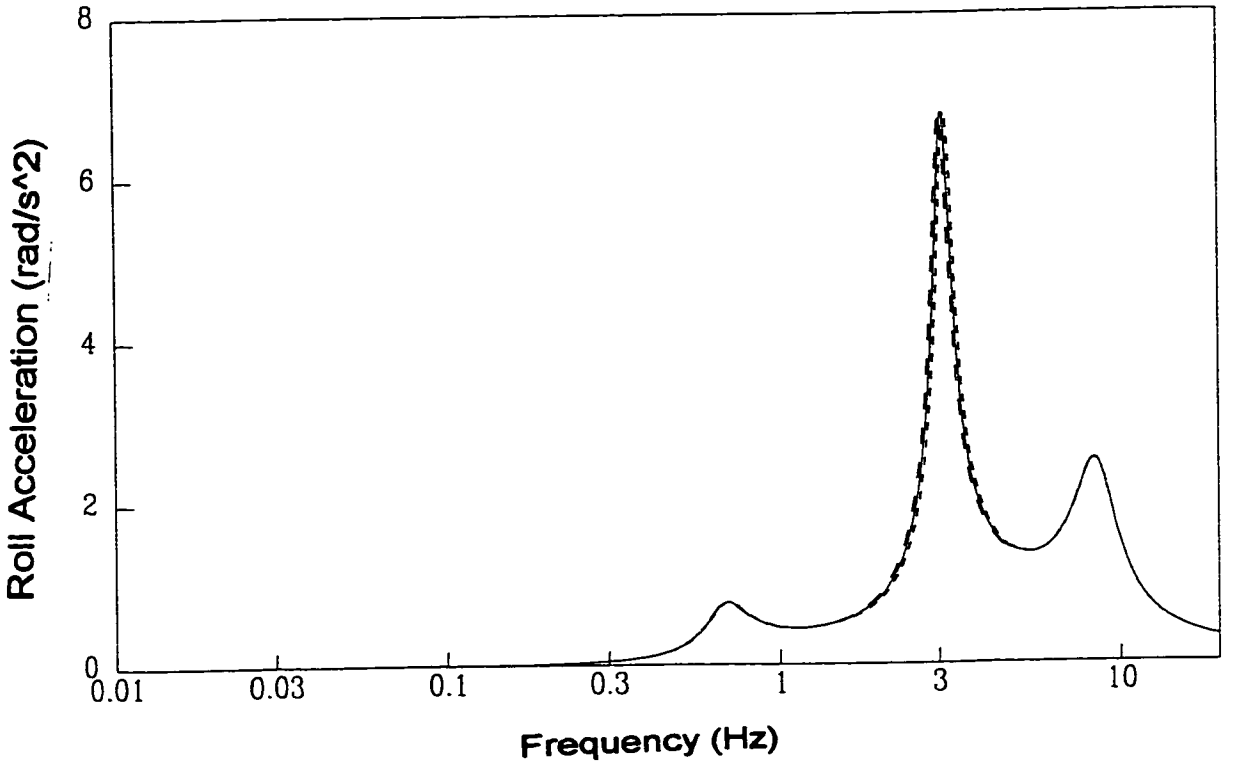


Figure 4.37 Influence of sprung mass weight on the roll response characteristics of the sprung mass (Excitation: 0.01 m harmonic out-of-phase displacement)

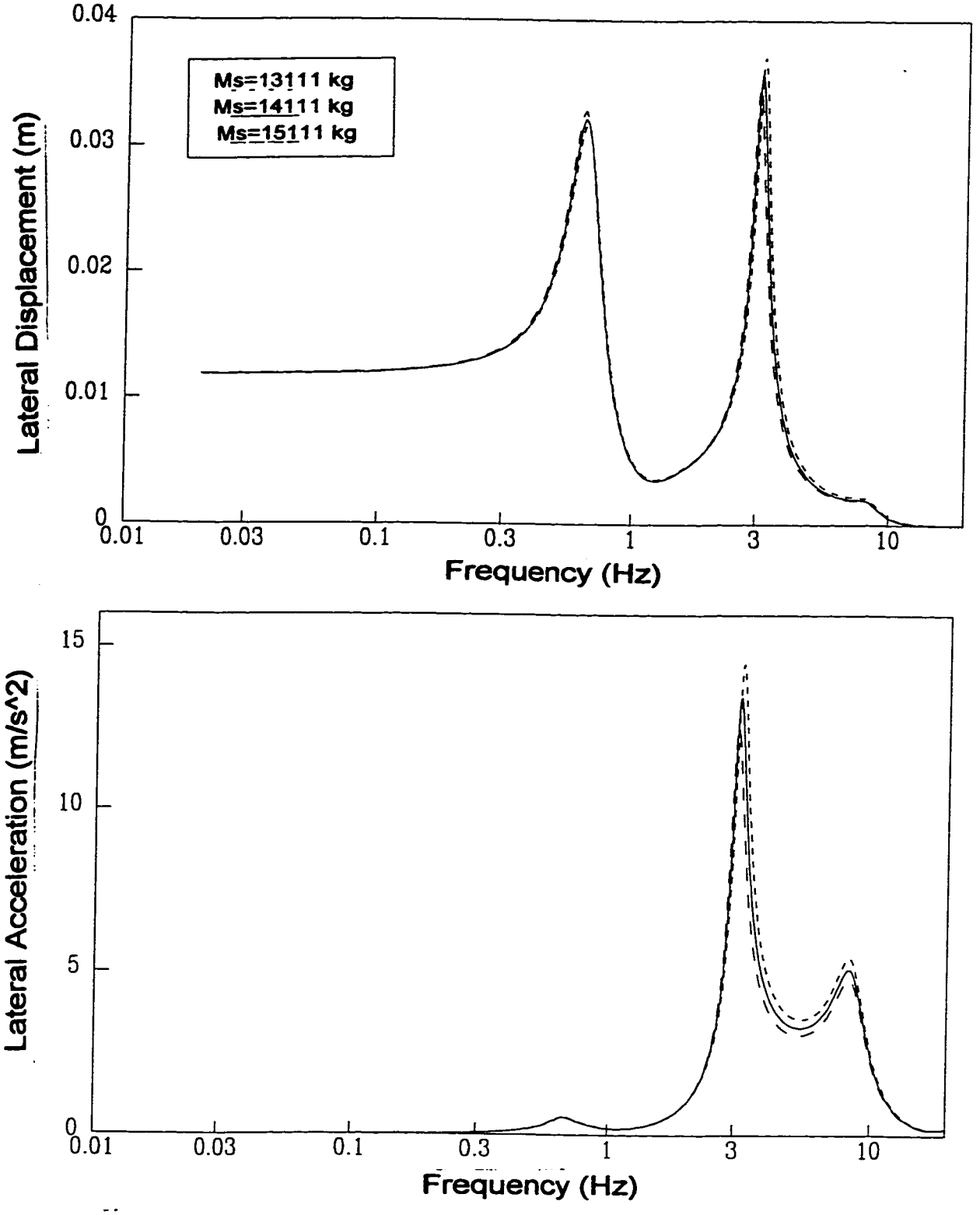


Figure 4.38 Influence of sprung mass weight on the lateral response characteristics of the sprung mass (Excitation: 0.01 m harmonic out-of-phase displacement)

of the frequencies lower than the sprung mass roll and lateral resonant frequencies. Lighter suspension load especially results lower roll and lateral responses of the sprung mass at ordinary steering frequencies, which is desirable for handling performance.

The effect of suspension load on the sprung mass dynamic characteristics for given harmonic out-of-phase road excitation is presented in Figures 4.37 to 4.38. Slight reductions in the roll and lateral responses of the sprung mass at the sprung mass roll natural frequency are observed when the suspension is lighter. While at higher frequency of the sprung mass lateral resonant frequency, the lighter suspension will result higher peaks of the sprung mass roll and lateral responses. Similar effect is applied on the sprung mass lateral responses near the unsprung mass natural frequency, while the effect on the corresponding sprung mass roll responses is noticed insignificant.

The random road roll and lateral response PSD of the sprung mass corresponding to different suspension loads are illustrated in Figures 4.39 to 4.42. The dominant PSD peaks of the roll and lateral displacement response characteristics of the sprung mass are yielded at the sprung mass roll resonant frequency, while the dominant PSD peaks of the roll and lateral acceleration response characteristics of the sprung mass occur at the sprung mass lateral resonant frequency. The results reveal that heavier suspension sprung weight tends to increase the these dominant roll and lateral displacement peaks, while reduce the corresponding dominant roll and lateral acceleration peaks. Furthermore, heavier sprung weight tends to reduce the lateral displacement peak attributed to the sprung mass lateral resonant mode. The results also show that the suspension sprung weight doesn't have apparent influence on the peak values of the roll displacement response near the sprung mass lateral resonant mode, roll and lateral acceleration response near the unsprung mass roll resonant mode.

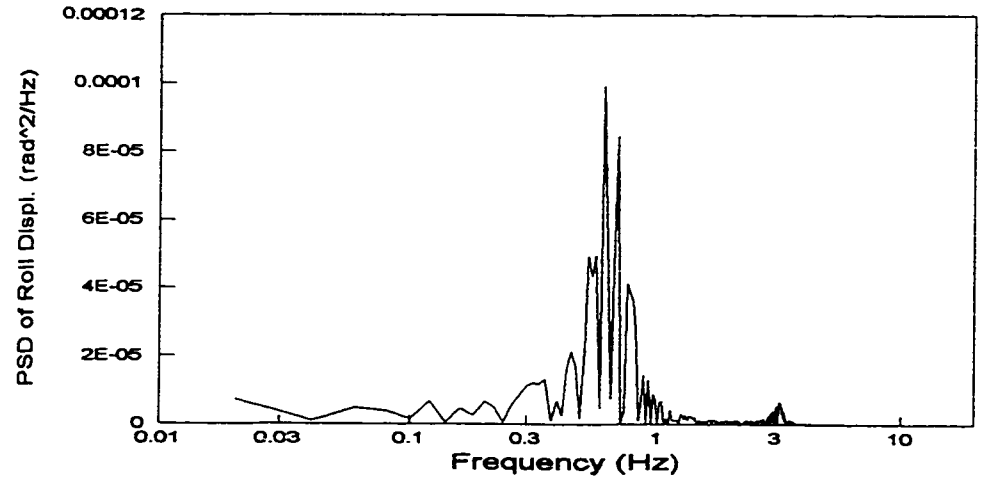


13111 kg

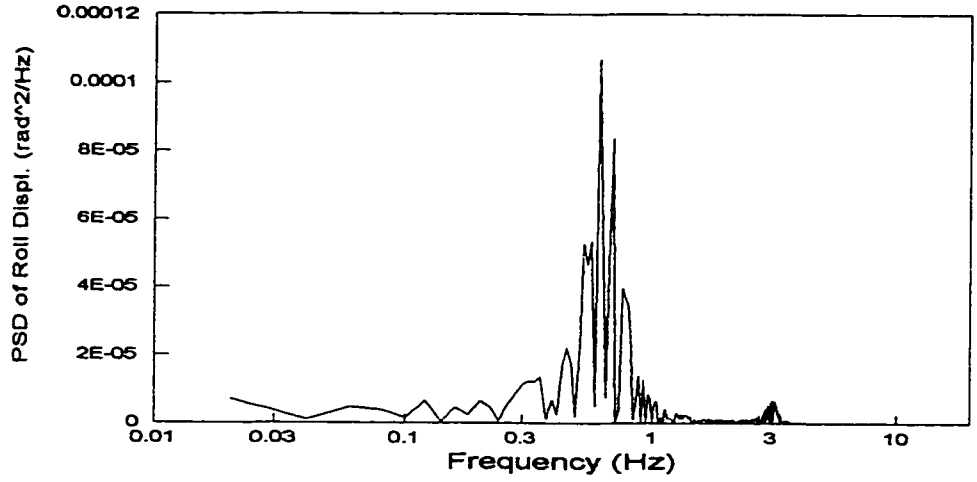


14111 kg

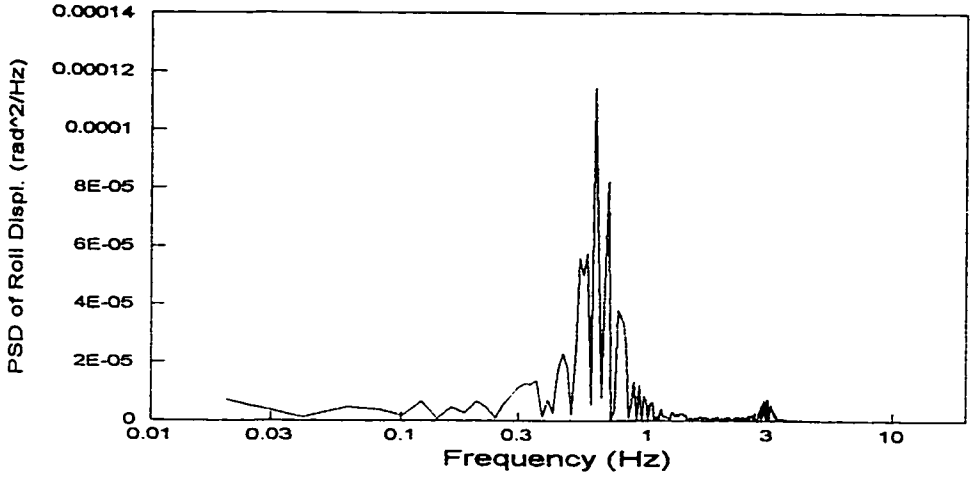


15111 kg

Figure 4.39 Influence of sprung mass weight on PSD of roll displacement of the sprung mass for rough random road with random cross-slope between left and right wheels.

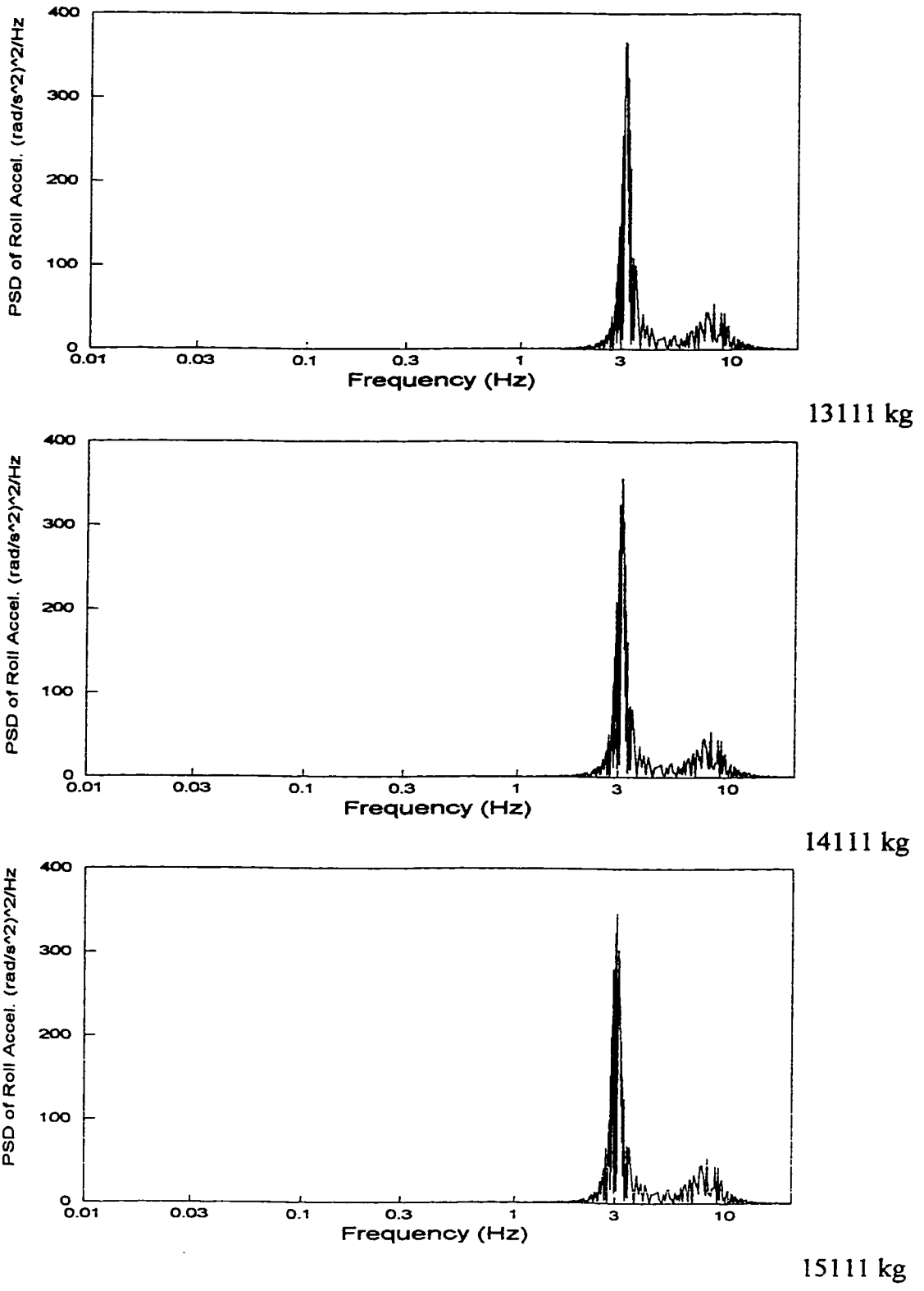


Figure 4.40 Influence of sprung mass weight on PSD of roll acceleration of the sprung mass for rough random road with random cross-slope between left and right wheels.

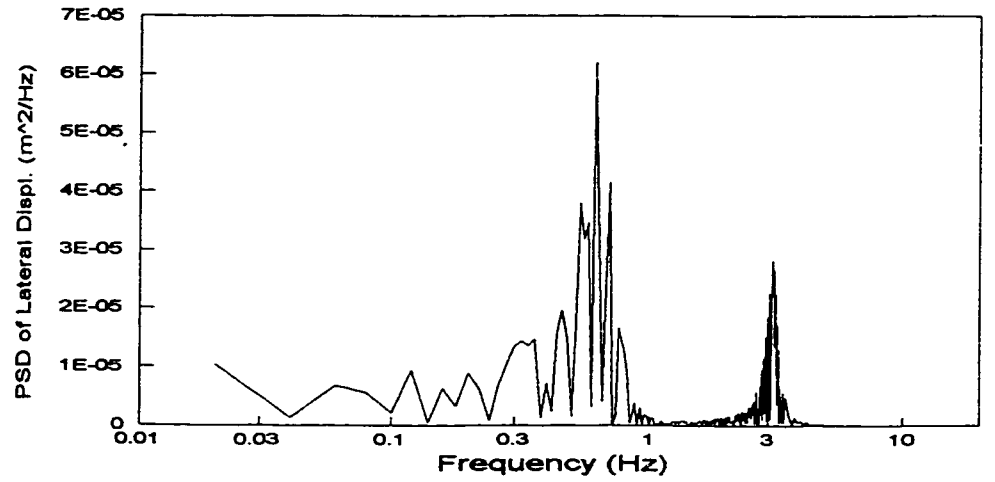


13111 kg

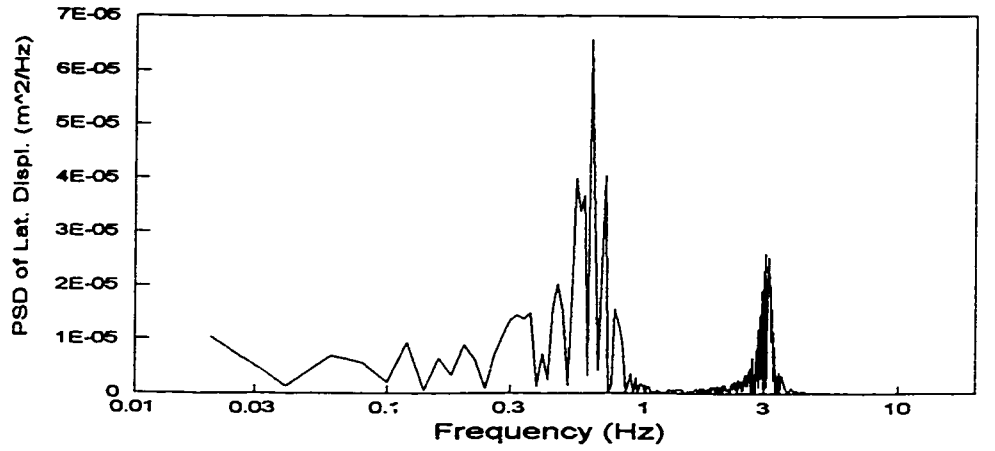


14111 kg

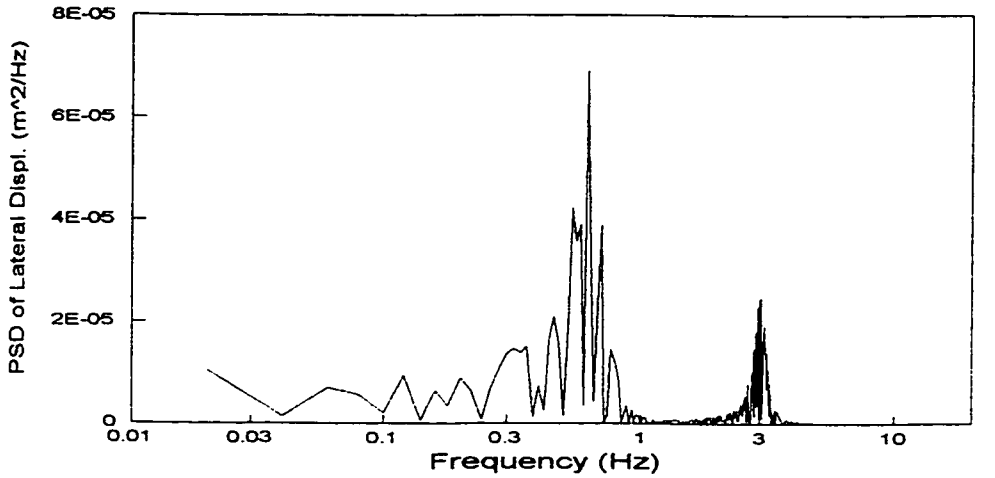


15111 kg

Figure 4.41 Influence of sprung mass weight on PSD of lateral displacement of the sprung mass for rough random road with random cross-slope between left and right wheels.

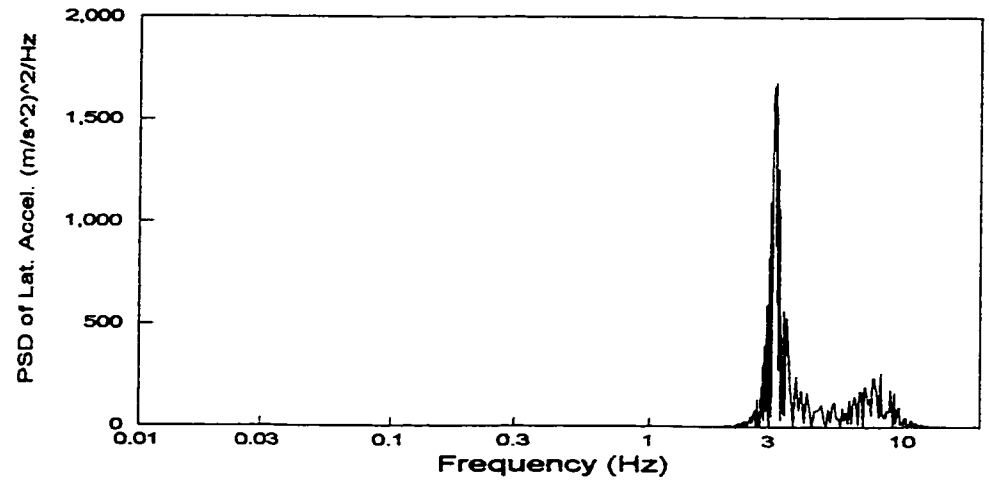


13111 kg

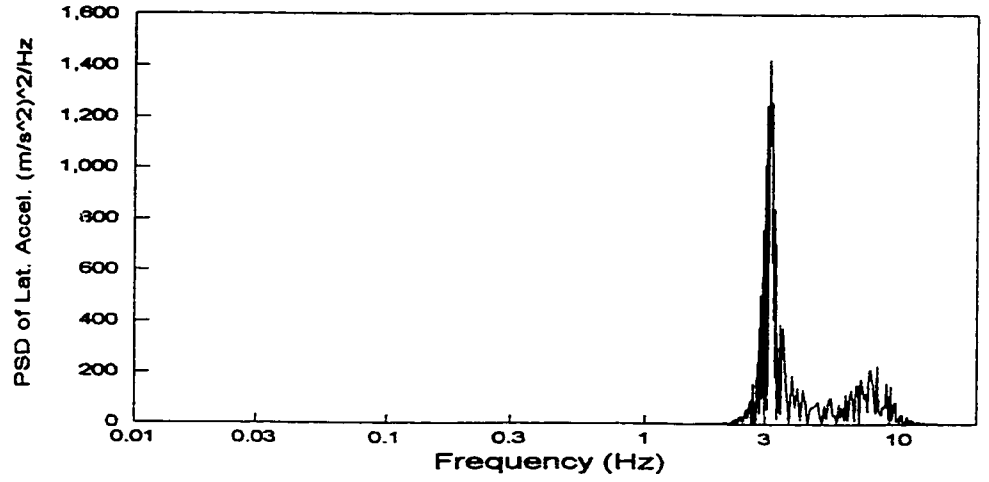


14111 kg

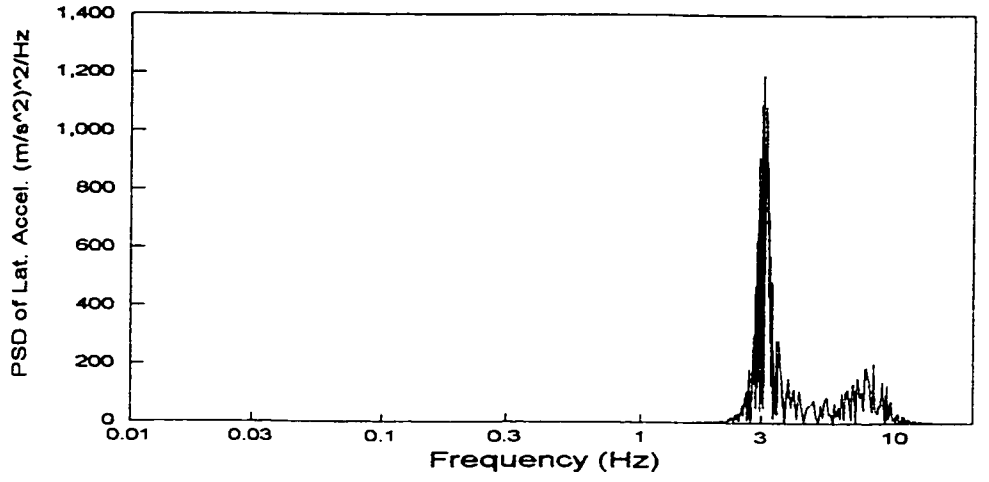


15111 kg

Figure 4.42 Influence of sprung mass weight on PSD of lateral acceleration of the sprung mass for rough random road with random cross-slope between left and right wheels.

### 4.5.5 Influence of Vehicle Speed

The influence of vehicle speed on the response PSD characteristics of the candidate vehicle is evaluated for given Gaussian random road excitation subject to variation in vehicle speed from 110 km/h to 70 km/h. The response PSD of the sprung mass is presented in Figures 4.43 to 4.46. The results clearly show that the roll and lateral displacement response PSD characteristics of the sprung mass exhibit a dominant peak at its roll natural frequency, while the roll and lateral acceleration response PSD characteristics of the sprung mass display a dominant peak at its lateral resonant frequency. These dominant roll and lateral displacement peak magnitudes tend to increase with decrease in vehicle speed, while the dominant roll and lateral acceleration peak magnitudes tend to decrease with decrease in vehicle speed. The amplitudes of the roll and lateral displacement response peaks near the sprung mass lateral resonant mode, and the roll and lateral acceleration response peaks near the unsprung mass roll resonant mode decrease with decrease in vehicle speed.

### 4.5.6 Influence of Random Road Roughness

The influence of random road roughness on the random response PSD characteristics of the candidate vehicle is evaluated for given random roadway excitation subject to road roughness coefficient varying from 0.15 to 0.4 and variance coefficient varying from 0.0033 to 0.012. The random response PSD of the sprung mass is illustrated in Figures 4.47 to 4.50. The results show that the PSD characteristics of the sprung mass roll and lateral displacement response exhibit considerable large resonant at the sprung mass roll natural frequency, while the corresponding acceleration PSD exhibit significant resonances at the sprung mass lateral natural frequency. Furthermore, the roughness of the random road affects the sprung mass response PSD amplitudes in a consistant and

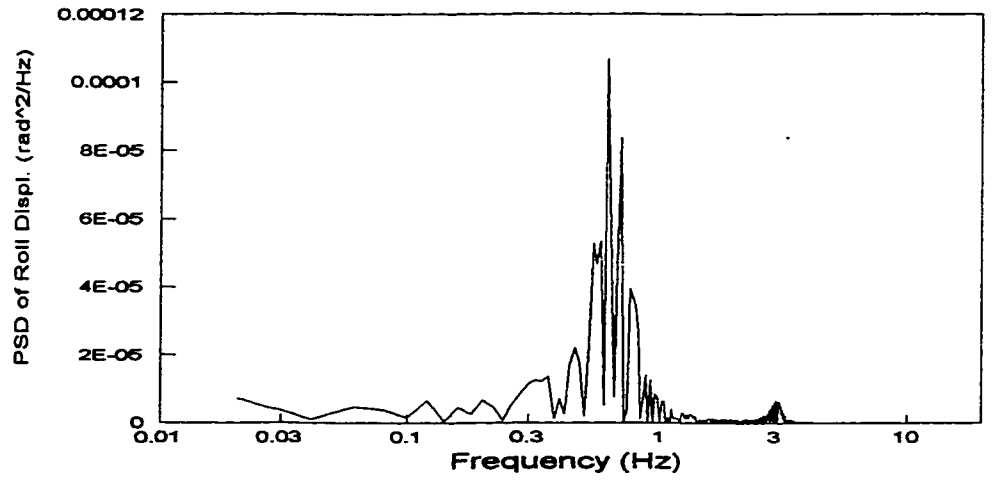


110 km/h

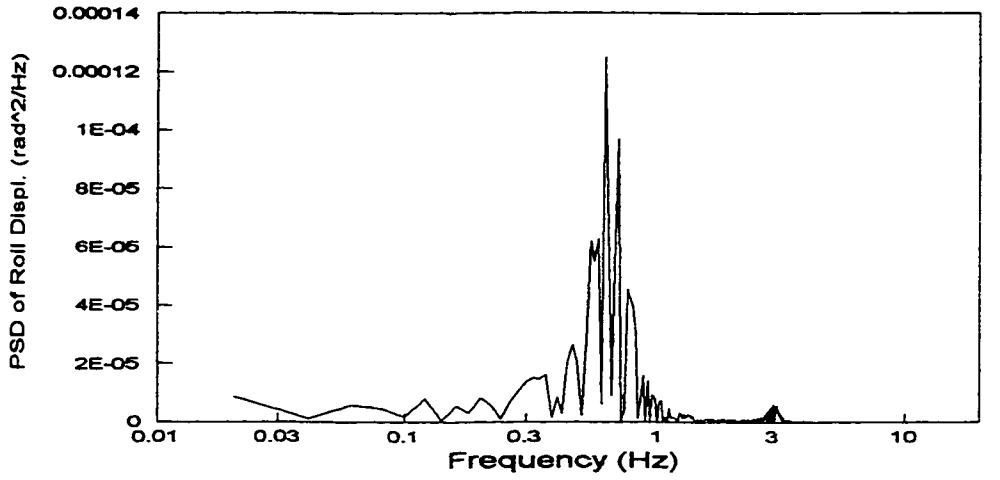


90 km/h

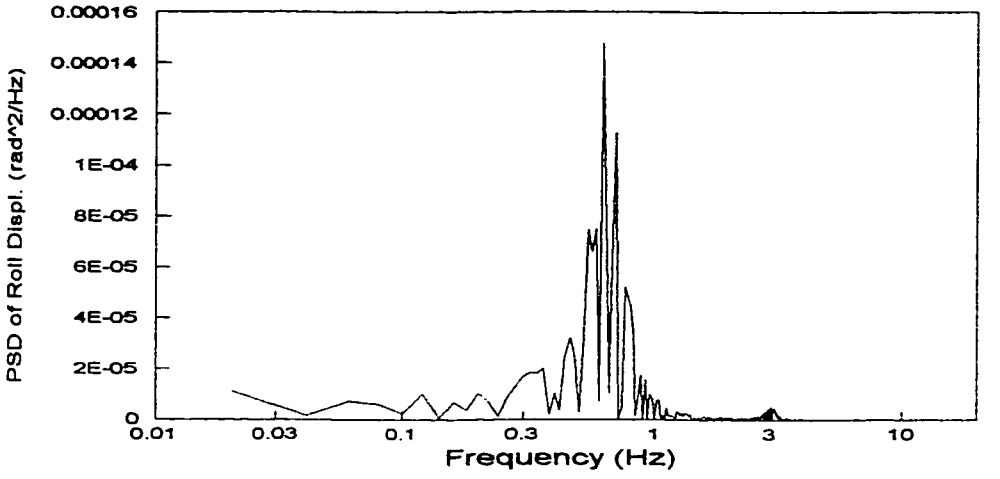


70 km/h

Figure 4.43 Influence of vehicle speed on PSD of roll displacement of the sprung mass for rough random road with random cross-slope between left and right wheels.

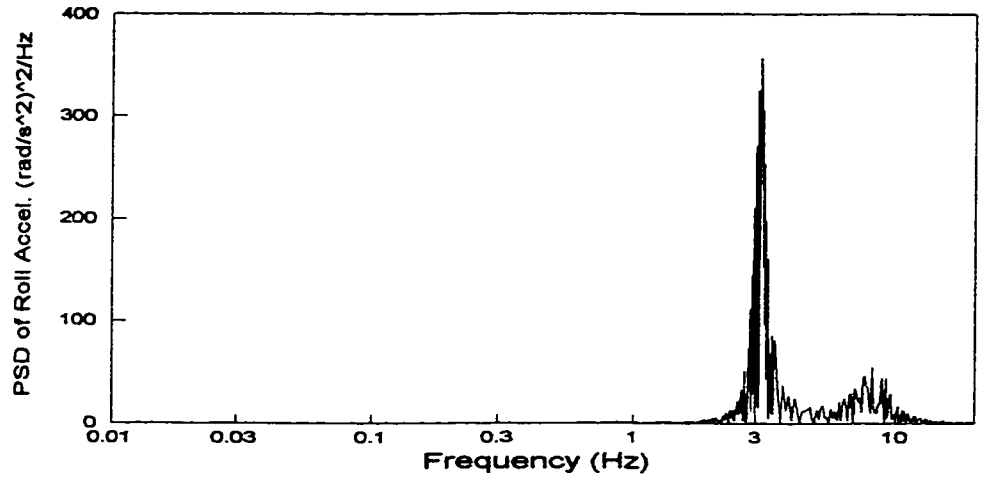


110 km/h

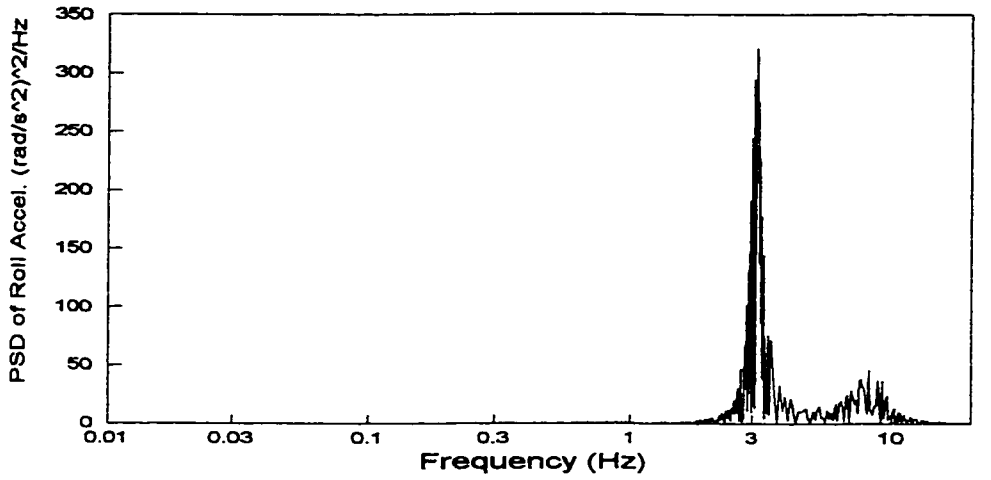


90 km/h

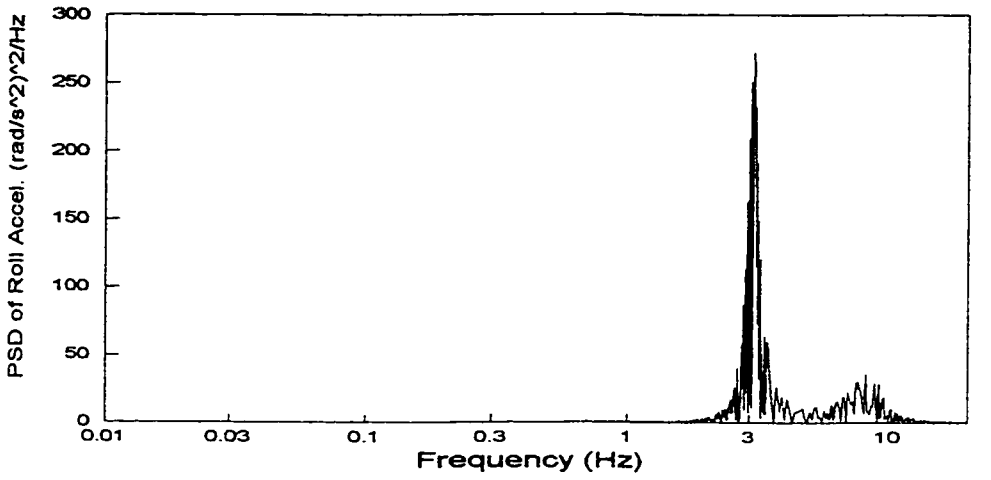


70 km/h

Figure 4.44 Influence of vehicle speed on PSD of roll acceleration of the sprung mass for rough random road with random cross-slope between left and right wheels.

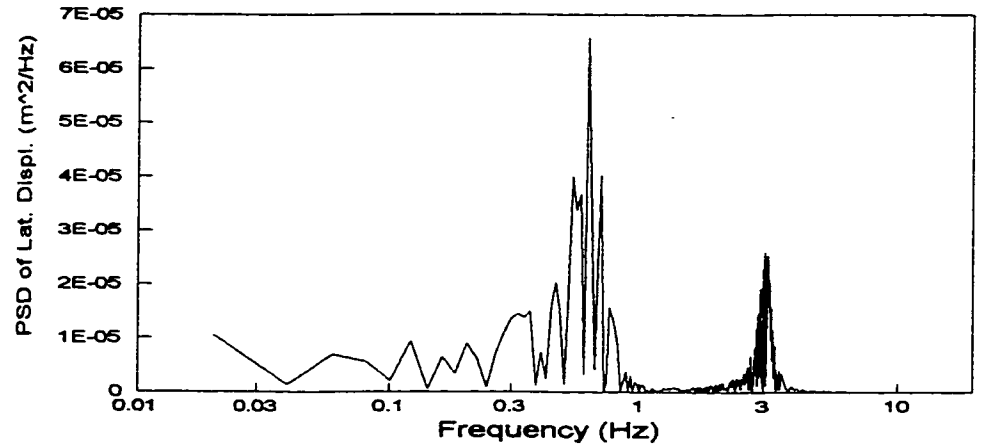


110 km/h

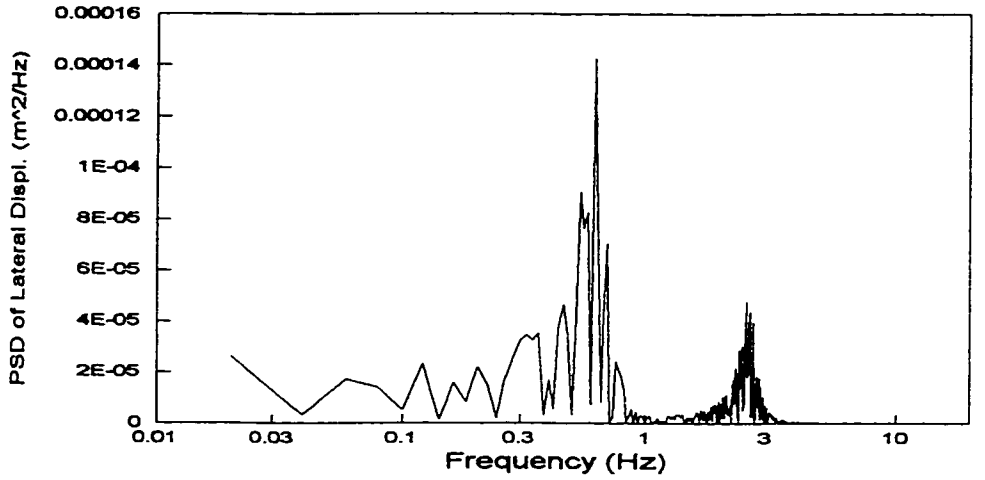


90 km/h

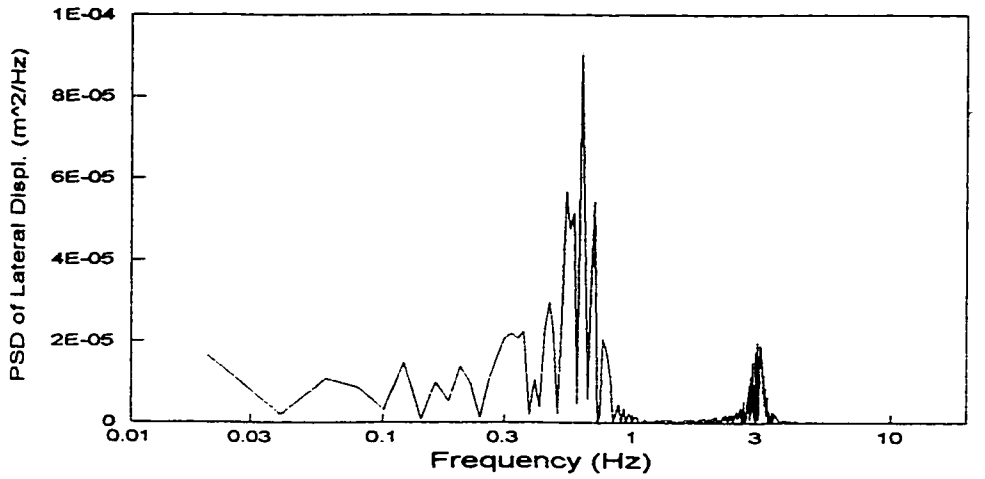


70 km/h

Figure 4.45 Influence of vehicle speed on PSD of lateral displacement of the sprung mass for rough random road with random cross-slope between left and right wheels.

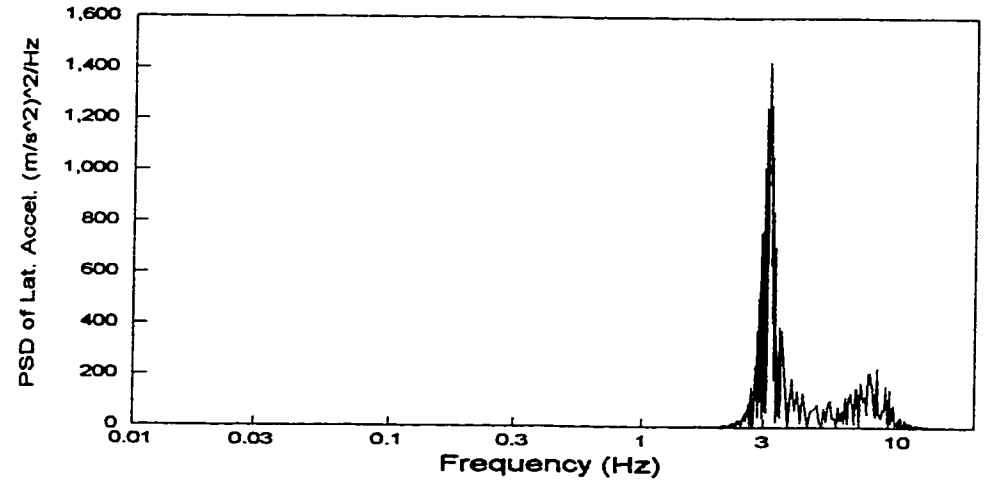


110 km/h

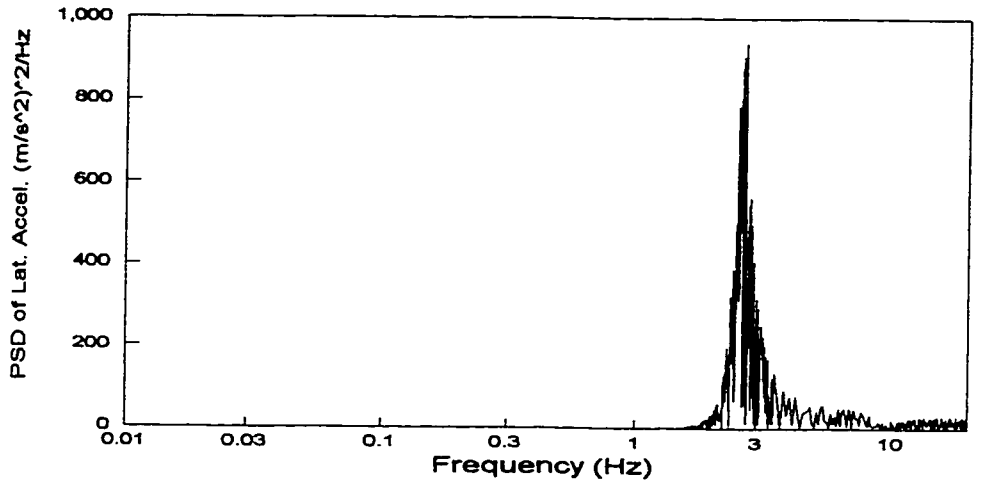


90 km/h

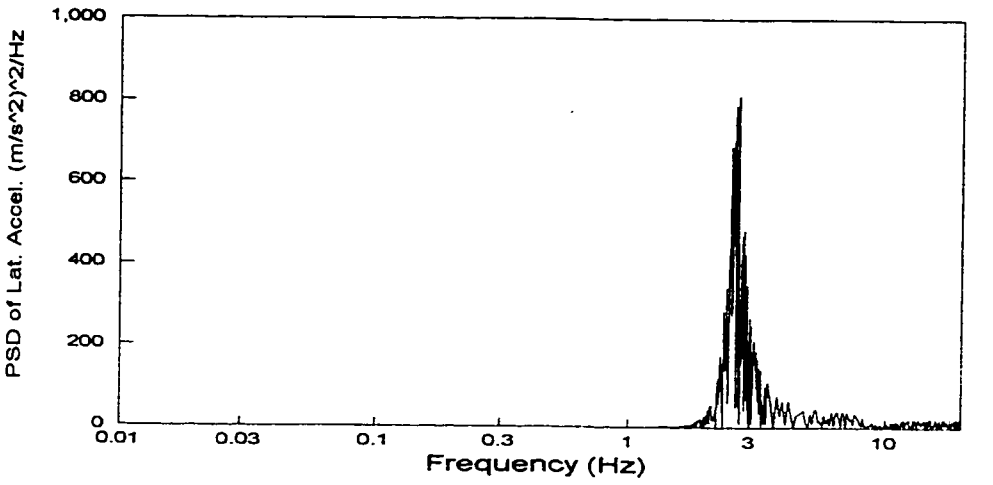


70 km/h

Figure 4.46 Influence of vehicle speed on PSD of lateral acceleration of the sprung mass for rough random road with random cross-slope between left and right wheels.

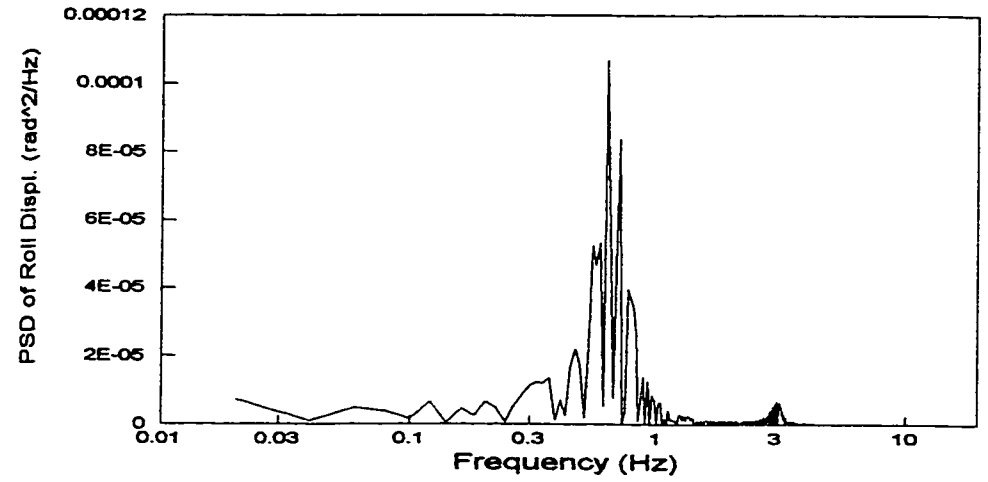


rough

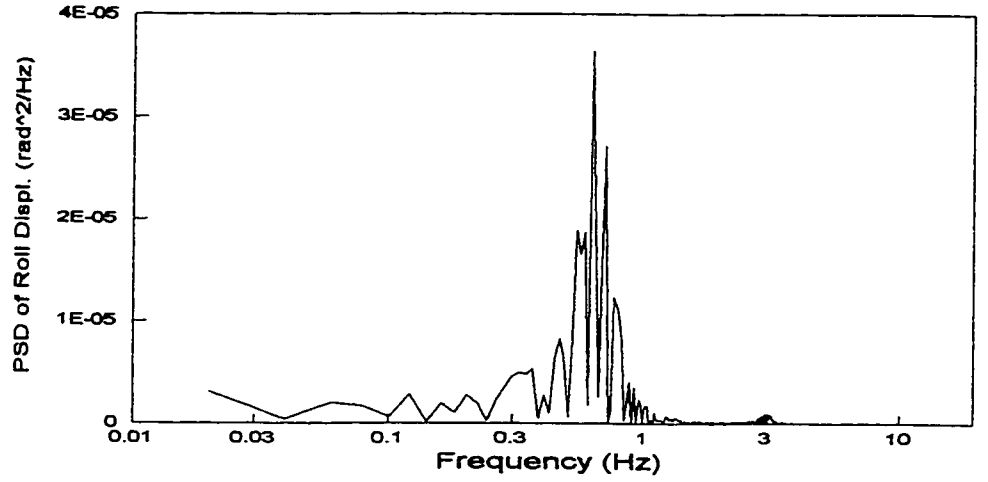


medium

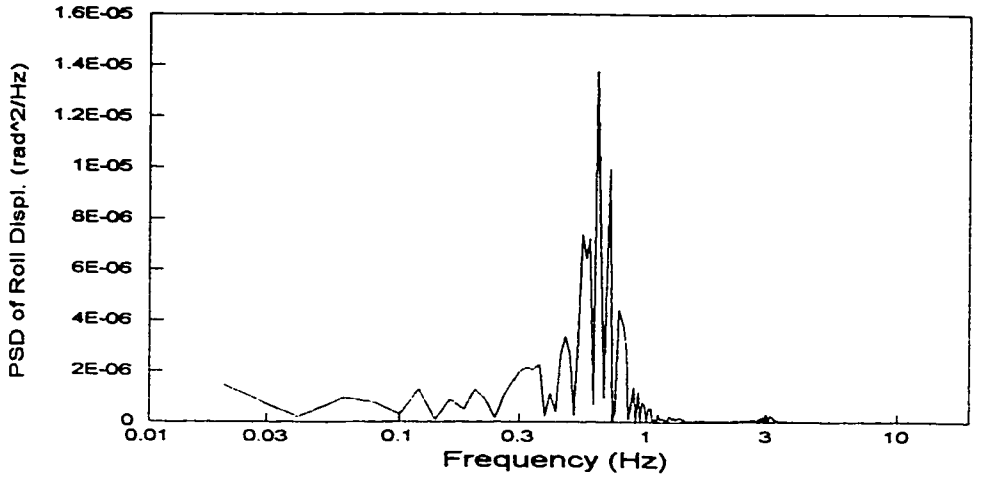


smooth

Figure 4.47 Influence of road roughness on PSD of roll displacement of the sprung mass for random cross-slope between left and right wheels.

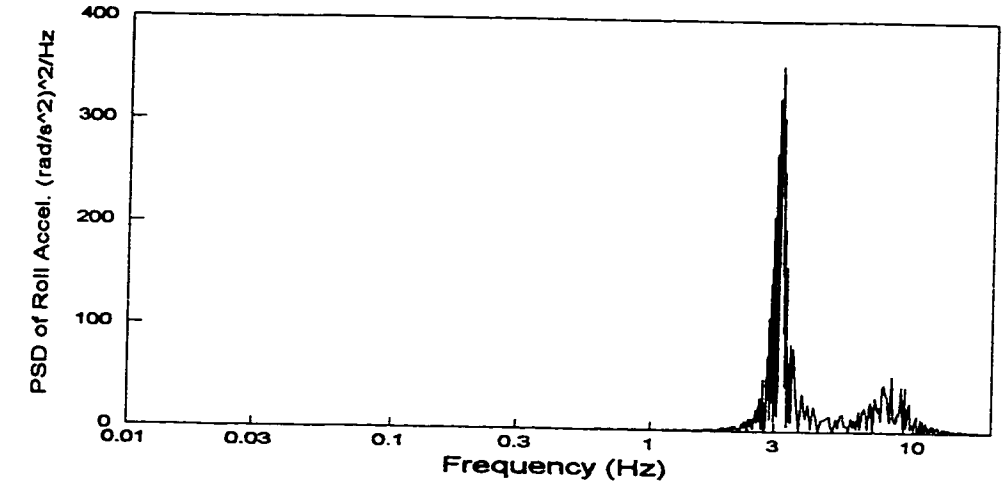


rough

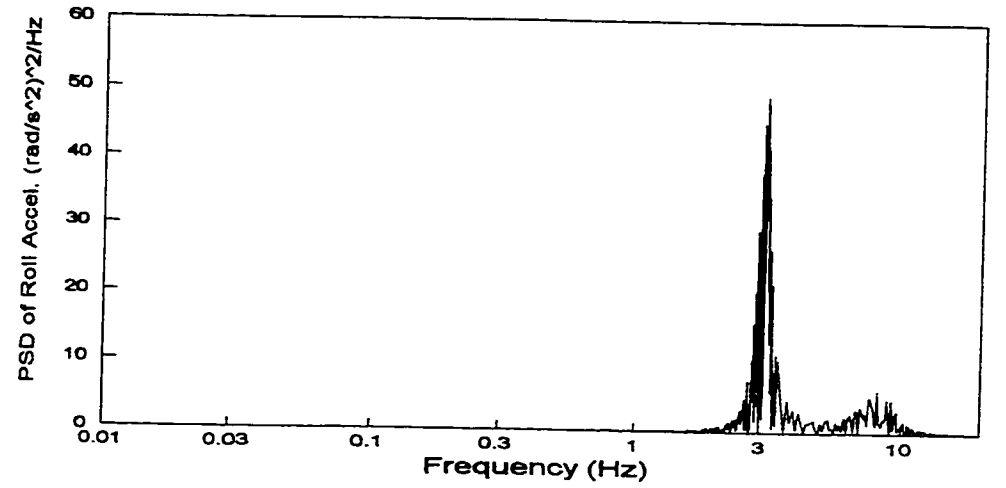


medium

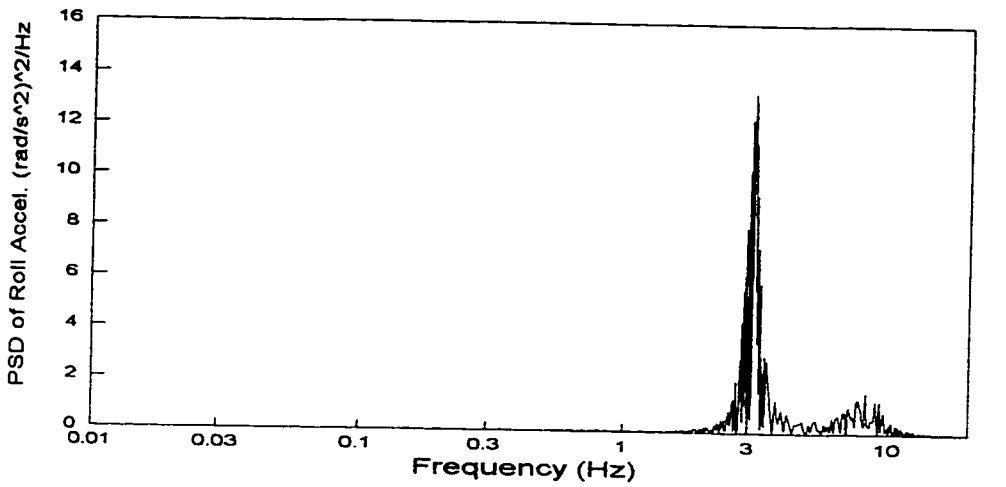


smooth

Figure 4.48 Influence of road roughness on PSD of roll acceleration of the sprung mass for random cross-slope between left and right wheels.

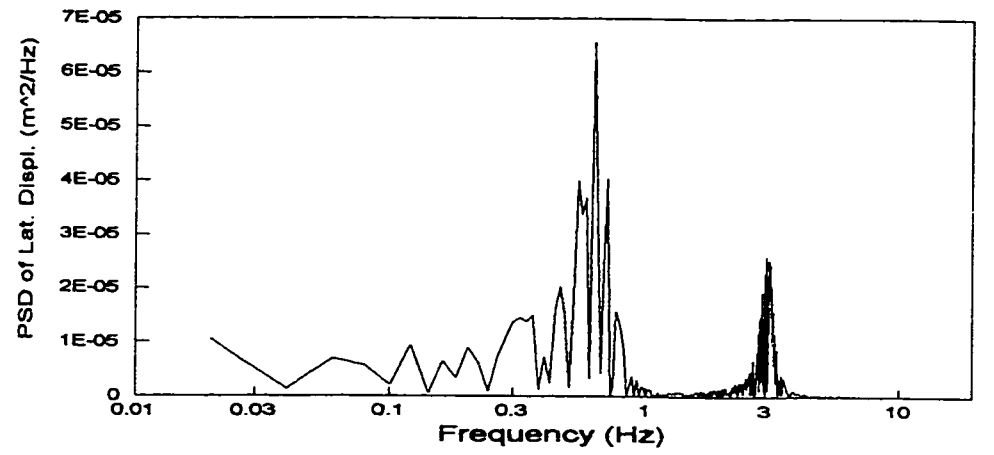


rough

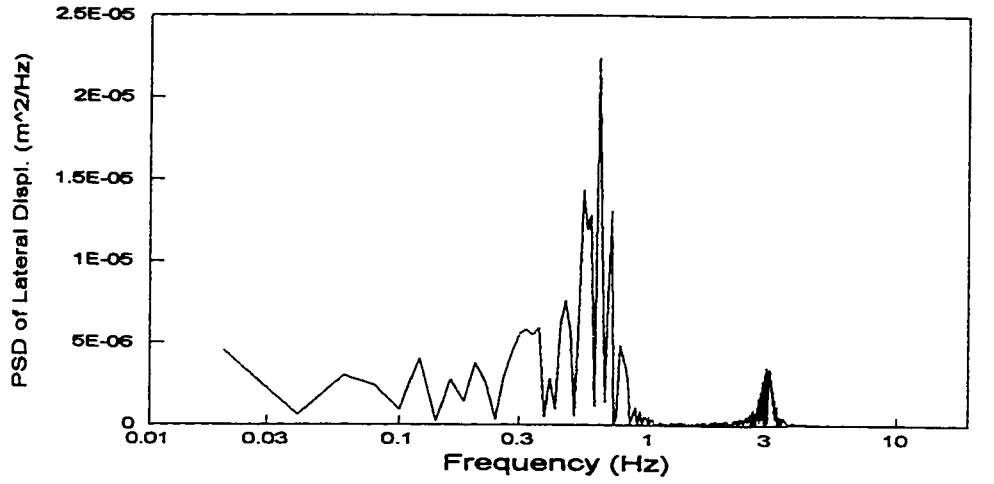


medium

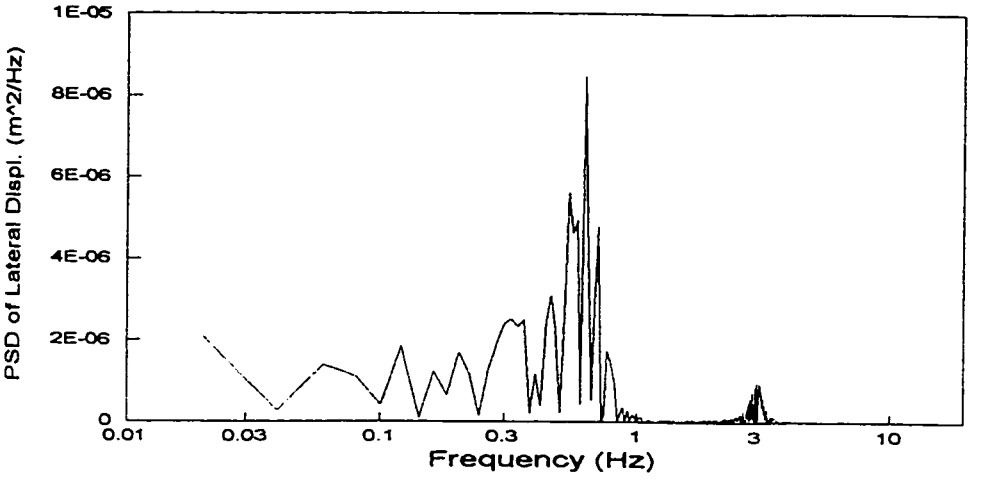


smooth

Figure 4.49 Influence of road roughness on PSD of lateral displacement of the sprung mass for random cross-slope between left and right wheels.

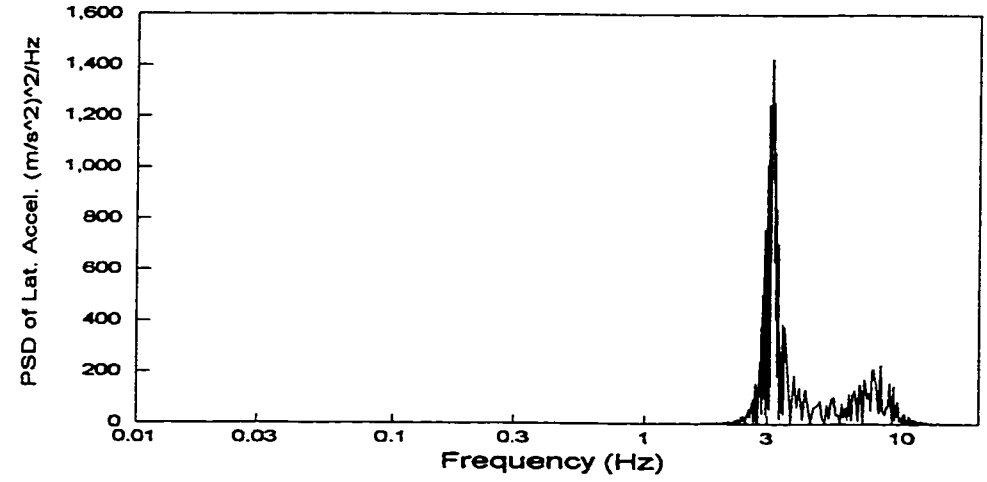


rough

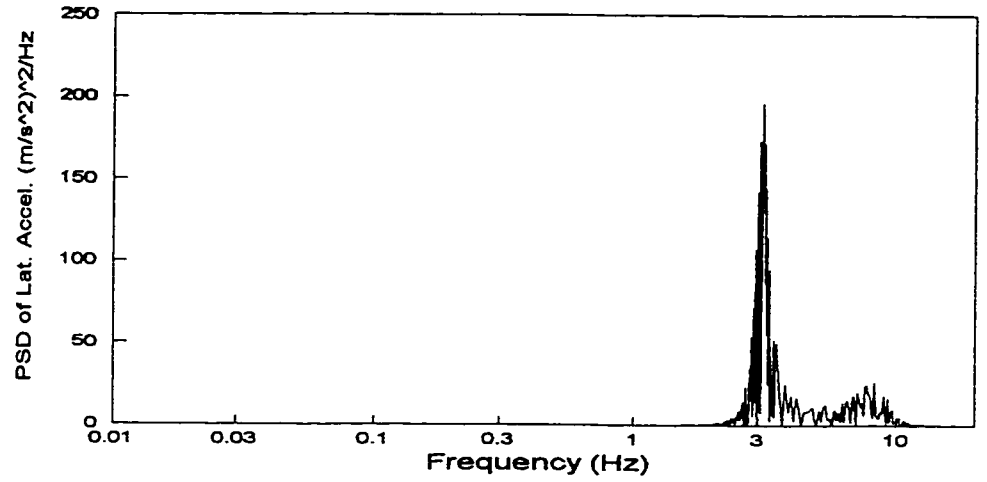


medium

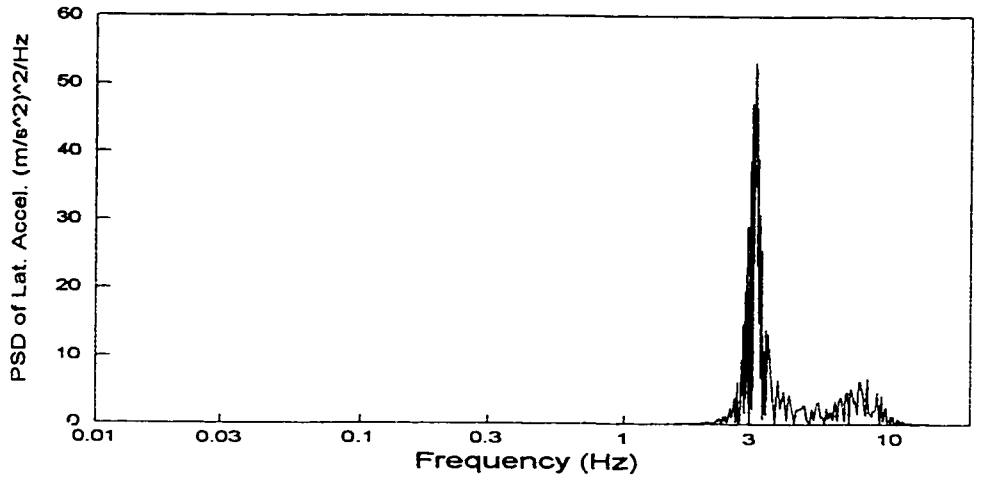


smooth

Figure 4.50 Influence of road roughness on PSD of lateral acceleration of the sprung mass for random cross-slope between left and right wheels.

significant manner that rougher road surface yields higher resonant peak magnitudes of the displacement and acceleration response PSD of the sprung mass.

## 4.6 Summary

In this chapter, the ride and handling performance of two analytical models with nine-DOF and five-DOF of the candidate vehicle in the roll plane are investigated. System properties such as natural frequencies, damping ratio and dominant coordinates corresponding to each resonant mode are studied. The fundamental properties of the suspension system are analyzed for harmonic lateral acceleration excitation, harmonic out-of-phase and random road excitations. The influences of the suspension parameters and vehicle operating conditions on the candidate vehicle's ride and handling characteristics are studied based upon the simplified five-DOF analytical model.

# Chapter 5

# Conclusions and Recommendations for Future Work

## 5.1 General

In this dissertation, an analytical investigation is performed to study the ride and handling performance characteristics of road vehicles equipped with beam-axle suspensions and the effects of their restraining linkages. A modern high-decker highway bus is considered as the candidate vehicle for the study. Three mathematical models are sequentially formulated with different complexities in the roll plane comprising a single composite beam-axle suspension constrained by a rigid transverse Panhard rod to investigate the ride and handling performance of the candidate vehicle.

A kineto-static model is initially developed to study the kinematic chartacteristics of the beam-axle suspension with transverse constraining linkage. The roll characteristics of the beam-axle suspension subject to constant lateral forces arising from cornering maneuvers and the deflection of the sprung mass center of gravity are studied. The influence of the suspension parameters, such as the Panhard rod length and its geometric location, and the static roll inputs induced from the tire-road interface are analyzed. A comprehensive nine-DOF dynamic analysis model is developed to investigate the dynamic response characteristics of the beam-axle suspension subject to cornering/directional maneuvers and road irregularities. The mass and mass moment of inertia of the Panhard rod, and the elasticity of the Panhard rod bushings are appropriately incorporated in the vehicle model. A simplified five-DOF model is further derived upon neglecting the mass of the rigid Panhard rod and the flexibility of the Panhard rod bushings. Both dynamic models are validated with the available test data on the dominant ride frequencies of the

highway bus. The results suggest that the simplified model can be effectively used to characterize the roll plane dynamics of the vehicle.

The handling performance characteristics of the beam-axle suspension with Panhard rod constraint are analyzed specifically in terms of the roll and lateral frequency response characteristics of the sprung mass, when the vehicle experiences harmonic centrifugal acceleration excitations. The ride performance of the vehicle is evaluated for excitations due to tire-terrain interface irregularities, such as harmonic out-of-phase displacement excitations, and in a more general sense, random phase with Gaussian random displacement excitations. The Gaussian random input density matrix is formulated by taking into account primarily the vehicle speed and the terrain roughness. The ride responses of the beam-axle suspension with the Panhard rod constraint subject to the random terrain are evaluated and presented in terms of power spectral densities of displacement and acceleration of the roll and lateral vibrations of the sprung mass. Sensitivity of the ride and handling characteristics of the suspension with respect to its parameters' variations is investigated to enhance the understanding of the effects of the Panhard rod constraint on the suspension ride and handling performance.

## 5.2 Highlights Of Investigation

This investigation is performed in three sequential phases. The major highlights of each phase are summarized in the following sections.

### 5.2.1 Development of a Candidate Vehicle Model

Based upon the survey of the reported literature on road vehicles with beam-axle suspensions constrained by auxiliary linkages, such as the transverse Panhard rod, a high-deck highway bus is selected for this investigation. The candidate vehicle comprising the front, dual-tire drive and rear beam-axle suspensions is represented in the roll plane by a single composite lumped beam-axle suspension constrained by a Panhard rod. The

suspension air bellows and shock absorbers are assumed to deflect along the axial directions and represented by linear springs and dampers. The tire terrain interactions are represented by the linear force-defection properties of the lumped tires assuming point-contact with the non-deformable road. The analytical model of the candidate vehicle comprises the sprung and unsprung masses, parallel combinations of a vertical linear spring and a vertical linear damper representing suspension air bellows and shock absorbers, parallel combinations of a linear spring and a damper in both vertical and lateral directions representing the linear force-defection properties of the lumped tire terrain interactions, and a rigid transverse Panhard rod and its bushings. Centrifugal and vertical excitations are formulated to represent the external loads due to directional maneuvers and tire-road interactions, respectively.

### 5.2.2 Kinetostatic Characteristics of the Panhard Rod Beam-Axle Suspension

A simplified two-DOF non-linear roll plane model is developed to study the kineto-static deflection behavior of the sprung mass of the candidate vehicle subject to different levels of cornering/directional maneuvers. Kinematic analyses are performed with and without roll motion of the unsprung mass to study the influence of the constraint on the coordinates of the roll center and the sprung mass center of gravity. A constant lateral force varying from -44.5 kN to 44.5 kN is applied to the center of gravity of the sprung mass to represent the centrifugal loads encountered during turns. A roll angle of the unsprung mass is introduced to represent the effect of the roll input arising from the tire-terrain interfaces. The non-linear algebraic equations of the kineto-static model of the candidate vehicle subjected to centrifugal forces are solved using the Newton iteration scheme. The roll motion of the sprung mass, the vertical deflection of the center of gravity of the sprung mass, the instantaneous roll center of the suspension, and the suspension roll stiffness are evaluated for different centrifugal accelerations to demonstrate the influence of constraining linkage on the suspension performance.

### 5.2.3 Dynamic Characteristics of the Panhard Rod Beam-Axle Suspension

Two lumped-parameter roll plane models of the vehicle with beam-axle suspension are developed to investigate the ride and handling performance characteristics. A comprehensive nine-DOF model incorporating the inertia and compliance of the Panhard rod and its bushings is initially developed, which is simplified to a five-DOF model upon neglecting the contribution due to inertia and compliance of the constraint. A free-vibration analysis of the two models is performed and the results are compared with the measured dominant ride frequencies of the candidate vehicle. The validity of the mathematical models is assessed upon comparison between the analytical resonant frequencies and the available experimental data on the dominant ride frequencies. The results of the study suggested that the contributions due to dynamics of the Panhard rod constraints to the low frequency ride and handling measures are negligible. The simplified five-DOF can thus be effectively used to study the ride and handling performance. The kinematics of the Panhard rod, however, strongly influences the response behavior of the vehicle and the suspension.

The simplified vehicle model is thus used to derive the ride and handling response of the vehicle subject to harmonic and random road excitations, and harmonic centrifugal acceleration excitations. A performance criteria comprising roll and lateral displacement and acceleration response is formulated to assess the effects of constraining linkage and suspension parameters on the ride and handling response.

A parametric study is performed to establish an understanding on the influence of variations in the suspension parameters and vehicle operating conditions, such as Panhard rod length and its location, suspension stiffness and damping properties, load condition, road condition and vehicle speed, on the dynamic ride and handling performance of the candidate vehicle.

## 5.3 Conclusions

The conclusions drawn from this investigation are summarized as follows:

- The suspension roll center can be assumed to be located at the intersection of the vertical axis of the sprung mass and the geometric center of the Panhard rod for centrifugal acceleration ranging from -0.3g to 0.3g.
- The roll deflections of the sprung mass and the Panhard rod, the lateral deflection of the sprung mass center of gravity, the lateral and vertical deflections of the suspension roll center, and the relative vertical displacement between the suspension roll center and the sprung mass center of gravity, vary in a nearly linear manner with the centrifugal force, ranging from -44.5 kN to 44.5 kN.
- The effective suspension roll stiffness exhibits linear and asymmetric characteristics corresponding to the centrifugal force. The negative lateral force yields higher suspension roll stiffness compared to that under positive lateral force.
- The asymmetric response characteristics of the sprung mass roll angle and the suspension roll stiffness under positive and negative centrifugal forces arising from the left and right turns, respectively, are insignificant and can thus be ignored.
- The sprung mass roll angle is insignificantly influenced by the variations in the Panhard rod orientation angle and the Panhard rod length, while it is apparently influenced by the unsprung mass roll angle and the suspension spring rate.
- The suspension roll stiffness increases with the increase in the suspension spring rate, irrespective of the direction of the centrifugal force. For negative lateral force, larger suspension roll stiffness is obtained with positive Panhard rod orientation angle, the unsprung mass roll angle, and the longer Panhard rod.
- Smaller relative vertical displacement of the suspension roll center relative to the sprung mass center of gravity is observed with positive Panhard rod orientation angle,

the positive unsprung mass roll angle and the suspension spring rate, while a stiffer suspension spring yields small relative lateral displacement.

- Variations in the Panhard rod orientation angle from $-3^{\circ}$ to $+3^{\circ}$ and the Panhard rod length from 0.6 m to 1.0 m have insignificant influence on the suspension dynamic behavior.

The following conclusions are in agreement with suspension tuning practice.

- Softer suspension deteriorates the roll stability and the handling quality, while a stiffer suspension deteriorates the ride quality due to road irregularities.
- An increase in suspension damping can effectively reduce the suspension resonant deflections at lower frequencies, leading to improved handling performance, while a lightly damping suspension is desirable to achieve better ride quality at higher frequencies.
- A stiffer tire offers advantage in reducing the magnitudes of roll and lateral deflection response at low frequencies, while a softer tire shows apparent decrease in the resonant deflections at higher frequencies.
- Heavier sprung mass tends to deteriorate the handling quality slightly, while lighter sprung mass slightly deteriorates the ride quality at higher frequencies.

## 5.4 Recommendations for Future Work

This thesis is carried out to evaluate the ride and handling characteristics of the beam-axle suspension with Panhard rod constraint of a candidate highway bus for centrifugal acceleration excitations and roll inputs due to road unevenness. It is recommended to undertake the following future works to further explore its performance potentials:

- A more elaborate three-dimensional analytical model of the candidate highway bus should be developed and analyzed to assess its ride and handling characteristics. This model should include its three beam-axle suspensions: the front, drive and rear beam-axle suspensions. Other considerations should include: a more sophisticated three-dimensional tire model and the effect of the steering linkage, etc.
- The ride and handling response characteristics need to be evaluated under transient steering maneuvers, where the contributions due to effective roll stiffness, and kinematics and dynamics of constraining linkage are expected to be significant.
- In this study, the coordinates of the suspension roll center and the resultant suspension roll stiffness are analyzed using single composite roll plane. A comprehensive three-dimensional model is highly desirable to account for the different axle loads and suspension properties.
- The non-linear properties of the suspension springs and dampers should be included in the dynamic modeling of road vehicle.
- The optimization on the parameters of beam-axle suspensions with Panhard rod constraints of road vehicles should be performed to enhance the ride and handling performance.

The concepts suggested in this thesis can be applied to broader applications, such as light weight, high speed and high performance race cars. Further recommendations are made accordingly as follows:

- The flexibility of the suspension sprung and unsprung masses, the restraining linkages, and the non-linear characteristics of the suspension springs and dampers should be taken into account.
- The effect of the restraining force properties posed by the Panhard rod on the handling performance of the vehicles should be further investigated.
- The potential of replacing rigid Panhard rod with an active Panhard rod should be explored to enhance the lateral stability and ride performance of the vehicle.

## References


1. H. Horntrich, "Rear Suspension Design with Front Wheel drive Vehicle," SAE Paper 810421.

2. D. A. Crolla, G. R. Firth and D. N. L. Horton, "Independent vs. Axle Suspension for On/Off Road Vehicles," SAE Paper 921662.

3. E. P. Timoney, S. S. Timoney and S. G. Timoney, "Heavy Vehicle Independent Suspension," Paper C434/88, Proc. I. Mech. E. Conf. on Advanced Suspension, London, 1988.

4. E. P. Timoney, S. S. Timoney and S. G. Timoney, "Independent Suspension for Heavy Armoured Vehicles," Autotech, Birmingham, 1989.

5. K. N. Moman and F. Giannopoulos, "Recent Advances in the Analytical and Computational Aspects of Modeling Active and Passive Vehicle Suspensions," Computational Methods in Ground Transportation Vehicles, AMD Vol. 50, 1982, pp. 75-115.

6. T. D. Gillespie, "Fundamentals of Vehicle Dynamics," SAE, 1992.

7. A. G. Nalecz and A. C. Bindemann, "Investigation into the Stability of Four Wheel Steering Vehicles," International Journal of Vehicle Design, 9(2), pp. 159-178, 1988.

8. A. G. Nalecz and A. C. Bindemann, "Analysis of the Dynamic Response of Four Wheel Steering Vehicles at High Speed," International Journal of Vehicle Design, 9(2), pp.179-202, 1988.

9. S. Rakheja et al., "Ride Vibrations of Articulated Vehicles and Significance of Secondary Suspension," SAE 1989 Noise and Vibration Conference, SAE Publ. No. P-222, May 16-18, pp. 139-147.

10. G. J. Heydinger et al., "Validation of Vehicle Stability and Control Simulations," SAE Paper 900128, 1990.

11. R. W. Allen and T. J. Rosenthal et al., "Validation of Ground Vehicle Computer Simulations Developed for Dynamics Stability Analysis," SAE Paper 920054, 1992.

12. H. S. Radt, Jr. and D. J. V. Dis, "Vehicle handling Responses Using Stability Derivatives," SAE paper 960483, 1996.

13. M. G. Kim, H. I Jeong and W. S. Yoo, "Sensitivity Analysis of Chassis System to Improve Shimmy and Brake Judder Vibration on Steering Wheel," SAE Paper 960734.

14. A. B. Patil, "Dynamic Analysis of Scooter (Two Wheeler) for Ride Evaluation," SAE Paper 911875.

15. C. D. Carter, C. B. Sherman and R. D. Matthews, "Design of a Formula SAE Race Car: Vehicle Dynamics and Performance," SAE Paper 821092.

16. C. H. Suh, "Modeling the McPherson Suspension," Computers in Mechanical Engineering, Sep/Oct 1988, pp. 52-56.

17. M. Rghavan, "An Atlas of Linkages for Independent Suspensions," SAE Paper 911925

18. E. Saibel and M. C. Tsao, "Further Investigations in Vehicle Dynamics," SAE Paper 700173, 1970.

19. M. A. Dorgham and J. R. Ellis, "Digital Simulation of the Kinematic and Dynamic Behaviour of Road Vehicle Suspensions: Part 1 - Planar Suspensions," ASME 74-DET-17, 1974.

20. P. J. Liu, "An Analytical Study of Ride and Handling Performance of An Interconnected Vehisle Suspension," Master Dissertation, Concordia University, Montreal, 1994.

21. P. Pintado and F. G. Benitez, "Optimization for Vehicle Suspension I: Time Domain," Vehicle Systems Dynamics, 19(1990), pp. 273-288.

22. T. C. Crahan, "Modeling Steady-State Suspension Kinematics and Vehicle Dynamics of Road Racing Cars - Part I: Theory and Methodology," SAE Paper 940505, 1994.

23. T. C. Crahan, "Modeling Steady-State Suspension Kinematics and Vehicle Dynamics of Road Racing Cars - Part II: Examples," SAE Paper 942506, 1994.

24. L. J. Howell, "Power Spectral Density Analysis of Vehicle Vibration Using the NASTRAN Computing Program," SAE Paper 740328, 1974.

25. A. E. Duncan, "Application of Modal Modeling and Mount System Optimization to Light Duty Truck Ride Analysis," SAE Paper 811313, 1981.

26. S. S. Kim, A. A. Shabana and E. J. Haug, "Automated Vehicle Dynamic Analysis with Flexible Components," Trans. of the ASME, Vol. 106, March 1984, pp.126-133.

27. S. H. Crandall, "Perturbation Techniques for Random Vibration of Non-lineart System," The Journal of the Acoustical Society of America, Vol. 35, No. 11, pp. 1700-1705, 1963.

28. J. B. Roberts, "Response of Non-linear Mechanical Systems to Random Excitation Part I: Markov Methods," Shock and Vibration Digest, Vol. 13, No. 4, pp. 17-28, 1981.

29. B. D. Van Deusen, "Truck Suspension System Optimization," Journal of Terramechanics, Vol. 9, no. 2, pp.83-100, 1973.

30. G. Dailey, W. C. Caywood and J. C. O'Connor, "A General Purpose Computer Program for the Dynamic Simulation of Vehicle-Guideway Interactions," AIAA Journal, Vol. 3, No. 3, pp. 278-288, 1973.

31. R. C. Bootan, "Nonlinear Control Systems with Random Inputs," Trans. IRE Circuit Theory, CT-1, pp. 9-18, 1954.

32. T. K. Caughy, "Equivalent Linearization Techniques," The Journal of the Acoustical Society of America, Vol. 35, No. 11, pp.1706-1711, 1963.

33. J. B. Roberts, "Response of Nonlinear Mechanical Systems to Random Excitaiton - Part II: Equivalent Linearization of Other Methods," shock and Vibration Digest, Vol. 13, No. 11, pp. 15-29, 1981.

34. S. Rakheja, M. Van Vliet and S. Sankar, "A Discrete Harmonic Linearization Technique for Simulation of Nonlinear Mechanical Systems," Journal of Sound and Vibration, 100(4), pp. 511-526, 1985.

35. M. M. ElMadany and M. A. Dokainish, "Articulated Vehicle Dynamics Analysis using Equivalent Linearization Technique," SAE Paper 801421, 1980.

36. P. Michelberger and D. Szoke, "Speed Dependent Vertical Vibrations of Elastic Vehicle Bodies," Int. J. Vehicle Design, 8(1), pp.8-95, 1985.

37. K. N. Norman Jr. and F. Giannopoulos, "Recent Advances in Analytical and Computational Aspects of Modeling Active and Passive Vehicle Suspensions," Computational Methods in Ground transportation vehicles, AMD-Vol. 50, ASME, 1982, pp.75-115.

38. N. Fujiwara and Y. Murotsu, "Design of Vibration Isolators Optimizing Riding Comfort," Bulletin of JSME, Vol. 19, No. 138, Dec. 1976.

39. D. Ryba, "Improvements in Dynamic Characteristics of Automobile Suspension Systems, Part I: Two Mass Systems," Vehicle Dynamics 3(1974), pp.17-46.

40. S. Rakheja, H. Su and T. S. Sankar, "Analysis of a Passive Sequential Hydraulic Damper for Vehicle Suspension," Vehicle System Dynamics, 19(1990), pp.289-312.

41. X. P. Lu, H. L. Li and P. Papalambros, "A Design Procedure for the Optimization of Vehicle Suspensions," Int. J. of Vehicle Design, Vol. 5, nos. ½, 1984.

42. M. F. R. Afonso, "Ride Dynamic Analysis of Tracked Vehicles," Master Dissertation, Concordia University, Montreal , 1989.

43. C. B. Winkler, S. M. karamihas and S. E. Bogard, "Roll-Stability Performance ofHeavy-Vehicle Suspensions," SAE Paper 922426, 1992.

44. H. S. Radt, Jr. and D. J. Van Dis, "Vehicle Handling Responses Using Stability Derivatives," SAE Paper 960483, 1996.

45. M. W. Sayers and S. M. Riley, "Modeling Assumptions for Realistic Multibody Simulations of the Yaw and Roll Behavior of Heavy Trucks," SAE Paper 960173.

46. A. Dulac, 'An Investigation of Ride and Handling Performance of Passive and Combined Active-Passive-Bus-Suspension,' Master Dissertation, Concordia University, 1992.

47. C. B. Winkler, S. M. Karamihas and S. E. Bogard, 'Roll-Stability Performance of Heavy-Vehicle Suspensions,' SAE Paper 922426, 1992.

48. C. J. Dodds and J. D. Robson, "The Description of Road Surface Roughness," Journal of Sound and Vibration, Vol. 31, No. 2, pp.175-184, 1973.

49. K. M. A. Kamash and J. D. Robson, "The Application of Isotrophy in Road Surface Modeling," Journal of Sound and Vibration, Vol. 57, No. 1, pp. 89-100, 1987.

50. J. Y. Wong, Theory of Ground Vehicles, John Wiley & Sons, New York, 1978.

51. B. Maclaurin, "Progress in British Tracked Vehicle Suspension Systems," SAE Paper 830442, 1983.

52. M. M. ElMadany and M. E. Samaha, "Optimum Response of a Stochastic Model of a Tractor Semitrailer Vehicle - Part II: Ride Control of an Active Suspension Vehicle," ASME Vibration Conference, Proceedings on Vehicle Dynamics and Special Topics, Montreal, Sept. 17-21, pp. 177-184, 1989.

53. F. Oueslati, "An Analytical Investigation of Passive and Active Suspension Systems for Articulated Freight Vehicles," Ph. D. Dissertation, Concordia University, 1995.

54. K. M. Captain, A. B. Boghani and D. M. Wormley, "Analytical Tire Models for Dynamic Vehicle Simulation," vehicle System Dynamics, Vol. 8, pp. 1-32, 1979.

55. D. C. Creighton, "Revised Vehicle Dynamic Module: User's Guide for Computer Program VEHDYNII," Research Note No. SL-86-9, U.S. Army Engineer Waterways Experiment Station, Vicksburg, Miss., May 1986.

56. R. M. Chalasani, "Ride Performance Potential of Active Suspension Systems - Part I: Simplified Analysis Based on a Quarter Car Model," ASME Winter Annual Meeting, AMD-Vol. 80, pp. 187-204, 1986.

57. R. Karadayi and G. Y. Masada, "A Nonlinear Shock Absorber Model," Proc. of ASME Winter Annual Meeting, 1988.

58. E. Saibel and M. C. C Tsao, "Dynamics of Pneumatic Tire Vehicles with Connected Suspension Systems," Vehicle System Dynamics, Vol. 1, pp. 89-102, 1972.

59. M. M. ElMadany, "a Procedure for Optimization of Truck Suspensions," Vehicle System Dynamics, 16(1987), pp.297-312.

60. R. E. Allen, "Cab Isolation and Ride Quality," SAE Paper 750165, 1975.

61. A. E. Duncan, "Application of Modal Modeling and Mount System Optimization to Light Duty Truck Ride Analysis," SAE Paper 811313, 1981.

62. P. Pintado and F. G. Benitez, "Optimization for Vehicle Suspension I: Time Domain," Vehicle System Dynamics, 19(1990), pp. 273-288.

63. J. M. Del Castillo, P. Pintado and F. G. Benitez, "Optimization for Vehicle Suspension II: Frequency Domain," Vehicle System Dynamics, 19(1990), pp.331-352.

64. T. Dahlberg, "Optimization Criteria for Vehicle Travelling on a Randomly Profiled Road - a Survey," Vehicle System Dynamics, 8(1979), pp. 239-252.

65. G. R. George and J. P. Sadler, "Kinetostatic Analysis and Optimization of Beam-Axle Vehicle Suspension Geometries," Trends in Vehicle Design Research, ASME Publication DE-Vol. 11(1987), pp. 27-34.

66. J. P. Sadler, H. C. Chou and G. R. George, "On the application of Straight-lines Linkages to Vehicle Suspension,"Transactions of the ASME, Vol. 111(1989), pp.208-214.

67. A. G. Nalecz, "Investigation into the Effects of Suspension Design on Stability of Light Vehicle," Society of Automotive Engineering, 1988, pp.2.512-2.541.

68. M. Ksminaga, M. Murata and Y. Tateishi, "Factoring Nonlinear Kinematics into New Suspension Design: A CAE Approach to Vehicle Roll Dynamics," SAE Paper 940871.